THE UNIVERSITY
of EDINBURGH

From the Conventional MIMO to Massive MIMO Systems: Performance Analysis and Energy Efficiency Optimization

Wenjun Fu

A thesis submitted for the degree of Doctor of Philosophy.
The University of Edinburgh.
July 2017

Abstract

The main topic of this thesis is based on multiple-input multiple-output (MIMO) wireless communications, which is a novel technology that has attracted great interest in the last twenty years. Conventional MIMO systems using up to eight antennas play a vital role in the urban cellular network, where the deployment of multiple antennas have significantly enhanced the throughput without taking extra spectrum or power resources. The massive MIMO systems "scales" up the benefits that offered by the conventional MIMO systems. Using sixty four or more antennas at the BS not only improves the spectrum efficiency significantly, but also provides additional link robustness. It is considered as a key technology in the fifth generation of mobile communication technology standards network, and the design of new algorithms for these two systems is the basis of the research in this thesis.

Firstly, at the receiver side of the conventional MIMO systems, a general framework of bit error rate (BER) approximation for the detection algorithms is proposed, which aims to support an adaptive modulation scheme. The main idea is to utilize a simplified BER approximation scheme, which is based on the union bound of the maximum-likelihood detector (MLD), whereby the bit error rate (BER) performance of the detector for the varying channel qualities can be efficiently predicted. The K-best detector is utilized in the thesis because its quasi-MLD performance and the parallel computational structure. The simulation results have clearly shown the adaptive K-best algorithm, by applying the simplified approximation method, has much reduced computational complexity while still maintaining a promising BER performance.

Secondly, in terms of the uplink channel estimation for the massive MIMO systems with the time-division-duplex operation, the performance of the Grassmannian line packing (GLP) based uplink pilot codebook design is investigated. It aims to eliminate the pilot contamination effect in order to increase the downlink achievable rate. In the case of a limited channel coherence interval, the uplink codebook design can be treated as a line packing problem in a Grassmannian manifold. The closed-form analytical expressions of downlink achievable rate for both the single-cell and multi-cell systems are proposed, which are intended for performance analysis and optimization. The numerical results validate the proposed analytical expressions and the rate gains by using the GLP-based uplink codebook design.

Finally, the study is extended to the energy efficiency (EE) of the massive MIMO system, as the reduction carbon emissions from the information and communication technology is a long-term target for the researchers. An effective framework of maximizing the EE for the massive MIMO systems is proposed in this thesis. The optimization starts from the maximization of the minimum user rate, which is aiming to increase the quality-of-service and provide a feasible constraint for the EE maximization problem. Secondly, the EE problem is a non-concave problem and can not be solved directly, so the combination of fractional programming and the successive concave approximation based algorithm are proposed to find a good suboptimal solution. It has been shown that the proposed optimization algorithm provides a significant EE improvement compared to a baseline case.

Declaration of originality

I hereby declare that the research recorded in this thesis and the thesis itself was composed and originated entirely by myself in the Department of Electronics and Electrical Engineering at The University of Edinburgh.

List your exceptions here and sign before your printed name.

Wenjun Fu

Acknowledgements

First and foremost, I would like to express my heartily profound thanks and deepest gratitude to my supervisor Professor John S. Thompson for his insightful technical and editorial advice, suggestions, and discussions. It would have been impossible to carry out this research without his continuous help both technically and personally during my time at the University of Edinburgh. His wise suggestions have always helped me and most of them have gone into the thesis. Also, I would like to thank Dr. Pan Cao. Your suggestions and helps on my Ph.D study is extremely valuable to me.

I also want to thank Dr. Khaled Benkrid for offering me this opportunity to study in this great university. I would also like to sincerely thank Dr.David I. Laurenson and Professor Tharmalingam Ratnarajah for their constructive comments and helpful discussions. I want to thank Mr. Michael J. Hunt for reading this thesis.

Secondly, the current and former colleagues who create a harmonious academic environment at the Institute for Digital Communications (IDCOM), and I can not finish this Ph.D study without their valuable helps, discussions and encouragements. I would like to thank Dr.Shendi Wang, Dr. Yichen Li, Dr. Zhe Chen, Dr. Cheng Chen, Mr. Yibo He and Mr. Kimin Kim, Miss Yuchang Wang, Dr. Nina Tadza, Mr. Yong Bao, Mr. Hancong Hu and etc..

A very special thank to Dr. Yung-chen Yuan for her encouragements within these eight years, from my first MSc degree until now.

Lastly, and most importantly, I wish to thank my parents, Mr. Taichang Fu and Mrs. Jihong Dai. I would like to express my deepest gratitude for their support and boundless love.

Contents

List of figures

List of tables

Acronyms and abbreviations

3G	The third generation of mobile communication technology standards network
4G	The fourth generation of mobile communication technology standards network
5G	The fifth generation of mobile communication technology standards network
ADC	Analog to digital converter
ANN	Artificial neural network
AWGN	Additive white Gaussian noise
AR	Augmented reality
BER	Bit error rate
BPSK	Binary phase-shift keying
BS	Base station
CDF	Cumulative distribution function
CDMA	Code division multiple access
CSI	Channel state information
DAC	Digital to analogue converter
EE	Energy efficiency
ED	Euclidean distance
FDD	Frequency-division-duplex
FDMA	Frequency division multiple access
FPGA	Field-programmable gate array
FSD	Fixed sphere decoder
GLP	Grassmannian line packing
GSM	Global System for Mobile Communications
ICT	Information and communication technology
i.i.d.	independent and identically distributed
IoT	Internet of Things
LUT	Look-up table
LR	Lattice reduction
LS	Least squares

MED	Minimum Euclidean distance
MIMO	Multiple-input multiple-output
MISO	Multiple-input single-output
MLD	Maximum likelihood detection
MMSE	Minimum mean square error
MRT	Maximum-ratio transmission
NP-hard	Non-deterministic polynomial-time hard
OFDMA	Orthogonal frequency division multiple access
OSIC	Ordered successive interference cancellation
PED	Partial Euclidean distances
PEP	Pairwise error probability
PSK	Phase-shift keying
QAM	Quadrature modulation
QoS	Quality of Service
RF	Reuse factor
SCA	Sequential concave approximation
SD	Sphere decoder
SDR	Semidefinite relaxation
SDMA	Space division multiple access
SISO	Single-input single-output
SIMO	Single-input multiple-output
SINR	Signal-to-interference-and-nosie ratio
SNR	Signal-to-noise ratio
STBC	Space-time block coding
SVD	Singular value decomposition
TDD	Time-division-duplex
TDMA	Time division multiple access
UB	Union bound
UE	User-equipment
V-BLAST	Vertical-Bell laboratories layered space-time
VLSI	Very-large-scale integration
VR	Virtual reality
ZF	Zero-forcing

Nomenclature

β	Large-scale fading coefficient
β_s	Path loss
B_c	Coherence bandwidth
B_s	Bandwidth of transmit signal
c	Speed of light
C_M	Channel capacity
C_{MIMO}	Capacity of the MIMO systems
$C_{MIMO,ergodic}$	Ergodic capacity of the MIMO systems
$C_{MIMO,EP}$	Capacity of the MIMO systems with equal transmit power
C_{MISO}	Capacity of the MISO systems
C_{SIMO}	Capacity of the SIMO systems
C_{SISO}	Capacity of the SISO systems
$C_{SISO,AWGN}$	AWGN capacity of the SISO systems
$\mathbb{C}$	Circular symmetric complex Gaussian factor
d	Distance between transmitter and receiver
d_a	Distances of the line-of-sight
d_b	Distance of reflection
d_0	Reference distance
d_{min}	The minimum Euclidean distance between transmit signal and constellation point
E_i	The allocated power of each antenna
EE	The energy efficiency of the system
E_s	Transmit power of conventional MIMO systems
f_c	Carrier frequency
$\mathcal{G}$	The Grassmannian manifold
h_c	Elements of the conventional MIMO channel matrix $\mathbf{H}_c$
$\mathbf{H}_c$	Channel matrix of conventional MIMO systems
$\mathbf{H}_{c,r}$	Real value form of channel matrix in the conventional MIMO systems
H_e	The entropy
$\mathbf{h}_k$	The channel state information to the BS

$\mathbf{I}_{M_r}$	Identity matrix
$I\left(\right)$	Mutual information
K	The number of UEs in the cell
M_n	The M_n-ary QAM constellation
M	The number of BS antennas
M_t	Number of antennas at transmitter in conventional MIMO
M_r	Number of antennas at receiver in conventional MIMO
n_c	Element of noise vector $\mathbf{s}_c$
$\mathbf{n}_c$	Additive white circularly symmetric complex Gaussian noise of the conventional MIMO
$\mathbf{n}_{c,r}$	Real value form of noise vector in the conventional MIMO systems
$\mathrm{P}_{\mathbf{s}_{\mathrm{c},i}\rightarrow\mathbf{s}'_{\mathrm{c},j}}$	Pairwise error probability
$p^d_{c,dac}$	The power consumptions of digital-analogue-converter
$p^d_{c,mix}$	The power consumptions of mixer
$p^d_{c,filt}$	The power consumptions of filter
$p^d_{c,syn}$	The power consumptions of frequency synthesizer
p^d_{bf}	The power consumptions of beamforming
P^{UL}_{max}	The maximum uplink transmit power
P^{DL}_{min}	The maximum downlink transmit power
p^d_i	The downlink transmit power
p^u_i	The uplink transmit power
P_c	The circuit power
p_t	The transmit power
P_{sum}	The total power consumption
P^U	The total power consumption of uplink transmission
P^D	The total power consumption of downlink transmission
P_{ub}	The union bound of the MLD
$\mathbf{Q}_c$	Unitary matrix from the QR decomposition
PED	Partial Euclidean distance
$P_{ub,MED}$	The union bound of the MLD with the MED events considered only
$Q(\cdot)$	The Marcum Q-function
$\mathbf{R}_c$	Upper triangular matrix from the QR decomposition
$\mathbf{R}_{\mathbf{y}_c}$	The covariance matrix

r_i	The received signal of UE i
R_i^d	The downlink rate of the UE i
$R_{ij}^{d,pr}$	The downlink rate of UE i in cell j with the pilot reuse scheme
R_{min}^D	The minimum downlink UE rate
γ_i	The downlink SINR of the UE i
RF	The reuse factor
$\mathcal{S}$	Constellation set of transmit symbols
$\hat{\mathbf{s}}_{ZF}$	Detected signal from the ZF
$\hat{\mathbf{s}}_{ML}$	Detected signal from the MLD
$\hat{s}_{c,ML}$	Detection results from the MLD
$\hat{\mathbf{s}}_{c,SD}$	Detection candidate from the SD
$\mathbf{s}_{c,r}$	Real value form of transmit signal in the conventional MIMO systems
$\mathbf{s}_c$	Transmitted vector in the conventional MIMO systems
s_c	Transmit signal element in conventional MIMO
$\mathbf{t}_k$	The MRT precoding vector
T	Coherence interval
T_c	Coherence time
T_s	Coherence bandwidth
$\mathbf{U}$	The complex unitary matrix from the SVD
$\mathbf{V}$	The complex unitary matrix from the SVD
v	Mobility speed
$\mathbf{y}$	The received vector at the BS
$\mathbf{y}_{c,r}$	Real value form of received signal in the conventional MIMO systems
$\mathbf{y}_c$	Received signal of conventional
y_c	Received bits
$\mathbf{\Sigma}$	The diagonal matrix from the SVD
$\kappa_{\mathbf{H}}$	The conditional number of channel matrix
γ_s	Path loss attenuation constant
$\mathrm{E}[\cdot]$	The expectation value
τ	The length of coherence interval
$\gamma_{ij}^{d,pr}$	The downlink SINR of the UE i in cell j with the pilot reuse scheme
ρ_{ij}	The correlation between pilot i and j

λ_i	The i-th element of eigenvalue
μ	Threshold for water-filling power allocation
$\|\|(\cdot)\|\|$	The norm of the vector
β_j^t	The threshold to distinguish cell centre and edge UE
η_{UE}	The power amplifier efficiency ratio of UE
η_{PA}	The power amplifier efficiency of the BS
η_{BS}	The power amplifier efficiency ratio of the BS
σ_{DC}	The loss factor due to DC power supply
σ_{MS}	The loss factor due to the main supply
σ_{cool}	The loss factor due to the cooling
$\mathcal{X}_s$	Randon variable follows the Gaussian distribution
σ_n^2	Variance of addictive white Gaussian noise (AWGN)
$\lambda_{\mathbf{H}_c}$	Eigenvalue of channel matrix
λ	Wavelength

Chapter 1
Introduction

This thesis will concentrate on the system design and performance analysis in both conventional multiple-input multiple-output (MIMO) and massive MIMO systems, along with the energy efficiency optimizations. The first chapter will provide an overview of the thesis, which will start in Section 1.1 with the motivation and origin of the work. It will be followed in Section 1.2 by an account of various contributions to the thesis. Finally, Section 1.3 will present an overview of the organizational content.

1.1 Motivation

The demand for data traffic in the recent decades has increased enormously because of the widespread use of smart devices. According to the report in [3], the global mobile data traffic has increased 4000 times between 2006 and 2016. By 2015, an incredible 563 million mobile connections were recorded, while mobile entertainment, such as video streaming, which requires huge amounts of data traffic, had become extremely popular. Consequently, the wireless communication industry has come to play a vital role in the fundamental operation of a society.

Moreover, the future demand for data traffic is set to grow exponentially, since the report in [3] also pointed out that the monthly traffic by year 2021 will have increased six times from its recorded 2016 level due to current and future demands from the mobile entertainment industry because of emerging innovative techniques, such as Virtual Reality (VR), Augmented Reality (AR) and the Internet of Things (IoT) [4] which are likely to be very much more widespread within the next five to ten years. Consequently, all these new applications will be based on platforms and services that will require ever faster connection speeds in order to provide more efficient coverage.

Clearly, such developmental demands on the wireless communication technology industry will need to meet the growing public demand. In order to achieve this, the fourth generation of mobile phone mobile communication technology standards networks (4G) becomes more sophisticated and by 2015 [3] they had already gone way beyond the third generation of mobile

phone mobile communication technology standards networks (3G) to such an extent that by 2021, it has been predicted that over 79% of mobile data traffic will be provided by the 4G networks. However, there is an expectation that current technology will soon be pushed to its limits; hence, with the aim of meeting such massive future demands for the IoT, enhanced broadband and critical communications [5], great efforts by both academia and the industry to research of the fifth generation of mobile phone mobile communication technology standards network (5G), therefore there is considerable optimism in both quarters regarding the prototypes that have been developed by various companies to date [6]; consequently, the standards that will be required from the 5G network by 2021 is confidently being predicted.

In terms of the 5G network, it is expected to provide the service for a massive number of devices and a wide range of applications with very high data rate, very low latency and energy-efficient network [7]. Firstly, according to the technical report in [7], the data rate is expected to reach 10Gbps for better propagation environment, such as the case of indoor or dense outdoor; the data rate is expected to reach 100Mbps in urban or suburban area and it is expected to reach 10Mbps almost everywhere. Secondly, in terms of the low latency requirement, it is required by the upcoming applications, such as smart vehicles. Thirdly, the energy-efficiency of the 5G network is required from both economic and environment perspective, where the network operator needs to concern about the operation costs and the CO_2 emissions.

The 4G multiple-input multiple-output (MIMO), which is wireless communication technology that produce those vital extra gains required for enhanced transmission [8], employed multiple antennas at both the transmitter and receiver devices. Compared with the traditional single-input single-output (SISO) systems, the deployment of multiple antennas offered extra diversity gain in order to combat wireless channel fading. Additionally, the MIMO systems offer spatial multiplexing gain whereby, if a greater number of antennas are deployed, the system capacity increases linearly without it requiring extra system bandwidth and power consumption. Due to such benefits, the MIMO technology has become an essential technology to meet wireless communication systems demands.

However, alongside the benefits from the deployment of multiple antennas, challenges also arise, especially at the receiver side since the computational complexity for detecting the transmitted signals increases exponentially with the numbers of antennas and modulation schemes. However, while some detection algorithms, such as the Maximum likelihood detector (MLD), guarantee performance, this comes at the cost of extremely high complexity [9]. On the other

hand, linear detectors - e.g. zero-forcing (ZF) or minimum mean square error (MMSE) - are straightforward to be implemented in MIMO systems, but give limited performance [10]. However, the K-best detector utilizes tree-search, which simplified the detection process and meanwhile have a promising bit error rate (BER) performance [11]. Hence, in terms of the algorithm regarding balancing the computational complexity and the BER, the K-best detector is a favourable option [12].

The combination of the K-best algorithm and adaptive modulation and coding scheme is an interesting topic, but did not attract attention from researchers. The main reason is the complexity of predicting the performance in different channel conditions. Adaptive modulation and coding is an effective scheme for improving spectrum efficiency with given a BER constraint [13]. Based on the channel condition, such schemes are selected to meet this constraint. One challenge is the difficulty of received signal-to-noise ratio (SINR) calculation for the K-best detection algorithm, which makes it difficult to predict the BER performance for the given channel condition. Additionally, because of the limited length of coherence interval, performance prediction needs to be simplified. Motivated by the superior BER performance of the K-best detector and the enhancement of spectrum efficiency in the adaptive modulation and coding scheme, this thesis will investigate the feasibility of combining these two method.

In recently years, antenna technology has been critical to the development of massive MIMO systems for use in the 5G networks [14, 15]. Unlike in the 4G MIMO systems, in the 5G networks, in order to serve tens of single antenna user equipments (UEs), a large number of antennas are intending to be deployed at the base station (BS) [16]. Consequently. the diversity and spatial multiplexing gains that offered by MIMO systems can be scaled up considerably, enabling them to achieve much higher spectrum efficiency. Moreover, because the linear detectors are able to achieve excellent performance, the problem of the design complexity at the receiver side has been greatly reduced.

However, the larger number of BS antennas has also increased pilot contamination, which is considered to be a particular performance limiting issue for the massive MIMO systems with time-division-duplex (TDD) operation, since the reduced length of the coherence intervals makes it impossible for an orthogonal pilot sequence for uplink training to be assigned to each UE [17]. As a result, the reuse of orthogonal pilot sequences becomes a common scheme for eliminating the effect of pilot contamination. Motivated by the deduction of system performance from pilot contamination, an investigation on the design of uplink pilot sequences

codebook other than pilot reuse scheme will be presented in this thesis.

Besides meeting the higher data rate and better coverage targets, the power consumption in cellular networks has attracted much pubic attention [18, 19]. Also, the reduction of CO_2 has been listed as a long-term target, not only for the cellular networks suppliers, but also for the other related information and communication technology (ICT) industries [20–22]. In accordance with the prediction in [23], the ICT industry, which was responsible for 2% of the global carbon footprint in 2007, will be responsible for its increase to 2.7% by 2021; more than 50% of the power consumption that creates this comes from BSs [24]. Consequently, motivated by reducing the power consumption while achieving high energy efficiency, this thesis will propose the establishment of an optimization based power allocation scheme.

1.2 Objectives and contributions

1.2.1 Objectives

The objective of this thesis has been to study the performance improvement of both the conventional MIMO and massive MIMO systems. On the one hand, it has set out to evaluate the performance of conventional MIMO systems with the K-best detector at receiver and adaptive modulation scheme to enhance the throughput. On the other hand, it has aimed to study the downlink achievable sum rate of multi-cell massive MIMO system with TDD operation, which utilizes the Grassmannian line packing based uplink training codebook design. This thesis has further aimed to maximize the energy efficiency of massive MIMO system by utilizing the proposed optimization framework.

1.2.2 Key contributions

The key contributions to this thesis will be:

1. The K-best detector with an adaptive modulation scheme is proposed for conventional MIMO systems. To predict the BER performance of the K-best detector in different channel conditions, a simplified BER estimation method based on the union bound (UB) of MLD is proposed. However, only the closest error events are considered in the estimation, which has significantly reduces the estimation accuracy. A look-up-table (LUT) has generated for improving the estimation accuracy with different K values.

2. Closed-form analytical expressions of downlink achievable sum rates are proposed for both single-cell and multi-cell massive MIMO systems with TDD operation. The propositions clearly demonstrate how the system performances are influenced by pilot contamination and the number of BS antennas. Furthermore, this thesis proposes a closed-form analytical expression of downlink achievable sum rate with the pilot reuse scheme has been proposed. This clearly reveals how the downlink rate is affected by the selected reuse factor. Comparisons have been made between the Grassmannian line packing based pilot codebook design and the pilot reuse scheme. If the pilot length is less than the total number of UEs, the Grassmannian line packing based pilot codebook design outperforms the pilot reuse scheme. The numerical results have validated the propositions and the gain of downlink achievable rate.

3. A general framework of energy efficiency maximization is proposed. The optimization algorithm starts with a minimum UE rate maximization, which aims to provide a feasible constraint for solving the energy efficiency problem. The combination of fractional programming and sequential concave approximation (SCA) algorithm are utilized in the proposition, where the local optimal solution can be sequentially calculated with polynomial-time complexity. The numerical results have validated the improvement of the minimum UE rate and the energy efficiency, together with the convergence of the algorithm.

1.3 The Organization of the Thesis

The remainder of this thesis will be organized as follows.

Chapter 2

The Chapter 2 will describe the general background knowledge and principles related to the thesis by, (i) presenting a review of the fading in wireless channels, (ii) describing the conventional MIMO systems, including diversity and spatial multiplexing gain, channel capacity and commonly utilized receiver-side detectors, (iii) giving a brief introduction to multi-UE MIMO systems, during which different multiple access schemes will be mentioned, (iv) describing the massive MIMO systems, and (v) introducing and comparing the TDD and frequency-division-duplex (FDD) operations.

Chapter 3

This chapter will propose the K-best detector with adaptive modulation scheme and the performance analysis by, (i) presenting a brief literature review on the development of detection algorithm and research of adaptive modulation and coding, (ii) describing the system model of the conventional MIMO systems, (iii) introducing the tree structure search, which is considered to be the key mechanism behind the K-best detector, (iv) offering a detailed explanation of the MLD union bound, (v) proposing a simplified prediction method for the adaptive modulation, and (vi) presenting numerical results that will support the various novel propositions made at the conclusion of this thesis.

Chapter 4

The Chapter 4 will focus on the multi-cell massive MIMO system with TDD operations by, (i) offering a general literature review of the related works, (ii) illustrating the system model of both single-cell and multi-cell massive MIMO, (iii) proposing of the downlink achievable sum rate analytical expressions for both single-cell and multi-cell massive MIMO systems, (iv) presenting the analytical expression of the pilot reuse scheme, and (v) by validating the analytical propositions by way of simulations.

Chapter 5

The Chapter 5 will propose a general framework of energy efficiency maximization with minimum UE rate constraint by, (i) introducing the power consumption model for both uplink and downlink transmission, (ii) formulating the energy efficiency maximization problem, (iii) providing a brief overview of the fractional programming theory and the sequential concave approximation (SCA) algorithm, and (iv) providing simulation results to proof the validity of the proposed optimization framework.

Chapter 6

This Chapter 6 will, (i) present the conclusions of the thesis, and (ii) indicate the directions for future work.

Chapter 2
Background

This chapter, which will present the necessary background knowledge about wireless communication technology essential for understanding this thesis, will be generally divided into two topics, (i) the conventional multiple-input multiple output (MIMO) systems, and (ii) the multi user equipment (UE) MIMO systems. An overview of the conventional MIMO systems starts with its basic system structure and then examines the advantages, disadvantages and the diversity of operations. It will then offer an overview of common detection algorithms. Secondly, the multi-UE MIMO systems will be introduced by way of a system model and the various multiple access schemes. Finally, the massive MIMO system will also be mentioned, together with uplink channel estimation and downlink precoding techniques.

2.1 Fading and Wireless Channels

Various factors limit system performance in wireless communication - (i) thermal noise at the receiver side, (ii) noise from the natural environment, and (iii) noise in the urban environment; these are known as *antenna noise temperatures* [25]. Because the statistical characteristic of these noises is flat in terms of power density, it follows a Gaussian distribution with zero mean and variance σ_{n}^2, otherwise known as *white Gaussian noise*. An ideal channel model for research is known as additive-white-Gaussian-noise (AWGN) channel, in which AWGN noise only exists. Also, researchers into mobile communication technology should consider other possible sources of degradation in the wireless propagation.

Two physical phenomenon - *fading* and *interference* - are the core challenges currently faced by mobile communications [26]. In previously wired communication systems, the attenuation in a wire line channel does not change rapidly over time. However, because communication in a wireless environment has dispensed with a wire line as it is based on electromagnetic spectrum. Consequently, the attenuation of a wireless channel emanates from these factors, such as large-scale fading due to path loss and shadowing, and small-scale fading due to multipath

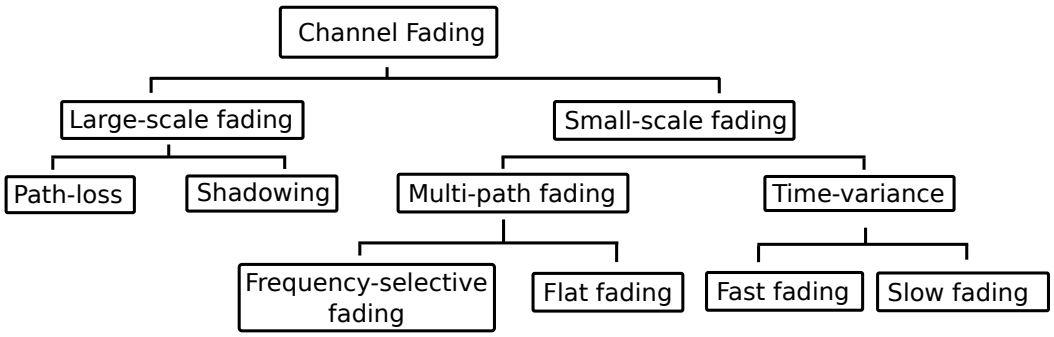

Figure 2.1: *Classification of fading in wireless channel [1]*

propagations, all of which makes the research additionally challenging. There are also different types of interference in cellular network that possibly come from either uplink or downlink transmission. Figure.2.1 shows the catalogue of fading in wireless channels [1].

Before the MIMO systems are discussed,however, fading in wireless channels will be considered.

2.1.1 Large-scale Fading

Large-scale fading describes the attenuation in signal power due to the long distance transmission, which is known as path loss, or the shadowing from big objects, such as buildings and mountains. This model is based on an average of these two influences, which has a function with distance as the variable. Power variation is slow in the large-scale fading, where it is assumed to be constant during numbers of time intervals.

A general way of modelling large-scale fading coefficient β (in dB) is the *log-normal* shadowing model, which is given as [25]

$$\beta = \beta_{\mathrm{s}}\left(d_0\right) + 10\gamma_{\mathrm{s}}\log_{10}\left(\frac{d}{d_0}\right) + \mathcal{X}_{\mathrm{s}}, \tag{2.1}$$

where β_{s} represents the path loss with unit dB, which is a function of distance d between the transmitter and receiver; d_0 is a reference distance and its value depends on the size of the cell; γ_{s} is a path loss attenuation constant, which is modelled according to different transmission environments; $\mathcal{X}_{\mathrm{s}}$ denotes the random variable which follows the Gaussian distribution, with a zero mean and variance of σ_{n}^2. The utilization of random variable $\mathcal{X}_{\mathrm{s}}$ indicates the attenuation

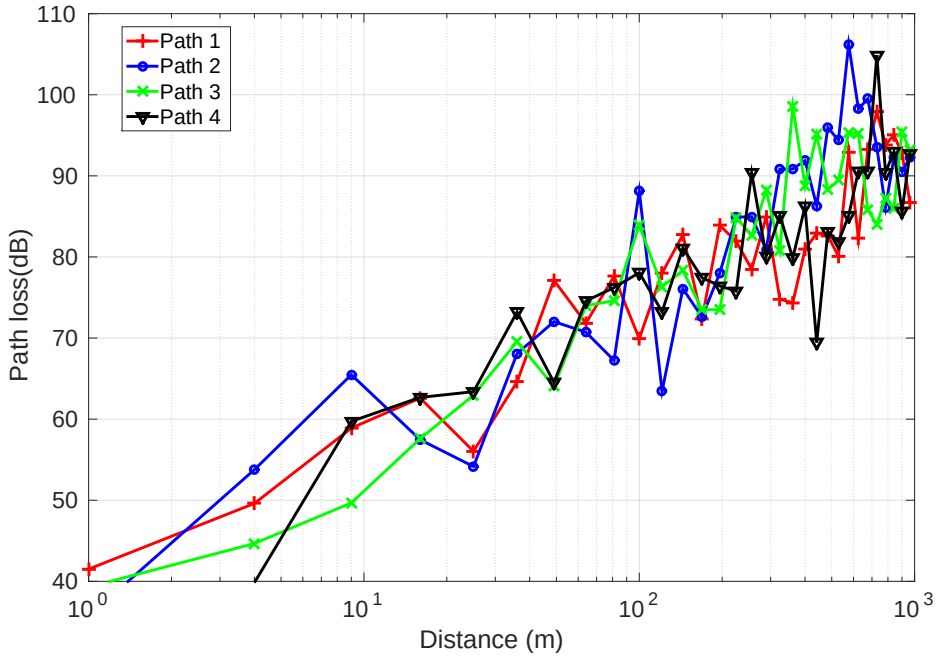

Figure 2.2: *Path loss versus distance with carrier frequency of 1.5GHz,* $d_0 = 100m$*,* $\sigma = 6dB$

caused by flat fading. Moreover, even if two receivers are at the same distance from the transmitter, their large-scale fading coefficients may not be equal because of shadowing. Large-scale fading will be utilized in the simulations included in Chapters 4 and 5.

Figure.2.2 shows the path loss of four paths calculated with equation (2.13). The carrier frequency is equal to 1.5GHz, and the four paths share the same distance where d is in a range from 1 to 1000 meters. The reference distance d_0 is equal to 100m, and σ is equal to 6dB. It can be seen that, due to the attenuation of path loss, path loss increases with the distance. Furthermore, all the values of path loss fluctuate randomly because of the random shadowing effect within each path.

2.1.2 Small-Scale Fading

Small-scale fading describes the variations in the propagation environment, where the amplitude and phase of received signals fluctuates rapidly within a limited time scale. It is different from the slow variation process in large-scale fading. One of the reasons for fluctuation is the multipath propagation environment, where transmitted signals reflects and scatters during transmission and multiple copies are received at the receiver side with distortions in amplitude

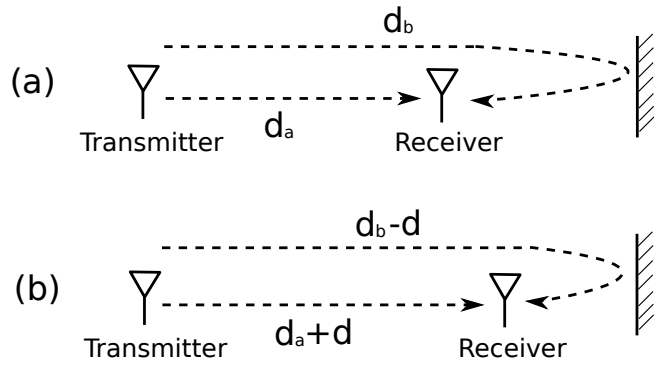

Figure 2.3: *Example of two path propagations with one transmitter and receiver*

and phase. Before the introduction of small-scale fading, a brief introduction will be given regarding the calculation of coherence time, coherence bandwidth and coherence interval.

2.1.2.1 Coherence Time, Coherence Bandwidth and Coherence Interval

- *Coherence Time*: is denoted by T_c in unit of seconds, is defined as the time period that the channel is assumed to be invariant. The explanation starts from a simple example, which is illustrated in Fig.2.3. Consider one transmitter and receiver, where both have only one antenna and there is a line-of-sight (LoS) path between them. The received signal y in Figure.2.3(a) is a combination of LoS signal that is directly transmitted plus the signal after reflection, which can be expressed as

$$y\left(t\right)=\left(e^{-i2\pi f_\mathrm{c}\frac{d_a}{c}}+e^{-i2\pi f_\mathrm{c}\frac{d_b}{c}}\right)s\left(t\right)=\left(e^{-i2\pi\frac{d_a}{\lambda}}+e^{-i2\pi\frac{d_b}{\lambda}}\right)s\left(t\right), \tag{2.2}$$

  where f_c is the carrier frequency and c denotes the speed of light. The distance d_a and d_b represents the distances of the LoS path and reflection from the transmitter to the receiver respectively. The wavelength is denoted by λ with $\lambda=\frac{c}{f_\mathrm{c}}$. If the receiver shifts to the right direction for a distance of d as shown in Fig.2.3 (b), the received signal can be expressed as

$$y\left(t\right)=\left(e^{-i2\pi\frac{d}{\lambda}}+e^{-i2\pi\frac{-d}{\lambda}}\right)s\left(t\right)=2\cos\left(2\pi\frac{d}{\lambda}\right)s\left(t\right). \tag{2.3}$$

  From equation (2.3), it can be found that the received signal will be zero if $d>\frac{\lambda}{2}$. This implies the movement distance of $\frac{\lambda}{2}$ guarantees the invariance of the channel [27]. The

coherence time T_{s} is approximated as follows with movement speed v [27],

$$T_{\mathrm{c}} = \frac{\lambda}{2v}. \tag{2.4}$$

- *Coherence Bandwidth*: is denoted by B_{c} with a unit of Hz, is defined as the interval in the frequency domain, where the magnitude of the channel frequency response stays constant. By utilizing the example in Figure.2.3 (a), if the transmitter sends signal with sinusoidal wave where $x\left(t\right) = e^{i2\pi ft}$, the channel frequency response is expressed as

$$G_h\left(f\right) = e^{-i2\pi(f_{\mathrm{c}}+f)\frac{d_a}{c}} + e^{-i2\pi(f_{\mathrm{c}}+f)\frac{d_b}{c}} = e^{-i2\pi f\frac{d_a}{c}} + e^{-i2\pi f\frac{d_b}{c}}, \tag{2.5}$$

  where the channel frequency response fluctuates with frequency f and $|G_h\left(f\right)|$ is the magnitude of the frequency response, which is given as

$$|G_h\left(f\right)| = \left|e^{-i2\pi f\frac{d_a}{c}} + e^{-i2\pi f\frac{d_b}{c}}\right| = 2\left|\cos\left(\pi f\frac{d_a - d_b}{c}\right)\right|. \tag{2.6}$$

  The coherence bandwidth is the interval between the zero value of $|G_H(f)|$, which is defined as

$$B_{\mathrm{c}} = \frac{c}{d_a - d_b}. \tag{2.7}$$

- *Coherence Interval*: T quantifies the number of samples within the period of time T_{s} seconds and the bandwidth B_{c} Hz, which is based on the Nyquist-Shannon sampling theorem, which is a part of a signal with a T_{c} seconds time period and a B_{c} Hz bandwidth that contains T samples inside, which is expressed as

$$T = T_{\mathrm{s}}B_{\mathrm{c}}. \tag{2.8}$$

2.1.2.2 Classification of Small-Scale Fading

As shown in Figure.2.1, by comparing the transmit signal and the characteristic of the channel, the small-scale fading can be classified into the following two approaches.

1. This classification is based on the multipath spread, which results in time dispersion. If the bandwidth of transmit signal is denoted by B_{s}, the channel is known as frequency-

selective fading orflat fading based on the following conditions.

$$\text{Frequency-selective fading} : B_{\text{s}} > B_{\text{c}} \tag{2.9}$$

$$\text{Flat fading} : B_{\text{s}} < B_{\text{c}}. \tag{2.10}$$

In a frequency-selective channel, the relationship of $B_{\text{s}} > B_{\text{c}}$ implies that the transmit signal has a smaller symbol time period than the delay spread of the channel. As a result, the frequency components of the transmit signal might result in inconsistent fading conditions. In a flat fading channel, the relationship of $B_{\text{s}} < B_{\text{c}}$ implies that the transmit signal has a larger symbol time than the delay spread of the channel. Consequently, the frequency components of the transmit signal experiences the same fading conditions. The flat fading channel is also known as the narrowband channel, which is because the coherence bandwidth of the transmit signal is lower than the coherence bandwidth of the channel.

2. The second classification is based on the Doppler spread, where it results in frequency dispersion. The channel, which is known either as *fast fading* or *slow fading*, is based on the following conditions.

$$\text{Fast fading} : T_{\text{s}} > T_{\text{c}} \tag{2.11}$$

$$\text{Slow fading} : T_{\text{s}} < T_{\text{c}}. \tag{2.12}$$

The fast fading channel means the channel coherence time is lower than the one of transmit signal, which suggests that the impulse response fluctuates during the time period of the transmit signal. Whereas the slow fading channel means that the channel stays constant during the time period of the transmit signal. In this thesis, the small-scale fading is based on flat, slow fading.

2.2 MIMO Systems

Because the transmitted power fluctuates rapidly due to fading in the wireless channel, the system performance, such as the BER at the receiver side, is heavily influenced. To combat fading, the MIMO technique is proposed for improving throughput and provide a reliable communication service. Compared with the single-input single-output (SISO) systems, the deployment

of multiple antennas at both the transmitter and receiver improves gains in spatial and time domains, which enhances the performance without taking up extra spectrum resource. Before the detailed introduction of MIMO systems, the following are some of the terms and their meanings that are used throughout this thesis.

- *Point-to-point MIMO systems*: has one device serving one terminal device both of which are equipped with multiple antennas.

- *Multi-user MIMO systems*: has one device with multiple antennas - such as BS - which serves multiple terminal devices with single or multiple antennas, such as the current cellular network.

- *Conventional MIMO systems*: MIMO technology is a broad catalogue describing the utilization of multiple antennas at both transmitter and receiver. The term "conventional" describes the MIMO technique in the fourth generation of mobile phone mobile communication technology standards network (4G) [28].

- *Massive MIMO systems*: has a large array of antennas utilized at BS-this could be hundreds or even thousands-serving tens or hundreds of single antenna UEs. It will play an important role in the up and coming the fifth generation of mobile phone mobile communication technology standards network (5G) [15, 29].

2.2.1 Point-to-point Conventional MIMO System Model

Consider a point-to-point conventional MIMO system with M_{t} and M_{r} antennas at both the transmitter and receiver. Note that $M_{\mathrm{r}} \geq M_{\mathrm{t}}$. The channel follows block flat fading, where the channel state information (CSI) stays constant within each communication block, and stays independent from each block to each block. The received signal $\mathbf{y}$ is represented as

$$\mathbf{y} = \mathbf{H}\mathbf{s} + \mathbf{n}, \tag{2.13}$$

also equation (2.13) can be interpreted in the following form,

$$\underbrace{\begin{bmatrix} y_1 \\ y_2 \\ \vdots \\ y_{M_\mathrm{r}} \end{bmatrix}}_{M_\mathrm{r}\times 1} = \underbrace{\begin{bmatrix} h_{11} & h_{12} & \dots & h_{1M_\mathrm{t}} \\ h_{21} & h_{22} & \dots & h_{2M_\mathrm{t}} \\ \vdots & \vdots & \vdots & \vdots \\ h_{M_\mathrm{r}1} & h_{M_\mathrm{r}2} & \dots & h_{M_\mathrm{r}M_\mathrm{t}} \end{bmatrix}}_{M_\mathrm{r}\times M_\mathrm{t}} \underbrace{\begin{bmatrix} s_1 \\ s_2 \\ \vdots \\ s_{M_\mathrm{t}} \end{bmatrix}}_{M_\mathrm{t}\times 1} + \underbrace{\begin{bmatrix} n_1 \\ n_2 \\ \vdots \\ n_{M_\mathrm{r}} \end{bmatrix}}_{M_\mathrm{r}\times 1}, \tag{2.14}$$

where $\mathbf{y} \in \mathbb{C}^{M_\mathrm{r}\times 1}$ denotes the received signal with vector element y_{M_r} representing the received term from the M_r-th antenna, where $\mathbf{s} \in \mathbb{C}^{M_\mathrm{t}\times 1}$ is the transmitted signal with the element s_{M_t} denoting the signal sent from M_t-th antenna, and $\mathbf{H} \in \mathbb{C}^{M_\mathrm{r}\times M_\mathrm{t}}$ represents the channel matrix with elements $h_{M_\mathrm{r}M_\mathrm{t}}$ representing the channel gain from the M_t-th transmitting antenna to the M_r-th receiving antenna, which is independent and identically distributed (i.i.d). Normalization is applied on the channel matrix with $\mathrm{E}\left[|h_{M_\mathrm{r}M_\mathrm{t}}|^2\right] = 1$. The variable $\mathbf{n} \in \mathbb{C}^{M_\mathrm{r}\times 1}$ is the AWGN and element n_{M_r} is a complex random variable with a zero mean and a variance of N_0, which follows a Gaussian distribution.

2.2.2 The Advantages of MIMO Systems - Diversity Gain

Compared with a SISO system, the main advantages of MIMO technology is because of the gains from diversity and spatial multiplexing [30]. Due to the randomness of the wireless channel, one path is very likely to fall into deep fade, even in the case of high SNR. However, if the same information can be transmitted through multiple paths, each of which has independent fading conditions, the transmitted information, there will be a lower chance of it falling into deep fading, or at least one copy can be sent to the receiver through a better propagation environment. This is naturally achieved by the deployment of multiple antennas and it is known as the "diversity gain", which is intended both to combat small-scale fading and improve the reliability and spectrum efficiency of systems. The diversity gain can be achieved from the various sources described as follows:

1. Time domain: the time diversity gain is achieved by transmitting the same signal repeatedly within different coherence intervals; the repetition needs to be large enough, so that each signal may have independent fading conditions.

2. Frequency domain: the frequency diversity gain is similar to time diversity, but it is

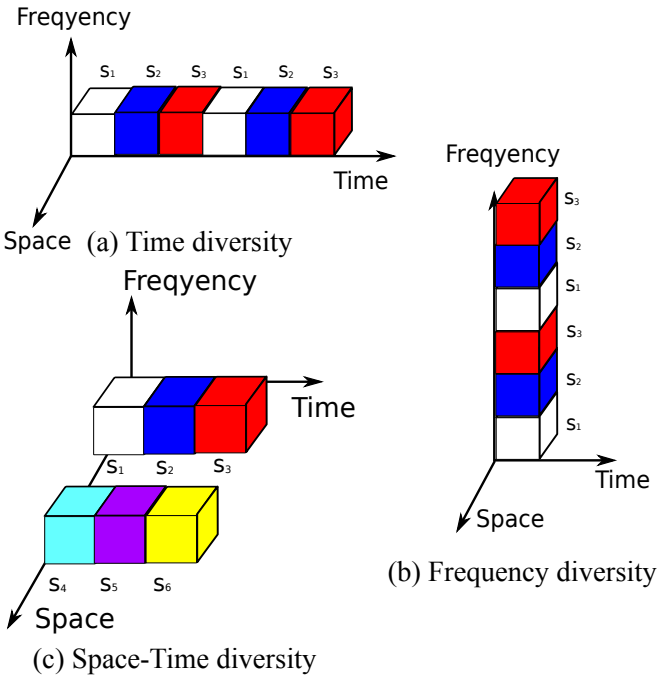

Figure 2.4: *Examples of frequency,time and space-time diversity technique in communication systems*

explored in frequency domains, where the same signal is repeatedly sent within different frequency bands.

3. Space domain: the space diversity gain is achieved by the deployment of multiple antennas at both the transmitter and receiver, assuming there is sufficient space in between antennas.

Figure.2.4 shows examples of how to achieve diversity gain in the domains described above. It is noticeable that extra time and frequency resources are required to achieve diversity gain with both of these schemes because additional time slots or frequency bands are occupied for the transmission of the repeated signals. In terms of space diversity, MIMO systems utilize the spatial domain for performance enhancement; most importantly this does not require additional time or frequency resources. In order to achieve diversity gain with high rate performance, an optimal coding scheme is also required. The Alamouti space-time block coding (STBC) is a powerful scheme designed for MIMO systems [31]. Figure.2.4 (c) illustrates the mechanism of the space-time scheme with repeated signals simultaneously transmitted through independent channels. The Alamouti STBC represents an improvement over the traditional space-time code

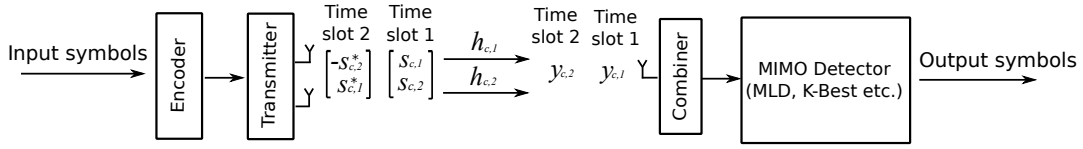

Figure 2.5: *Block diagram of MISO system with Alamouti STBC*

by introducing a simple coding scheme at the transmitter, while, at the same time, transmit and receive diversity can easily be achieved. An introduction to the Alamouti STBC scheme is given below in order to explain the diversity gain in MIMO systems.

Consider a simple example of a 2×1 multiple-input single-output (MISO) system with binary phase-shift keying (BPSK) modulation scheme. The symbol sequence to be transmitted is given as $[s_1, s_2, \cdots, s_n]$, where n complex symbols are sent within n time slots. If the repetition coding scheme is considered, the first transmit vector is expressed as $\mathbf{s}_1 = [s_1, s_1]^T$ and the second vector as $\mathbf{s}_2 = [s_2, s_2]^T$ and so on. However, in the Alamouti STBC scheme, two complex symbols are encoded as follows [26, 31]

$$\mathbf{s} = \begin{bmatrix} s_1 & -s_2^* \\ s_2 & s_1^* \end{bmatrix}, \tag{2.15}$$

where $\mathbf{s}$ denotes the encoded symbols for two time slots. During the transmission, the elements in the first column of equation (2.15) will be assigned to each antenna for transmission in the first time slot and followed by the second column. Note that $\mathbf{s}$ is a complex-orthogonal matrix. It is assumed that the channel state information remains invariant during these two time slots. The received signal of two time slots are denoted by y_1 and y_2, which is expressed as

$$y_1 = \begin{bmatrix} h_1 & h_2 \end{bmatrix} \begin{bmatrix} s_1 \\ s_2 \end{bmatrix} + n_1 \tag{2.16}$$

$$y_2 = \begin{bmatrix} h_1 & h_2 \end{bmatrix} \begin{bmatrix} -s_2^* \\ s_1^* \end{bmatrix} + n_2, \tag{2.17}$$

where h_n denotes the CSI in the n-th time slot and n_n represents the AWGN in the n-th time slot. Equation (2.16) and (2.17) can be combined and rewritten for detection in the following

form

$$\mathbf{y} = \begin{bmatrix} y_1 \\ y_2^* \end{bmatrix} = \begin{bmatrix} h_1 & h_2 \\ h_2^* & -h_1^* \end{bmatrix} \begin{bmatrix} s_1 \\ s_2 \end{bmatrix} + \begin{bmatrix} n_1 \\ n_2^* \end{bmatrix} = \mathbf{Hs} + \mathbf{n}. \tag{2.18}$$

It is assumed that the channel state information (CSI) is known at the receiver in this example, or alternatively it can be obtained by utilizing channel estimation scheme. By multiplying the Hermitian transpose of $\mathbf{H}$ at the receiver side, the received vector $\mathbf{y}$ can be separated into two individual streams, which is given as

$$\mathbf{r} = \mathbf{H}^H\mathbf{y} = \mathbf{H}^H\mathbf{Hs} + \mathbf{H}^H\mathbf{n}$$

$$r_1 = \left[|h_1|^2 + |h_2|^2\right] s_1 + h_1^* n_1 + h_2 n_2^* \tag{2.19}$$

$$r_2 = \left[|h_1|^2 + |h_2|^2\right] s_2 - h_1^* n_2^* + h_2^* n_2 \tag{2.20}$$

The detection algorithm, such as the maximum likelihood detector (MLD), can be applied in equation (2.19) and (2.20). More importantly, two symbols are transmitted in two time slots, where no additional resource - either in time or frequency - is required to double the rate compared with the repetition coding scheme. Additionally, if it is assumed that same transmit power is applied in both the Alamouti STBC and the repetition coding scheme, it has been reduced by 50%. In this MISO example, the transmission diversity gain by utilizing Alamouti STBC is 2, because each received signal in equation (2.19) and (2.20) only contains one symbol and not a combination of two. Consider the MISO system with transmit antenna equals to M_{t}, the diversity gain will increased to M_{t}. In MIMO systems, if there are M_{t} transmitting and M_{r} receive antennas with i.i.d. Rayleigh fading channel, the diversity gain will be $M_{\mathrm{t}}M_{\mathrm{r}}$.

Figure.2.6 shows the comparison of bit-error-rate (BER) performance. The following three systems are considered with BPSK modulation scheme and the MLD for detection at receiver: (i) uncoded SISO ($M_{\mathrm{t}} = M_{\mathrm{r}} = 1$), (ii) MISO ($M_{\mathrm{t}} = 2, M_{\mathrm{r}} = 1$) and (iii) MIMO ($M_{\mathrm{t}} = M_{\mathrm{r}} = 2$) with the Alamouti STBC scheme. The channel, which utilizes Rayleigh fading, has a zero mean and a unit variance. The total power constrain is the same for all three systems. It is noticeable that both the MISO and MIMO systems outperform the SISO system because of the diversity gain. By utilizing one more antenna at the receiver, the MIMO system has a better BER performance over the MISO system, which is also because of its receiving diversity gain.

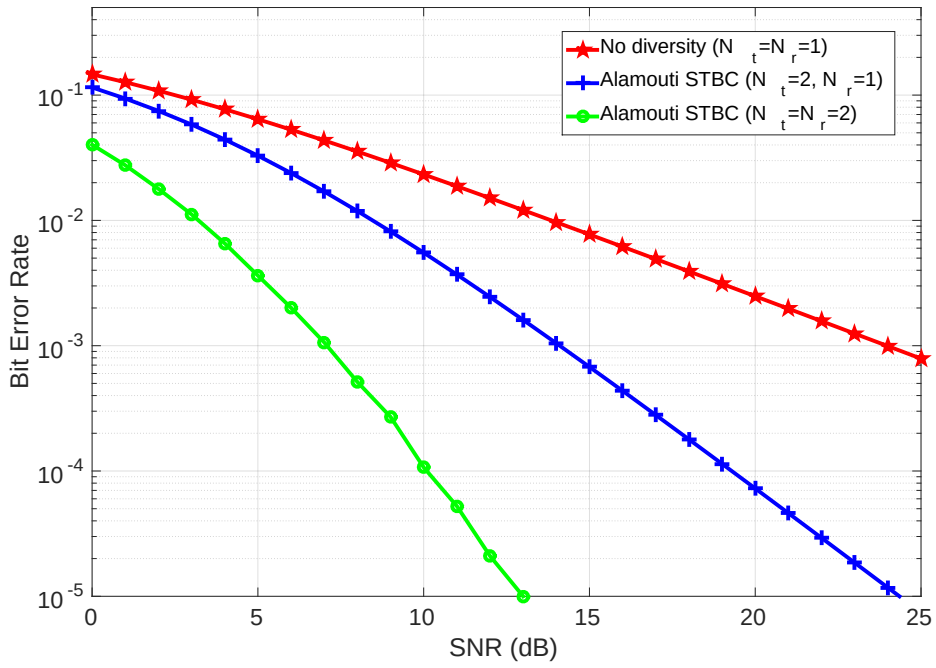

Figure 2.6: *BER performance of SISO, MISO and MIMO systems with Alamouti STBC*

2.2.3 The Advantage of MIMO Systems - Spatial Multiplexing Gain

The diversity gain in MIMO systems combat fading in channel and improve the transmission reliability. However, the fading can also provide an extra degree of freedom for the system, which comes from the multiple arrival directions at the receiver side with rich reflection and scattering in multipath propagation. If multiple independent signals are transmitted simultaneously without interleaving in between, the system throughput can be much increased without taking up extra time and frequency resources. This is known as the spatial multiplexing gain that is offered by MIMO systems.

Figure.2.7 shows a block-diagram of the vertical Bell Laboratories layered space-time (V-BLAST) architecture of MIMO systems [32]. At the transmitter side, the input data streams will firstly be divided into M_{t} independent sub-streams prior to symbol mapping; they will then be send through M_{t} transmit antennas simultaneously over same frequency band. Each receive antenna will receive all these sub-streams with different signatures of the propagation environment. The received signal will be multiplexed and if the CSI is known at the receiver, the transmit data can be jointly detected. By comparison, in the Alamouti STBC scheme, the V-LBAST offers much higher data throughput, which increases with the number of antennas

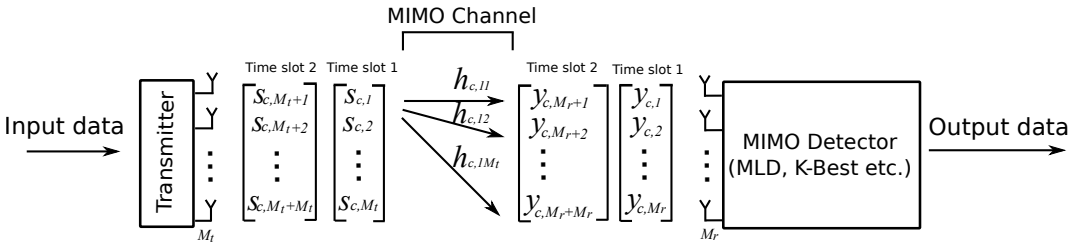

Figure 2.7: *Block diagram of MIMO systems with V-BLAST architecture*

deployed, whereby the maximum degree of freedom is $\min(M_{\mathrm{t}}, M_{\mathrm{r}})$.

MIMO systems provide both diversity gain and spatial multiplexing gain, but with a trade-off in between. Consequently, it is difficult to achieve the theoretical maximum reliability and data throughput that the MIMO architecture offers at the same time.

The capacity of MIMO system will be introduced in the following section.

2.2.4 The Capacity of MIMO Systems

The previous section demonstrated that MIMO systems offer diversity gains and spatial multiplexing gains for performance improvements in fading combat and data throughput, with the ideal values of both gains can be achieved being $M_{\mathrm{t}}M_{\mathrm{r}}$ and $\min(M_{\mathrm{t}}, M_{\mathrm{r}})$. Capacity is enhanced by transmitting data over multiple independent channels in a rich scattering environment. In the following section, the enhanced capacity of MIMO systems over SISO will be discussed.

2.2.4.1 Capacity of MIMO Systems with a Deterministic Channel

The analysis of the capacity of MIMO systems can be divided into two approaches, (i)deterministic channel, and (ii) random channel. The system model utilized in the following section is based on the equation (2.13), where the channel matrix $\mathbf{H}$ is assumed to be deterministic. The channel capacity is defined as the maximum mutual information between transmit signal $\mathbf{s}$ and received signal $\mathbf{y}$, which is expressed as [1, 25]

$$C_M = \max_{f(\mathbf{s})} \quad I(\mathbf{s}; \mathbf{y}), \tag{2.21}$$

where $f(\mathbf{s})$ is the probability density function (PDF) of transmit random signal $\mathbf{s}$, $I(\mathbf{s};\mathbf{y})$ denotes the mutual information of both $\mathbf{s}$ and $\mathbf{y}$, and it is given as

$$I(\mathbf{s};\mathbf{y}) = H_e(\mathbf{y}) - H_e(\mathbf{y}|\mathbf{s}), \tag{2.22}$$

where $H_e(\mathbf{y})$ represents the entropy of $\mathbf{y}$ and $H_e(\mathbf{y}|\mathbf{s})$ denotes the conditional entropy of $\mathbf{y}$ with given $\mathbf{s}$. As $\mathbf{n}$ and $\mathbf{s}$ are two independent random vectors, the conditional entropy can be transformed as $H_e(\mathbf{y}|\mathbf{s}) = H_e(\mathbf{n})$. And consequently the mutual information is equivalent to

$$I(\mathbf{s};\mathbf{y}) = H_e(\mathbf{y}) - H_e(\mathbf{n}). \tag{2.23}$$

As the entropy of noise term is a constant, therefore the maximization of channel capacity comes from maximizing the entropy of receive signal $\mathbf{y}$.

SISO channel capacity

Consider a SISO system with limited transmit power, where $\mathrm{E}\left[|\mathbf{s}|^2 \leq E_\mathrm{s}\right]$ and E_s denotes the transmit power. In this case, both the transmit and receive signal and channel plus noise is transferred from matrix into scalers if utilizing equation (2.13). If only the AWGN channel is considered, both transmit and receive signal needs to follow Gaussian distribution to reach the maximum capacity with transmit signal $s \sim \mathcal{CN}(0, E_\mathrm{s})$ and receive signal $y \sim \mathcal{CN}\left(0, E_\mathrm{s} + \sigma_\mathrm{n}^2\right)$, where σ_n^2 denotes the noise variance. As a result, the entropy $H_e(n)$ equals to $\log_2\left(\pi e \sigma_\mathrm{n}^2\right)$ and $H_e(y)$ equals to $\log_2\left(\pi e\left(E_\mathrm{s} + \sigma_\mathrm{n}^2\right)\right)$. The AWGN channel capacity of SISO system is expressed as [25, 26]

$$C_{\text{SISO,AWGN}} = \log_2\left(1 + \frac{E_\mathrm{s}}{\sigma_\mathrm{n}^2}\right) \text{(bit/s/Hz)}, \tag{2.24}$$

where $\frac{E_\mathrm{s}}{\sigma_\mathrm{n}^2}$ is the SNR of SISO systems. In a more general case, the receive signal will also be affected by the randomness from channel if Rayleigh flat fading is considered rather than the AWGN case. The entropy $H_\mathrm{e}(y_\mathrm{c})$ becomes $\log_2\left(\pi e\left(|h|^2 E_\mathrm{s} + \sigma_\mathrm{n}^2\right)\right)$ and the corresponding capacity of SISO systems is expressed as

$$C_{\text{SISO}} = \log_2\left(1 + \frac{E_\mathrm{s}}{\sigma_\mathrm{n}^2}|h|^2\right) \text{(bit/s/Hz)}. \tag{2.25}$$

SIMO channel capacity

Consider a single-input multiple-output (SIMO) system with one transmit and M_r receive an-

tennas. Now both the receive signal and channel plus noise are in the form of vector if utilizing equation (2.13), with $\mathbf{H} = [h_1, h_2, \cdots, h_{\mathrm{r}}]^T$. The transmit signal is a scaler now. The entropy $H_{\mathrm{e}}(\mathbf{y})$ becomes $\log_2\left(\pi e\left(\sum_{i=1}^{M_{\mathrm{r}}}|h_i|^2 E_{\mathrm{s}} + \sigma_{\mathrm{n}}^2\right)\right)$ and the corresponding capacity of SIMO systems is expressed as [1, 26]

$$C_{\text{SIMO}} = \log_2\left(1 + \frac{E_{\mathrm{s}}}{\sigma_{\mathrm{n}}^2}\sum_{i=1}^{M_{\mathrm{r}}}|h_i|^2\right)\text{(bit/s/Hz)}\,. \tag{2.26}$$

It can be observed from equation (2.26) that the channel capacity is logarithmic increase with the number of receive antenna M_{r} with the spatial multiplexing gain of M_{r}.

MISO channel capacity

Consider a MISO system with M_{t} transmit antenna and one receive antenna. Now the transmit signal and channel are in the form of vector, which are expressed as $\mathbf{s} = [s_1, s_2, \cdots, s_{M_{\mathrm{t}}}]^T$ and $\mathbf{H} = [h_1, h_2, \cdots, h_{M_{\mathrm{t}}}]$. The receive signal and noise are both scalers. If each transmit antenna has the same power with the total constrain as E_{s}, the entropy $H_{\mathrm{e}}(y)$ becomes $\log_2\left(\pi e\left(\sum_{i=1}^{M_{\mathrm{t}}}|h_i|^2\frac{E_{\mathrm{s}}}{M_{\mathrm{t}}} + \sigma_{\mathrm{n}}^2\right)\right)$ and the corresponding capacity of MISO systems is expressed as [33]

$$C_{\text{MISO}} = \log_2\left(1 + \frac{E_{\mathrm{s}}}{M_{\mathrm{t}}\sigma_{\mathrm{n}}^2}\sum_{i=1}^{M_{\mathrm{t}}}|h_i|^2\right)\text{(bit/s/Hz)}\,. \tag{2.27}$$

From equation (2.27), it can be found that the MISO channel capacity is logarithmically increase with the number of transmit antenna M_{t} with the spatial multiplexing gain of M_{t}.

MIMO channel capacity

Consider a MIMO system with M_{t} transmit and M_{r} receive antennas. The covariance matrix of receive signal $\mathbf{y}$ is interpreted as

$$\begin{aligned}\mathbf{R}_{\mathbf{y}} = \mathrm{E}\{\mathbf{y}\mathbf{y}^H\} &= \mathrm{E}\left\{\frac{E_{\mathrm{s}}}{M_{\mathrm{t}}}\mathbf{H}\mathbf{s}\mathbf{s}^H\mathbf{H}^H + \mathbf{n}\mathbf{n}^H\right\}\\ &= \frac{E_{\mathrm{s}}}{M_{\mathrm{t}}}\mathbf{H}\mathrm{E}\left\{\mathbf{s}\mathbf{s}^H\right\}\mathbf{H}^H + \mathrm{E}\left\{\mathbf{n}\mathbf{n}^H\right\}\\ &= \frac{E_{\mathrm{s}}}{M_{\mathrm{t}}}\mathbf{H}\mathbf{R}_{\mathbf{s}}\mathbf{H}^H + \sigma_{\mathrm{n}}^2\mathbf{I}_{M_{\mathrm{r}}},\end{aligned} \tag{2.28}$$

where $\mathbf{I}$ is an $M_{\mathrm{r}} \times M_{\mathrm{r}}$ identity matrix. Both the entropy $H_{\mathrm{e}}(\mathbf{y})$ and $H_{\mathrm{e}}(\mathbf{n})$ can be expressed

as

$$H_{\mathrm{e}}\left(\mathbf{y}\right)=\log_2\left[\det\left(\pi e\mathbf{R}_{\mathbf{y}}\right)\right]=\log_2\left[\det\left(\pi e\left(\frac{E_{\mathrm{s}}}{M_{\mathrm{t}}}\mathbf{H}\mathbf{R}_{\mathbf{s}}\mathbf{H}^{H}+\sigma_{\mathrm{n}}^{2}\mathbf{I}_{M_{\mathrm{r}}}\right)\right)\right] \tag{2.29}$$

$$H_{\mathrm{e}}\left(\mathbf{n}\right)=\log_2\left[\det\left(\pi e\mathbf{R}_{\mathbf{n}}\right)\right]=\log_2\left[\det\left(\pi e\sigma_{\mathrm{n}}^{2}\mathbf{I}_{M_{\mathrm{r}}}\right)\right]. \tag{2.30}$$

Consequently, the channel capacity of MIMO systems is expressed as

$$\begin{aligned}C_{\text{MIMO}}&=\log_2\left[\det\left(\pi e\left(\frac{E_{\mathrm{s}}}{M_{\mathrm{t}}}\mathbf{H}\mathbf{R}_{\mathbf{s}}\mathbf{H}^{H}+\sigma_{\mathrm{n}}^{2}\mathbf{I}_{M_{\mathrm{r}}}\right)\right)\right]-\log_2\left[\det\left(\pi e\sigma_{\mathrm{n}}^{2}\mathbf{I}_{M_{\mathrm{r}}}\right)\right]\\&=\log_2\left[\det\left(\mathbf{I}_{M_{\mathrm{r}}}+\frac{E_{\mathrm{s}}}{M_{\mathrm{t}}\sigma_{\mathrm{n}}^{2}}\mathbf{H}\mathbf{R}_{\mathbf{s}}\mathbf{H}^{H}\right)\right]\text{(bit/s/Hz)}.\end{aligned} \tag{2.31}$$

2.2.5 Capacity of MIMO Systems With CSI Not Known at the Transmitter

In the case of CSI not known at the transmitter side, the transmit power can be equally allocated. As a result, with M_{t} transmit antennas, the autocorrelation matrix $\mathbf{R}_{\mathbf{s}}$ in equation (2.31) becomes a identity matrix $\mathbf{I}_{M_{\mathrm{t}}}$, which is expressed as [34]

$$C_{\text{MIMO,EP}}=\log_2\left[\det\left(\mathbf{I}_{M_{\mathrm{r}}}+\frac{E_{\mathrm{s}}}{M_{\mathrm{t}}\sigma_{\mathrm{n}}^{2}}\mathbf{H}\mathbf{H}^{H}\right)\right]. \tag{2.32}$$

If $\mathbf{H}\mathbf{H}^{H}$ has the SVD decomposition as $\mathbf{H}\mathbf{H}^{H}=\mathbf{U}\sum\mathbf{V}^{H}$, equation (2.32) can be simplified as

$$\begin{aligned}C_{\text{MIMO,EP}}&=\log_2\left[\det\left(\mathbf{I}_{M_{\mathrm{r}}}+\frac{E_{\mathrm{s}}}{M_{\mathrm{t}}\sigma_{\mathrm{n}}^{2}}\mathbf{U}\sum\mathbf{V}^{H}\right)\right]\\&=\sum_{i=1}^{\min(M_{\mathrm{t}},M_{\mathrm{r}})}\log_2\left(1+\frac{E_{\mathrm{s}}}{M_{\mathrm{t}}\sigma_{\mathrm{n}}^{2}}\lambda_{\mathbf{H}}^{2}\right),\end{aligned} \tag{2.33}$$

where $\lambda_{\mathbf{H}}$ denotes the eigenvalue of $\mathbf{H}\mathbf{H}^{H}$. Equation (2.33) indicates that the channel capacity of $M_{\mathrm{t}}\times M_{\mathrm{r}}$ MIMO can be seen as a combination of $\min\left(M_{\mathrm{t}},M_{\mathrm{r}}\right)$ SISO channel with equal power allocation.

2.2.5.1 Capacity of MIMO Systems with CSI Known at the Transmitter

At the transmitter side of MIMO systems, the CSI can be available from different techniques, such as feedback (FDD) or channel reciprocity (TDD). The transmit power can be adaptively allocated based on the channel quality, which is known as water-filling power allocation algo-

rithm and it is considered as an useful technique for improving system capacity [34].

The optimal achievable capacity with power allocation can be formulated as follows

$$\max_{E_i} \sum_{i=1}^{\min(M_\mathrm{t},M_\mathrm{r})} \log_2\left(1+\frac{E_i}{\sigma_\mathrm{n}^2}\lambda_i\right) \tag{2.34a}$$

$$\text{Subject to} \quad \sum_{i=1}^{M_\mathrm{t}} \leq E_\mathrm{s} \tag{2.34b}$$

$$E_i \geq 0 \tag{2.34c}$$

where E_i denotes the allocated power of each antenna. The solution of this problem can be achieved by water-filling power allocation algorithm, where the optimal power E_i should meet the following constrain

$$\left(\frac{\sigma_\mathrm{n}^2}{\lambda_i^2}+E_i\right)=\mu, \quad \forall\, i \tag{2.35}$$

where μ denotes the chosen threshold for water-filling power allocation algorithm. From equation (2.35), the optimal power for each antenna E_i is expressed as

$$E_i^* = \left(\mu-\frac{\sigma_\mathrm{n}^2}{\lambda_i}\right)^+, \tag{2.36}$$

where "+" represents the positive term only. As a result, the capacity with CSI at the transmitter is given as

$$C_{\text{MIMO,WF}} = \sum_{i=1}^{M_\mathrm{t}} \log_2\left(1+\frac{E_i^*}{\sigma_\mathrm{n}^2}\lambda_i\right). \tag{2.37}$$

2.2.5.2 Capacity of MIMO Systems with Random Channels

The capacity introduced previously is based on a deterministic channel model. However, random channel, which changes as a function of time, is a more realistic model and $\mathbf{H}$ is considered to be a random matrix. The capacity will also be random by the utilization of random channel in calculation.

Ergodic capacity of MIMO systems

Consider a MIMO system with an ergodic flat fading channel, where the channel stays independent between each time period and constant within each period. If there are *N* time periods,

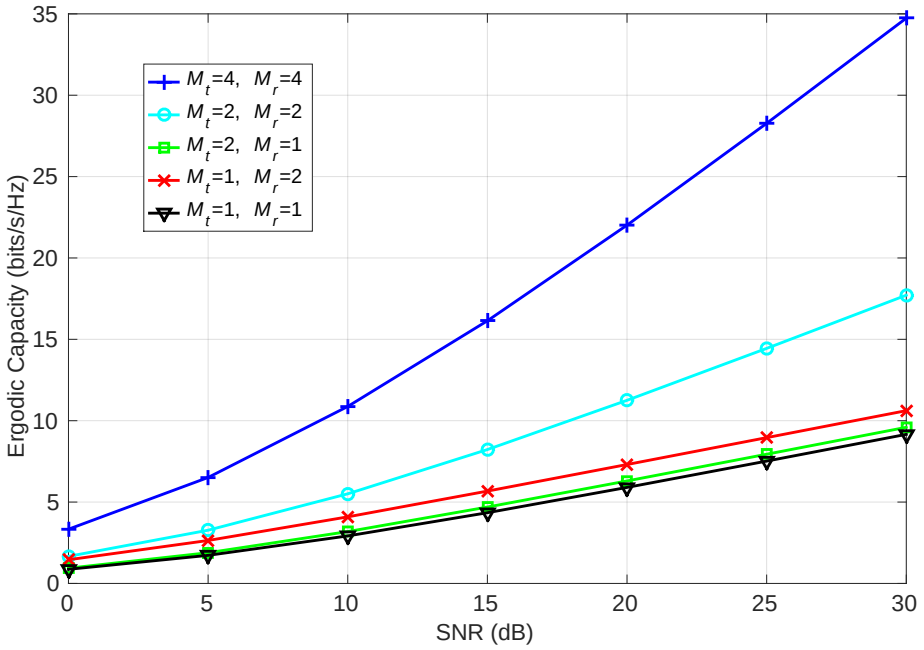

Figure 2.8: *Ergodic capacity of different MIMO configurations*

the capacity of MIMO systems will be the average performance, which is expressed as

$$C_{\text{MIMO}} = \frac{1}{N}\sum_{n=1}^{N}\log_2\left(\mathbf{I}_{M_\text{r}} + \frac{E_\text{s}}{M_\text{t}\sigma_\text{n}^2}\mathbf{H}\left[n\right]\mathbf{R}_\text{s}\mathbf{H}^H\left[n\right]\right)\text{(bit/s/Hz)}\,. \tag{2.38}$$

The ergodic capacity is the expectation of equation (2.31) in the case of $N \to \infty$, which is presented as

$$C_{\text{MIMO,ergodic}} = \text{E}\left[\sum_{n=1}^{N}\log_2\left(\mathbf{I}_{M_\text{r}} + \frac{E_\text{s}}{M_\text{t}\sigma_\text{n}^2}\mathbf{H}\mathbf{R}_\text{s}\mathbf{H}^H\right)\text{(bit/s/Hz)}\right]. \tag{2.39}$$

Fig.2.8 shows the simulation results of ergodic capacity over SNR, which includes SISO, SIMO, MISO and MIMO systems. Firstly, it can be observed that all the capacity results increase linearly regarding to the SNR. Secondly, the capacity of MIMO with $M_\text{t} = M_\text{r} = 4$ is almost triple over the SISO case when SNR is 15dB. Even in the case of low SNR, the MIMO system still outperforms the SISO system. Thirdly, the SIMO performs better than MISO because of the power gain, which is scaled with M_r. To be more specific, the multiple antennas deployed at the receiver in SIMO system is able to coherently combine the received signal, which results to a power boost.

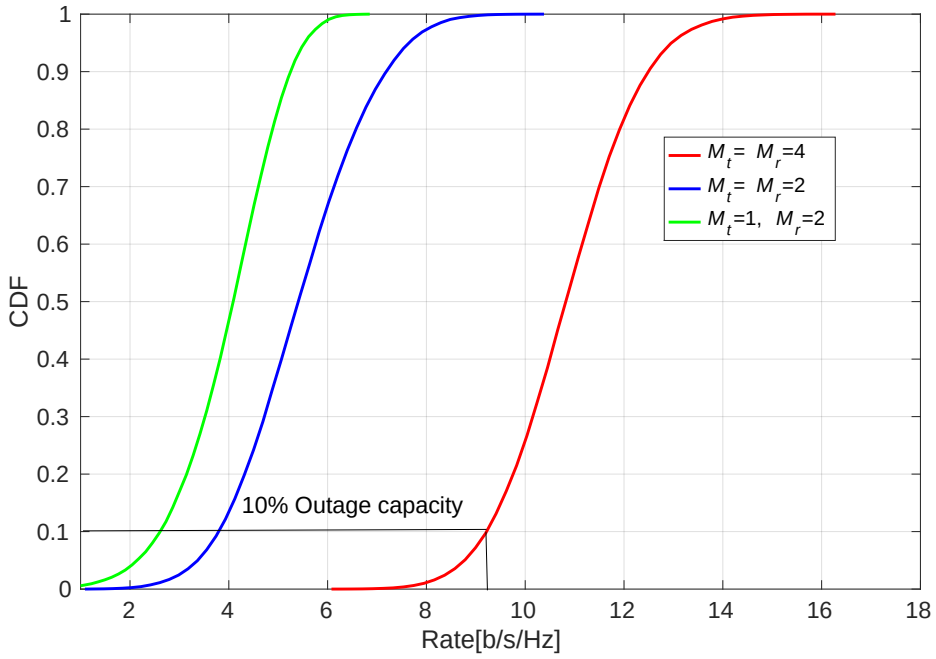

Figure 2.9: *Outage capacity of different MIMO configurations*

Outage capacity of MIMO systems

The $q\%$-outage capacity, $C_{\text{MIMO,outage}}$, is defined as the maximum possible capacity for $(100-q)\%$ channel samples [33]. Fig.2.9 shows the cumulative density function (CDF) of capacity with $SNR = 10$dB. The 10 % outage capacity of different number of antennas are highlighted in the figure. Again, MIMO system is outperformed over SISO system with improvement about 50% in the case of $M_{\text{t}} = M_{\text{r}} = 2$ and 260 % in the case of $M_{\text{t}} = M_{\text{r}} = 4$.

2.2.6 MIMO Detection Algorithms

The MIMO detection algorithm is the signal processing technique which is applied to detect the transmitted signals at the receiver side. To be more specific, at the transmitter side, M_{t} independent data streams will be modulated and transmitted by the M_{t} antennas. At the receiver side of system, M_{r} antennas receive signals that contains CSI and thermal noise. As a result, detection algorithm is applied to jointly detect the signal.

2.2.6.1 Maximum likelihood detection

The MLD adopts an exhaustive search approach for signal detection [35]. A search will be conducted over all the possible combinations of candidate symbols. The detection, which calculates the Euclidean distance between received noisy signals and all the possible candidate vectors, is formulated as:

$$\hat{\mathbf{s}}_{\mathrm{ML}} = \arg\min_{\mathbf{s}\in\mathcal{S}} \|\mathbf{y} - \mathbf{H}\mathbf{s}\|^2 \tag{2.40}$$

where $\mathcal{S}$ denotes the constellation set of transmit symbols and the $\|(\cdot)\|$ denotes the norm of the vector. The optimal detection resulting from the MLD will be the vector with minimum Euclidean distance, which indicates the smallest error probability. Due to the exhaustive search, the optimal detection result also leads to the optimal BER performance. However, there is a trade-off between the optimal detection performance and the computational complexity, since the computational complexity will increase exponentially with the number of antennas in the MIMO system and the modulation constellation. For example, if the MLD is used on a 16×16 MIMO system with 256-QAM, the detection of one symbol vector involves a search of over 256^{16} lattice points, which limits the practical use of the MLD.

2.2.6.2 Linear detection

Linear detection algorithms are proposed in order to reduce the computational complexity of the MLD to compensate for detection performance [36]. The basic idea behind the algorithm is to invert the action of the channel matrix $\mathbf{H}$ in the received signal by applying a matrix filter, the main purpose of which is to obtain the desired signal by filtering out the channel information and noise. One approach to a linear detection algorithm is called zero forcing (ZF). It utilizes the pseudo inverse of the channel matrix which is $\mathbf{H}^{\dagger} = \left(\mathbf{H}^H\mathbf{H}\right)^{-1}\mathbf{H}^H$. By applying on the received signal, the estimated detection result is given as [36]

$$\hat{\mathbf{s}}_{\mathrm{ZF}} = \mathbf{H}^{\dagger}\mathbf{y} = \mathbf{s} + \mathbf{H}^{\dagger}\mathbf{n} \tag{2.41}$$

From the above equation, it can be observed that the noise effect, $\mathbf{H}^{\dagger}\mathbf{n}$, will be enhanced in the detected result. However, this degrades the detection accuracy and leads to a sub-optimal detection result. To reduce the noise effect, a minimum mean square error (MMSE) criterion is proposed. The MMSE receiver adds the power of noise in the pseudo inverse calculation so that after the multiplication, both the effect of channel and noise can be filtered. The MMSE

receiver can be written as [36]

$$\mathbf{W}_{\text{MMSE}} = (\mathbf{H}^H\mathbf{H} + N_0\mathbf{I}_{M_\text{t}})^{-1}\mathbf{H}^H \tag{2.42}$$

where N_0 and $\mathbf{I}_{M_\text{t}}$ denote noise power and identity matrix with the size of M_t respectively. Note that the initial results calculated from the linear detection algorithms are not the constellation points from set $\mathcal{S}$, therefore, the detection results will be rounded to the closest constellation points.

2.2.6.3 Ordered successive interference cancellation detection

The ordered successive interference cancellation (OSIC), which is known as Vertical Bell Laboratories Layered Space-Time (V-BLAST) receiver [37], is developed which further reduces the interference between transmitted signals. To compare it with the linear detectors, the V-BLAST detector applies a non-linear detection algorithm and it splits the detection into stages. Each substream of the received signal is detected individually while the other substreams are treated as "interference". The detection of each substream can utilize either the ZF or the MMSE algorithm as the nulling vector. After the detection of one substream, the interference cancellation is achieved by subtracting the detected vector from the original received signal. One important issue is that the detection performance is significantly influenced by the cancellation order, which is based on the post-detection SNR of each vector stream. The optimal cancellation order always starts the detection of the vector with the post-detection SNR in a descending order. The detection has M_i iterations with $i = 1, 2, \cdots, M_\text{t}$. The detection process is summarized as follows:

- *Ordering step*: the detection order defines the sequence of detecting individual signals from the received signal vector. It is based on the Euclidian norm value for each row of the channel matrix. We will rank the Euclidian norm value and detection order starting from row with the minimum value which represents the maximum SNR.

$$k = \arg\min_j \| \left(\mathbf{H}_i^\dagger\right)_j \|^2 \tag{2.43}$$

  where $\left(\mathbf{H}_i^\dagger\right)_j$ represents the j-th row of the pseudoinverse of $\mathbf{H}_i$. Please note that the j-th row can only be selected from the signals that have not been detected yet.

- *Nulling step*: after defining the detection order,the kth row of $(\mathbf{H}^{\dagger})$ is chosen as the nulling vector $\mathbf{w}_k$ to null out the weaker transmitted signals for purpose of reducing interference which can be expressed as:

$$\hat{\mathbf{s}}_{k,i} = \mathbf{w}_k^T \mathbf{y}_i \tag{2.44}$$

- *Slicing step*: we need to slice the signal obtained from the nulling step to the nearest constellation point $\tilde{\mathbf{s}}_{k,i}$, in order to recover the transmitted data.

- *Cancellation step*: in this step, we need to remove the detected signal from the received vector using the result of the slicing step. The purpose of this cancellation is to reduce the interference caused by this signal. ...

$$\mathbf{y}_{i+1} = \mathbf{y}_i - \tilde{\mathbf{s}}_{k,i}(\mathbf{H})^k \tag{2.45}$$

  where $(\mathbf{H})^k$ represents the kth row of $\mathbf{H}$. The nulling the k-th column of $\mathbf{H}_i$ results the channel matrix $\mathbf{H}_{i+1}$ for the following iteration.

The V-BLAST algorithm will repeat these steps until all the transmitted signals are detected. Both ZF and MMSE detectors can be applied in the V-BLAST detector for the single stream detection. Also the application of MMSE detector can further reduce the noise effect.

Figure.2.10 shows the uncoded BER performance of the five detection algorithms. The simulation considers a 16-QAM 4×4 MIMO systems. The top two curves are linear detectors. We can find that MMSE has better performance than ZF. It can be seen that at BER of 10^{-2}, the performance gap between these two linear detectors is 2dB. However, linear detectors have the worst performance among these five algorithms. V-BLAST has better BER performance over linear detectors. It can be seen V-BLAST-ZF has 3dB gains over MMSE at BER of 10^{-2}. As mentioned before, V-BLAST-MMSE has slightly better performance than V-BLAST-ZF which is 2dB at BER of 10^{-2}. Finally, it is noticeable that the MLD has the best performance of the group.

This section focused on the point-to-point MIMO systems, where one device is designed to serve another device and where both are equipped with multiple antennas to create a single-UE MIMO system and where BS serves on UE with multiple antennas. The following section will describe another type of MIMO system-the multi-UE MIMO system-which is like the cellular

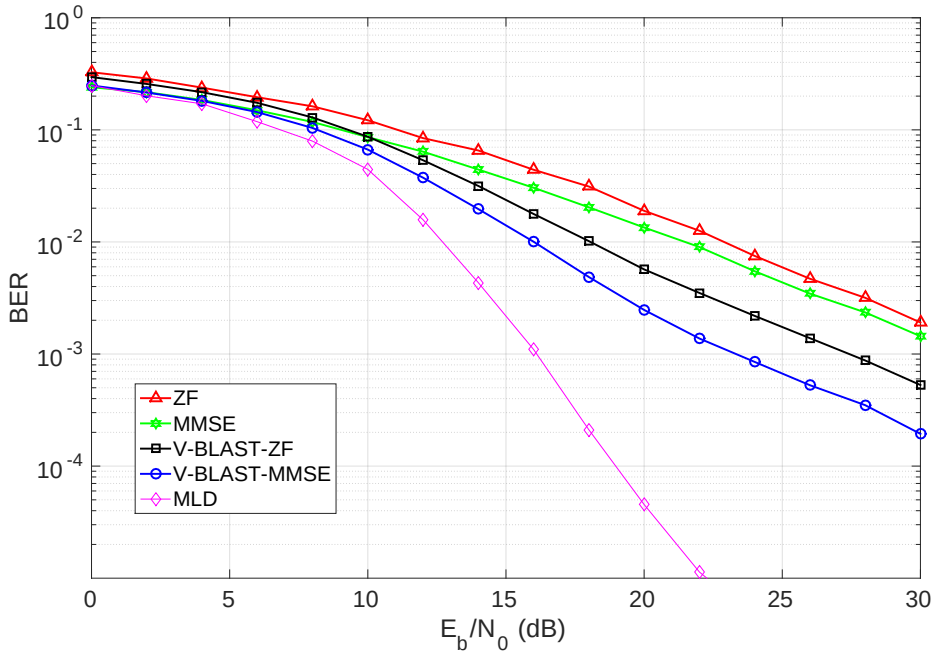

Figure 2.10: *BER of* 4×4 *MIMO system with 16-QAM and different detection algorithms*

network, where one BS serves multiple single antenna UEs with the same time and frequency resource, and where, if there are M antennas at the BS serving K single-antenna UEs are in a single hexagon shaped cell, they will form a $M \times K$ multi-UE MIMO system.

2.2.6.4 Semidefinite Relaxation Programming Based Detection

Although the MLD achieves the optimal detection performance, the computational complexity increases exponentially with the modulation order and the number of antennas. To simplified the complexity, an alternative approach of detection in MIMO systems is to convert the MLD into a optimization problem and utilize semidefinite relaxation (SDR) programming to solve it, which is known as the SDR-based detection [38, 39].

Different from the exhaustive search that utilized in the MLD, the SDR-based detection reformulates the original MLD detection problem and the near-MLD result can be found with polynomial worst-case complexity. To be more specific, consider BPSK modulation scheme,

Equation (2.40) can be reformulated into a minimization problem as [40]

$$\underset{\mathbf{s}}{\text{minimize}} \quad \text{tr}\left(\mathbf{Q}_{\text{SDR}}\mathbf{X}_{\text{SDR}}\right) \tag{2.46a}$$

$$\text{subject to} \quad \mathbf{X}_{\text{SDR}} = \mathbf{x}_{\text{SDR}}\mathbf{x}_{\text{SDR}}^{H} \tag{2.46b}$$

$$\mathbf{x}_{\text{SDR}} \in \mathcal{S}_{\text{BPSK}}, \tag{2.46c}$$

where $\mathbf{Q}_{\text{SDR}}$ and $\mathbf{X}_{\text{SDR}}$ are defined as

$$\mathbf{Q}_{\text{SDR}} = \begin{bmatrix} \mathbf{H}^{H}\mathbf{H} & -\mathbf{H}^{H}\mathbf{y} \\ -\mathbf{y}^{H}\mathbf{H} & \|\mathbf{y}\|^{2} \end{bmatrix}, \quad \mathbf{X}_{\text{SDR}} = \begin{bmatrix} \mathbf{s} \\ 1 \end{bmatrix}. \tag{2.47}$$

Consider $\text{diag}\left(\mathbf{X}_{\text{SDR}}\right)$ is defined as a vector with elements from the diagonal entries of $\mathbf{X}_{\text{SDR}}$ and $\mathbf{e}_{\text{SDR}}$ is defined as a vector with all the elements equal to one. Additionally, it is defined that $\mathbf{X}_{\text{SDR}} \succeq 0$ represents the matrix $\mathbf{X}_{\text{SDR}}$ is positive semidefinite. In the SDR-based detection, Constraint (2.46b) and (2.46c) can be replaced and it becomes a typical semidefinite programming problem, which is expressed as

$$\underset{\mathbf{s}}{\text{minimize}} \quad \text{tr}\left(\mathbf{Q}_{\text{SDR}}\mathbf{X}_{\text{SDR}}\right) \tag{2.48a}$$

$$\text{subject to} \quad \text{diag}\left(\mathbf{X}_{\text{SDR}}\right) = \mathbf{e}_{\text{SDR}} \tag{2.48b}$$

$$\mathbf{X}_{\text{SDR}} \succeq 0. \tag{2.48c}$$

Problem (2.48a) can be solved iteratively by utilizing common optimization algorithms and the detection result $\mathbf{s}$ can be found by adopting various methods, such as rounding quantizations [41]. The SDR-based detection achieves quasi-MLD BER with reduced complexity, however, the performance still needs to be improved when detecting the symbol with high order modulation scheme [9].

2.3 Multi-UE MIMO and Massive MIMO Systems

The following section will describe the multi-UE MIMO systems and explain its basic structure and the advantages it offers. It will also introduce the massive MIMO systems-a novel communication technology that has attracted great interests from both academia and industries-which, although it belongs to multi-UE MIMO system, because the number of BS antennas has been greatly increased, it has brought about many exciting innovations.

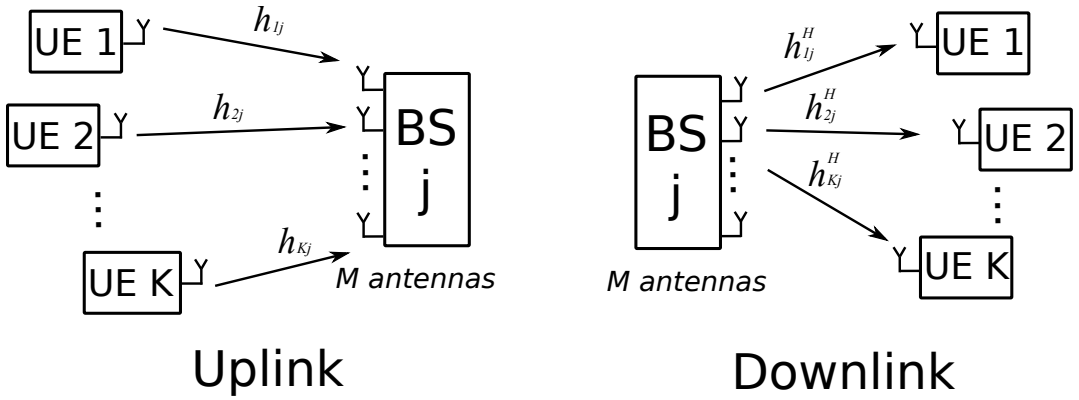

Figure 2.11: *Block diagram of multi-UE MIMO system including uplink and downlink transmission*

2.3.1 Single-cell Multi-UE MIMO systems

Figure.2.11 shows a simplified block digram of multi-UE MIMO system. As listed in the figure, uplink and downlink are two communication stages in multi-UE MIMO systems. In the uplink stage (also known as multiple access), multiple UEs send independent data streams to one BS with multiple antennas, which can be seen as a "many-to-one" transmission. As the UEs are assumed to be distributed in the cell randomly, the uplink data streams are expected to have different distortions. In the downlink stage (also known as broadcasting), BS transmits the data streams to the serving UEs, which can be seen as a "one-to-many" transmission. Different from the uplink stage, in downlink transmission, the UE will receive the signal and interference in one channel. To be more specific, UE k will receive both the desired downlink signal x_k and the interference x_j where $j \neq k$ in the downlink channel between UE k and BS. As a result, precoding can be utilized in downlink transmission to reduce the interference. The detailed discussion will be given in the section latter.

2.3.1.1 Multiple Access Scheme

In multi-UE MIMO systems, BS is designed to serve multiple UEs within the same time-frequency resource. Multiple access schemes are proposed as a resource allocation strategy for the serving UEs in order to share the limited resources efficiently.

Similar to the diversity gain, as described above, the multiple access scheme can utilize the resources from different dimensions. The common techniques include frequency division mul-

tiple access (FDMA), time division multiple access (TDMA), code division multiple access (CDMA) and space division frequency multiple access (SDMA) [42]. A brief introduction is given as follows.

- *FDMA*: its resource sharing is based on the division in frequency spectrum, where a different frequency band is assigned to each UE, meaning that UEs can communicate with the BS simultaneously. Its advantages are, (i) the easy implementation of its system design, (ii) it suffers less inter-symbol interference, and (iii) it needs fewer overheads for the synchronization with BS.
- *TDMA*: its resource sharing is based on the division in time period, where the serving UEs share the entire frequency band, but different time slots are assigned to each UE. It has been utilized in the Global System for Mobile Communications (GSM). However, its one drawback is the large overhead cost of synchronization.
- *CDMA*: it is designed to allow the serving UEs to share both the spectrum and time resource simultaneously, since a unique spreading code for signal encoding is assigned to each UE. The codebook, which is known by BS, is used to distinguish the data transmitted from multiple UEs.
- *SDMA*: it is achieved by allocating an array of M antennas at the BS, where the distinguish of UEs is based on the beam pattern. This can be jointly used with the other three schemes.

2.3.2 Massive MIMO Systems

The massive MIMO technique can be seen as an "upgraded" version of multi-UE MIMO systems. A principle feature is that BS utilizes a large-array of antennas with the number of hundreds or even thousands simultaneously serving tens or even hundreds of single antenna UEs within the same time-frequency resources. This adoption of excess antennas has enhanced the gains that the conventional MIMO systems offer, bringing additional benefits.

2.3.2.1 Frequency-division-duplex and Time-division-duplex

As mentioned above, the CSI is crucial to the performance of all MIMO systems. To be more specific, an accurate estimation of CSI is essential for both the detector at the receiver and

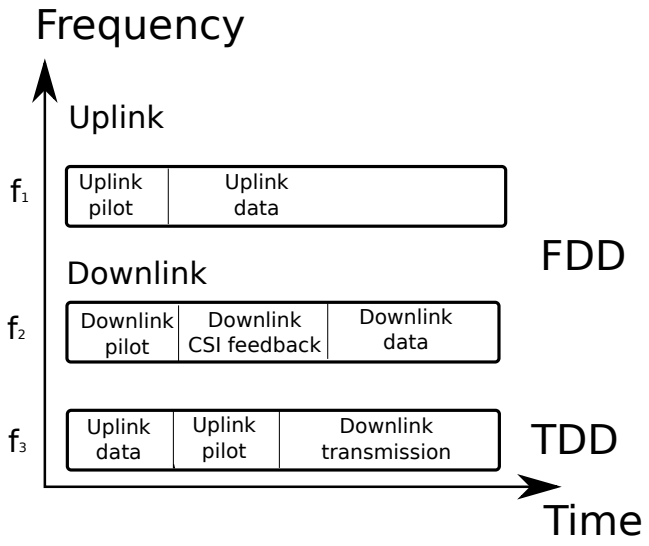

Figure 2.12: *Frame structures of FDD and TDD operations*

the BS for downlink precoding. TDD and frequency-division-duplex (FDD) are two common traffic modes in the urban cellular systems with different CSI acquisition schemes [43], which are illustrated in Fig.2.12. It is assumed that the pilot aided scheme is utilized for channel estimation in which the CSI is estimated from the received known pilot sequences straightforwardly. However, part of the coherence interval needs to be allocated for the transmission of pilot sequences. Meanwhile, if many resources are allocated for channel estimation, the data transmission rate will definitely be influenced. The consumption of resources with both the FDD and TDD operations are listed below.

FDD Operation

In the FDD operation, both uplink and downlink transmission operates in the same coherence time; however different frequency bands are assigned. The basic operation procedures are:

1. *Uplink-channel estimation*: uplink CSI is estimated from all the UEs that send their own assigned pilot sequences, presumably simultaneously, to their BS. The channel estimation is performed based on the known pilot sequences.

2. *Uplink-data transmission and detection*: the UEs start to send data after sending the pilot sequences. Based on the estimated uplink CSI, the detection is performed at BS to achieve the uplink data.

3. *Downlink-channel estimation*: The downlink CSI needs to be estimated again. The BS

sends the downlink pilot sequence to each UE and channel estimation is performed at UE side.

4. *Downlink-CSI feedback*: The estimated CSI is fed back to the BS from the uplink control channel.

5. *Downlink-precoding and data transmission*: The downlink data is passed through the precoder and transmitted to UEs.

When counting the resources that are needed for channel estimation in FDD operation, the uplink CSI pilot needs a minimum length of K and the length of downlink pilot should be equal to the number of BS antennas M. Consequently, the pilot length in the FDD operation needs to be at least $K + M$. This limits the application of FDD operation in massive MIMO system because of the large array of BS antennas.

TDD operation

In the TDD operation, both uplink and downlink transmission are designed to share the same frequency spectrum, but in different time slots. For this the following three steps are taken:

1. *Uplink training and channel estimation*: the TDD operation starts with all the active UEs sending their own assigned pilot sequence to the BS. It is assumed to be simultaneously and it is also assumed that the BS received the known pilot sequences synchronously and perform channel estimation to obtain the uplink CSI. Since the same frequency band is utilized for both uplink and downlink traffic, the downlink CSI for precoding is assumed to be consistent with the one from the uplink estimation because of the channel reciprocity. This is considered to be a principle advantage of the TDD operation.

2. *Uplink data transmission and detection*: the UEs transmit data streams after sending the pilot sequences. The estimated CSI is utilized for detecting the transmitted data streams from UEs. In massive MIMO systems, low complexity detectors such as linear detection, is capable of achieving optimal performance.

3. *Downlink precoding and data transmission*: The estimated CSI is also utilized for downlink precoding. The downlink data streams will pass to the precoder and then they will be sent to UEs.

In this thesis, the TDD operation is selected for massive MIMO systems. The main reason is the

resources for channel estimation are not proportional to the number of BS antennas. To achieve the benefits the massive MIMO systems offer, an essential condition is that access number of antennas serves single antenna UEs, where $M >> K$. Comparing with the pilot length in the TDD operation is scaled with K, the FDD operation needs a minimum length of $M+K$, which limits the application in the case of large M.

2.3.2.2 Uplink in massive MIMO system with TDD operation

The least squared (LS) method is a useful channel estimation scheme in massive MIMO systems. Consider UE i is assigned with the pilot sequence $\mathbf{s}_i \in \mathbb{R}^{\tau \times 1}$. The received signal at the BS in cell j is expressed as

$$\mathbf{y}_j = \sum_{i=1}^{K} \mathbf{s}_i \mathbf{h}_i + \mathbf{n}_j, \tag{2.49}$$

where $\mathbf{s}_i \in \mathbf{R}^{\tau M \times M}$ denotes the pilot received at BS with $\mathbf{s}_i = \mathbf{s}_i \otimes \mathbf{I}_M$ and $\mathbf{I}_M$ is a $M \times M$ identity matrix. The estimated CSI $\widehat{\mathbf{h}}_i$ of UE i from LS method is expressed as

$$\widehat{\mathbf{h}}_i = \mathbf{s}^H \mathbf{y}_j \tag{2.50}$$

2.3.2.3 Downlink in Massive MIMO System with TDD Operation

The channel reciprocity in TDD operation results in the utilization of estimated uplink CSI in downlink transmission. With the CSI known at BS, the precoding technique can be adopted for performance enhancement [44] from various different aspects.

Precoding technique both eliminates interference between UEs and reduces the size and energy consumption of terminal equipments. In multi-UE MIMO system of the uplink detection at BS, when serving large number of UEs the computational complexity will be very high, because the received signal at BS is a combination of multiple streams and the jointly detection is computation intensive. In the downlink transmission, high energy consumption arises with the high computational detection at the UE side, which will limit the mobility service of equipments. Consequently, a precoding technique is applied for "pre-processing" before the downlink transmission in order to increase the spatial multiplexing gain that UEs have achieved. This helps to improve the detection performance at the UE side and also to increase the system's capacity.

Linear precoding schemes are generally utilized in massive MIMO systems; this is similar to the

adoption of linear detection for uplink, where the large number of antennas result in favourable propagation and the complexity for both detection and precoding design is reduced. Maximum ratio transmission (MRT) belongs to the linear precoding schemes, which is aiming to maximize the SNR in downlink transmission. The received signal $r_i \in \mathbb{C}$ of UE i is expressed as

$$r_i = \sum_{k=1}^{K} \mathbf{h}_i^H \mathbf{t}_k x_k + z_i, \tag{2.51}$$

where $\mathbf{t}_k \in \mathbb{C}^{M\times 1}$ denotes the precoding vector, x_k represents the transmit data symbols and $z_i \in \mathbb{C}$ is the receiver noise and $z_i \in \mathcal{CN}(0,1)$. As the TDD operation is considered, the downlink channel utilized the Hermitian transpose of the uplink channel. The MRT precoding vector is given as

$$\mathbf{t}_k = \frac{\mathbf{h}_k}{\|\mathbf{h}_k\|} \tag{2.52}$$

2.4 Chapter summary

The first part of this chapter, which has introduced the background knowledge regarding both the conventional MIMO and massive MIMO systems as used in this thesis, started with a point-to-point description of the conventional MIMO systems. Firstly, the fading in wireless propagation environment was introduced, together with the concept of both large- and small-scale fading, which will be applied in the system model, to be presented in the next three chapters. Secondly, a detailed description of the advantages that offered by MIMO systems was covered, revealing a principle benefit of diversity gain that can be achieved in time, frequency and space dimensions, where it has been much enhanced both by the deployment of multiple antennas and by reaching up to $M_{\mathrm{t}}M_{\mathrm{r}}$ in MIMO systems. Thirdly, this chapter revealed that another benefit is the spatial multiplexing gain, where the system capacity linearly increases with $\min(M_{\mathrm{t}}, M_{\mathrm{r}})$. Fourthly, a comparison channel capacity has been established between SISO, SIMO, MISO and MIMO systems, with the simulation result verifying a capacity improvement by incorporating additional antennas.

The second part of this chapter considered multi-UE MIMO and massive MIMO systems. Firstly, the multiple access scheme that was utilized in the multi-UE MIMO system is introduced. The CDMA scheme is considered in the following system design. Secondly, a brief introduction of massive MIMO system has been given. An introduction of the advantages that

is offered by massive MIMO systems has been given, where it not only brings a great enhancement of system capacity but also reduces the computational complexity at the BS side. The research into the TDD or FDD operation based massive MIMO system have attracted great interests; hence, in this thesis, the TDD operation is utilized because of the channel reciprocity.

The next chapter will consider the conventional MIMO systems, where the combination of the K-best detector with adaptive modulation scheme will be proposed. The chapter 4 will present the analytical results based on massive MIMO systems, followed by the chapter 5, where the system's energy efficiency will be maximized.

Chapter 3

Performance Analysis of the K-Best Detector with Adaptive Modulation

This chapter describes an error probability approximation framework for multiple-input multiple-output (MIMO) systems with the K-Best detection algorithm at receiver side, which aims to serve for the adaptive modulation scheme. The basic idea of this work is to utilize a simplified error probability approximation scheme based on the union bound (UB) of the maximum likelihood detector (MLD) such that the bit error rate (BER) performance of the K-Best algorithm in various channel qualities can be efficiently predicted. Instead of considering all the error events, we only apply the minimum Euclidean distance (MED) errors in the UB calculation will be applied - this amounts to only a small portion, especially since the number of antenna is large. This will be suitable for real-time adaptive modulation systems because the computational complexity has been much reduced. To improve the accuracy of prediction, the signal-to-noise ratio (SNR) gaps between the simplified UB and the full UB in different channel conditions are estimated and recorded in a look-up-table (LUT). By applying the simplified approximation method, simulation results have clearly shown the adaptive K-Best algorithm to have a much reduced computational complexity while still maintaining a promising BER performance.

The remainder of this chapter will be organized as follows: section 3.1 will introduce of the background and purpose of this chapter by giving a brief literature review of the MIMO detection algorithm with the adaptive modulation. Section 3.2 will focus on the system model and the detection algorithms, both of which will be utilised in this chapter. Section 3.3 will present a detailed explanation of the UB of the MLD. Section 3.4 will describe the procedures of how adaptation works and how the LUT that contains SNR gaps between predictions and actual results are generated. Section 3.5 will bring the chapter to this conclusion with a demonstration of the simulation results and its corresponding analysis.

3.1 Introduction

As stated in Chapter 2, MIMO is an advanced wireless communication technology that has attracted great interest from both researchers and industrialists. The deployment of multiple antennas at both transmitter and receiver is a promising technique designed to increase spectrum efficiency with a high order of diversity [26, 37, 45]. Multiple data streams are sent simultaneously from the transmitter, but each stream will suffer independent fading through different channels. Therefore, the joint-detection of transmitted information from the received signal at the receiver side becomes both important and challenging because it is crucial that the system should achieve a high data rate while maintaining an acceptable detection error probability at the receiver side. Consequently, there has to be a trade-off between detection performance and computational complexity at the receiver side.

Convincing detection results often entail a the high computational complexity, hence the MLD, which is an optimal receiver designed for the MIMO systems, guarantees robust detection performance. However, an exhaustive search over the large lattice point space leads to high computational complexity, which makes it unrealistic for practical application, whereas the linear detector can be implemented simply, although it needs a higher SNR in order to achieve the desired performance. Therefore, over the last decade a considerable number of detection algorithms have been proposed in order to achieve a quasi-MLD performance with an manageable level of complexity. For instance, numerous novel tree-search based detection algorithms have been proposed, such as the fixed sphere decoder (FSD) [46] and the K-Best detector [11]. The K-Best detector is a non-linear algorithm that achieves the quasi-ML performance with fixed degree of complexity allowing detection to be executed simultaneously by applying a breadth-first tree search with a fixed number of searching paths at each level, which is a feature has great potential for parallel hardware platforms implementation as well as for practical applications [47, 48].

In terms of spectrum efficient transmission in MIMO systems, an adaptive transmission technique is an convincing means of improving data throughput over time-varying channels [49–51]. The adaptive transmission method estimates the channel condition at the receiver and feeds back the relevant transmission parameter, which matches the instantaneous channel quality in order for it to transmit based on the channel condition estimation. The typical transmission parameter can be modified to includes transmit power, modulation scheme, and coding scheme. By employing the adaptive transmission scheme, the system throughput can either be max-

imised by setting a target BER, or BER can be reduced under a fixed throughput requirement [52].

Related work: the K-Best detector is based on a tree-search based algorithm which was first proposed in [9, 53]. Until recently the development of the K-Best algorithm focused mainly on the complexity reductions and detection performance improvements. However, in [54], the authors proposed an adaptive K-value method according to the channel condition and an adaptive K values will be employed in the detection according to the varying channel conditions at each tree level. In [55] the authors considered the complexity reduction on higher order modulation schemes in the K-Best algorithm. In contrast to the conventional K-Best algorithm, which implements a full expansion at each level, the proposed algorithm expands to only partial constellation sets at certain levels thus providing good detection performance with fewer computations. A lattice reduction (LR) aiding K-Best algorithm was proposed in [56], hence the authors claim to reduce computational complexity; therefore the proposed algorithm is suitable for massive MIMO systems. A combination of the MMSE and the K-Best algorithm was proposed in [57] where the complexity is reduced firstly by utilizing MMSE detection followed by the reduced-dimension K-Best algorithm. In [58], an improved K-Best algorithm was proposed whereby a flexible number of nodes are utilized in the detection; these are determined by a pre-defined adaptive threshold value, thus achieving quasi-MLD performance by considering more nodes at an early detection stage than the conventional K-Best algorithm.

The adaptive transmission scheme has become a significant technology that has been used in the third and forth generation of mobile communication technology standards network (3G & 4G) [49, 59]. In [60] the authors proposed a joint power control and adaptive modulation scheme for uplink transmission in massive MIMO systems, which increases the average spectrum efficiency. In [61], the adaptive transmission was applied to virtual-MIMO systems and this gave a promising performance. The imperfect CSI in an adaptive transmission is another topic that has attracted great interest. The authors in [62] proposed a scheme with outdated CSI where the coefficient of time correction was calculated based on SINR and BER. In [63], the adaptation was based on the mean of channel feedback with the Alamouti structure.

Contribution: this chapter will now focus on the K-Best algorithm with an adaptive transmission scheme for the uplink transmission. An estimation scheme is proposed to predict the performance of the K-Best algorithm in time varying channels with different transmission parameters, which, in order to estimate the error probability rate will entail the application of a

simplified error probability approximation method based on the UB of the MLD. Compared with the original UB of the MLD, the proposed method utilizes the MED events only in the approximation. This simplification is computationally complex, hence it is more suitable to be used for performance predictions in real-time adaptive modulation setups. The channel condition number is utilized as the channel quality indicator in the system. Furthermore, by setting up the target BER, a look-up table (LUT) approach is applied to approximate performance gaps between the proposed simplified approximation and the conventional UB or the K-Best detector with different K values.

At this point, the BER performance of the K-Best algorithm can be predicted accurately in the adaptive modulation scheme by using this pre-estimated table, thus allowing the modulation schemes that achieve the target BER to be sent back to the users. So far, numerical results have shown that the proposed scheme guarantees a promising error rate performance under different channel conditions with much reduced computational complexity.

3.2 The System Model

3.2.1 The MIMO System Model

This model assumes an uncoded conventional point-to-point MIMO system with M_{t} transmit antennas and M_{r} receive antennas, denoted as $M_{\mathrm{t}} \times M_{\mathrm{r}}$. It is further assumed that $M_{\mathrm{r}} \geq M_{\mathrm{t}}$ and where the received vector $\mathbf{y}$ with size $M_{\mathrm{r}} \times 1$ can be denoted as

$$\mathbf{y} = \mathbf{H}\mathbf{s} + \mathbf{n}, \tag{3.1}$$

where $\mathbf{s} = [s_1, s_2, \ldots, s_{M_{\mathrm{t}}}]^T$ denotes the transmitted symbol vector of size $M_{\mathrm{t}} \times 1$ and each symbol is modulated with a complex constellation based on M-ary quadrature amplitude modulation (M-QAM). The received complex vector is represented as $\mathbf{y} = [y_1, y_2, \ldots, y_{M_{\mathrm{r}}}]^T$ with $\mathbf{n} = [n_1, n_2, \ldots, n_{M_{\mathrm{r}}}]^T$ as the additive white Gaussian noise (AWGN) vector with elements of independent and identically distributed (i.i.d) complex Gaussian noise. In addition, the complex noise elements have a zero mean and a variance of σ_{n}^2. The channel $\mathbf{H} \in \mathbb{C}^{M_{\mathrm{r}} \times M_{\mathrm{t}}}$ has i.i.d elements $h_{ji} \sim \mathcal{CN}(0, 1)$ indicating the uncorrelated Rayleigh fading propagation environment. An assumption is made that the CSI is perfectly known at the receiver side.

3.2.2 The Tree-search Based Detection and K-Best Algorithm

The K-Best algorithm is a detection method that can be seen as an extension over the sphere decoder (SD). If the search for an optimal detection is accomplished by a tree-search based method, the K-Best algorithm performs a breadth-first search from the top to the bottom with fixed K points at each level. The following section will give a brief introduction to the SD and the tree-search, which will be followed by an explanation of the K-Best algorithm.

The MLD performs exhaustive searches over all the candidate vectors. Figure.3.1(a) shows an example of the MLD search principle, where the red cross represents the received noisy signal and the blue points denote the noiseless constellation set. The search is based on a calculation of the Euclidean distances (ED) between the received signal and all the other candidate points. Therefore it is proposed that the SD reduces the computational complexity by searching only a subset of the constellations [64]. Figure.3.1 shows the principle of the SD where the constellation points in the subset are selected inside a sphere with a pre-defined radius R and the received signal is the centre point, with the detection result, which is obtained by comparing the ED between the received signal and the points in the subset and it is written as [64]

$$\widehat{\mathbf{s}}_{\mathrm{SD}} = \|\mathbf{y} - \mathbf{H}\hat{\mathbf{s}}\|^2 \leq R_{\mathrm{SD}}^2. \tag{3.2}$$

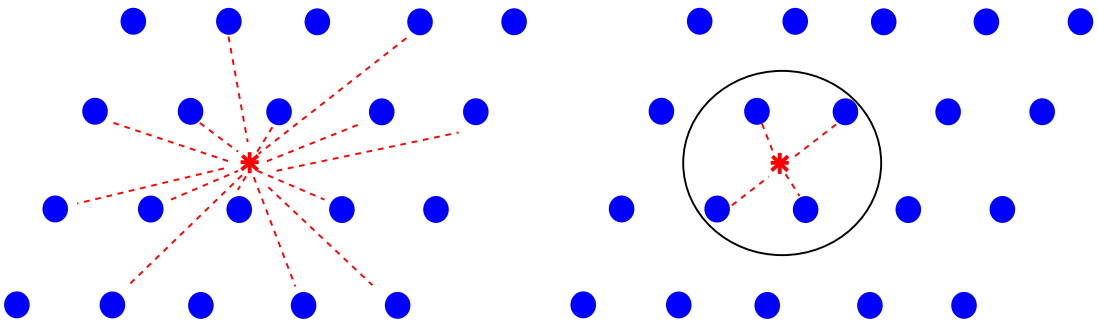

(a) MLD - exhaustive search (b) SD - search within pre-defined sphere

Figure 3.1: *Comparison of MLD and SD search principles*

The detection search shown in Fig.3.1 can also be viewed as a tree-search problem, in which the decision tree contains all the points in the constellation set as leaf *nodes*, and the search starts from the top to the bottom. The tree pruning generally starts with converting the received

symbols from a complex value into a real value form, which is given as

$$\begin{aligned}\mathbf{y}_{\mathrm{r}} &= \begin{bmatrix}\Re(\mathbf{y})\\ \Im(\mathbf{y})\end{bmatrix} = \begin{bmatrix}\Re(\mathbf{H}) & -\Im(\mathbf{H})\\ \Im(\mathbf{H}) & \Re(\mathbf{H})\end{bmatrix}\begin{bmatrix}\Re(\mathbf{s})\\ \Im(\mathbf{s})\end{bmatrix} + \begin{bmatrix}\Re(\mathbf{n})\\ \Im(\mathbf{n})\end{bmatrix}\\ &= \mathbf{H}_{\mathrm{r}}\mathbf{s}_r + \mathbf{n}_r, \end{aligned} \tag{3.3}$$

where $\Re\{\cdot\}$ denotes the real, and $\Im\{\cdot\}$ represents the imaginary part of the symbol vectors; $\mathbf{y}_{\mathrm{r}}, \mathbf{H}_{\mathrm{r}}, \mathbf{s}_r$ and $\mathbf{n}_r$ are the real value vectors. Note that the size of the real vectors are doubled over complex vectors after the conversions. Following the conversion, the QR decomposition is applied on the real valued channel matrix, which comes to

$$\mathbf{H}_{\mathrm{r}} = \mathbf{Q}\mathbf{R}, \tag{3.4}$$

where $\mathbf{Q} \in \mathbb{R}^{2M_{\mathrm{r}}\times 2M_{\mathrm{t}}}$ is a unitary real value matrix and $\mathbf{R} \in \mathbb{R}^{2M_{\mathrm{t}}\times 2M_{\mathrm{t}}}$ is an upper triangular real value matrix with entries r_{mn}. By multiplying the nulling term $\mathbf{Q}^H$ on the MLD equation, the reformulation is represented as

$$\begin{aligned}\hat{\mathbf{s}}_{\mathrm{ML}} &= \underset{\hat{\mathbf{s}}_{\mathrm{r}}\in\mathcal{S}_{\mathrm{r}}^{2M_{\mathrm{t}}}}{\arg\min} \|\mathbf{Q}^H(\mathbf{y}_{\mathrm{r}} - \mathbf{H}_{\mathrm{r}}\hat{\mathbf{s}}_{\mathrm{r}})\|^2\\ &= \underset{\hat{\mathbf{s}}_{\mathrm{r}}\in\mathcal{S}_{\mathrm{r}}^{2M_{\mathrm{t}}}}{\arg\min} \|\mathbf{Q}^H\mathbf{y}_{\mathrm{r}} - \mathbf{Q}^H\mathbf{Q}\mathbf{R}\hat{\mathbf{s}}_{\mathrm{r}}\|^2\\ &= \underset{\hat{\mathbf{s}}_{\mathrm{r}}\in\mathcal{S}_{\mathrm{r}}^{2M_{\mathrm{t}}}}{\arg\min} \|\tilde{\mathbf{y}}_r - \mathbf{R}\hat{\mathbf{s}}_{\mathrm{r}}\|^2\\ &= \underset{\hat{s}_{\mathrm{r},n}\in\mathcal{S}_{\mathrm{r}}^{2M_{\mathrm{t}}}}{\arg\min} \sum_{m=1}^{2M_{\mathrm{t}}} |\tilde{y}_{r,m} - \sum_{n=1}^{2M_{\mathrm{t}}} r_{mn}\hat{s}_{\mathrm{r},n}|^2, \end{aligned} \tag{3.5}$$

where $\mathcal{S}_{\mathrm{r}}$ represents a real-valued constellation set. Note that $\tilde{\mathbf{y}}_{\mathrm{r}} = \mathbf{Q}^H\mathbf{y}_{\mathrm{r}} = \mathbf{R}\mathbf{H}_{\mathrm{r}}^H\mathbf{y}_{\mathrm{r}}$. Due to $\mathbf{R}_c$ is an upper triangular matrix with zero elements under the matrix diagonal, the search of the closest lattice point as the optimal detection result in equation (3.5) can be transformed into a tree structure search. Fig.3.2 shows an example of the expanded tree structure. The lattice point tree contains $2M_{\mathrm{r}} + 1$ tree levels and tree level starts from $2M_{\mathrm{r}} + 1$ to 1. If we have level *m* lies above the *m-1* level, the nodes in level *m* are *parent nodes* and each node in level $m - 1$ is a *child node*. Each parent node contains a number of $\sqrt{\mathcal{S}_{\mathrm{r}}}$ real valued child nodes. The paths between parent nodes and child nodes are named as the partial Euclidean distances

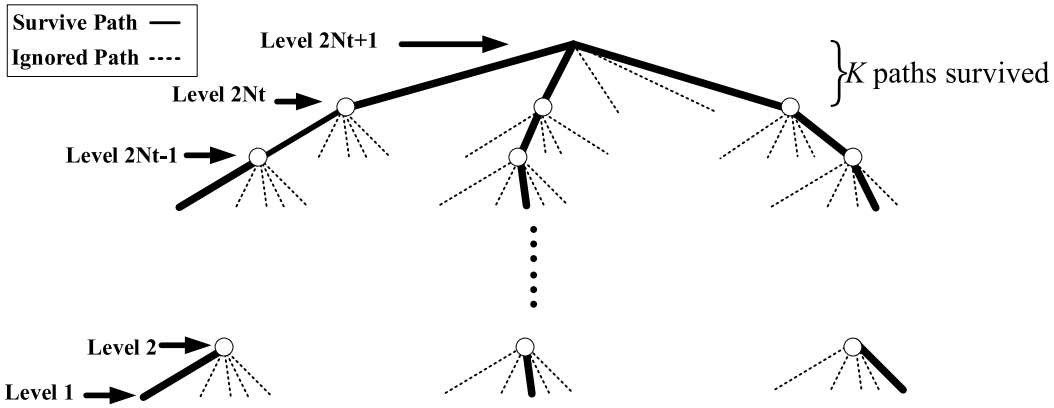

Figure 3.2: *The K-Best detection tree diagram*

(PEDs) between the lattice points. The PED of the level *m* can be represented as

$$PED_m = PED_{m+1} + |\tilde{y}_{\mathrm{r},m} - \sum_{n=1}^{2M_{\mathrm{t}}} r_{mn}\hat{s}_{\mathrm{r},n}|^2, \tag{3.6}$$

where PED_m records the PEDs of both the previous level PED_{m+1} and the current level. In the end, the path with the smallest acccumulative PEDs is chosen and the node points on this path is sorted as the detection result. The computational complexity depends on the number of nodes that were visited during the traversal. The MLD utilises the exhaustive traversal, which calculates the acccumulative PEDs of each path and select the minimum one as the detection result. The SD only visit the path with the accumulative PEDs that less or equal to R. The SD reduces the computational complexity involved in detection from the reduction of the number of nodes visit while keeps acceptable detection errors.

Two traversal approaches are utilized in the tree-structure in order to establish a detection result, which are *depth-first* and *breadth-first*. The depth-first approach is commonly utilised by the SD, where the search moves from the top to the bottom repeatedly until the accumulative PEDs meet the constraints. Once the search finds that the accumulative PEDs exceed R, it moves backward to the parent node and tries the other branches, after which all the candidates are stored and compared. Although the SD is an efficient detection algorithm, there are two potential problems exist [46]: firstly, the choice of radius R_{SD} is significant to the overall performance; hence, if the radius is set as a large number, the detection performance can only be guarantee by sacrificing computational complexity. However, if the radius is small, the correct transmitted signal is more likely to be neglected, which indicates an uncertain complexity of the

SD. The second potential problem is that the sequential nature of the depth-first search limits the wider applications of the SD in parallel hardware platforms.

The K-Best algorithm is a detection method which can be seen as an extension of the SD, which aims to tackle the uncertain complexity and sequential nature problems. The breadth-first search is considered in the K-Best algorithm, whereas, by contrast, the depth-first search in the search of the K-Best algorithm is only one directional. The search at each level only keeps K nodes with the smallest PEDs and the expansion of the child nodes follows these K candidates. When the search reaches Level 1, the path with the smallest accumulative PEDs is selected from the fixed number of candidates. The value K has significantly influenced the detection performance and complexity, therefore, if the intention is to maximize the detection performance, the K value should be set as a large number. In summary, the nature of a breadth-first search shows that it has a fixed complexity, which not only reduces the searching candidates but also make it suitable for the implementation with the practical hardware platform consisting of very-large-scale integration (VLSI) or field-programmable gate array (FPGA).

Compared with the MLD, the computational complexity in the K-Best algorithm has been much reduced. As discussed in Chapter 2, the detection of one vector in the MLD needs to search $M_{\mathrm{n}}^{M_{\mathrm{r}}}$ possible vectors in MIMO systems, where M_{n} is the size of constellation set and M_{r} is the number of receive antennas. However, the K-Best algorithm only needs $K^{M_{\mathrm{r}}}$. As a result, both the detection performance and complexity is determined by the choice of K.

After the introduction of the K-Best algorithm, the UB of the MLD will be introduced in the next section, where the prediction of the K-Best algorithm will be based on it.

3.2.3 The UB of the MLD

The UB for the BER of the MLD is a simple, but widely used upper bound, which acts as an indicator of the MLD detection performance by providing a theoretical approximation of the error probability. It is tight especially at high SNRs [65, 66]. The calculation of the UB generally starts with the most basic element, the Pairwise Error Probability (PEP) which is denoted as $\mathrm{P}_{\mathbf{s}_i \to \mathbf{s}'_j}$. It indicates the probability that the receiver detected vector $\mathbf{s}'_j$ but the vector

$\mathbf{s}_i$ was actually sent. The $\mathrm{P}_{\mathbf{s}_i \to \mathbf{s}'_j}$ is formulated as

$$\begin{aligned}
\mathrm{P}_{\mathbf{s}_i \to \mathbf{s}'_j} &= \mathrm{P}\left(\|\mathbf{y} - \mathbf{H}\mathbf{s}_i\|^2 > \|\mathbf{y} - \mathbf{H}\mathbf{s}'_j\|^2\right) \\
&= \mathrm{P}\left(\|\mathbf{H}\mathbf{s}_i + \mathbf{n} - \mathbf{H}\mathbf{s}_i\|^2 > \|\mathbf{H}\mathbf{s}_i + \mathbf{n} - \mathbf{H}\mathbf{s}'_j\|^2\right) \\
&= \mathrm{P}\left(\|\mathbf{n}\|^2 > \|\mathbf{n} + \mathbf{H}\left(\mathbf{s}_i - \mathbf{s}'_j\right)\|^2\right)
\end{aligned} \tag{3.7}$$

where $\left(\mathbf{s}_i - \mathbf{s}'_j\right)$ is the difference between two signal vectors. If we have $\delta_{i,j'} = \left(\mathbf{s}_i - \mathbf{s}'_j\right)$, then equation (3.7) can be transformed as follows

$$\begin{aligned}
\mathrm{P}_{\mathbf{s}_i \to \mathbf{s}'_j} &= \mathrm{P}\left(\mathbf{n}^H\mathbf{n} > \left(\mathbf{n} + \mathbf{H}\delta_{i,j'}\right)^H\left(\mathbf{n} + \mathbf{H}\delta_{i,j'}\right)\right) \\
&= \mathrm{P}\left(\mathbf{n}^H\mathbf{n} > \mathbf{n}^H\mathbf{n} + \mathbf{n}^H\mathbf{H}\delta_{i,j'} + \delta_{i,j'}^H\mathbf{H}^H\mathbf{n} + \delta_{i,j'}^H\mathbf{H}^H\mathbf{H}\delta_{i,j'}\right) \\
&= \mathrm{P}\left(-\delta_{i,j'}^H\mathbf{H}^H\mathbf{H}\delta_{i,j'} > 2Re\{\mathbf{n}^H\mathbf{H}\delta_{i,j'}\}\right).
\end{aligned} \tag{3.8}$$

The $2Re\{\mathbf{n}^H\mathbf{H}\delta_{i,j'}\}$ is denoted by $\xi_{i,j'}$. As mentioned above, the noise vector $\mathbf{n}$ has Gaussian distribution. Then we have the mean value of $\xi_{i,j'}$ is 0 and variance $\sigma^2_{\xi_{i,j'}}$ is $2\sigma^2_{\mathbf{n}}\delta_{i,j'}^H\mathbf{H}^H\mathbf{H}\delta_{i,j'}$. We can formally define the conditional probability density function (PDF) of detecting $\mathbf{s}'_j$ but actually $\mathbf{s}_i$ was send over channel $\mathbf{H}$

$$\begin{aligned}
\mathrm{P}_{\mathbf{s}_i \to \mathbf{s}'_j} &= \frac{1}{\sqrt{2\pi\sigma^2_{\xi_{i,j'}}}} \int_{-\infty}^{-\delta_{i,j'}^H\mathbf{H}^H\mathbf{H}\delta_{i,j'}} e^{\frac{\left(\xi_{i,j'}-0\right)^2}{2\sigma^2_{\xi_{i,j'}}}} d\xi_{i,j'} \\
&= \frac{1}{\sqrt{2\pi}} \int_{\frac{\delta_{i,j'}^H\mathbf{H}^H\mathbf{H}\delta_{i,j'}}{\sigma_{\xi_{i,j'}}}}^{\infty} e^{\frac{\xi_{i,j'}^2}{2}} d\xi_{i,j'} \\
&= Q\left(\frac{\delta_{i,j'}^H\mathbf{H}^H\mathbf{H}\delta_{i,j'}}{\sigma_{\xi_{i,j'}}}\right) \\
&= Q\left(\frac{\delta_{i,j'}^H\mathbf{H}^H\mathbf{H}\delta_{i,j'}}{\sqrt{2\sigma^2_{\mathbf{n}}\delta_{i,j'}^H\mathbf{H}^H\mathbf{H}\delta_{i,j'}}}\right) \\
&= Q\left(\sqrt{\frac{\delta_{i,j'}^H\mathbf{H}^H\mathbf{H}\delta_{i,j'}}{2\sigma^2_{\mathrm{n}}}}\right)
\end{aligned} \tag{3.9}$$

where $Q(\cdot)$ is the Marcum Q-function. The numerator in equation (3.9) represents the euclidean distance between vector $\mathbf{s}_i$ and $\mathbf{s}_{\mathrm{c},j'}$ under the given channel realization $\mathbf{H}$, which is interpreted

as

$$\begin{aligned} d^2_{\mathbf{s}_i \to \mathbf{s}'_j} &= \delta^H_{i,j'} \mathbf{H}^H \mathbf{H} \delta_{i,j'} \\ &= \left(\mathbf{s}_i - \mathbf{s}'_j\right)^H \mathbf{H}^H \mathbf{H} \left(\mathbf{s}_i - \mathbf{s}'_j\right) \\ &= \| \mathbf{H} \left(\mathbf{s}_i - \mathbf{s}'_j\right) \|^2 \end{aligned} \tag{3.10}$$

According to equation (3.10), the PEP of one symbol vector can be calculated. The UB of the MLD is sum of the mean PEP of all the candidate symbol vectors. The first step is to calculate the mean PEP over i.i.d. uncorrelated Gaussian distributed channels. The mean PEP is given as [66]

$$\begin{aligned} PEP_{i,j} &= \mathrm{E}\left\{ Q\left(\sqrt{\frac{d^2_{\mathbf{s}_i \to \mathbf{s}'_j}}{2\sigma^2_{\mathrm{n}}}} \right) \right\} \\ &= \left(\frac{1-\mu_{i,j}}{2}\right)^{M_{\mathrm{r}}} \sum_{k=1}^{M_{\mathrm{r}}-1} \binom{M_{\mathrm{r}}-1+k}{k} \left(\frac{1+\mu_{i,j}}{2}\right)^k \end{aligned} \tag{3.11}$$

where

$$\mu_{i,j} = \sqrt{\frac{\gamma_{i,j}}{1+\gamma_{i,j}}} \tag{3.12}$$

and

$$\gamma_{i,j} = \frac{\|\delta_{i,j'}\|^2 \sum\limits_{n=1}^{M_{\mathrm{t}}} \log_2(M_{\mathrm{n}})}{4M_{\mathrm{r}} \sum\limits_{n=1}^{M_{\mathrm{t}}} \mathrm{E}\left(|s_n|^2\right)} \frac{E_{\mathrm{b}}}{N_0}. \tag{3.13}$$

The UB of the MLD can be represented as

$$\begin{aligned} P_{\mathrm{ub}} = & \frac{1}{\sum\limits_{n=1}^{M_{\mathrm{t}}} \log_2(M_{\mathrm{n}})} \frac{1}{\prod\limits_{n=1}^{M_{\mathrm{t}}} M_{\mathrm{n}}} \sum_{i=1}^{M_{\mathrm{n}}^{M_{\mathrm{t}}}} \sum_{j=1 \& j \neq i}^{M_{\mathrm{n}}^{M_{\mathrm{t}}}} e_b(\mathbf{s}_i, \mathbf{s}^*_j) \\ & \times \mathrm{E}\left\{ Q\left(\sqrt{\frac{\|\mathbf{H}(\mathbf{s}_i - \mathbf{s}^*_j)\|^2}{2\sigma^2_{\mathrm{n}}}} \right) \right\}, \end{aligned} \tag{3.14}$$

where $e_b(\mathbf{s}_i, \mathbf{s}^*_j)$ is the number of bit errors between the vectors $\mathbf{s}_i$ and $\mathbf{s}_j$.

Consequently, it is noticeable that the UB of the MLD includes all the error events in the calculation. This comprehensive calculation provides an accurate estimation of the BER per-

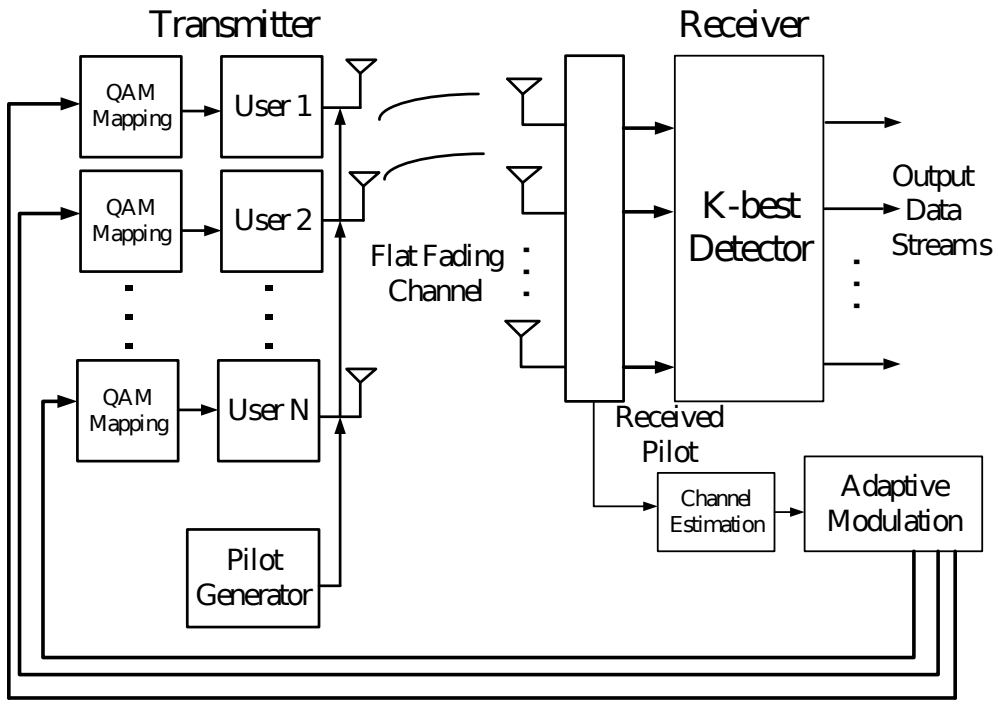

Figure 3.3: *System diagram of the K-Best adaptive modulation scheme*

formance in high SNR region. However, due to the high computational complexity, it is not suitable for real-time implementation. In terms of the application in prediction of the K-Best performance in adaptive modulation scheme, it needs simplifications, which will be introduced in the following section.

3.3 The K-Best Algorithm with Adaptive Modulation Scheme

In this section, firstly an overview of the proposed adaptive MIMO system with the K-Best algorithm will be given. Secondly, how the detection performance is affected by the channel condition number will be investigated and thirdly a comprehensive introduction will be presented on the simplified UB with MED events method.

Fig.3.3 shows the block diagram of the MIMO systems with the adaptive modulation scheme. Here, the transmitters are considered as users with either a single antenna devices or a device with multiple antennas. The receiver is the device with multiple antennas using the K-Best algorithm as the detector. The detailed description of the systems is given as follows:

1. Measure the MIMO channel and the transmit powers: each transmitter will first transmit pilot symbols to perform channel estimation. At the receiver, the channel estimation module predicts the channel state information (CSI) according to the received pilot symbols.

2. Estimate the error rate for different modulation scheme combinations: the adaptive modulation module computes the error probability using perfect CSI with different modulation scheme set-ups for users.

3. Select the modulation schemes combinations: after the calculation of error probabilities, the modulation combination reaches the target BER, which is chosen for the adaptive modulation.

4. Feed back the chosen modulation schemes to users at the transmitter side: finally, the combination of modulation schemes, which maximizing data throughput and still meets the target error rate, is feed back to the users. The users then transmit data symbols according to the feed back information. Note that this scheme is most suitable for the channel with slow fading.

A simple example is presented to explain the principle of adaptive modulation scheme. Considered a single-input single-output (SISO) system with AWGN channel. The modulation scheme can be utilized is quadrature phase-shift keying (QPSK) and 8PSK. The target BER for adaptive modulation equals to 10^{-3}. In [25, 49], the error probability of QPSK and 8PSK are expressed as

$$P_{\text{QPSK}} \approx Q\left(\sqrt{\gamma}\right) \tag{3.15}$$

$$P_{\text{8PSK}} \approx 0.666Q\left(\sqrt{2\gamma}\sin\left(\pi/8\right)\right), \tag{3.16}$$

where γ denotes the SNR. As a result, based on equations (3.15) and (3.16), it can be calculated that the minimum SNRs to reach the 10^{-3} are 10.35dB and 14.79dB respectively. Consequently, when the instantaneous SNR of this system is between 10.35dB and 14.79dB, the QPSK modulation scheme can be utilized. If the SNR is bigger than 14.79dB, the 8PSK modulation can be utilized. If the SNR is less than 10.35dB, the system can choose to transmit nothing or use lower order modulation scheme.

However, the BER performance of K-Best detector in the channel with Rayleigh fading is more

difficult to predict, since there is no closed-form expression of estimating it. Consequently, in terms of utilizing the K-Best detector with the adaptive modulation scheme in MIMO systems, a simplified prediction method is required for estimating the BER performance in different channel conditions. In the following section, one of the channel quality metric, the channel conditional number, will first be discussed. Then, the proposed simplified prediction scheme will be introduced.

3.3.1 Influence of Channel Condition Number on Detection Performance

The propagation environment has a significant influence on the performance of the K-Best detector. One of the channel quality metrics is the channel condition number, denoted as κ_{H}. The calculation of κ_{H} starts from applying the singular value decomposition (SVD) of the channel matrix, which is given as

$$\mathbf{H} = \mathbf{U}\mathbf{\Sigma}\mathbf{V}^{H}, \tag{3.17}$$

where $\mathbf{U}$ is a $M_{\mathrm{r}} \times M_{\mathrm{r}}$ complex unitary matrix, $\mathbf{V}$ is a $M_{\mathrm{t}} \times M_{\mathrm{t}}$ complex unitary and $\mathbf{\Sigma}$ is a $M_{\mathrm{r}} \times M_{\mathrm{t}}$ diagonal matrix with non-zero real elements on the diagonal. The singular values of matrix $\mathbf{H}$ are the diagonal entries of $\mathbf{\Sigma}$, which is denoted as λ_{H}. Then κ_{H} is defined as

$$\kappa_{\mathrm{H}} = \frac{\lambda_{\mathrm{H,max}}}{\lambda_{\mathrm{H,min}}} \geq 1, \tag{3.18}$$

where $\lambda_{\mathrm{H,max}}$ and $\lambda_{\mathrm{H,min}}$ represents the maximum and minimum singular value. The singular values are located in a decreasing order over the diagonal of $\mathbf{\Sigma}$. If $\kappa_{\mathrm{H}} = 1$, the channel is considered as well-conditioned channel. In this case, the receiver can equalise the channel without losing performance. When $\kappa_{\mathrm{H}} > 1$, the channel quality deteriorates with an increasing κ_{H} value. In [67], the authors provided simulation which shows how the κ_{H} influences the detection performance of the linear detectors (i.e., ZF and MMSE). The interest here is the influence of κ_{H} on the non-linear detectors such as the K-Best algorithm.

Regarding an uncoded point-to-point MIMO system with $M_{\mathrm{t}} = M_{\mathrm{r}} = 4$; the transmit signal is modulated with a $16 - QAM$ scheme for each transmitter and with the MLD and K-Best with $K = 4, 8, 12, 16$ are adopted as the detection algorithm. Fig.3.4 illustrates how the BER of K-Best is degraded by the increasing value of κ_{H}. In the case of $\kappa_{\mathrm{H}} < 10$, only the MLD and $K = 16$ have an acceptable BER performance, which is below 10^{-3}. However, the performance drops dramatically when $\kappa_{\mathrm{H}} > 10$. Furthermore, the degradation in BER is significant in both

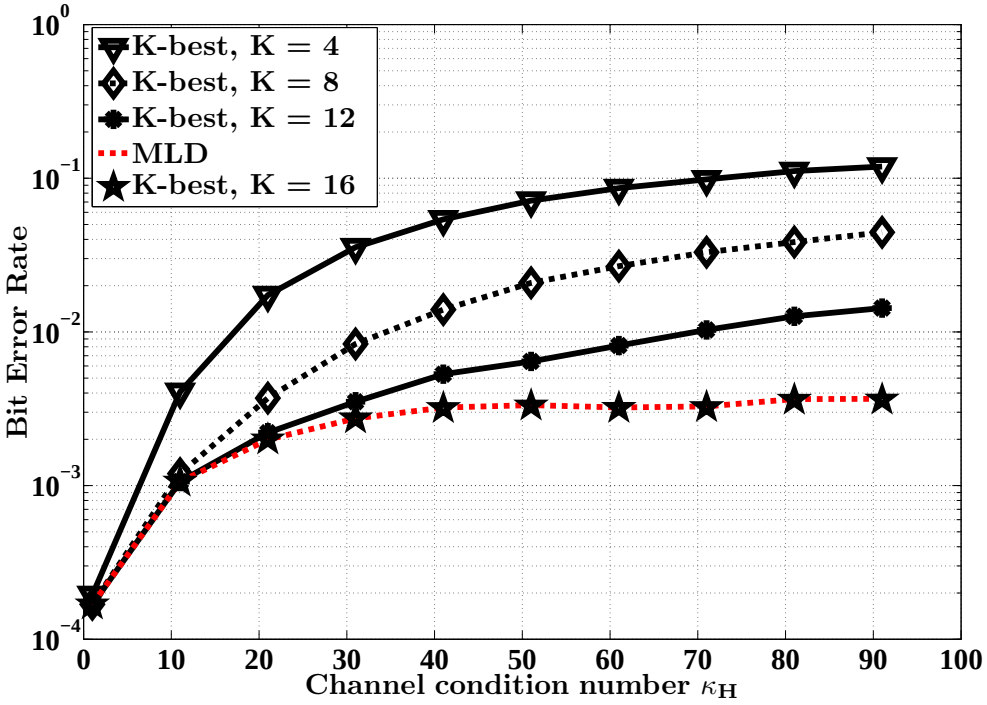

Figure 3.4: *System diagram of the K-Best adaptive modulation scheme*

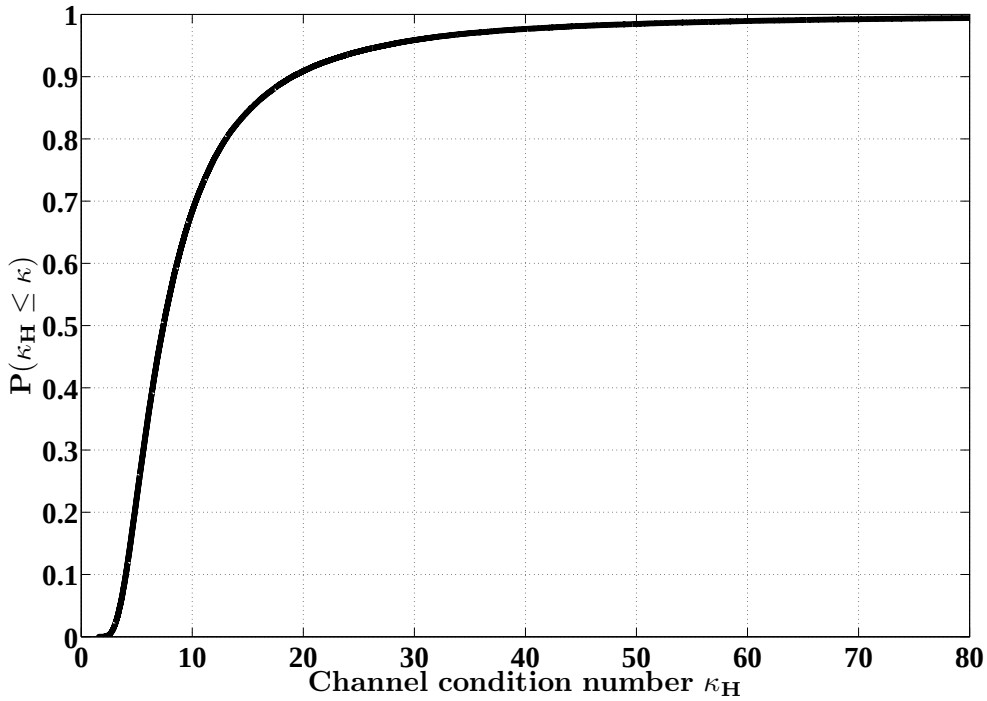

Figure 3.5: *System diagram of the K-Best adaptive modulation scheme*

large K values (e.g.,$K = 16$) and small K values (e.g.,$K = 4$). Fig.3.5 plots the acccumulative distribution function (CDF) simulation of κ_{H} for an i.i.d Rayleigh fading channel. This shows that there is an approximately a 30% chance that $\kappa_{\mathrm{H}} > 10$ and a 15% chance that $\kappa_{\mathrm{H}} > 15$. The CDF result indicates that the high condition number channel events occur frequently, which significantly affects the overall detection performance. Based on the characteristics of channel observed in Fig.3.5 and the degradation observed in Fig.3.4, it has clearly shown that the uncertainty of channel quality and its impact on the detection performance of the receiver.

The adaptive K-Best algorithm is proposed, since the main goal of the adaptive K-Best algorithm is to combat influences brought by the varying channel conditions and that by selecting feasible modulation schemes which fit the channel condition, the detection performance can achieve the target BER.

3.3.2 The Simplified UB with MED

In adaptive modulation, one important step is to achieve an accurate prediction of the error rate under varying channel conditions. It has been mentioned in [11] that with a sufficiently large K value, the K-Best detector performs closely to the MLD, while in [65] it is shown that the UB is a tight upper bound of the MLD. As a result, the approximation of the K-Best error probability employs the UB of MLD for each channel realization. However, equation (3.14) has shown a high computational complexity that is not suitable for practical implementation of the adaptive modulation scheme. For example, if a 4×4 MIMO utilizes 64-QAM scheme, the UB needs to calculate 64^4 PEPs, where each PEP averages over 64^4 pairs of vectors, which is a very high computational complexity. Therefore , approximation needs to be accurate and with less computations. The simplified approximation method of the error probability is proposed to overcome the high computational requirement while maintaining a high level of accuracy. The simplified approximation uses only the MED events for the calculation of the PEP if comparing with the conventional UB of the MLD. The MED events indicate error events of the constellation points that are at a MED from the transmitted symbols. The MED is expressed as

$$d_{\min} = \min_{\mathbf{s} \in M_{\mathrm{n}}^{M_{\mathrm{t}}} \& \mathbf{s} \neq \mathbf{s}'} \|\mathbf{s} - \mathbf{s}'\|. \tag{3.19}$$

In order to compare with the non MED events, the MED events have a relation of

$$Q\left(\sqrt{\frac{d^2_{\mathbf{s}\to\mathbf{s}'}}{2\sigma^2_{\mathrm{n}}}}\right) \leq Q\left(\sqrt{\frac{d^2_{\min}}{2\sigma^2_{\mathrm{n}}}}\right). \tag{3.20}$$

In equation (3.20), the reason for the MED events having higher probabilities than the other error events is because the Q-function is a decreasing function of the Euclidean distance. Since the MED events have significant influence on the overall error probability approximation, the simplified UB utilizes MED events in the PEP calculation in order to obtain a rough approximation of the full UB. If the set Λ_{MED} denotes the subset of the constellation points with the MED to the transmit signal, then it is clear that Λ_{MED} is much lower than the full constellation point set. Also, the lattice space of Λ_{MED} is also smaller than the full constellation point lattice space. Therefore, the proposed simplified UB approximation of the K-Best algorithm's performance is derived as

$$\begin{aligned} P_{\text{ub,MED}} = & \frac{1}{\sum_{n=1}^{M_{\mathrm{t}}} \log_2(M_{\mathrm{n}})} \frac{1}{\prod_{n=1}^{M_{\mathrm{t}}} M_{\mathrm{n}}} \sum_{i=1}^{M_{\mathrm{n}}^{M_{\mathrm{t}}}} \sum_{\text{MED}=1}^{\Lambda_{\mathrm{MED}}} e_b(\mathbf{s}_i, \mathbf{s}^*_{\text{MED}}) \\ & \times \mathrm{E}\left\{ Q\left(\sqrt{\frac{\|\mathbf{H}(\mathbf{s}_i - \mathbf{s}^*_{\text{MED}})\|^2}{2\sigma^2_{\mathrm{n}}}} + \Delta SNR \right) \right\}, \end{aligned} \tag{3.21}$$

where $P_{\text{ub,MED}}$ denotes the error probability approximation using the UB with MED events only. By comparing Equation (3.14) and (3.21), we can find that the utilization of Λ_{MED} has much reduced the computational complexity of UB. The utilization of closest error events has reduced the computational complexity from $M_{\mathrm{n}}^{M_{\mathrm{t}}}$ to Λ_{MED}, which is approximately 94% to 99.8% of the error events are neglected. This reduction is important for enabling the proposition in real-time error performance prediction.

Although the UB approximations with the MED events are not tight enough to yield an accurate approximation, it has the same PEP trend in the high SNR region. The gaps between the UB with MED events and the full UB in SNR are estimated as error rate corrections for the use in the adaptive modulation algorithm. Therefore, if the SNR gap is denoted as ΔSNR, it is represented as

$$\Delta SNR = \Delta SNR_{\mathrm{UB}} + \Delta SNR_{\mathrm{kbest}}. \tag{3.22}$$

The estimation of the ΔSNR value starts from setting the modulation combinations, which

indicates the combinations of the possible feeding of modulation schemes to different users. Then the channel condition numbers κ_{H} are divided into different groups with small value intervals based on the CDF of κ_{H}. Finally, the ΔSNR_{UB} between the simplified UB and the full UB within each group of κ_{H} are estimated and recorded.

Compare with single-input single-output (SISO) systems, the estimation of ΔSNR_{UB} is difficult in MIMO systems. In [68], the author mentioned the error probability estimation method based on the closest error events in SISO systems. As a single antenna is utilised in both transmitter and receiver, the received signal and channel are all scalars;thus, the distances between signals when calculating union bounds multiplies a scalar rather than a matrix in MIMO systems. As a result, the smallest error events definitely dominate the UB calculation. Furthermore, the distance between the transmit signal and its neighbouring points will not be changed after passing through channels. This is the reason why closest error events in SISO systems are reliable when estimating the error probability in them. However, the channel becomes a matrix in MIMO systems, which adds much uncertainty and influences to the error probability estimations. Here is a simple examples containing several random channel realizations, which aims to give an impression of error events calculation in MIMO systems. An uncoded point-to-point MIMO systems may be considered with $M_{\mathrm{t}} = M_{\mathrm{r}} = 2$ in which the BPSK modulation scheme is utilised in the system for simplicity. Parts of the possible transmit vectors are selected and given as follows

$$\mathbf{s}_{\mathrm{cb}} = \begin{bmatrix} 1-i & 1+i & -1+i & -1+i & -1+i \\ 1-i & 1-i & 1-i & 1+i & -1+i \end{bmatrix}$$

where the columns of $\mathbf{s}_{\mathrm{cb}}$ are named from $\mathbf{s}_1$ to $\mathbf{s}_5$. Because the $d^2_{\mathbf{s}_i \to \mathbf{s}'_j}$ dominates the UB, it is of interest to see how the $d^2_{\mathbf{s}_i \to \mathbf{s}'_j}$ is influenced by the channel matrix with different κ_{H}. The squared distance between $\mathbf{s}_1$ and the rest of the four vectors are 4, 8, 12, 16 respectively. The following table shows the impact on distance when $\mathbf{s}_1$ is transmitted through four different channel realisations. Table 3.1 shows the distance changes in four different channel realisations,

	Original distance	Channel 1	Channel 2	Channel 3	Channel 4
$d^2_{\mathbf{s}_1 \to \mathbf{s}'_2}$	4	2.1445	11.2174	13.8237	22.3411
$d^2_{\mathbf{s}_1 \to \mathbf{s}'_3}$	8	4.2889	22.4349	27.6473	44.6823
$d^2_{\mathbf{s}_1 \to \mathbf{s}'_4}$	12	58.1617	45.9433	6.1513	32.3765
$d^2_{\mathbf{s}_1 \to \mathbf{s}'_5}$	16	90.8377	160.3259	74.4302	7.9302

Table 3.1: *Cases of $d^2_{\mathbf{s}_i \to \mathbf{s}'_j}$ in different channel realisations*

which are given as

$$\mathbf{H}_1 = \begin{bmatrix} -0.1792 + 0.2255i & 0.4377 - 2.7430i \\ 0.2259 - 0.6341i & 0.4938 + 2.7395i \end{bmatrix}$$

$$\mathbf{H}_2 = \begin{bmatrix} 1.2608 + 0.8006i & 2.7421 - 2.0351i \\ -0.5512 + 0.5197i & 0.6471 + 1.0565i \end{bmatrix}$$

$$\mathbf{H}_3 = \begin{bmatrix} 1.1239 + 0.3740i & -0.6434 - 1.8919i \\ 0.0737 - 1.4309i & -2.6654 + 1.2026i \end{bmatrix}$$

$$\mathbf{H}_4 = \begin{bmatrix} 1.4580 - 1.2397i & -1.8630 + 2.1348i \\ -0.6280 + 1.2363i & 0.7278 - 1.3626i \end{bmatrix}$$

In channel 1, both $d^2_{\mathbf{s}_1 \to \mathbf{s}'_2}$ and $d^3_{\mathbf{s}_1 \to \mathbf{s}'_2}$ are reduced and the closest point is still the smallest distance. However, in both channels 3 and 4, the error events, which are not the closest point before transmission, have the smallest distance after passing the channels. The results indicate that the MED events might not always have the smallest distance in every channel realisations of MIMO systems. But, referring to the calculation of UB, which considers average distance over many channel realisations, the MED events still provides precise prediction of the error probability. Table 3.2 shows the average distance values over 10,000 channel realisations. It is

	Original distance	$\mathrm{E}[d^2_{\mathbf{s}_1 \to \mathbf{s}'_2}]$
$d^2_{\mathbf{s}_1 \to \mathbf{s}'_2}$	4	32.1391
$d^2_{\mathbf{s}_1 \to \mathbf{s}'_3}$	8	64.2781
$d^2_{\mathbf{s}_1 \to \mathbf{s}'_4}$	12	96.1996
$d^2_{\mathbf{s}_1 \to \mathbf{s}'_5}$	16	128.3895

Table 3.2: *Cases of average* $d^2_{\mathbf{s}_i \to \mathbf{s}'_j}$

noticeable that the closest point before the transmission still has the smallest average distance which dominates the union bound calculation.

The other key point is to estimate the gap between the K-Best algorithm with different K value configurations. Although a large K value leads to a quasi-MLD performance, under well conditioned channels, small K values can also be used to obtain optimal result with fewer computations. Therefore, small K value cases are included in the adaptive scheme. The performance gaps $\Delta SNR_{\mathrm{kbest}}$ are estimated so that the simplified UB is able to predict the K-Best

algorithm with different K values. The accurate predications of error probability are based on the above two performance gaps. An LUT can be built with ΔSNR under different channel conditions, therefore the LUT is crucial to the adaptive modulation scheme.

As mentioned above that the uncoded MIMO system is considered in this study. However, the proposed scheme can be extended to coded MIMO systems. LUTs of ΔSNR can be estimated and recorded which target to different coding schemes. Consequently, the proposed adaptive scheme can choose the corresponding LUT for BER performance analysis.

3.4 Simulation Results

In this section, the simulation results are given on performance of the K-Best algorithm with the adaptive modulation scheme. The first step of simulation was to build the LUT of ΔSNR_{t} and $\Delta SNR_{\mathrm{kbest}}$. For the estimations of ΔSNR, simulations have been made on a 4×4 MIMO systems; there are four users at the transmitter and the receiver has four antennas with the K-Best SD algorithm as detector. The M_{n}-ary QAM modulation scheme is used in the simulation with $M = 4, 16$. Based on the CDF of κ_{H}, it has been divided into eight groups with interval value of 5 from $\kappa_{H\mathrm{H}} = 1$ to $\kappa_{\mathrm{H}} = 40$. For example, group 1 is from $\kappa_{\mathrm{H}} = 1$ to $\kappa_{\mathrm{H}} = 5$, and group 2 is from $\kappa_{\mathrm{H}} = 6$ to $\kappa_{\mathrm{H}} = 10$ etc.. Within each group of κ_{H}, there are a minimum 10,000 of randomly generated channel realizations that have κ_{H} distributed within the range.

Fig.3.6 shows an example of how the ΔSNR_{UB} between the UB with MED events and the full UB are constructed. The figure shows the BER performance as a function of SNR of the fully calculated UB versus the UB with MED events only. The BER curves of these two bounds are consistent with fixed SNR gaps between each other. With the target BER as 10^{-3}, the ΔSNR_{UB} values between the full UB and the UB with MED events have been estimated.

Fig.3.7 shows an example of how the $\Delta SNR_{\mathrm{kbest}}$ was estimated between the UB using only the MED events and the K-Best algorithm with different K values within different κ_{H} value ranges. It is clear that with larger K values, the K-Best algorithm will produce a better performance. The reduction of the performance of the K-Best algorithm with different K values at the target BER were estimated. In the simulation, there were a total $M_{\mathrm{n}}^{M_{\mathrm{t}}} = 65536$ possible transmit vectors and for each vector, the subset Λ_{MED} approximate ranges from 2^4 to 8^4. Compared to the full UB with the set 16^4, the proposed scheme can reduce the computation between 94% to 99.98% by utilizing the closest points in the UB calculation.

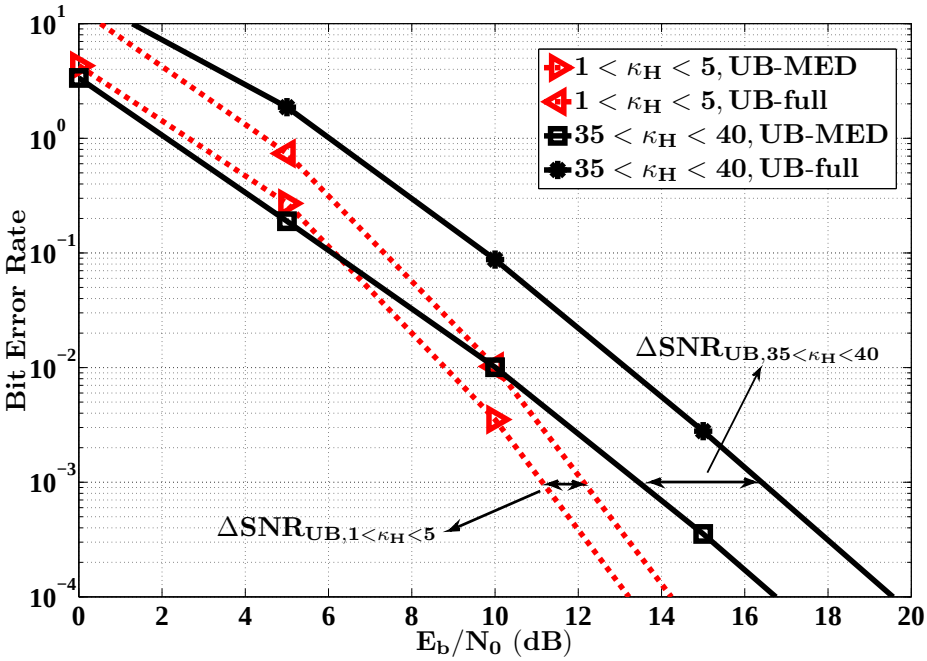

Figure 3.6: *The UB with MED events and the full UB, in MIMO with $M_t = M_r = 4$, 16-QAM*

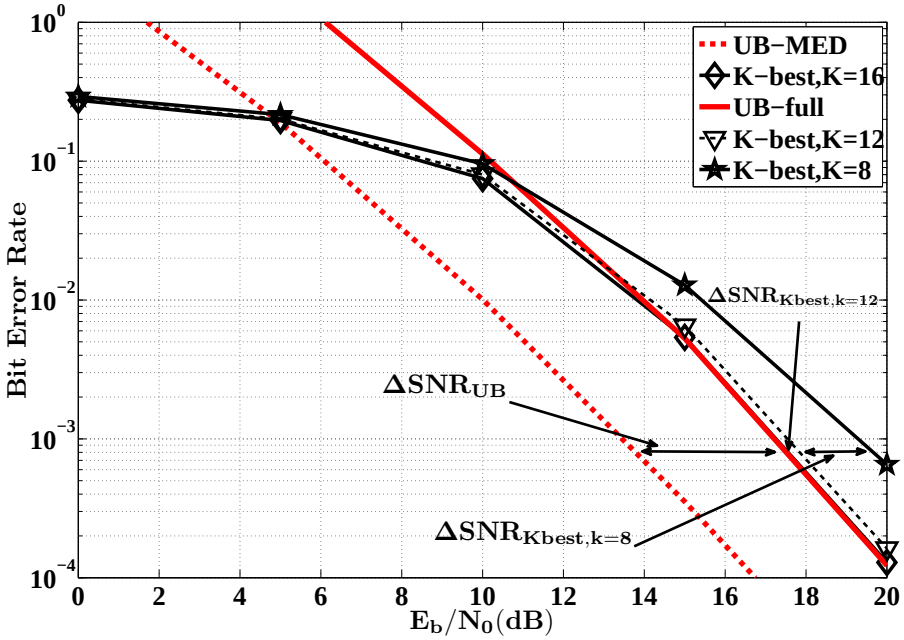

Figure 3.7: *The UB with MED events versus the full UB and K-Best with different K values, in MIMO systems with $M_t = M_r = 4$, 16-QAM, $35 \leq \kappa \leq 40$. The K values are $K = 8, 12, 16$*

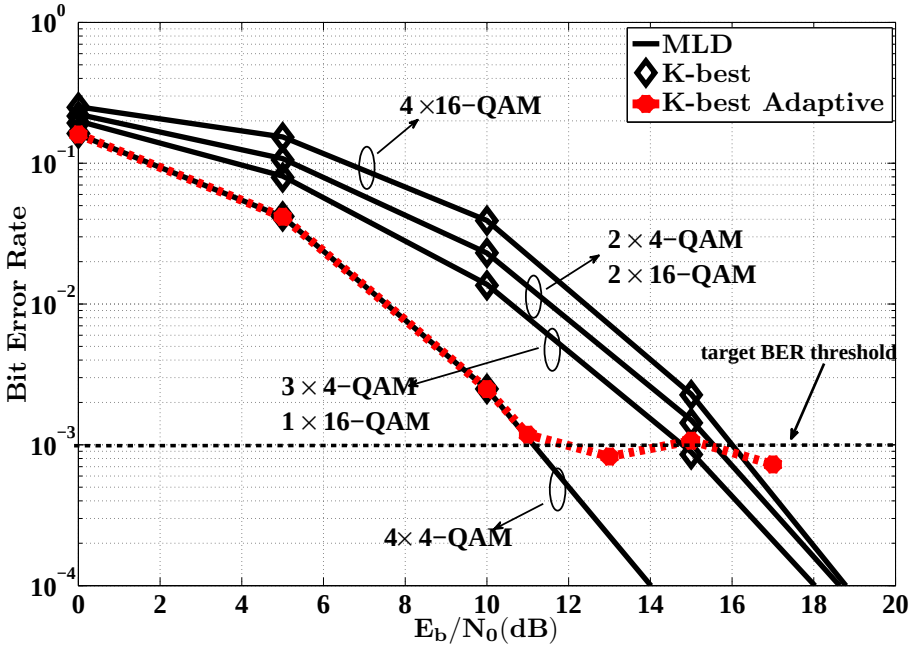

Figure 3.8: *BER of the K-Best with adaptive modulation scheme versus the MLD and K-Best with different modulation combinations, in MIMO systems with $M_t = M_r = 4$ and modulation combinations listed in Table I.*

Table 3.4 is built with the $\Delta SNR_{\text{kbest}}$ covering eight different ranges of κ_{H} values. Note that the number (1) to (8) in Table 3.4 represents eight different combinations of modulation scheme in a 4×4 MIMO systems, which is given as

Groups	Combinations
(1)	$4 \times 4 -$ QAM
(2)	$[16, 4, 4, 4]$ with $K = 16$ for 16-QAM and $K = 4$ for 4-QAM
(3)	$[16, 16, 4, 4]$ with $K = 16$ for 16-QAM and $K = 4$ for 4-QAM
(4)	$4 \times 16 -$ QAM with $K = 16$
(5)	$4 \times 16 -$ QAM with $K = 12$
(6)	$4 \times 16 -$ QAM with $K = 8$

Table 3.3: *Notes of combinations in LUT*

The ΔSNR values of the K-Best algorithm for both small and big K values are similar for small values of κ_{H}. This indicates that with the well-conditioned channels, the K-Best algorithm can use small K values in order to reduce computational complexity. In the case of large value of κ_{H}, the difference of ΔSNR with different modulation configurations becomes significant. The performance degradations caused by high κ_{H} is obvious in higher order modulation

schemes with small K values.

Fig.3.8 shows the BER performance of the K-Best adaptive modulation scheme versus the MLD and the K-Best algorithm. For the users at the transmitter side, there are six different modulation configurations to select according to the channel conditions in adaptive modulation scheme, following Table 3.3. The target BER is set to $BER_{\mathrm{t}} = 10^{-3}$. For each channel realization, the predicted performance of different modulation combinations will be calculated with the simplified UB and the pre-recorded LUT. In Fig.3.8, it can be observed that the K-Best algorithm has similar performance with the MLD. Additionally, the K-Best with the adaptive modulation scheme follows the BER of 4×4-QAM modulations until the SNR is approximately 11dB. When the SNR is greater than 11dB, the BER performance of the K-Best algorithm fluctuates around BER_{t} with higher data rate than the fix modulation configurations.

κ_{H}	(1)	(2)	(3)	(4)	(5)	(6)
1∼5	0.33	1.66	1.66	1.43	1.43	1.43
6∼10	0.40	2.24	2.33	2.20	2.20	2.20
11∼15	0.46	2.40	2.65	2.60	2.60	2.60
16∼20	0.50	2.50	2.80	2.75	2.75	2.85
21∼25	0.55	2.62	2.90	2.82	2.84	3.10
26∼30	0.55	2.65	2.96	2.91	3.02	3.52
31∼35	0.60	2.65	3.00	2.94	3.15	4.61
36∼40	0.60	2.70	3.05	2.96	3.40	5.46

Table 3.4: *LUT of* ΔSNR (dB)

3.5 Conclusion

The K-Best algorithm with adaptive modulation scheme was proposed in this chapter. A simplified approach was given to approximate the error probability with the minimum Euclidean distance events considered only. By estimating the performance gaps between the conventional union bound and the simplified union bound, accurate predictions were made on the BER performance of the K-Best algorithm with far fewer computations. From the simulations, the adaptive K-Best has guaranteed the BER performance with an approximately 94% to 99% reduction of computations compared with the conventional union bound in one search iteration. Future work will consider the performance in the cases of imperfect CSI and correlated channels.

The receiver side of MIMO systems is computation intensive, which scales with the number of antennas at the transmitter side. As a result, research in detection algorithms is accompanied

by the development of MIMO systems. However, with the proposition of massive MIMO systems, the design of receivers is less challenging compared to the difficulty that the transmitter side faces. Massive MIMO system deploys a large array of antennas at base station (BS), usually hundreds or even thousands, to serve tens of single-antenna user equipments (UEs). Following the scale up of antennas, the random channel becomes more deterministic, which leads to the adaptation of simple linear detectors that can achieve a good performance. A detailed introduction to the benefits that brought by massive MIMO systems will be presented in the following chapter.

The pilot contamination issue arises with the proposition of massive MIMO systems [69, 70]. To be more specific, the pilot sequences utilised in training-based uplink channel estimation can not all be orthogonal with each other under a limited coherence interval. As a result, the reuse of orthogonal pilots across different cells becomes a straight forward solution. However, the pilot reuse scheme causes inter-cell interference, which significantly influences the quality of CSI and constantly limits the overall performance of massive MIMO systems. In the next chapter, an uplink codebook design will be proposed to eliminate the pilot contamination effect.

Chapter 4
Achievable Rate Performance of TDD Multi-cell Massive MIMO with Non-Orthogonal Pilots

The advantages that offered by multiple-input multiple-output (MIMO) systems were discussed in Chapters 2 and 3. Basically, thanks to the deployment of multiple antennas at both the transmitter and receiver sides, the throughput was shown to be much enhanced, even under the channel with fading, interference and limited bandwidth conditions. However, signal processing complexity increases exponentially with the number of antennas deployed, especially at the receiver side. By thinking through both the advantages and challenges offered by the MIMO systems, various questions occur to researchers, such as, if the MIMO systems was scaled up, would it offer further advantages or would it create greater problems? After scaling up the system is named massive MIMO, or large-scale antennas MIMO systems, which was first introduced in [71] and studied in [72]. In the following four years, much literatures focused on the performance analysis, propositions for schemes involving both uplink and downlink transmissions and system optimizations.

This chapter describes an uplink pilot codebook design method for the multi-cell massive MIMO systems with time-division-duplex (TDD) operations, which aims to eliminate pilot contamination and increase the downlink achievable sum rate. Basically, the idea behind the proposition is to treat the pilot codebook design as a problem of optimal line packing in a Grassmannian manifold. A closed-form downlink achievable sum rate expression is proposed to demonstrate how the system performance is influenced by the cross-correlations between uplink pilots and the number of antennas at base station (BS). The simulation results have verified the proposition by comparing it with the pilot reuse scheme.

The chapter will be organized as follows: Section 4.1 will explain the purpose of this chapter, then it will offer a brief literature review of the massive MIMO systems. Section 4.2 will focus on the system model. Section 4.3 will explain the proposed downlink achievable sum rate

results. Section 4.4 will introduce the pilot reuse scheme and followed by the introduction of Grassmannian line packing (GLP) and its application for uplink channel estimation in Section 4.5. Finally, Section 4.6 will demonstrate the simulation results, together with the corresponding analysis, and it will also bring the chapter to a conclusion in Section 4.7.

4.1 Introduction

The massive MIMO systems are an advanced cellular network architecture that is regarded as a promising technology for the fifth generation of mobile communication technology standards network (5G) [71, 73–75]. Compared with the conventional multi-user MIMO systems, a large-array of antennas - i.e. hundreds or even thousands -has bee designed to be deployed at BS in the massive MIMO systems, which offers high data rate and robustness to tens, or even hundreds, of single-antenna user-equipments (UEs) within the same time-frequency resources. The utilization of excess antennas has solved many difficult technical issues and brought extra advantages, which will be described as follows:

- Firstly, the size of the channel matrix is enlarged along with the array of antennas, where the random matrix theory can be utilized for the analysis of channel characteristics. The channel gains inside the channel matrix tend to be pair-wisely orthogonal by utilizing the law of large numbers in the random channel matrix theory, which is considered to be a *favourable propagation* environment. As a result, the system capacity can be maximized under a desirable environment. Moreover, simple signal processing techniques, such as linear processing can achieve optimal performance in both uplink channel estimation and signal detection with much reduced computational complexity.
- Secondly, the massive MIMO systems guarantee high multiplexing gain. As long as the distance between antennas is large and rich scattering exists in the environment and signals will pass through channels with independent fading. Thus, the spatial multiplexing gain can be dramatically enhanced, which will increases the capacity significantly.
- Thirdly, the massive MIMO systems provide promising robustness. In LTE systems, there are typically 4 to 8 antennas at deployed at the BS [59], where the failure of one antenna unit may significantly influence the system performance. However, the massive MIMO systems deploy hundreds or even thousands of antennas, which do not suffer much overall impact on the whole system with the case of one or two antenna failures.

The benefits that are offered by massive MIMO systems relies heavily on an accurate channel estimation. For the detection at BS, channel state information (CSI) is required if the linear detection algorithms are utilized [9]. For beamforming, the deployment of more antennas means narrower beams, where the high quality CSI plays an important role in beamforming. Recent literature has focused on the research of channel estimation in both TDD and frequency-division-duplex (FDD) based massive MIMO systems [76–79]. However, TDD operation is preferred in massive MIMO systems because of channel reciprocity, where the training overhead depends only on the number of UEs rather on than the number of antennas at the BSs [27].

Pilot contamination is a common phenomenon that exists in the multi-user system with TDD operation, but it has become an issue that fundamentally limits the capacity of massive MIMO systems. In a pilot-aided uplink channel estimation, each UE should be assigned with an orthogonal pilot sequence, and pilot codebook is known by the BSs. Based on this known pilot codebook, the BSs estimate the CSI of the UEs in their home cell by various algorithms. However, in multi-cell systems, the allocation of orthogonal pilot sequence to each UE is impractical with a limited length of the coherence interval. Consequently, a common solution is to allocate orthogonal pilot sequences to a fraction of the UEs while the remainder are designed to reuse these pilots, this is known as *pilot reuse* scheme. If the BS receives the same pilot sequences from different UEs, it may degrade the accuracy of channel estimation, whereby this effect is known as *pilot contamination* phenomenon.

Related work: Following the initial idea massive MIMO systems, the researchers focused on the study of system capacity and performance analysis. In [70], the researchers provide a general overview and analysis of research directions in massive MIMO systems. Experimental results were based on the testbed with 128 BS antennas serving 4 UEs in a single-cell scenario, which shows a good performance of spectrum efficiency. A discussion of the optimal number of BS antennas is provided in [80]. The expressions of achievable sum rate for multi-cell massive MIMO systems were proposed with various linear precoders and detectors. The researchers believe that the deployment of the minimum mean squared errors (MMSE) algorithm for detection and zero-forcing (ZF) for precoding would perform better than the maximum ratio transmission (MRT) and eigenbeamforming.

In [81], both the spectrum and energy efficiency of massive MIMO systems have been investigated. The deployment of a large BS antenna array has been shown to provide a significant

increase in spectrum efficiency. However, the authors only considered small-scale fading and no large-scale fading in the simulations. The closed-form expressions of downlink achievable sum rates in the massive MIMO are proposed in [82]. The optimization of per UE rate, also known as "fairness", was implemented based on the proposed expression. However, the problem was that closed-form expression did not clearly show how the rate was influenced by pilot contamination.

Because the pilot contamination phenomenon is considered to be a principle factor that limits the system performance, numerous propositions were proposed to eliminate it. The existing channel estimation techniques in the massive MIMO system can generally be categorized into two schemes: (i) pilot-aided, and (ii) subspace-based schemes [69]. In [79], a detailed analysis is given regarding how the pilot contamination in the uplink influences the downlink achievable rates. Based on the proposed rate expression, the researchers believe that the rate will be saturated due to pilot contamination. Therefore, a downlink precoding scheme aiming at reducing both intra-cell and inter-cell interference was proposed.

In [83, 84], the pilot codebook was divided into several subsets while UEs were divided into cell-centre and cell-edge groups according to path-loss and shadowing. Following the division, one subset was reused and the remaining subsets were assigned to the remaining UEs. This pilot allocation improved the quality-of-service (QoS) of cell-edge UEs with the rate decrease of reused UEs as a compensation.

In [85] the researchers examined the covariance between the desired and the interfering UE channels because the channel estimation performance depends on the overlapping condition of their dominant subspaces. The pilot contamination was much reduced under the condition of limited angle of arrival at BS. In [86], an analysis was made on the allocation of UEs with a given number of antennas and coherence intervals. Other than the conventional pilot reuse scheme, the researchers in [87] first proposed the design of the pilot codebook with GLP method under the condition of not sufficiently large training section. In [88] the generalized welch bound equality sequence design was proposed. However, only a single-cell case was considered, while a multi-cell case is considered in [89]; the authors make an invalid assumption about power control.

Contributions: In contrast with pilot reuse schemes, this chapter has focused on the GLP based pilot codebook design. Although it is not the first time GLP has been applied to eliminate pilot

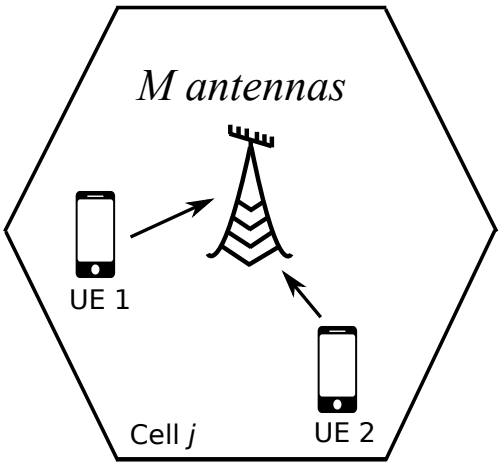

Figure 4.1: *Single-cell diagram of massive MIMO systems with* K *single-antenna UEs and a large array of* M *antennas at BS*

contamination, the aim of this chapter is to provide a comprehensive analysis of the downlink achievable rate improvements the system offers. Closed-form expressions of downlink achievable rate are proposed for both single-cell and multi-cell massive MIMO systems with TDD operations as these have clearly shown how the pilot contamination and BS antenna number influences the system's performance. Additionally, the closed-form expression of multi-cell massive MIMO systems with pilot reuse scheme for training sequence scheduling is proposed. Comparisons were made with conventional pilot reuse scheme and the numerical results showed that the GLP-based pilot design outperformed the pilot reuse scheme thereby bringing large gains in the system throughput.

4.2 System Model

4.2.1 Single-cell Massive MIMO System Model

A more general single-cell case without considering uplink power control is introduced before the multi-cell model. Consider a single-cell massive MIMO cellular network as illustrated in Figure.4.1, where a central BS equipped with an array of M antennas serving K single-antenna UEs. Note that $M \gg K$. A block-fading channel is considered and the channel vector from UE i to the BS can be represented as $\sqrt{\beta_i}\mathbf{h}_i$, where β_i represents the large-scale fading coefficient that models the effect of path-loss and shadowing; $\mathbf{h}_i$ represents the small-scale fading and vector contains independent and identically distributed (i.i.d) random variables

where $\mathbf{h}_i \in \mathcal{CN}(0, \mathbf{I}_M)$. It is assumed that the channel model $\sqrt{\beta_i}\mathbf{h}_i$ remains constant during one coherence interval.

4.2.1.1 Single-cell Uplink Channel Estimation

The single-cell uplink transmission starts with UEs sending their own training sequences to their home cell BS simultaneously. The UE i will be assigned a pilot sequence vector $\mathbf{s}_i$, where $\mathbf{s}_i \in \mathbb{C}^{\tau \times 1}$ has a length of τ samples and $\mathrm{E}[|\mathbf{s}_i|^2] = 1$. The correlation coefficient of pilot sequences between the UE i_1 and the UE i_2 is given as

$$\rho^2_{i_1,i_2} \triangleq |\mathbf{s}^H_{i_1}\mathbf{s}_{i_2}|^2, \tag{4.1}$$

where in the perfect orthogonality condition it has

$$\rho^2_{i_1,i_2} = \begin{cases} 0, & if \quad i_1 \neq i_2 \\ 1, & if \quad i_1 = i_2. \end{cases} \tag{4.2}$$

Non perfect orthogonality is considered in the system model, where the possible factors of orthogonality loss are the utilization of finite precision analog to digital converters (ADCs)or digital to analogue converters (DACs) at transmitter or receiver side. As mentioned in [70, 71], a large number of cheap antennas will be deployed at the BS in the massive MIMO systems. The finite precision devices might brings quantization noises, which causes the imperfect orthogonality between pilot sequences. The average impairment exists in both GLP-based uplink codebook and pilot reuse scheme, which is expressed as

$$\mathrm{E}\left[\rho^2_{i_1,i_2}\right] = \begin{cases} 0.01, & if \quad i_1 \neq i_2 \\ 0.99, & if \quad i_1 = i_2. \end{cases} \tag{4.3}$$

It is assumed that UEs send their uplink pilot sequence simultaneously to the BSs, where the received signal at BS j is expressed as

$$\mathbf{y} = \sum_{k=1}^{K} \sqrt{p^{\mathrm{u}}_k \beta_k}\mathbf{S}_k\mathbf{h}_k + \mathbf{n}_j, \tag{4.4}$$

where $\mathbf{y} \in \mathbb{C}^{\tau M \times 1}$ is the received signal; p^{u}_k denotes the uplink transmit power; $\mathbf{n}_j \in \mathbb{C}^{\tau M \times 1}$

represents additive white Gaussian noise (AWGN) at the BS with elements $n_M \in \mathcal{CN}(0, \sigma_{\mathrm{n}}^2 \mathbf{I}_M)$; $\mathbf{S}_k \in \mathbb{C}^{\tau M \times M}$ denotes the matrix including the pilot sequence from UE k to BS j and $\mathbf{S}_k = s_k \otimes \mathbf{I}_M$. Once the BS receives the uplink training sequences, the least-squares (LS) method is applied for estimating CSI [90], where the estimated CSI of UE i is represented as

$$\begin{aligned}\hat{\mathbf{h}}_i &= \frac{1}{\sqrt{p_i^{\mathrm{u}}}}\mathbf{S}_i^H \mathbf{y} \\ &= \underbrace{\sqrt{\beta_i}\mathbf{h}_i}_{\text{desired CSI}} + \underbrace{\frac{1}{\sqrt{p_i^{\mathrm{u}}}}\left(\sum_{k\neq i}^{K}\sqrt{p_k^{\mathrm{u}}\beta_k}\rho_{i,k}\mathbf{h}_k + \mathbf{S}_i^H \mathbf{n}_j\right)}_{\text{interferece \& noise}}.\end{aligned} \tag{4.5}$$

Equation (4.5) shows that the channel estimation result consists the desired CSI and interference. The intra-cell interference exists if $K > \tau$, where $\rho_{i,k} \neq 0$. Otherwise, if the assigned pilots are all orthogonal, the intra-cell interference vanishes and only thermal noise is left.

4.2.1.2 Single-cell Downlink Transmission

Recall that reciprocity in the TDD operation leads to a downlink transmission utilizes the estimated CSI in uplink training. The maximum ratio transmission (MRT) scheme is applied for downlink precoding [91], where the received noisy signal for UE i is expressed as

$$r_i = \sum_{k=1}^{K}\sqrt{p_i^{\mathrm{d}}\beta_i}\mathbf{h}_i^H \mathbf{t}_k x_k + z_i, \tag{4.6}$$

where p_i^{d} is the downlink transmit power; $\sqrt{\beta_i}\mathbf{h}_i^H$ denotes the downlink CSI, which utilized the uplink CSI; z_i represents the AWGN and $z_i \in \mathcal{CN}(0, \sigma_z^2 \mathbf{I}_M)$; x_k represents the data symbols streams to UE k and $\mathbf{t}_k$ is MRT linear precoding vector, which is expressed as

$$\mathbf{t}_k = \frac{\hat{\mathbf{h}}_k}{\|\hat{\mathbf{h}}_k\|}. \tag{4.7}$$

4.2.2 Multi-cell Massive MIMO System Model

Consider a multi-cell massive MIMO cellular network with TDD operation, where multiple central BS equipped with an array of M antennas serving K single-antenna UEs and is illustrated in Figure.4.2. Note that $M \gg K$. A block-fading channel is considered and the channel vector from UE i in cell j to the BS l can be represented as $\sqrt{\beta_{ij,l}}\mathbf{h}_{ij,l}$, where $\beta_{ij,l}$ represents

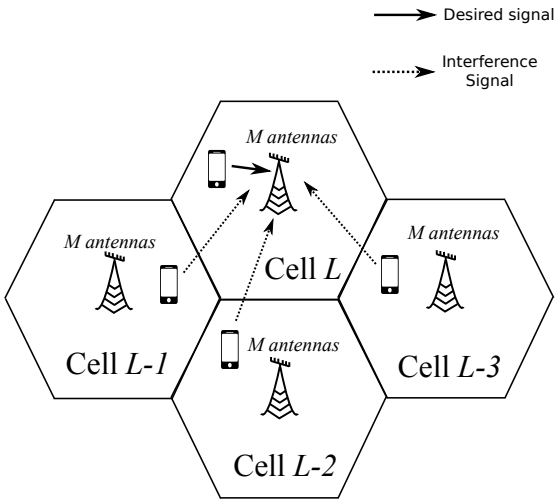

Figure 4.2: *Cell diagram of massive MIMO systems with* L *cells,* K *single-antenna UEs and a large array of* M *antennas at BS*

the large-scale fading coefficient that models the effect of path-loss and shadowing; $\mathbf{h}_{ij,l}$ represents the small-scale fading and vector contains independent and identically distributed (i.i.d) random variables where $\mathbf{h}_{ij,l} \in \mathcal{CN}(0, \mathbf{I}_M)$. It is assumed that the channel model $\sqrt{\beta_{ij,l}}\mathbf{h}_{ij,l}$ remains constant during one coherence interval.

4.2.2.1 Multi-cell Uplink Channel Estimation

The multi-cell uplink transmission starts with UEs sending their own training sequences to their home cell BS simultaneously. The UE i in cell j will be assigned a pilot sequence vector $\mathbf{s}_{ij}$, where $\mathbf{s}_{ij} \in \mathbb{C}^{\tau \times 1}$ has a length of τ samples and $\mathrm{E}[|\mathbf{s}_{ij}|^2] = 1$. The correlation coefficient of pilot sequences between the UE i_1 and the UE i_2 in cell j is given as

$$\rho^2_{i_1 j, i_2 j} \triangleq |\mathbf{s}^H_{i_1 j} \mathbf{s}_{i_2 j}|^2, \tag{4.8}$$

where in the perfect orthogonality condition it has

$$\rho^2_{i_1 j, i_2 j} = \begin{cases} 0, & if \quad i_1 \neq i_2 \\ 1, & if \quad i_1 = i_2. \end{cases} \tag{4.9}$$

It is assumed that UEs send their uplink pilot sequence simultaneously and the BS received the uplink pilot sequence from both the home cell and the other $L - 1$ cells synchronously, where

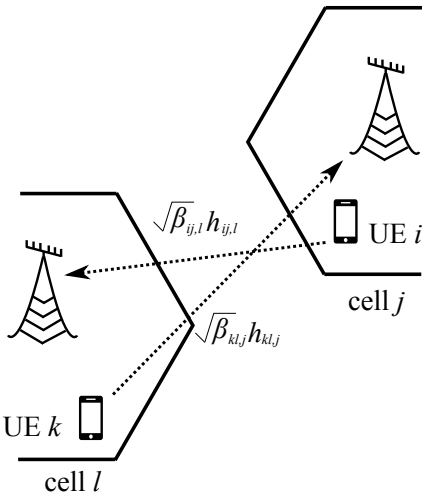

Figure 4.3: *Cell diagram of massive MIMO systems with* L *cells,* K *single-antenna UEs and a large array of M antennas at BS*

the received signal at BS j is expressed as

$$\begin{aligned}\mathbf{y}_j &= \underbrace{\sum_{k=1}^{K}\sqrt{p_{kj}^{\mathrm{u}}\beta_{kj,j}}\mathbf{S}_{kj}\mathbf{h}_{kj,j}}_{\text{cell } j} + \underbrace{\sum_{l\neq j}^{L}\sum_{k=1}^{K}\sqrt{p_{kl}^{\mathrm{u}}\beta_{kl,j}}\mathbf{S}_{kl}\mathbf{h}_{kl,j}}_{\text{other } L-1 \text{ cells}} + \mathbf{n}_j \\ &= \sum_{l=1}^{L}\sum_{k=1}^{K}\sqrt{p_{kl}^{\mathrm{u}}\beta_{kl,j}}\mathbf{S}_{kl}\mathbf{h}_{kl,j} + \mathbf{n}_j, \end{aligned} \tag{4.10}$$

where $\mathbf{y}_j \in \mathbb{C}^{\tau M\times 1}$ is the received signal; p_{kj}^{u} denotes the uplink transmit power; $\mathbf{n}_j \in \mathbb{C}^{\tau M\times 1}$ represents additive white Gaussian noise (AWGN) at the BS with elements $n_M \in \mathcal{CN}(0,\sigma_{\mathrm{n}}^2\mathbf{I}_M)$; $\mathbf{S}_{kj} \in \mathbb{C}^{\tau M\times M}$ denotes the matrix includes the pilot sequence from UE k to BS j and $\mathbf{S}_k = s_k \otimes \mathbf{I}_M$. Once the BS receives the uplink training sequences, the LS method is applied for estimating CSI, where the estimated CSI of UE i is represented as

$$\begin{aligned}\hat{\mathbf{h}}_{ij,j} &= \frac{1}{\sqrt{p_{ij}^{\mathrm{u}}}}\mathbf{S}_{ij}^T\mathbf{y}_j \\ &= \sqrt{\beta_{ij,j}}\mathbf{h}_{ij,j} + \frac{1}{\sqrt{p_{ij}^{\mathrm{u}}}}\left(\sum_{k\neq i}^{K}\sqrt{p_{kj}^{\mathrm{u}}\beta_{kj,j}}\rho_{ij,kj}\mathbf{h}_{kj,j} + \sum_{l\neq j}^{L}\sum_{k=1}^{K}\sqrt{p_{kl}^{\mathrm{u}}\beta_{kl,j}}\rho_{ij,kl}\mathbf{h}_{kl,j} + \mathbf{S}_{ij}^T\mathbf{n}_j\right). \end{aligned} \tag{4.11}$$

Equation (4.11) shows how the correlation between uplink training sequences influence the accuracy of estimation result. If there is no pilot contamination exists, the desired CSI is only affected by thermal noise. However, due to the limited coherence interval and large number of UEs, pilot contamination is difficult to be eliminated. Therefore, an uplink training scheme with mitigation of the pilot correlation becomes important to the system.

4.2.2.2 Multi-cell Downlink Transmission

It is assumed that the estimated CSI in uplink training is utilized in downlink transmission because of channel reciprocity in TDD operation. The MRT scheme is applied in downlink precoding, where the received noisy signal by UE i in cell j is expressed as

$$\begin{aligned} r_{ij} &= \underbrace{\sqrt{p_{ij}^{\mathrm{d}}\beta_{ij,j}}\mathbf{h}_{ij,j}^{H}(\sum_{k=1}^{K}\mathbf{h}_{ij,j}^{H}\mathbf{t}_{ij,j}x_{ij,j})}_{cell\ j} + \underbrace{\sum_{l\neq j}^{L}\sum_{k=1}^{K}\sqrt{p_{il}^{\mathrm{d}}\beta_{ij,l}}\mathbf{h}_{ij,l}^{H}\mathbf{t}_{kl,l}x_{kl,l}}_{other\ L-1\ cells} + z_{ij} \\ &= \sum_{l=1}^{L}\sum_{k=1}^{K}\sqrt{p_{ij,l}^{\mathrm{d}}\beta_{ij,l}}\mathbf{h}_{ij,l}^{H}\mathbf{t}_{kl,l}x_{kl,l} + z_{ij}, \end{aligned} \tag{4.12}$$

where p_{ij}^{d} is the downlink transmit power; $\sqrt{\beta_{ij,j}}\mathbf{h}_{ij,j}^{H}$ denotes the downlink CSI, which utilized the uplink CSI; z_{ij} represents the AWGN and $z_{ij} \in \mathcal{CN}(0, \sigma_{\mathrm{w}}^{2}\mathbf{I}_{M})$; $x_{kl,l}$ represents the data symbols streams to UE k in cell l from BS l and $\mathbf{t}_{kl,l}$ is linear precoding vector where $\mathbf{t}_{kl,l} = \frac{\hat{\mathbf{h}}_{kl,l}}{\|\hat{\mathbf{h}}_{kl,l}\|}$.

4.3 Downlink Achievable Sum Rate

4.3.1 Single-cell Massive MIMO Achievable Sum Rate

As mentioned above, the law of large numbers in random matrix theory is utilized in analysing the characteristics of the massive MIMO channel, which defines the asymptotic orthogonality between channels because of the utilization of a large antenna array at the BS. If the assumption is made that the number of BS antennas increase to infinity, the following results, known as

asymptotically favourable propagation environment [27, 81, 88], is expressed as

$$\lim_{M\to\infty}\frac{1}{M}\mathbf{h}_i^H\mathbf{h}_j=\begin{cases}0, & \text{if } i\neq j\\ 1, & \text{if } i=j.\end{cases} \tag{4.13}$$

The results in (4.13) can be applied to simplify the denominator of downlink precoding vector $\|\hat{\mathbf{h}}_i\|$, where

$$\|\hat{\mathbf{h}}_i\|=\sqrt{\|\hat{\mathbf{h}}_i\|^2}=\sqrt{\hat{\mathbf{h}}_i^H\hat{\mathbf{h}}_i}. \tag{4.14}$$

The term $\hat{\mathbf{h}}_i^H\hat{\mathbf{h}}_i$ can be simplified as

$$\begin{aligned}\hat{\mathbf{h}}_i^H\hat{\mathbf{h}}_i&=\frac{1}{\sqrt{p_i^{\mathrm{u}}}}\left(\sum_{n_1=1}^{K}\sqrt{p_{n_1}^{\mathrm{u}}\beta_{n_1}}\rho_{i,n_1}\mathbf{h}_{n_1}+\mathbf{S}_i^H\mathbf{n}_j\right)^H\times\frac{1}{\sqrt{p_i^{\mathrm{u}}}}\left(\sum_{n_2=1}^{K}\sqrt{p_{n_2}^{\mathrm{u}}\beta_{n_2}}\rho_{i,n_2}\mathbf{h}_{n_2}+\mathbf{S}_i^T\mathbf{n}_j\right)\\&=\frac{1}{p_i^{\mathrm{u}}}\sum_{n_1=1}^{K}\sum_{n_2=1}^{K}\sqrt{p_{n_1}^{\mathrm{u}}\beta_{n_1}}\sqrt{p_{n_2}^{\mathrm{u}}\beta_{n_2}}\rho_{i,n_1}\rho_{i,n_2}\mathbf{h}_{n_1}^H\mathbf{h}_{n_2}+\frac{1}{p_i^{\mathrm{u}}}\sum_{n_1=1}^{K}\sqrt{p_{n_1}^{\mathrm{u}}\beta_{n_1}}\rho_{i,n_1}\mathbf{h}_{n_1}^H\mathbf{S}_i^H\mathbf{n}_j\\&+\frac{1}{p_i^{\mathrm{u}}}\sum_{n_2=1}^{K}\sqrt{p_{n_2}^{\mathrm{u}}\beta_{n_2}}\rho_{i,n_2}\mathbf{n}_j^H\mathbf{S}_i\mathbf{h}_{n_2}+\frac{1}{p_i^{\mathrm{u}}}\mathbf{n}_j^H\mathbf{S}_i\mathbf{S}_i^T\mathbf{n}_j\end{aligned} \tag{4.15}$$

Then, $\mathrm{E}\|\hat{\mathbf{h}}_i^H\hat{\mathbf{h}}_i\|$ is expressed as

$$\begin{aligned}\mathrm{E}\|\hat{\mathbf{h}}_i^H\hat{\mathbf{h}}_i\|&=\frac{1}{p_i^{\mathrm{u}}}\sum_{n_1=1}^{K}\sum_{n_2=1}^{K}\sqrt{p_{n_1}^{\mathrm{u}}\beta_{n_1}}\sqrt{p_{n_2}^{\mathrm{u}}\beta_{n_2}}\rho_{i,n_1}\rho_{i,n_2}\mathrm{E}\left[\mathbf{h}_{n_1}^H\mathbf{h}_{n_2}\right]+\frac{1}{p_i^{\mathrm{u}}}\mathrm{E}\left[\mathbf{n}_j^H\mathbf{S}_i\mathbf{S}_i^T\mathbf{n}_j\right]\\&=\beta_iM+\frac{1}{p_i^{\mathrm{u}}}\Bigg(\sum_{n_1=n_2\neq i}^{K}p_{n_1}^{\mathrm{u}}\beta_{n_1}\rho_{i,n_1}^2\mathrm{E}\left[\mathbf{h}_{n_1}^H\mathbf{h}_{n_1}\right]\\&+\sum_{n_1\neq n_2}^{K}\sqrt{p_{n_1}^{\mathrm{u}}\beta_{n_1}}\sqrt{p_{n_2}^{\mathrm{u}}\beta_{n_2}}\rho_{i,n_1}\rho_{i,n_2}\mathrm{E}\left[\mathbf{h}_{n_1}^H\mathbf{h}_{n_2}\right]+\mathrm{E}\left[\mathrm{tr}(\mathbf{S}_i^H\mathbf{n}_j\mathbf{n}_j^H\mathbf{S}_i)\right]\Bigg)\\&=M\left(\frac{1}{p_i^{\mathrm{u}}}\sum_{n=1}^{K}\left(p_n^{\mathrm{u}}\beta_n\rho_{i,n}^2+\sigma^2\right)\right)=M\alpha_{i,n}.\end{aligned} \tag{4.16}$$

The UE received signal can be derived into the form of the desired signal plus the effective noise, where the effective noise includes the intra-cell interference and thermal noise [79]. Let $g_i=\sqrt{p_i^{\mathrm{d}}\beta_i}\mathbf{h}_i^H\mathbf{t}_i$, then the received signal of UE i is represented as

$$r_i=\mathbb{E}[g_i]x_i+z_i^{'}, \tag{4.17}$$

where $z_i^{'}$ represents the effective noise and is expressed as

$$z_i^{'} = (g_i - \mathbb{E}[g_i])x_i + \left(\sum_{k \neq i}^{K} g_k x_k\right) + z_i. \tag{4.18}$$

The expression of received signal in (4.17) and the effective noise in (4.18) follows the methods proposed in [79, 92, 93]. It is assumed that for pilot-aided channel estimation, each estimated instantaneous CSI is known by the BS. It is also assumed that the UEs know the expectation of channel $\mathbb{E}[g_i]$ not the instantaneous CSI. It is because the distribution of channel is straightforward to calculate. Refer to the instantaneous CSI, as the assumption has been made on single-antenna UEs, the CSI between one UE and BS is a scaler. Consequently, for the detection of downlink signal at the UE side, the CSI is not as important as the detection in MIMO systems. Following these assumptions, in [80], an ergodic downlink achievable rate of UE i is proposed, which is given as

$$\begin{aligned} R_i^{\mathrm{d}} &= \left(1 - \frac{\tau}{T}\right) \log_2\left(1 + \gamma_i^{\mathrm{d}}\right) \\ &= \left(1 - \frac{\tau}{T}\right) \log_2 \left(1 + \frac{\left(\mathrm{E}\left[\mathbf{h}_i^H \mathbf{t}_i\right]\right)^2 \beta_i p_i^{\mathrm{d}}}{\mathrm{Var}\left[\mathbf{h}_i^H \mathbf{t}_i\right] \beta_i p_i^{\mathrm{d}} + \sum\limits_{m \neq i}^{K} \mathrm{E}\left|\mathbf{h}_i^H \mathbf{t}_m\right|^2 \beta_i p_m^{\mathrm{d}} + \sigma_{\mathrm{D}}^2} \right), \end{aligned} \tag{4.19}$$

where γ_i denotes the downlink SINR of UE i, and $\mathrm{Var}\left[\mathbf{h}_i^H \mathbf{t}_i\right]$ is defined as $\mathrm{Var}\left[\mathbf{h}_i^H \mathbf{t}_i\right] = \mathrm{E}|\left(\mathbf{h}_i^H \mathbf{t}_i - \mathrm{E}\left[\mathbf{h}_i^H \mathbf{t}_i\right]\right)|^2$. Based on equation (4.19), the following theorem is proposed with a closed-form expression of downlink rate in single-cell massive MIMO system.

Theorem 1. *Consider a single-cell massive MIMO system with TDD operation utilizing LS method for uplink channel estimation and MRT method for downlink precoding, the following rates are achievable for UE i in downlink transmission*

$$R_i^d = \left(1 - \frac{\tau}{T}\right) \log_2\left(1 + \gamma_i^d\right) \tag{4.20}$$

where γ_{ij}^d denotes the SINR of UE i. The closed-form expression of SINR γ_i^d is proposed and expressed as

$$\gamma_{ij}^d = \frac{M \beta_i^2 p_i^d}{\alpha_{i,n} \left(\beta_i p_i^d + \sum\limits_{m \neq i}^{K} \left(1 + \frac{M \beta_i p_i^u \rho_{m,i}^2}{p_m^u \alpha_{m,n}}\right) \beta_i p_m^d + \sigma_w^2 \right)}, \tag{4.21}$$

with $\alpha_{i,n} = \sum_{n=1}^{K} \frac{1}{p_i^{\mathrm{u}}} \left(\beta_n \rho_{i,n}^2 + \sigma_w^2 \right)$.

Proof. See Appendix. □

The proposed closed-form expression can be utilized to study the downlink throughput of single-cell massive MIMO system. The more important feature is that it clearly shows how the number of BS antennas and intra-cell interference limits the system throughput.

4.3.2 Multi-cell Massive MIMO Downlink Achievable Sum Rate

The result of the asymptotically favourable propagation environment can also be applied in deriving the downlink achievable sum rate in multi-cell scenario, which is expressed as

$$\lim_{M\to\infty} \frac{1}{M} \mathbf{h}_{ij,j}^H \mathbf{h}_{kj,j} = \begin{cases} 0, & \text{if } i \neq k \\ 1, & \text{if } i = k. \end{cases} \tag{4.22}$$

The results shown in (4.22) are the channel of UE i and UE k in cell j. It can also be extended into multi-cell case. Following this result, the term $\hat{\mathbf{h}}_{ij,j}^H \hat{\mathbf{h}}_{ij,j}$ is simplified as

$$\begin{aligned} \hat{\mathbf{h}}_{ij,j}^H \hat{\mathbf{h}}_{ij,j} = & \frac{1}{\sqrt{p_{ij}^{\mathrm{u}}}} \left(\sum_{l_1=1}^{L} \sum_{n_1=1}^{K} \sqrt{p_{n_1 l_1}^{\mathrm{u}} \beta_{n_1 l_1, j}} \rho_{ij, n_1 l_1} \mathbf{h}_{n_1 l_1, j} + \mathbf{S}_{ij}^T \mathbf{n}_j \right)^H \times \\ & \frac{1}{\sqrt{p_{ij}^{\mathrm{u}}}} \left(\sum_{l_2=1}^{L} \sum_{n_2=1}^{K} \sqrt{p_{n_2 l_2}^{\mathrm{u}} \beta_{n_2 l_2, j}} \rho_{ij, n_2 l_2} \mathbf{h}_{n_2 l_2, j} + \mathbf{S}_{ij}^T \mathbf{n}_j \right) \\ = & \frac{1}{p_{ij}^{\mathrm{u}}} \sum_{l_1=1}^{L} \sum_{n_1=1}^{K} \sum_{l_2=1}^{L} \sum_{n_2=1}^{K} \sqrt{p_{n_1 l_1}^{\mathrm{u}} \beta_{n_1 l_1, j}} \sqrt{p_{n_2 l_2}^{\mathrm{u}} \beta_{n_2 l_2, j}} \rho_{ij, n_1 l_1} \rho_{ij, n_2 l_2} \mathbf{h}_{n_1 l_1, j}^H \mathbf{h}_{n_2 l_2, j} \\ & + \frac{1}{p_{ij}^{\mathrm{u}}} \sum_{l_1=1}^{L} \sum_{n_1=1}^{K} \sqrt{p_{n_1 l_1}^{\mathrm{u}} \beta_{n_1 l_1, j}} \rho_{ij, n_1 l_1} \mathbf{h}_{n_1 l_1, j}^H \mathbf{S}_{ij}^T \mathbf{n}_j \\ & + \frac{1}{p_{ij}^{\mathrm{u}}} \sum_{l_2=1}^{L} \sum_{n_2=1}^{K} \sqrt{p_{n_2 l_2}^{\mathrm{u}} \beta_{n_2 l_2, j}} \rho_{ij, n_2 l_2} \mathbf{n}_j^H \mathbf{S}_{ij} \mathbf{h}_{n_2 l_2, j} + \frac{1}{p_{ij}^{\mathrm{u}}} \mathbf{n}_j^H \mathbf{S}_{ij} \mathbf{S}_{ij}^T \mathbf{n}_j \end{aligned} \tag{4.23}$$

Consequently, $\mathrm{E}\|\hat{\mathbf{h}}_{ij,j}^H \hat{\mathbf{h}}_{ij,j}\|$ can be simplified as

$$\begin{aligned}
&\mathrm{E}\|\hat{\mathbf{h}}_{ij,j}^H \hat{\mathbf{h}}_{ij,j}\| \\
&= \beta_{ij,j} M + \frac{1}{p_{ij}^{\mathrm{u}}} \sum_{n_1=n_2\neq i}^{K} p_{n_1 j}^{\mathrm{u}} \beta_{n_1 j,j} \rho_{ij,n_1 j}^2 M + \frac{1}{p_{ij}^{\mathrm{u}}} \sum_{l_1=l_2\neq j}^{L} \sum_{n_1=n_2}^{K} p_{n_1 l_1}^{\mathrm{u}} \beta_{n_1 l_1,j} \rho_{ij,n_1 l_1}^2 M + M\sigma^2 \\
&= M \left(\frac{1}{p_{ij,j}} \sum_{l=1}^{L} \sum_{n=1}^{K} \left(p_{nl}^{\mathrm{u}} \beta_{nl} \rho_{ij,nl}^2 + \sigma^2 \right) \right) = M \alpha_{ij,nl}
\end{aligned} \tag{4.24}$$

As a result, the precoding vector $\mathbf{t}_{ij,j}$ from BS j to UE i in cell j can also be expressed as

$$\mathbf{t}_{ij,j} = \frac{\hat{\mathbf{h}}_{ij,j}}{\sqrt{M \alpha_{ij,nl}}}. \tag{4.25}$$

In a multi-cell scenario, the received signal at the UE side can also be interpreted as the desired signal and effective noise, where the effective noise includes both possible intra-cell and inter-cell interference plus thermal noise. Let $g_{ij} = \sqrt{p_{ij}^{\mathrm{d}} \beta_{ij,j}} \mathbf{h}_{ij,j}^H \mathbf{t}_{ij}$, then the received signal of UE i in cell j is represented as

$$r_{ij} = \mathbb{E}[g_{ij}] x_{ij} + z_{ij}^{'}, \tag{4.26}$$

where $z_i^{'}$ represents the effective noise and is expressed as

$$z_{ij}^{'} = (g_{ij} - \mathbb{E}[g_{ij}]) x_{ij} + \sum_{k\neq i}^{K} g_{kj} x_{kj} + \sum_{l\neq j}^{L} \sum_{k=1}^{K} g_{kl} x_{kl} + z_{ij}. \tag{4.27}$$

The multi-cell ergodic downlink achievable rate of UE i in cell j is given as [80]

$$R_{ij}^{\mathrm{d}} = \left(1 - \frac{\tau}{T}\right) \log_2 \left(1 + \gamma_{ij}^{\mathrm{d}}\right), \tag{4.28}$$

with the downlink SINR γ_{ij}^{d} expressed as

$$\gamma_{ij}^{\mathrm{d}} = \frac{\left(\mathrm{E}\left[\mathbf{h}_{ij,j}^H \mathbf{t}_{ij,j}\right]\right)^2 \beta_{ij,j} p_{ij}^{\mathrm{d}}}{\mathrm{Var}\left[\mathbf{h}_{ij,j}^H \mathbf{t}_{ij,j}\right] \beta_{ij,j} p_{ij,j}^{\mathrm{d}} + \sum_{m\neq i}^{K} \mathrm{E}\left|\mathbf{h}_{ij,j}^H \mathbf{t}_{mj,j}\right|^2 \beta_{ij,j} p_{mj}^{\mathrm{d}} + \sum_{l\neq j}^{L} \sum_{k=1}^{K} \mathrm{E}\left|\mathbf{h}_{ij,l}^H \mathbf{t}_{kl,l}\right|^2 \beta_{ij,l} p_{kl}^{\mathrm{d}} + \sigma_{\mathrm{D}}^2} \tag{4.29}$$

Based on Equation (4.28), the following closed-form ergodic downlink achievable sum rate is proposed.

Theorem 2. *Consider a multi-cell massive MIMO system with TDD operation utilizing the LS*

method as uplink channel estimation and MRT method as downlink precoding, the following rates are achievable for UE i of cell j in downlink transmission

$$R_{ij}^{d} = \left(1 - \frac{\tau}{T}\right) \log_2 \left(1 - \gamma_{ij}^{d}\right) \tag{4.30}$$

where γ_{ij}^{d} denotes the SINR of UE i which is expressed as

$$\gamma_{ij}^{d} = \frac{M\beta_{ij,j}^{2} p_{ij}^{d}}{\alpha_{ij,nm}\left(\beta_{ij,j} p_{ij}^{d} + \sum\limits_{m\neq i}^{K}\left(1 + \frac{M\beta_{ij,j} p_{ij}^{u} \rho_{mj,ij}^{2}}{p_{mj}^{u}\alpha_{mj,nm}}\right)\beta_{ij,j} p_{mj}^{d} + \sum\limits_{l\neq j}^{L}\sum\limits_{k=1}^{K}\left(1 + \frac{M\beta_{il,l} p_{il}^{u} \rho_{kl,ij}^{2}}{p_{kl}^{u}\alpha_{kl,nm}}\right)\beta_{il,l} p_{kl}^{d} + \sigma^{2}\right)}, \tag{4.31}$$

with $\alpha_{ij,nm} = \sum\limits_{m=1}^{L}\sum\limits_{n=1}^{K} \frac{1}{p_{ij}^{u}}\left(\beta_{nm,j}\rho_{ij,nm}^{2} + \sigma_{D}^{2}\right)$.

Proof. See Appendix. □

The achievable rates expression given in Theorem 2 has clearly demonstrated how the system spectrum efficiency might be affected by correlations between pilot sequence and number of BS antennas. Both intra- and inter-cell interference will lead to non-zero correlations in the denominator of SINR expression which degrades the achievable rate. To maximize the achievable rate, the ideal case is that each UE assigned a uplink training sequence which is orthogonal with each other and interference will vanish.

4.4 Pilot Reuse Scheme

The pilot reuse is a common scheme that utilized in the multi-cell massive MIMO system for the pilot sequence distribution. Due to the limited length of the coherence interval, it is difficult to assign an orthogonal pilot signal to each UE. As a result, non-orthogonal pilot codebooks have to be adopted. If the orthogonal pilot codebook can satisfy the UEs in N cells, then the remaining $L - N$ cells are going to reuse these pilot sequences. The pilot reuse scheme that utilized in this thesis is based on the traditional frequency division multiple access (FDMA) with different reuse factors (RF) considered. There is a trade-off between RF and training overhead. If a bigger RF value is utilized, there will be fewer UEs that suffer inter-cell interference

and the downlink rate might be improved. However, a bigger RF value means a bigger training overhead, which might limit the downlink transmission. The following closed-form expression of downlink achievable sum rate with the pilot reuse scheme is proposed for the performance analysis.

Corollary 1. *If we assume the condition of perfect orthogonality between pilots and pilot reuse factor RF is positive integer which is larger or equal to 1, the achievable downlink rate of each UE with pilot reuse scheme for uplink channel estimation is given as*

$$R_{ij}^{d,pr} = \left(1 - \frac{\tau}{T}\right) \log_2 \left(1 - \gamma_{ij}^{d,pr}\right) \tag{4.32}$$

where $\gamma_{ij}^{d,pr}$ denotes the SINR of UE i in cell j using pilot reuse scheme which is expressed by

$$\gamma_{ij}^{d,pr} = \frac{M\beta_{ij,j}^2 p_{ij}^d}{\alpha_{ij,nm}\left(\sum\limits_{k=1}^{K} \beta_{ij,j} p_{kj}^d + \xi_{l_1} + \xi_{l_2} + \xi_{l_3} + \sigma_D^2\right)} \tag{4.33}$$

with

- $\xi_{l_1} = \sum\limits_{l_1 \neq j}^{L - \frac{L}{RF}} \sum\limits_{k_1=1}^{K} \beta_{ij,l_1} p_{k_1 l_1}^d$
- $\xi_{l_2} = \sum\limits_{l_2 \neq j}^{L/RF} \sum\limits_{k_2=1}^{K-1} \beta_{ij,l_2} p_{k_2 l_2}^d$
- $\xi_{l_3} = \sum\limits_{l_2 \neq j}^{L/RF} \sum\limits_{k_3}^{1} \left(1 + \frac{M\beta_{il_2,l_2} p_{il_2}^u}{p_{k_3 l_2}^u \alpha_{k_3 l_2,nl}}\right) \beta_{il_2,l_2} p_{k_3 l_2}^d$

Proof. Under the assumption that pilot reuse factor RF is positive integer and $RF \geq 1$, we have the number of UEs who are assigned orthogonal pilots is $\left(L - \frac{L}{RF}\right) \times K + \frac{L}{RF} \times (K-1)$. If there is perfect orthogonality between pilots, it comes to $\rho = 0$. The other $\frac{L}{RF}$ UEs reuse the pilot which comes to $\rho = 1$. As a result, equation (4.31) can be simplified and we can have the closed-form expression of downlink achievable rate using pilot reuse scheme. □

With given cell numbers and RF, the equation (4.32) clearly shows the impact to the downlink achievable rate with different RF values.

4.5 Grassmannian Line Packing based Pilot Design

Other than the pilot reuse scheme, the pilot codebook design can also be treated as a line packing problem in an Grassmannian manifold. The GLP problem is to find a optimal packing of N one-dimensional subspaces in a M-dimensional complex vector space by maximizing the minimum pairwise distance between subspaces [94]. It is a classic mathematical problem which has been well studied for downlink transmission for beamforming codebook design in the conventional multi-user MIMO systems [95, 96]. Inspired by this application, it is considered here in the pilot sequence design. In this section, we will introduce the GLP problem and investigate the application to the pilot sequence design for uplink channel estimation.

Consider two 1-dimensional unit vectors $\mathbf{w}_i$ and $\mathbf{w}_j$ all belong to a matrix Φ_M with $\mathbf{w}_i \equiv \mathbf{w}_j$. The equivalence of two vectors can be seen as two lines with same length in a complex vector space $\mathbb{C}^M$. The two lines can also be seen as two one-dimensional subspaces in $\mathbb{C}^M$. The set of all the one-dimensional subspaces in $\mathbb{C}^M$ is denoted as $\mathcal{G}(m, 1)$, which forms a Grassmann Manifold. Assume that there are N one-dimensional subspaces in the Grassmann manifold $\mathcal{G}(m, 1)$, the GLP problem is to find a codebook with optimally packing of these N subspaces, i.e. the N subspaces are equally separated in space with the largest possible adjacent distances. The GLP problem can be formulated as

$$\max_{\mathbf{s}_i, \mathbf{s}_j \in \mathcal{G}(m,1)} \quad \min_{i \neq j} \quad d_c\left(\mathbf{s}_i, \mathbf{s}_j\right), \tag{4.34}$$

where d_c denotes the distance between vector $\mathbf{s}_i$ and $\mathbf{s}_j$. In the Grassmann manifold, different metrics have been proposed for defining the distance between codewords. One is the choral distance. For the choral distance between two 1-dimensional subspace is expressed as

$$d_{ch}(\mathbf{s}_i, \mathbf{s}_j) = \sin\left(\theta_{1,2}\right) = \sqrt{1 - |\mathbf{s}_i^H \mathbf{s}_j|^2}. \tag{4.35}$$

The other one is the Fubini-Study distance, which is expressed as

$$d_{fs}(\mathbf{s}_i, \mathbf{s}_j) = \arccos |\det\left(\mathbf{s}_i^H \mathbf{s}_j\right)|. \tag{4.36}$$

The choral distance is chosen here as the distance metric, because of its previous application in downlink achievable rate analysis [97].

The GLP method can also be utilized in pilot sequence design. If each UE is assigned a training

$$SINR_{i,j} = \frac{\beta_{i,j} p_{i,j}}{\beta_{i,j}\left(\rho_G^2 \sum\limits_{k\neq i}^{K} p_{k,j} + \frac{K\rho_G^2+\sigma_{\mathrm{w}}^2}{M} \sum\limits_{m=1}^{K} p_{m,j}\right) + \sum\limits_{l\neq j}^{L}\sum\limits_{\bar{k}=1}^{K} \beta_{i,l} p_{\bar{k},l} \frac{(M+K)\rho_G^2+\sigma_{\mathrm{w}}^2}{M} + \frac{K\rho_G^2+\sigma_{\mathrm{w}}^2}{M}\sigma_i^2} \tag{4.37}$$

sequence with length τ and there are totally K UEs in the L cells, it forms a $\tau \times K$ matrix with the pilot sequence as the row vector. Due to the limited length of τ, it is not possible to assign each UE with orthogonal pilots in a TDD massive MIMO system. As a result, in the pilot reuse scheme [83], only some of the UEs are assigned with orthogonal pilots and the other UEs reuse these pilots. However, the pilot sequences can be treated as packing K one-dimensional subspaces in a $\mathcal{G}(\tau, 1)$ Grassmann manifold. With maximum adjacent distances between pilots, the correlations between pilot sequences will be minimized. The correlation between pilot sequence $\mathbf{s}_1$ and $\mathbf{s}_2$ can be written as

$$\rho^2_{\mathbf{s}_1,\mathbf{s}_2} = |\mathbf{s}_1^H \mathbf{s}_2|^2 = 1 - d_c^2(\mathbf{s}_1, \mathbf{s}_2). \tag{4.38}$$

The distance between codewords is upper bounded by the simplex and the orthoplex bound [94, 98]. The choral distance between codeword $\mathbf{w}_i$ and $\mathbf{w}_j$ is bounded as follows,

$$d_{ch}^2(\mathbf{s}_i, \mathbf{s}_j) \leq \begin{cases} \frac{(\tau-1)}{\tau} \cdot \frac{K}{K-1}, & \text{if } K \leq \tau(\tau+1)/2 \\ \frac{(\tau-1)}{\tau}, & \text{if } K > \tau(\tau+1)/2. \end{cases} \tag{4.39}$$

The above upper bound of distance can be utilized in bounding the correlations of the pilot sequences scheme with GLP. Consequently, we can estimate the achievable sum rate with the proposed pilot sequence design.

4.6 Simulation Results

In this section, numerical results are going to be presented. The aim is to verify the proposed closed-form expressions of downlink achievable sum rate for single-cell systems, multi-cell systems and pilot reuse scheme. Additionally, the performance of pilot reuse scheme and GLP-based codebook design will be compared.

The numerical results are generated by the following steps. Firstly, UEs are generated and

Number of antennas at BS, M	$64 \leq M \leq 256$
Number of single antenna UEs, K	$8 \leq M \leq 64$
Cell radius	500 m
UE minimum distance from BS	25 m
Carrier frequency	1.9 GHz
System bandwidth	20 MHz
Maximum UL power,P_{max}^{UL}	200 mW
Maximum DL power,P_{max}^{DL}	40 W
Thermal noise, σ_{n}^2	-174 dBm/Hz
Mobility speed	60 km/H
Path loss model	$35.3 + 37.6 \log_{10} d$ dB
Coherence bandwidth	100 kHz

Table 4.1: *Simulation parameters for the results in this section*

randomly located in each cell. Secondly, pilots for uplink channel estimation are generated. For the pilot reuse scheme, the Hadamard matrix is generated as the orthogonal pilot codebook with the vector length of τ. For the non-orthogonal pilot codebook, the algorithm proposed by [99] is utilized for generating the GLP-based pilot codebook. Thirdly, the pilot sequences are assigned to UEs for channel estimation. Fourthly, the estimated CSI is utilized for downlink transmission and we can calculate the downlink achievable sum rate. The downlink SINR of simulation results for each channel realization are calculated by utilizing Equation (4.19) and Equation (4.28) for single- and multi-cell respectively. The downlink SINR of analytical results for each channel realization are calculated by utilizing Equation (4.21) and Equation (4.31). Both the downlink achievable sum rate of simulation and analytical results are averaged over 10,000 channel realizations.

4.6.1 Verifications of Proposed Analytical Expressions

Firstly, the validity of single-cell analytical downlink achievable sum rate proposed in Theorem 1 will be verified. Consider a single-cell massive MIMO system with hexagonal shape cell and single-antenna UEs randomly located. Figure.4.4 shows an example layout of simulated single-cell massive MIMO system with $K = 8$, where the red triangle and blue squares represent BS and UEs respectively. The simulation parameters are listed in Table 4.1. The uplink pilot codebook is a normalized $\tau \times K$ Hadamard matrix, where column vector is assigned to each UE. The pilot sequence length τ is equal to the number of UE K. Both the UL and DL power utilize the maximum power for the sake of simplicity.

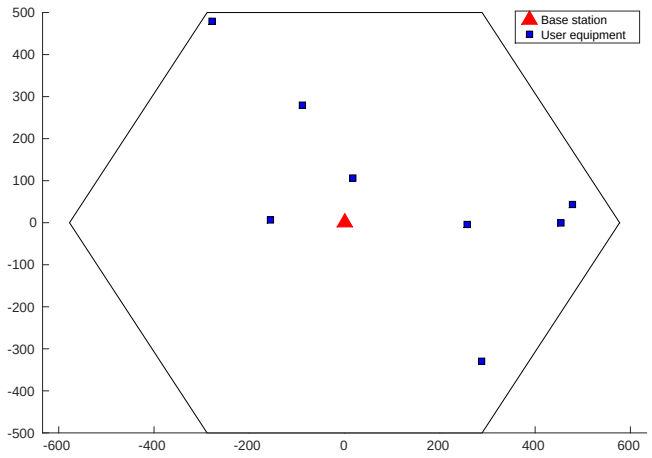

Figure 4.4: *Illustration of single hexagonal cell layout with* $K = 8$

Figure.4.5 shows the downlink achievable sum rate versus number of BS antennas. Four different configurations of K are considered with $K = \tau = 8, 16, 32, 64$. The analytical rate values are calculated by adopting equation (4.20) in Theorem 1 and the simulation rate values are based on 10,000 channel realizations. It can be observed that all the downlink achievable sum rate increase linearly with the number of antennas. The proposed analytical expression provides an accurate approximation of the downlink rate as the analytical results well matched with the simulation results.

Secondly, the validity of analytical multi-cell downlink achievable sum rate proposed in Theorem 2 will be verified. The simulation considers 19 cells system with a central cell surrounded by two layer of cells. Figure.4.6 shows an illustration of the system layout with $K = 8$ for each cell. The case of $RF = 1$ is considered in the simulation. Each cell has same number of UE and shares the same uplink codebook with $\tau = K$. This is illustrated in Figure.4.6 by utilizing same fill color (i.e. white). The configuration of simulation parameters is same with single-cell case, which is listed in Table 4.1.

Figure.4.7 shows the downlink achievable sum rate with $RF = 1$ versus number of BS antennas. Again, four different configurations of K are considered with $K = 8, 16, 32, 64$ for each cell. The analytical results are calculated by adopting equation (4.30) in Theorem 2 and simulation results from equation (4.28) with 10,000 channel realizations. It can be observed that the downlink achievable sum rate increases linearly with M. Additionally, the proposed analytical results match well with the simulation results, which has proofed the validity of Theorem 2.

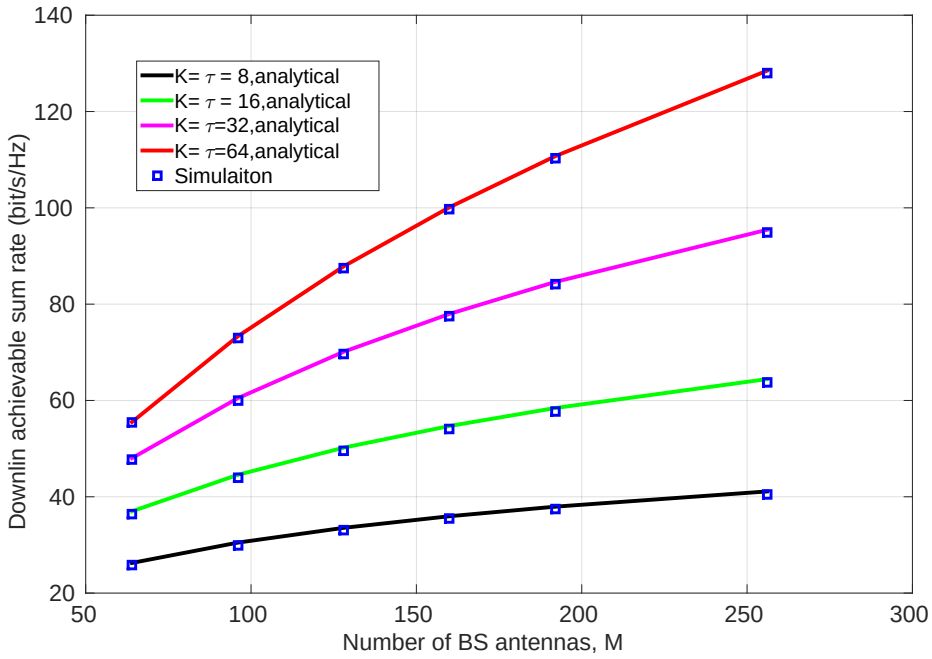

Figure 4.5: *Average downlink achievable sum rate versus the number of BS antennas M, with $\tau = K = 8, 16, 32, 64$*

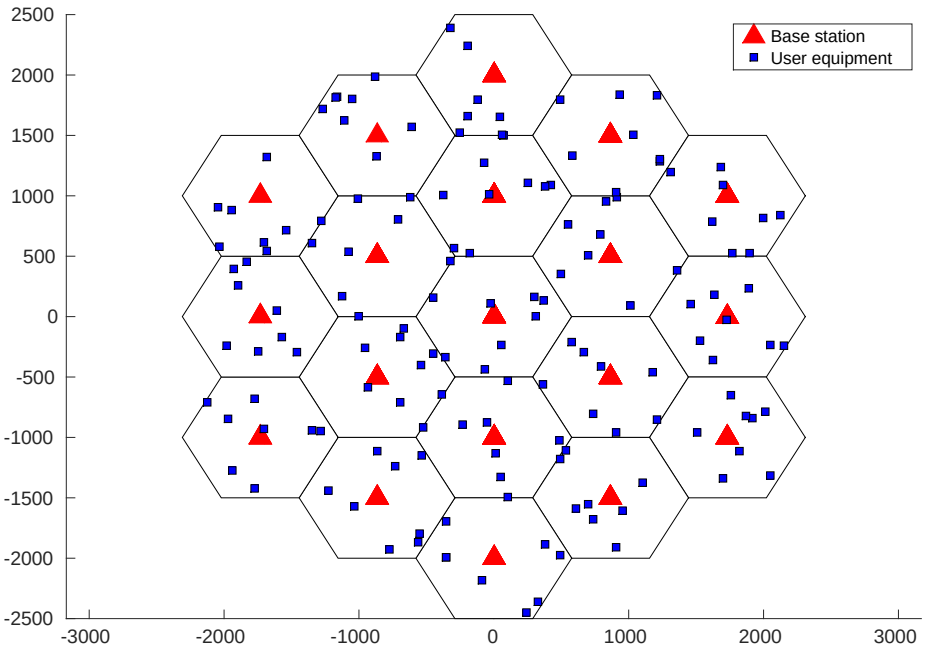

Figure 4.6: *Illustration of multi-cell massive MIMO systems with $L = 19$, $RF = 1$. The fill color uses white only represents the assignment of one set orthogonal pilot sequences in each cell. In this example, $K = 8$.*

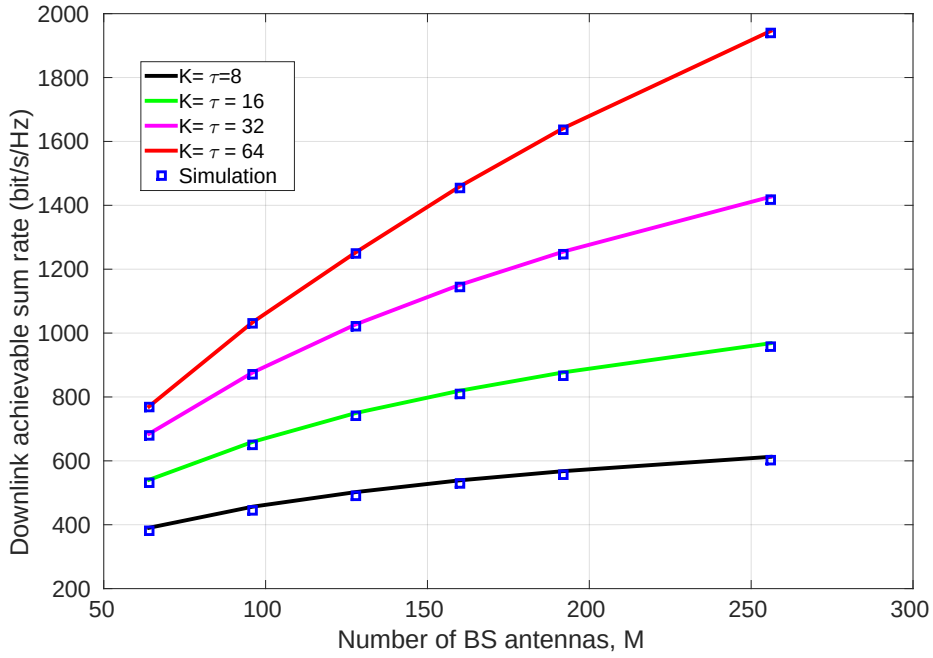

Figure 4.7: *Average downlink achievable sum rate versus the number of BS antennas M, with $L = 19$, $\tau = K = 8, 16, 32, 64$ and $RF = 1$*

pilot length,τ	K in white cell	K in green cell	K in yellow cell	Total number of UE
$\tau = 8$	$K = 2$	$K = 3$	$K = 3$	50
$\tau = 16$	$K = 5$	$K = 5$	$K = 6$	101
$\tau = 32$	$K = 10$	$K = 11$	$K = 11$	202
$\tau = 64$	$K = 20$	$K = 22$	$K = 22$	404

Table 4.2: *UE distribution when $RF = 3$*

Thirdly, the validity of the proposition of downlink achievable sum rate with pilot reuse scheme in Corollary 1 is verified. Figure.4.8 illustrates the layout of simulated system with $RF = 3$. Three different colors are applied in the layout to indicate the reuse of mutual orthogonal pilot sequences. The simulation parameters are consistent with the previous simulations. Three configurations of τ are considered with $\tau = 8, 16, 32, 64$ as the length of orthogonal pilot codebook. The UE distribution in different cells is listed in Figure.4.9 shows the downlink achievable sum rate with $RF = 3$ versus number of BS antennas. The analytical results are calculated by adopting equation (4.32) in Corollary 1 and the simulation results are calculated by adopting equation (4.28). It can be observed that the analytical results match well with the simulation results, which again shown the validity of the proposed analytical expression.

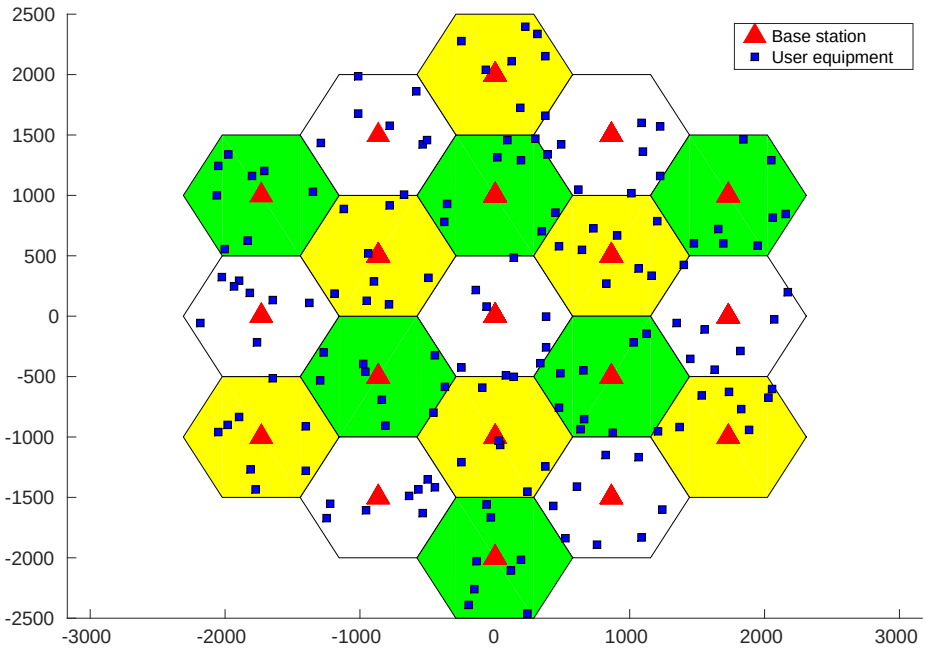

Figure 4.8: *Illustration of multi-cell massive MIMO systems with* $L = 19$, $RF = 3$. *Each fill color represents the assignment of one set orthogonal pilot sequences. In this example,* $K = 8$.

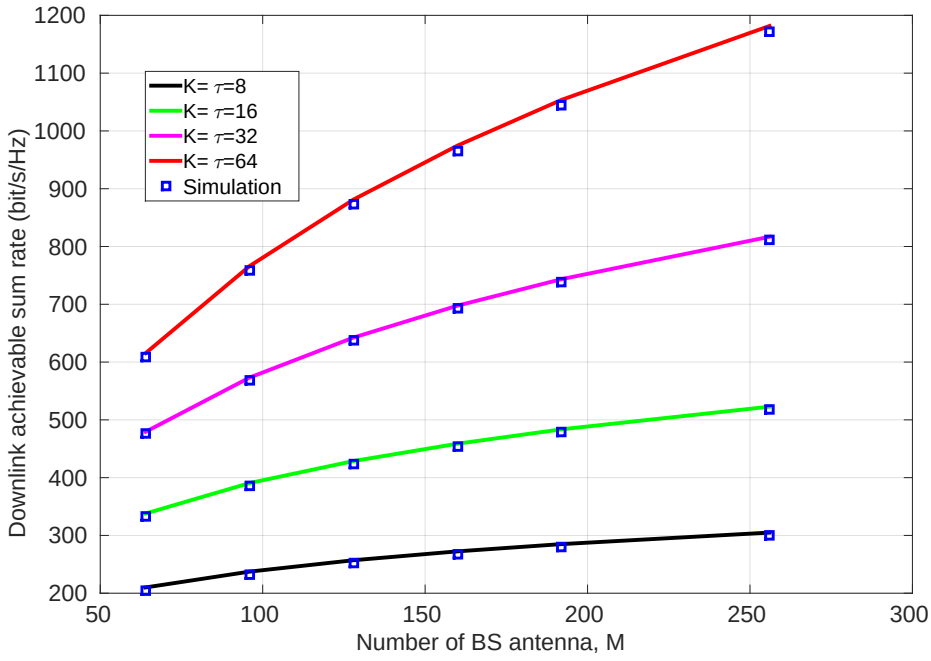

Figure 4.9: *Average downlink achievable sum rate versus the number of BS antennas* M, *with* $L = 19$, $\tau = K = 8, 16, 32, 64$ *and* $RF = 3$

4.6.2 Performance Comparison of GLP-based Codebook Design and Pilot Reuse Scheme

In the previous section, the proposed analytical achievable downlink rate of multi-cell massive MIMO systems have been verified. Simulation results have shown the validity of the propositions. In this section, the comparison of achievable downlink rate of proposed GLP-based uplink codebook design and pilot reuse scheme will be presented.

The performance comparison considers not only the average downlink achievable sum rate, but also the rate of both cell central and edge UEs. The classification method in each cell is consistent, which is compared with the following threshold β_j^t [83]

$$\beta_j^t = \frac{\varphi}{K} \sum_{i=1}^{K} \beta_{ij}^2, \tag{4.40}$$

where φ denotes the coefficient that defined based on the system configurations. The φ is chosen as 0.2 in this thesis. As a result, the classification of central and edge UE in cell j is expressed as

$$\begin{cases} \beta_{ij}^2 \geq \beta_j^t, & \text{central UE} \\ \beta_{ij}^2 < \beta_j^t, & \text{edge UE} \end{cases} . \tag{4.41}$$

The system parameters are consistent with the previous simulation of $RF = 3$. Figure.4.10 shows the average downlink achievable sum rate versus the number of BS antennas. The GLP-based design utilizes the codebook generated from the algorithm proposed in [99], which has constant modulus and a finite alphabet (i.e.phase-shift keying (PSK)). It can be observed that the GLP-based pilot codebook outperforms the pilot reuse scheme. Additionally, with the increase of τ, the rate gain becomes more significant. In the case of $\tau = 8$, the average improvement is about 0.5%. When τ increases to 16 and 32, the average improvement is about 3.4 %. In the case of $\tau = 64$, the rate improvement becomes 4.7%. The reason is due to the increase of choral distance between lines in Grassmannian manifold along with the vector space dimension. In another word, the correlation between codewords decreases as indicated by the upper bound. Figure.4.11 shows the downlink spectrum efficiency of both central and edge UEs. The simulation considers $\tau = 32$ with $M = 128, 256$. By observing at the 10th percentile, i.e., the 90% likely minimum UE rate, the improvement of central UE is about 70% and nearly two fold of edge UEs.

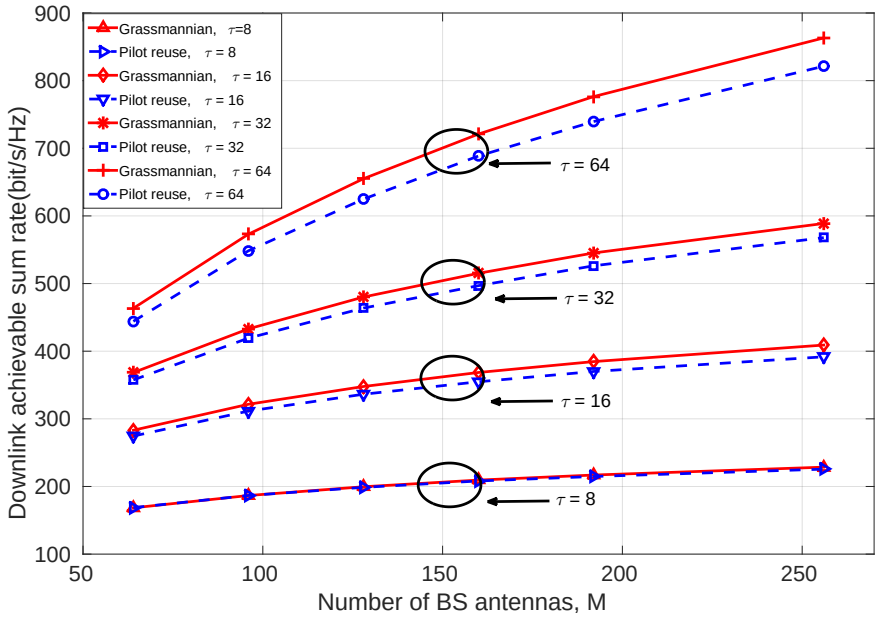

Figure 4.10: *Comparison of average downlink achievable sum rate versus the number of BS antennas M between GLP-based pilot codebook and pilot reuse scheme, with $L = 19$, $\tau = K = 8, 16, 32, 64$ and $RF = 3$*

4.7 Conclusion

This chapter has investigated the achievable sum rate of multi-cell massive MIMO system with TDD operation. Firstly, closed-form expressions of downlink rate for both single-cell and multi-cell configurations of massive MIMO systems were proposed. The LS method and MRT scheme were utilized for uplink channel estimation and downlink precoding. The proposed expression clearly shows how the number of BS antennas and correlation between uplink pilots influence the downlink achievable rate. Simulation results have shown the validity of propositions. Secondly, closed-form expression of downlink rate for massive MIMO systems with pilot reuse scheme as uplink pilot scheduling was proposed. This proposition shows the rate performance with any given reuse factors. Thirdly, the downlink rate performance of the Grassmannian line packing based uplink pilot codebook has been investigated. Comparisons have been made between pilot reuse scheme and Grassmannian line packing based pilot codebook design by utilizing the proposed expressions. The simulation results show that the Grassmannian line packing pilot codebook offers significant rate improvement.

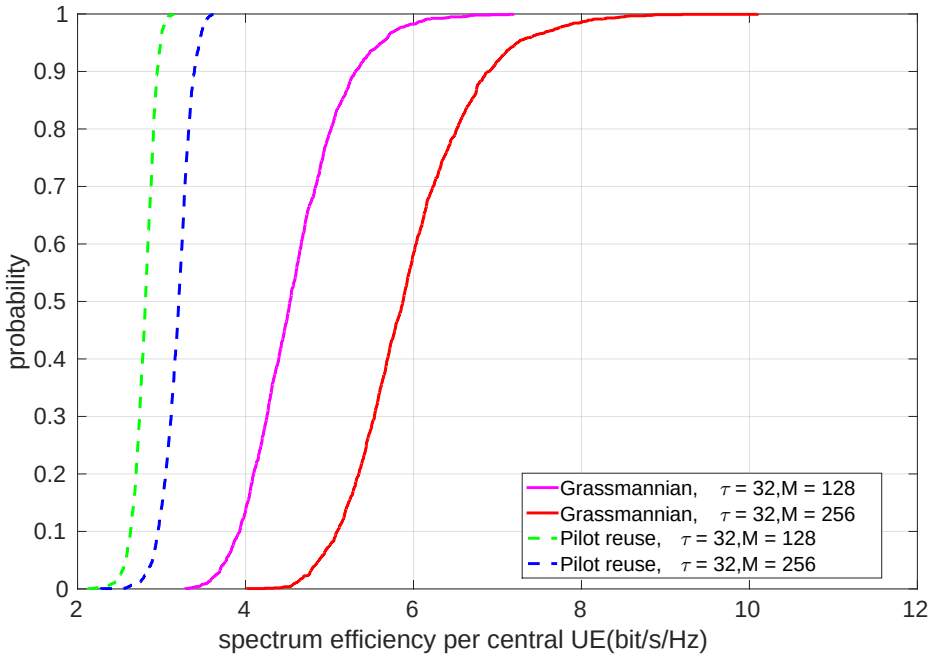

(a) Cumulative distribution function of spectrum efficiency per central UE, with $\tau = 32$ and $M = 128, 256$

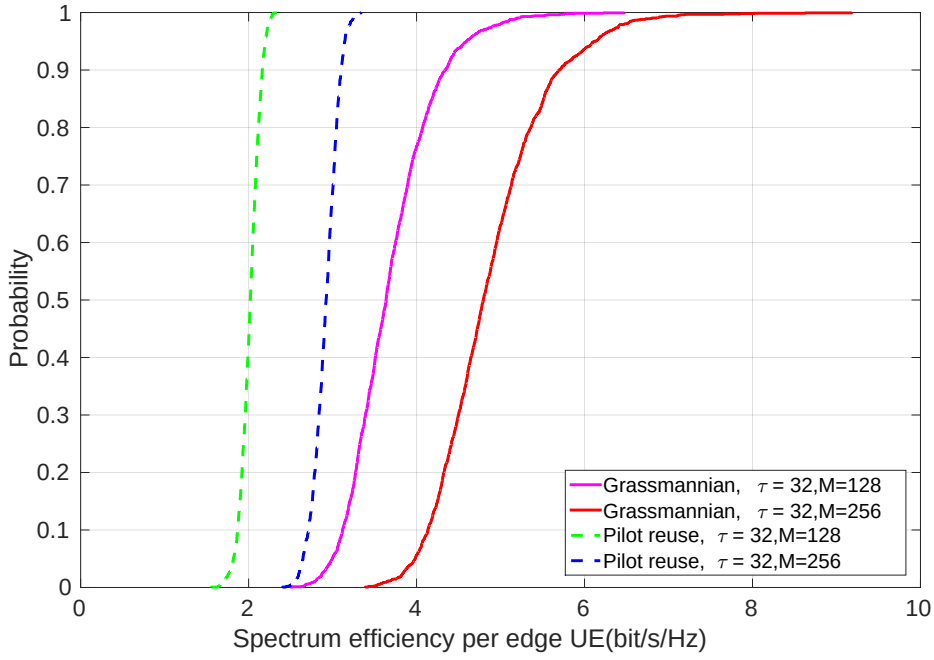

(b) Cumulative distribution function of spectrum efficiency per edge UE, with $\tau = 32$ and $M = 128, 256$

Figure 4.11: *The downlink spectrum efficiency comparison of central and edge UE*

Chapter 5
Energy-efficient power allocation in multi-cell massive MIMO systems

The performance benefits offered by massive multiple-input multiple-output (MIMO) systems and the deployment of large number of base station (BS) antennas that are capable of increasing system capacity and robustness have been discussed in Chapter 2 and 4. However, a further question that naturally arises is how energy efficient is the massive MIMO systems? While the large number of antennas at BS can dramatically increase capacity performance, like a double-edge sword, the restive power consumption might become problematic, since it is considered to be as important in communication systems design as capacity. In [100], it was pointed out that BS consumes 80% of the energy in cellular network operations, which means that the research into energy saving in massive MIMO systems is urgently required.

This chapter describes a general framework of optimization for maximizing global energy efficiency (EE) in massive MIMO systems, whereby the optimization starts with maximizing minimum user-equipment (UE) rate which aims to improve the quality-of-service (QoS) and provide a feasible condition for the EE maximization problem. Secondly, to solve the EE optimization which is considered to be a non-concave problem, the fractional programming and successive convex approximation (SCA)-based algorithm will be used to find a local optimal solution with affordable complexity.

The remainder of this chapter will consist of the following:

1. In Section 5.1, the background and purpose of this chapter will be described and a brief literature review of energy efficiency in both convention MIMO and massive MIMO systems will be given.
2. In Section 5.2, the system mode and the EE problem will be given.
3. In Section 5.3, a detailed explanation of the maximization of minimum UE rate will be presented.

4. In Section 5.4, an explanation of the fractional programming and SCA-based algorithm will be given.

5. In Section 5.5, the simulation results, together with the corresponding analysis will be demonstrated, and then will bring the chapter to its conclusion in Section 5.6.

5.1 Introduction

The development of cellular network has grown rapidly over the last twenty years. According to the report in [100], the CO_2 emission from information and communication technology weights approximately 2% in 2011, but it is predicted to increase dramatically up to 2021 due to the data communication demands [3]. Massive MIMO is an advanced cellular network architecture which is regarded to be a promising technology for the fifth generation of mobile phone mobile communication technology standards network (5G) [71, 73–75]. Consequently, the research into the EE in massive MIMO systems has become very important and it has attracted great interest from both academia and industry.

The optimization of EE, which is a ratio of sum rate over sum energy consumption as a benefit-to-cost ratio, generally utilizes fractional programming due to the natural of fraction expression. However, due to the effect of pilot contamination, this method is not suitable for optimizing massive MIMO systems. It is because the sum rate expression in the numerator is generally a non-convex problem, which can not be solved within polynomial time.

Related work: The concept of a green cellular network was proposed in [101], where the importance of developing mechanisms for reducing energy consumption was addressed. The reduction at BS side can be implemented in two different ways, (i) hardware improvement, and (ii) transmission protocol/allocation scheme development. This thesis will focus on the latter.

The statistics of daily data loads is unevenly distributed across the time periods and cells [102]. Consequently, the power consumption of the BS can be adaptive to the actual demands for the sake of energy efficiency. The adaptation of traffic loads is a popular research topic belongs to the catalogue of transmission protocol scheme, where under the condition of satisfying QoS, the operation mode of BS switches based on the varying traffic demands. In the off-peak time slots, such as midnight, BS can turn to sleep mode (also called lower power mode or deep idle mode) for the purpose of saving energy[102]. This adaptation allows for straightforward

implementation in an urban cellular system, but its drawback is that a selection has to be made between high performance and energy efficiency.

In [103], a mode switching algorithm between MIMO and SIMO was proposed. The results showed that transmission energy can be saved 50% by utilizing dynamic mode. The collaboration between BSs was also proposed for the adaptation of traffic loads [104]. Various cooperative initiatives were also recommended for the sake of increasing coverage and services for off-peak period. Additionally, an artificial neural network (ANN) was utilized for predicting traffic statistics [105], and BSs can dynamically change the working mode according to the prediction.

Other than the propositions of different transmission protocol, optimization techniques are also applied for resource allocation. Based on the cell condition, BSs optimally or sub-optimally allocate resource based on the calculation results from optimization algorithms. The object of optimization can vary according to specific requirements, such as the maximization of throughput for the purpose of system performance, or the maximization of EE as an energy saver. An optimization based scheduler for maximizing the EE in a MIMO system was proposed in [106] and a trade-off between the EE and the number of BS antennas is discussed, where the numerical results demonstrate that the system EE decrease with the number of antennas. In [107], a gradient-based method is also adopted for the optimization of EE in conventional MIMO systems, with close performance to the optimal linear solution. The Dinkelbach method is a powerful algorithm that is usually utilized for EE optimization in conventional MIMO systems [108–110]. Simulation results have shown that the optimal solution can be achieved within polynomial-time complexity.

There is also great research interest in EE optimization in massive MIMO systems; for instance, in [81] the EE problem in orthogonal frequency division multiple access (OFDMA) based system was formulated. An iterative algorithm that based on the Dinkelbach's method was proposed to optimize the power, subcarrier and antenna allocation policies. Also in [111], in order to maximize the EE, the optimal configuration of BS antennas and UEs inside each cell was focused on; a new power consumption model was proposed and closed-form expressions of EE were obtained for comparisons. In [112], the downlink EE performance was investigated and results showed that the circuit power consumption per antenna significantly influences the EE. In [113], a single-cell downlink power allocation algorithm was proposed to achieve EE and both transmit and circuit power were considered. In [114] a power allocation algorithm for

maximizing EE in massive MIMO systems was proposed.

Contributions: A general framework was proposed for the EE maximization in the massive MIMO systems with time-division-duplex (TDD) operation, where the minimum UE rate was firstly maximized in order to increase the QoS and provide a feasible constrain for the EE optimization latter. It is noticeable that the massive MIMO system is an interference-limited system, the optimization of EE was considered to be non-concave, which is a non-deterministic polynomial-time hard (NP-hard) problem. A combination of fractional programming and successive convex approximation (SCA)-based algorithm was proposed in order to tackle the EE maximization iteratively and efficiently. The local optimal solution of downlink power allocation can be found with acceptable complexity. Comparisons were made between the downlink power with equal division and the power allocation after the optimization. Furthermore, it considered the case of the GLP-based codebook design and the pilot reuse scheme. Numerical results proofed the validity of the proposed optimization methods, where the EE has been significantly improved. Additionally, it showed that the minimum UE rate was highly improved after the proposed optimization. The EE of the GLP-based codebook design also performed better thanthe pilot reuse scheme.

5.2 Energy Efficiency and Optimization Problem Formulation

For the purpose of this section, the general concept of efficiency (EE) was defined as the output with given resource that can be seen as a "benefit-cost ratio". Hence, high efficiency means that more output per unit of resource. In terms of the massive MIMO systems, the "benefit" is the amount of data that is successfully transmitted within a time period, while the "cost" is the total power consumption that is required for transmission. Consequently, the EE (measured in bit/Joules) of the massive MIMO systems in this thesis is defined as a fractional expression with the downlink achievable sum rate (measured in bit/seconds) over the total power consumption (measured in Watts, where Watts = Joules/second), which is expressed as

$$\text{Energy Efficiency} = \frac{\text{Downlink achievable sum rate}}{\text{Total power consumption}}. \tag{5.1}$$

It is noticeable that the EE can not only be expressed as a fractional expression, but also with a differential form, as mentioned in [110]. The reason for choosing the fractional form in this thesis is to try to be consistent with the common definition of spectral efficiency, which is

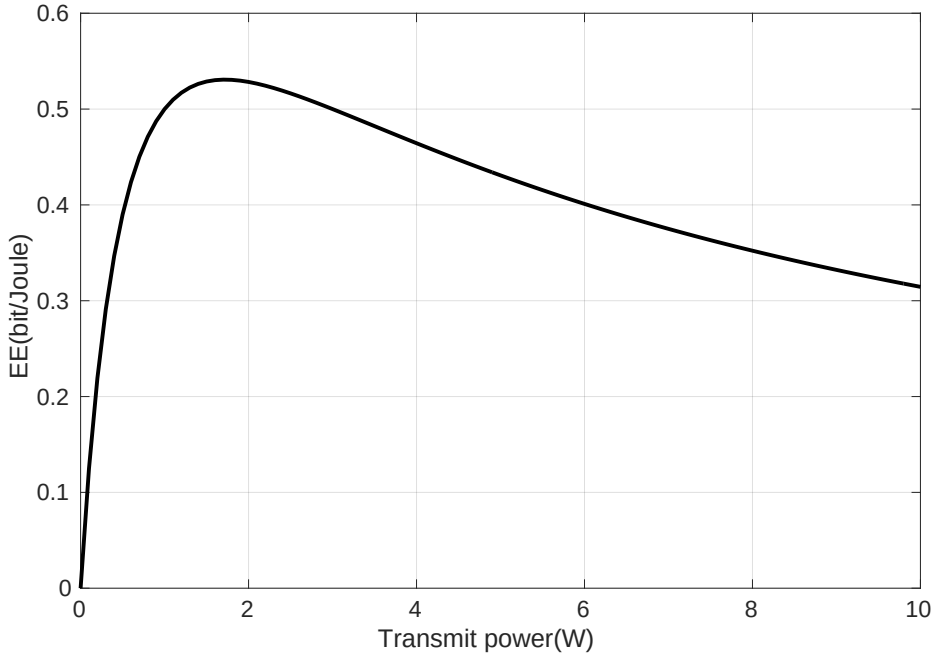

Figure 5.1: *Energy efficiency versus transmit power p_t, with $P_c = 1W$*

defined as the total number of bits over the system bandwidth [115].

The objective of this work was to develop an efficient power allocation algorithm to jointly allocate the power to all the UEs in the multi-cell massive MIMO systems, and meanwhile satisfy the transmit power limitation and minimum UE rate constraints, in order to maximize the EE as defined in (5.1). To be more specific, it is aiming to find a "balance" point of the achievable rate and the transmit power. Figure.5.1 shows a simple example of EE versus the transmit power, which is aiming to illustrate the trade-off between achievable rate and power consumption. The EE is expressed as

$$EE = \frac{\log_2(1 + p_t)}{p_t + P_{\mathrm{c}}}, \tag{5.2}$$

where p_t denotes the transmit power and P_{c} is the circuit power. In this example, P_{c} is a fixed constant and assumed to be equal to 1W. Figure.5.1 illustrates how the EE varies with the transmit power. Note that the EE is not monotonically increased with the transmit power and in this example the optimal p_t is equal to 1.7W, which means the rate and power meets the best trade-off when the transmit power is set to 1.7W.

The simple example showed here is to illustrate why the optimization of EE is essential. In

the following sections, the mathematical formulation of the EE for multi-cell massive MIMO systems with TDD operation will be presented, which starts with the power consumption modelling.

5.2.1 Power Consumption Model

To formulate the EE maximization problem, the total power consumption of P_{tot} the system will be first modelled, where P_{tot} is expressed as

$$P_{\text{tot}} = P_{\text{u}} + P_{\text{d}}, \tag{5.3}$$

where P_{u} and P_{d} denotes the total power for the uplink and downlink transmission respectively. In terms of the total power consumption model for the uplink transmission, it includes: (i) the transmit power for transmitting uplink pilot of single antenna UEs, and (ii) the circuit and signal processing power associated with transmission of uplink pilot. Without loss of generality, it follows the assumption below

Assumption 1. *For all the single-antenna UEs in the multi-cell massive MIMO systems with TDD operation, it is assumed that all the UEs have the same power amplifier (PA) efficiency, circuit and signal processing power consumption for each coherence interval. For all the BSs, it follows the assumptions below*

1. *All the BSs have the same PA ratio, circuit and signal processing power consumption for each coherence interval.*
2. *Each transceiver serves one antenna at the BS.*

Consequently, following the Assumption 1, the total power consumption for the uplink transmission P_{u} is defined as

$$P_{\text{u}} = \underbrace{\sum_{l=1}^{L}\sum_{k=1}^{K}\frac{\tau}{T}\frac{p_{kl}^{\text{u}}}{\eta_{UE}}}_{uplink\ transmit\ power} + \underbrace{L \cdot K \cdot p_{\text{c}}^{\text{u}}}_{\substack{uplink\ circuits\ and \\ signal\ processing\ power}}, \tag{5.4}$$

where p_{kl}^{u} denotes the uplink transmit power of UE k in cell l and $k \in \mathcal{K}$, $l \in \mathcal{L}$, η_{UE} is the PA efficiency of UE, $\frac{\tau}{T}p_{kl}^{\text{u}}$ denotes the transmit power for uplink pilot transmission, p_{c}^{u} represents the circuits and signal processing power of UEs.

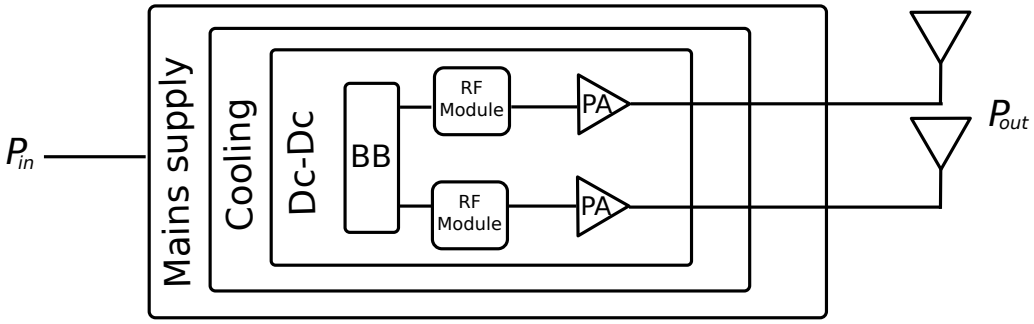

Figure 5.2: *Block diagram of BS transceiver [2]*

After the formulation of total power consumption of uplink transmission, it will focus on the total power consumption model for BS in downlink transmission P_{d}, which includes (i) the downlink transmit power, and (ii) the circuit and signal processing power for the BS in receiving and transmitting signal. The P_{d} is expressed as [2, 114]

$$P_{\mathrm{d}} = \frac{1}{\sigma_{\mathrm{BS}}} \left(\sum_{l=1}^{L} \sum_{k=1}^{K} \left(1 - \frac{\tau}{T}\right) \frac{p_{kl}^{\mathrm{d}}}{\eta_{\mathrm{BS}}} + L \cdot M \cdot p_{\mathrm{c}}^{\mathrm{d}} \right), \tag{5.5}$$

where p_{kl}^{d} denotes the downlink transmit power for UE k by the BS in cell l and $k \in \mathcal{K}$, $l \in \mathcal{L}$, η_{BS} denotes the PA efficiency and σ_{BS} represents the loss factors of BS, which is expressed as

$$\sigma_{\mathrm{BS}} = (1 - \sigma_{\mathrm{DC}})(1 - \sigma_{\mathrm{MS}})(1 - \sigma_{\mathrm{cool}}), \tag{5.6}$$

where σ_{DC}, σ_{MS} and σ_{cool} represents the loss factor due to (i) direct-current (DC) to DC power supply, (ii) mains supply indicating Alternating Current (AC) to DC unit and (iii) cooling system respectively [114] [2]. The $p_{\mathrm{c}}^{\mathrm{d}}$ is the circuit and signal processing power consumption of BS, which is modelled as

$$p_{\mathrm{c}}^{\mathrm{d}} = p_{\mathrm{c,dac}}^{\mathrm{d}} + p_{\mathrm{c,mix}}^{\mathrm{d}} + p_{\mathrm{c,filt}}^{\mathrm{d}} + p_{\mathrm{c,syn}}^{\mathrm{d}} + p_{\mathrm{bf}}^{\mathrm{d}}, \tag{5.7}$$

where $p_{\mathrm{c,dac}}^{\mathrm{d}}$, $p_{\mathrm{c,mix}}^{\mathrm{d}}$ and $p_{\mathrm{c,filt}}^{\mathrm{d}}$ represents the circuit power consumption of each BS antenna for the operation of (i) digital-analogue-converting, (ii) mixing, and (iii) filtering [103]. The $p_{\mathrm{c,syn}}^{\mathrm{d}}$ and $p_{\mathrm{bf}}^{\mathrm{d}}$ represents the consumption of frequency synthesizer and beamforming respectively.

Figure 5.2 shows a simplified block diagram of the BS transceiver structure [2], with the BB

Parameter	Description
P_{u}	Total uplink power consumption
p_{kl}^{u}	Uplink transmit power from the UE k in cell l
η_{UE}	Power amplifier efficiency ratio of UE
$p_{\mathrm{c}}^{\mathrm{u}}$	Total Circuit and signal processing power consumption of UE

Table 5.1: *Power model parameters for the uplink in multi-cell massive MIMO systems*

Parameter	Description
P_{d}	Total downlink power consumption
p_{kl}^{d}	Downlink transmit power to the UE k from BS l
η_{BS}	Power amplifier efficiency of BS
σ_{BS}	Loss factors of BS
σ_{DC}	Loss factor from direct-current to direct-current power supply
σ_{MS}	Loss factor from main supply
σ_{cool}	Loss factor from cooling
$p_{\mathrm{c}}^{\mathrm{d}}$	Total circuit and signal processing power consumption of BS
$p_{\mathrm{c,dac}}^{\mathrm{d}}$	BS power consumption of digital-analogue-converting
$p_{\mathrm{c,mix}}^{\mathrm{d}}$	BS power consumption of mixing
$p_{\mathrm{c,filt}}^{\mathrm{d}}$	BS power consumption of filtering
$p_{\mathrm{c,syn}}^{\mathrm{d}}$	BS power consumption of synchronization
$p_{\mathrm{c,syn}}^{\mathrm{d}}$	BS power consumption of beamforming

Table 5.2: *Power model parameters for the downlink in multi-cell massive MIMO systems*

denoting the baseband units. It is noticeable that the BS transceiver can be generally divided into three modules, which are

1. The BB unit: the power consumption from the operations of signal processing are produced from this unit, and it is represented by $p_{\mathrm{c}}^{\mathrm{d}}$.

2. The small radio frequency transceiver plus the PA units: the downlink transmit power is influence by the PA efficiency, because the PA units are intending to prevent adjacent channel interference, however, it has low efficiency, which is represented by η_{BS}.

3. The power loss from the combination of power supply units and the system cooling units are modelled with σ_{BS}.

For the sake of understanding, the power model parameters for the uplink and downlink transmission utilized in this thesis have been listed in Table 5.1 and Table 5.2 respectively. In terms of the typical values of the parameters, they are listed in Table 5.3 along with the references.

Following the formulation of the total power consumption of the system, the problem of maximizing the EE can be mathematically formulated in the next section.

5.2.2 Problem Formulation

The EE is defined as

$$EE\left(p_{kl}^{\mathrm{u}}, p_{kl}^{\mathrm{d}}\right)=\frac{\sum_{l=1}^{L}\sum_{k=1}^{K}\left(1-\frac{\tau}{T}\right)\log_2\left(1+\gamma_{kl}\left(p_{kl}^{\mathrm{u}}, p_{kl}^{\mathrm{d}}\right)\right)}{\left(\sum_{l=1}^{L}\sum_{k=1}^{K}\frac{\tau}{T}\frac{p_{kl}^{\mathrm{u}}}{\eta_{\mathrm{UE}}}+L\cdot K\cdot p_{\mathrm{c}}^{\mathrm{u}}\right)+\left(\frac{1}{\sigma_{\mathrm{BS}}}\left(\sum_{l=1}^{L}\sum_{k=1}^{K}\left(1-\frac{\tau}{T}\right)\frac{p_{kl}^{\mathrm{d}}}{\eta_{\mathrm{BS}}}+L\cdot M\cdot p_{\mathrm{c}}^{\mathrm{d}}\right)\right)} \tag{5.8}$$

where γ_{kl} denotes the SINR which utilizes the proposed SINR expression in Equation (4.31). As the EE is defined equation (5.8), power allocation will be applied on both uplink and downlink transmit power for maximizing the EE of systems. The optimization problem can be formulated as

$$\underset{p_{kl}^{\mathrm{u}}, p_{kl}^{\mathrm{d}}}{\text{maximize}} \quad EE\left(p_{kl}^{\mathrm{u}}, p_{kl}^{\mathrm{d}}\right) \tag{5.9a}$$

$$\text{subject to} \quad 0 < p_{kl}^{\mathrm{u}} \leq p_{\max}^{\mathrm{u}}\ ,\ \forall\,(k,l) \in (\mathcal{K}, \mathcal{L}) \tag{5.9b}$$

$$p_{kl}^{\mathrm{d}} \geq 0,\ \forall\,(k,l) \in (\mathcal{K}, \mathcal{L}) \tag{5.9c}$$

$$\sum_{k=1}^{K} p_{kl}^{\mathrm{d}} \leq p_{\max}^{\mathrm{d}}\ ,\ \forall\,(l) \in (\mathcal{L}) \tag{5.9d}$$

$$R_{kl}^{D}\left(p_{kl}^{\mathrm{u}}, p_{kl}^{\mathrm{d}}\right) \geq \zeta_{kl} R_{\min}\ ,\ \forall\,(k,l) \in (\mathcal{K}, \mathcal{L})\,, \tag{5.9e}$$

where $p_{\max}^{\mathrm{u}}$ and $p_{\max}^{\mathrm{d}}$ are the maximum uplink and downlink transmit power constrain at UE and BS side due to the hardware limitations, $R_{\min}$ represents the minimum downlink rate that guarantees the QoS, ζ_{kl} is a random scaler between 0 and 1. In (5.9), Constraint (5.9b) ensures that the uplink power is less or equal to the maximum limitation but larger than 0. Constraint (5.9c) and (5.9d) ensure that the downlink power to each UE is larger or equal to 0, and the sum power to all the UEs in one cell meets the maximum limitation. Constraint (5.9e) represents that the downlink achievable rate of each UE needs to larger or equal to the pre-defined minimum UE rate.

It is noticeable that the Problem (5.9a) that the maximization of EE is challenging to solve directly. The Problem (5.8) has a ratio form with a fractional structure and it belongs to the

fractional programming problem, it can not be directly solved with the existing algorithms belongs to the fractional programming theory [110, 116]. If the optimization problem has a concave and convex function in the numerator and the denominator respectively, it can be solved efficiently with a guaranteed polynomial-time complexity. However, it can be observed that the numerator in Problem (5.9a) and the Constraint (5.9e) includes the downlink achievable sum rate of a multi-cell massive MIMO systems, which is a difference of two concave functions. And it is noticeable that the optimization problem with difference of two concave functions is generally non-concave and challenge to find the globally optimal solution. In this thesis, the combination of the fractional programming and the SCA method are proposed to allocate the power effectively in order to achieve the optimal EE.

The proposed optimization method starts with the reformulation of (5.9), which aims to convert the variables in equation (5.8) into vector form. The purpose of conversion for the algorithm is for the jointly allocation of the transmit power for all the UEs in the multi-cell scenario. Following this reformulation, the optimization focuses on one single power vector, rather than multiple scaler power values.

In terms of the downlink achievable sum rate, the problem utilizes the proposition in Theorem 2. By observing the equation, it is noticeable that the jointly optimization of both uplink and downlink power for multi-cell massive MIMO systems is very complex, which is difficult for practical application. For the sake of solving the problem efficiently, it is assumed that all the UEs utilize full power for the transmission of uplink training sequences. It is because by observing the downlink SINR expression in equation (4.31), it can be found that the downlink achievable sum rates increase monotonically with the uplink power. Consequently, the optimization only considers the downlink transmit power as the variable, which is expressed as

$$\mathbf{p} \triangleq \left[p_{1l}^{\mathrm{d}}, p_{2l}^{\mathrm{d}}, \cdots, p_{kl}^{\mathrm{d}}\right]^T \in \mathbb{R}_{+}^{(LK\times 1)}, \tag{5.10}$$

where $\mathbf{p}$ is the vectors with elements of the downlink power for each UE. Consequently, the downlink SINR expression in equation (4.31) is reformulated in the following definition.

Definition 1. The downlink SINR of UE i in cell j is reformulated as

$$\gamma_{ij}\left(\mathbf{p}\right) = \frac{\mathbf{z}_{ij}^T\mathbf{p}}{\mathbf{b}_{ij}^T\mathbf{p} + \sigma_{\mathrm{n}}^2}, \tag{5.11}$$

with $\mathbf{z}_{ij} \triangleq \left[0, 0, \cdots, \frac{M}{\alpha_{ij,nj}}\beta_{ij,j}^2, 0, 0, \cdots\right]^T \in \mathbb{R}^{(LK\times 1)}$

$$\mathbf{b}_{ij} \triangleq \left[0, 0, \cdots, \beta_{ij,j}, \sum_{k\neq i}^{K} \frac{(M\beta_{ij,j}\rho_{kj,ij}^2+\alpha_{kj,nm})}{\alpha_{kj,nm}}\beta_{ij,j}, \sum_{l\neq j}^{L}\sum_{k=1}^{K} \frac{(M\beta_{ij,l}\rho_{kl,ij}^2+\alpha_{kl,nm})}{\alpha_{kl,nm}}\beta_{ij,l}, \cdots\right]^T,$$

where $\mathbf{z}_{ij}$ is a $LK \times 1$ all zero vector except for one corresponding position. The $\mathbf{b}_{ij} \in \mathbb{R}^{LK\times 1}$ is similarly defined, but for multiple non zero entries. For example, in terms of the the calculation of γ_{ij}, it has p_{ij}^{d} in the numerator. Consequently, the non zero entry in $\mathbf{z}_{ij}$ will be $\frac{M}{\alpha_{ij,nj}}\beta_{ij,j}^2$ and all the other entries will be zero. Then, the numerator of γ_{ij} equals to $\frac{M}{\alpha_{ij,nj}}\beta_{ij,j}^2 p_{ij}^{\mathrm{d}}$. In terms of $\mathbf{b}_{ij}$ in the denominator, it is similarly defined.

The total power consumption of the system can also be reformulated as

$$P_{\text{sum}}(\mathbf{p}) = P_{\mathrm{u}} + \left(\frac{1}{\sigma_{\text{BS}}}\left(\sum_{l=1}^{L}\sum_{k=1}^{K}\mathbf{c}_{\eta}^T\mathbf{p} + L\cdot M\cdot p_{\mathrm{c}}^{\mathrm{d}}\right)\right), \tag{5.12}$$

where $\mathbf{c}_{\eta}$ is a $LK \times 1$ vector with all the entries are $\left(1-\frac{\tau}{T}\right)\frac{1}{\eta_{\text{BS}}}$. Following the reformulation of the SINR and utilization of fixed uplink power, the Problem (5.9a) can be simplified as

$$\underset{\mathbf{p}}{\text{maximize}} \quad EE(\mathbf{p}) = \frac{\sum_{l=1}^{L}\sum_{k=1}^{K}\left(1-\frac{\tau}{T}\right)\log_2\left(1+\gamma_{kl}(\mathbf{p})\right)}{P_{\mathrm{u}} + \left(\frac{1}{\sigma_{\text{BS}}}\left(\sum_{l=1}^{L}\sum_{k=1}^{K}\mathbf{c}_{\eta}^T\mathbf{p} + L\cdot M\cdot p_{\mathrm{c}}^{\mathrm{d}}\right)\right)} \tag{5.13a}$$

$$\text{subject to} \quad \mathbf{t}_{kl}^T\mathbf{p} \geq 0,\ \forall(k,l) \in (\mathcal{K},\mathcal{L}) \tag{5.13b}$$

$$\sum_{k=1}^{K}\mathbf{t}_{kl}^T\mathbf{p} \leq p_{\text{max}}^{\mathrm{d}},\ \forall(l) \in (\mathcal{L}) \tag{5.13c}$$

$$R_{kl}^{\mathrm{d}}(\mathbf{p}) \geq \zeta_{kl}R_{\text{min}},\ \forall(k,l) \in (\mathcal{K},\mathcal{L}), \tag{5.13d}$$

where $\mathbf{t}_{kl} \triangleq [0, 0, \cdots, 1, 0, 0, \cdots]^T$ is a vector with $KL \times 1$ length and all zero elements but unit elements at corresponding position.

Compared with the Problem (5.9), the reformulated problem in (5.13) is more straightforward to understand. More importantly, the aim of the optimization algorithm is to jointly optimize the downlink transmit power for all the UEs of the cell, and it can be easily achieved after the reformulation. Also, the reformulated problem is suitable for utilizing the CVX [117] to solve it. In the following section, the optimization of the minimum UE rate will be considered. It is aiming not only to maximize the QoS for all the UEs, but also provide a feasible constraint for the EE optimization in the varying quality propagation environment.

5.3 Optimization of Max-min Rate

To solve the problem of EE maximization, the first step is to maximize the minimum UE rate, R_{min}. As the constraint that shown is in (5.13d), a fixed value of R_{min} is obviously not suitable. It is because the UE positions and propagation environment are always changing, where the minimum UE rate also varies. For example, the cell edge UEs may suffer strong interference which might influence the channel estimation quality and therefore the downlink transmission rate might be reduced. In order to tackle the Problem (5.13a), a proper constraint value of minimum UE rate is required at the beginning of EE maximization. Moreover, by maximizing the minimum UE rate, it solves the feasibility of EE optimization problem. The maximized minimum UE rate is the best downlink achievable rate that can be reached for a given channel realization. Consequently, it plays the role as an "upper bound" of the UE rate and the constraint of the maximized UE rate times a random scaler guarantees the feasibility of each iteration in the optimization algorithm.

On the other hand, fairness should also be considered in the system design. The object of fairness is to enhance the minimum UE rate, which improves the QoS of UE. The maximization problem of the minimum UE rate is formulated as follows

$$\underset{\mathbf{P}}{\text{maximize}} \quad \min_{k,l} \quad R_{kl}^{\text{d}}(\mathbf{p}) \tag{5.14a}$$

$$\text{Subject to} \quad \mathbf{t}_{kl}^{T}\mathbf{p} \geq 0, \ \forall\,(k,l) \in (\mathcal{K},\mathcal{L}) \tag{5.14b}$$

$$\sum_{k=1}^{K} \mathbf{t}_{kl}^{T}\mathbf{p} \leq p_{\text{max}}^{\text{d}} \ , \ \forall\,(l) \in (\mathcal{L})\,. \tag{5.14c}$$

To solve Problem (5.14a), it can be transferred into a epigraph form, which is commonly used for solving concave optimization problem [116]. The epigraph form is a reformulation of the concave problem by replacing the original objective function with a new variable and an equal constraints. Consequently, the Problem (5.14a) can be reformulated as

$$\underset{\chi,\mathbf{P}}{\text{maximize}} \quad \chi \tag{5.15a}$$

$$\text{subject to} \quad R_{kl}(\mathbf{p}) \geq \chi, \forall\,(k,l) \in (\mathcal{K},\mathcal{L}) \tag{5.15b}$$

$$\mathbf{t}_{kl}^{T}\mathbf{p} \geq 0, \ \forall\,(k,l) \in (\mathcal{K},\mathcal{L}) \tag{5.15c}$$

$$\sum_{k=1}^{K} \mathbf{t}_{kl}^{T}\mathbf{p} \leq p_{\text{max}}^{\text{d}} \ , \ \forall\,(l) \in (\mathcal{L})\,, \tag{5.15d}$$

where χ is the introduced variable. It can be found that Problem (5.15) is a linear programming problem and it is concave. It can be solved by the common optimization method, e.g. CVX, where the proof of concave is presented below.

Proposition 1. *The Problem (5.15) is linear programming problem.*

Proof. The constraint (5.15b) can be reformulated as follows

$$\begin{aligned}\left(1-\frac{\tau}{T}\right)\log_2\left(1+\frac{\mathbf{z}_{ij}^T\mathbf{p}}{\mathbf{b}_{ij}^T\mathbf{p}+\sigma_{\mathrm{n}}^2}\right) &\geq \chi \\ \log_2\left(1+\frac{\mathbf{z}_{ij}^T\mathbf{p}}{\mathbf{b}_{ij}^T\mathbf{p}+\sigma_{\mathrm{n}}^2}\right) &\geq \frac{\chi}{\left(1-\frac{\tau}{T}\right)} \\ \frac{\mathbf{z}_{ij}^T\mathbf{p}}{\mathbf{b}_{ij}^T\mathbf{p}+\sigma_{\mathrm{n}}^2} &\geq 2^{\frac{\chi}{\left(1-\frac{\tau}{T}\right)}}-1 \end{aligned} \tag{5.16}$$

Let $y \triangleq 2^{\frac{\chi}{\left(1-\frac{\tau}{T}\right)}}-1$, then equation (5.16) can be reformulated as

$$\begin{aligned}\mathbf{z}_{ij}^T\mathbf{p} &\geq y\mathbf{b}_{ij}^T\mathbf{p}+y\sigma_{\mathrm{n}}^2 \\ \left(\mathbf{z}_{ij}^T-y\mathbf{b}_{ij}^T\right)\mathbf{p} &\geq y\sigma^2 \\ \mathbf{p} &\geq \frac{y\sigma^2}{\left(\mathbf{z}_{ij}^T-y\mathbf{b}_{ij}^T\right)}\end{aligned} \tag{5.17}$$

As a result, the reformulation of constraint (5.15b) proofed that the Problem (5.15) is a linear programming problem. □

After the maximization of minimum UE rate, it provides a feasible constraints for optimizing EE. As Problem $(5.13a)$ is a fractional expression, the fractional programming, which is a useful branch of optimization theory [110], can be utilized for solving the problem. A brief introduction of fractional programming and the algorithm that utilized for solving the problem will be given below.

5.4 Introduction of Fractional Programming

Consider the following optimization problem

$$\underset{\mathbf{x}}{\text{maximize}} \quad \frac{y(\mathbf{x})}{z(\mathbf{x})} \tag{5.18a}$$

$$\text{subject to} \quad v_i(\mathbf{x}) \leq 0, \forall i = 1, 2, \cdots, I \tag{5.18b}$$

$$w_j(\mathbf{x}) = 0, \forall j = 1, 2, \cdots, J \tag{5.18c}$$

where $y(\mathbf{x})$ is a non-negative concave function, and $z(\mathbf{x})$ is a positive convex function, $v_i(\mathbf{x})$ is convex for all the i and $w_j(\mathbf{x})$ is affine for all the j. As proved in [110], equation $(5.18a)$ is a quasi-concave optimization problem.

One useful algorithm for solving the optimization with objective function as a fractional expression is the Dinkelbach algorithm [118]. it is a an approach of parametric convex programme, because of the introduction of an extra parameter λ. The fractional problem can be converted into linear form and iteratively solved. If the constraints (5.18b) and (5.18c) are denoted by $\mathcal{X}$, the Problem (5.18a) can be converted as

$$F(\lambda) = \underset{\mathbf{x}\in\mathcal{X}}{\text{maximize}} \quad y(\mathbf{x}) - \lambda(\mathbf{x}). \tag{5.19}$$

The function $F(\lambda)$ has the following properties [110, 118]

- $F(\lambda)$ is convex on $\mathbb{R}$

  Proof. if it is assumed that $u \in [0, 1]$, then it has

  $$\begin{aligned} &F(u\lambda_1 + (1-u)\lambda_2) = \max\{y(\mathbf{x}) - u\lambda_1(\mathbf{x}) - (1-u)\lambda_2(\mathbf{x})\} = \\ &\max\{u[y(\mathbf{x}) - \lambda_1(\mathbf{x})] + (1-u)[y(\mathbf{x}) - \lambda_2(\mathbf{x})]\} \leq \\ &u \cdot \max\{[y(\mathbf{x}) - \lambda_1(\mathbf{x})]\} + (1-u) \cdot \max\{[y(\mathbf{x}) - \lambda_2(\mathbf{x})]\} = \\ &uF(\lambda_1) + (1-u)F(\lambda_2) \end{aligned} \tag{5.20}$$

  □

- $F(\lambda)$ is monotonically decreasing, e.g. if $\lambda_2 > \lambda_1$, then $F(\lambda_2) < F(\lambda_1)$

Proof. Let $\lambda_2 > \lambda_1$, then $F(\lambda_2)$ has the following relationship

$$F(\lambda_2) = \max\{y(\mathbf{x}) - \lambda_2 z(\mathbf{x})\} = y(\mathbf{x_2}) - \lambda_2 z(\mathbf{x_2}) < y(\mathbf{x_2}) - \lambda_1 z(\mathbf{x_2}) \leq \max\{y(\mathbf{x}) - \lambda_1 z(\mathbf{x})\} = F(\lambda_1) \tag{5.21}$$

□

- $F(\lambda) = 0$ has a unique solution, λ_0

  Proof. As $F(\lambda)$ is monotonically decreasing, plus the following fact, where $\lim_{\lambda\to-\infty} F(\lambda) = +\infty$ and $\lim_{\lambda\to+\infty} F(\lambda) = -\infty$, $F(\lambda) = 0$ has a unique solution, λ_0. □

In addition, the connection of Problem (5.18a) and (5.19) is proved as follows [110, 118].

Proposition 2. *If $\mathbf{x}^* \in \mathcal{X}$ and $\lambda^* = \frac{y(\mathbf{x}^*)}{z(\mathbf{x}^*)}$, then $\mathbf{x}^*$ will be a solution of problem (5.18a) if and only if*

$$\mathbf{x}^* = \arg\max_{\mathbf{x}\in\mathcal{X}} \{y(\mathbf{x}) - \lambda^* z(\mathbf{x})\} \tag{5.22}$$

Proof. If $\mathbf{x}^*$ is the optimal solution of problem (5.18a), it comes to

$$\lambda^* = \frac{y(\mathbf{x}^*)}{z(\mathbf{x}^*)} > \frac{y(\mathbf{x})}{z(\mathbf{x})}, \forall \mathbf{x} \in \mathcal{X}. \tag{5.23}$$

As a result, $y(\mathbf{x}) - \lambda^* z(\mathbf{x}) \leq 0, \forall \mathbf{x} \in \mathcal{X}$ and $y(\mathbf{x}^*) - \lambda^* z(\mathbf{x}^*) = 0$. Consequently, $F(\lambda^* = 0)$ and it meets equation (5.22). On the other hand, if $\mathbf{x}^* = \arg\max_{\mathbf{x}\in\mathcal{X}} \{y(\mathbf{x}) - \lambda^* z(x)\}$, it comes to

$$y(\mathbf{x}) - \lambda^* z(\mathbf{x}) \leq y(\mathbf{x}^*) - \lambda^* z(\mathbf{x}^*) = F(\lambda^*) = 0, \forall \mathbf{x} \in \mathcal{X}. \tag{5.24}$$

As a result,

$$\lambda^* \geq \frac{y(\mathbf{x})}{z(\mathbf{x})}, \forall \mathbf{x} \in \mathcal{X} \tag{5.25}$$

$$\lambda^* = \frac{y(\mathbf{x}^*)}{z(\mathbf{x}^*)} \tag{5.26}$$

□

As a result, the Problem (5.18a) is converted into linear convex problems, where $F(\lambda)$ continuously decreases with the variable λ. The convergence point is found by iteratively updating

λ so that the numerator function can be maximized while the denominator function can be minimized, until $F(\lambda) = 0$ and $\mathbf{x}^*$ is equivalently the root of the function. The Dinkelbach algorithm is described in Algorithm 1.

Algorithm 1 The Dinkelbach method to solve optimization problem

Require:
$\lambda^{(0)}$ (initial value of λ where $F(\lambda_0) \geq 0$)
ϵ_{fp} (convergence tolerance)
$i = 0$ (iteration number)
Ensure:
λ^* (optimal λ)
$\mathbf{x}^*$ (optimal $\mathbf{x}$)
1: **while** $F(\lambda_i) \geq \epsilon_{fp}$ **do**
2: solve the problem $\mathbf{x}_i^* = \arg\max_{\mathbf{x}\in\mathcal{X}} \left(y(\mathbf{x}) - \lambda^{(i)} g(\mathbf{x})\right)$;
3: $i = i + 1$;
4: **end while**

The directly utilization of the fractional programming theory to solve the EE maximization problem is not capable because of the objective function and constraint has DC function. In the next section, the SCA algorithm will be introduced, where it will be combined with the fractional programming.

5.4.1 Introduction of the SCA Algorithm

The utilization of fractional programming theory converts the EE maximization problem into a series of concave problem, and the global optimal solution can be iteratively found by utilizing the Dinklebach algorithm. However, the directly adoption of fractional programming theory requires conditions on both the objective function and constraints, where $y(\mathbf{x})$ needs to be a concave function, $z(\mathbf{x})$ is a concave function and the constraints are all concave as well. In terms of the multi-cell massive MIMO system with TDD operation, the expression of downlink rate, which is the numerator in Problem (5.13a) and the constraint (5.13d), is a non-concave function [119, 120]. Consequently, the sequential concave approximation (SCA) algorithm is considered for combining with the fractional programming.

The SCA algorithm is an advanced scheme that utilized to solve the non-concave optimization problems, where the local optimal solutions can be found efficiently with acceptable complexity

[121, 122]. Consider a non-concave optimization problem

$$\underset{\mathbf{x}\in\mathbb{R}^M}{\text{maximize}} \quad y(\mathbf{x}) \tag{5.27a}$$

$$\text{s.t.} \quad c_j(\mathbf{x}) \leq 0\ ,\ j = 1, 2, \cdots, J, \mathbf{x} \in \Omega \tag{5.27b}$$

where y, c_j are both continuous and differentiable functions over $\mathbb{R}^M$. It is assumed that both y and c_j can be expanded as the difference of two non-negative concave functions, which are expressed as

$$y(\mathbf{x}) \triangleq y^+(\mathbf{x}) - y^-(\mathbf{x}) \tag{5.28}$$

$$c_j(\mathbf{x}) \triangleq c_j^+(\mathbf{x}) - c_j^-(\mathbf{x}) \tag{5.29}$$

where $y^+, y^-, c_j^+, c_j^- : \mathbb{R}^M \to \mathbb{R}$. It can be observed that both the objective function (5.27a) and the constraint (5.27b) are typical difference of concave functions (DC) programming of variable $\mathbf{x}$ [123] with DC constraint, which is generally considered as a non-concave problem. As a result, common concave optimization algorithms can not be directly applied on solving this kind of problems.

There are many algorithms that proposed for finding the global optimal solutions for the non-concave problems [124, 125]. However, the high computational complexity is not suitable in massive MIMO systems. One common scheme of solving a non-concave problem with local convergence is the approximation of concave functions. And the SCA algorithm adopts this scheme in solving the non-concave problem iteratively. A surrogate function is generated for the approximation iteratively by utilizing the first order Taylor series expansion, which is given as

$$y(\mathbf{x}, \mathbf{z}) = y(\mathbf{x})^+ - \left(y^-(\mathbf{z}) + (\nabla y(\mathbf{z}))^T(\mathbf{x} - \mathbf{z})\right). \tag{5.30}$$

The equation (5.30) is an approximation of function $y(\mathbf{x})$, which is tight when $\mathbf{x} = \mathbf{z}$. Otherwise it comes to $y(\mathbf{x}, \mathbf{z}) < y(\mathbf{x})$. Similarly, the surrogate functions can also be generated for the DC constraints. By replacing the non-concave functions in both the objective function and constraints with their surrogate functions, problem (5.27a) can be approximated linearly by a series of concave functions, which can be iteratively solved with acceptable complexity. The SCA algorithm is summarized in Algorithm 2.

After the introduction of fractional programming and the SCA algorithm, the proposed fractional SCA algorithm in solving the EE problem will be presented in the follow section.

5.4.2 Fractional SCA Algorithm

To solve the maximization of EE in multi-cell massive MIMO system with TDD operation, the combination of fractional programming and the SCA algorithm is proposed to jointly find the optimal downlink power allocation. The optimization firstly calculates the maximized minimum UE rate R^*_{min}, which provides a feasible constraints. Secondly, the surrogate function is generated for the downlink achievable rate, which is the numerator of the objective function (5.13a) and constraints (5.13d), where with feasible vector $\mathbf{q}$, the surrogate functions for the SCA algorithm are expressed as

$$R^{\text{d}}_{kl}(\mathbf{p},\mathbf{q}) \triangleq \left(1-\frac{\tau}{T}\right)\left(\log_2\left(\frac{\left(\mathbf{z}^T_{kl}+\mathbf{b}^T_{kl}\right)\mathbf{p}+\sigma^2_{\text{n}}}{\left(\mathbf{z}^T_{kl}+\mathbf{b}^T_{kl}\right)\mathbf{q}+\sigma^2_{\text{n}}}\right)-\frac{1}{\log\left(2\right)}\frac{\mathbf{b}^T_{kl}\left(\mathbf{p}-\mathbf{q}\right)}{\left(\mathbf{z}^T_{kl}+\mathbf{b}^T_{kl}\right)\mathbf{q}+\sigma^2_{\text{n}}}\right). \quad (5.31)$$

Thirdly, by utilizing the fractional programming in the (5.13a) with equation (5.31), the maximization problem is reformulated as

$$\begin{aligned}
\underset{\mathbf{p}}{\text{maximize}} \quad & \sum_{l=1}^{L}\sum_{k=1}^{K}\left(1-\frac{\tau}{T}\right)\left(\log_2\left(\frac{\left(\mathbf{z}^T_{kl}+\mathbf{b}^T_{kl}\right)\mathbf{p}+\sigma^2_{\text{n}}}{\left(\mathbf{z}^T_{kl}+\mathbf{b}^T_{kl}\right)\mathbf{q}+\sigma^2_{\text{n}}}\right)-\frac{1}{\log\left(2\right)}\frac{\mathbf{b}^T_{kl}\left(\mathbf{p}-\mathbf{q}\right)}{\left(\mathbf{z}^T_{kl}+\mathbf{b}^T_{kl}\right)\mathbf{q}+\sigma^2_{\text{n}}}\right) \\
& -\lambda P_{\text{tot}}\left(\mathbf{p}\right) && (5.32a)\\
\text{subject to} \quad & \mathbf{t}^T_{kl}\mathbf{p}\geq 0, \forall\left(k,l\right)\in\left(\mathcal{K},\mathcal{L}\right) && (5.32b)\\
& \sum_{k=1}^{K}\mathbf{t}^T_{kl}\mathbf{p}\leq p^{\text{d}}_{\text{max}}, \forall\left(l\right)\in\left(\mathcal{L}\right) && (5.32c)\\
& \left(1-\frac{\tau}{T}\right)\left(\log_2\left(\frac{\left(\mathbf{z}^T_{kl}+\mathbf{b}^T_{kl}\right)\mathbf{p}+\sigma^2_{\text{n}}}{\left(\mathbf{z}^T_{kl}+\mathbf{b}^T_{kl}\right)\mathbf{q}+\sigma^2_{\text{n}}}\right)-\frac{1}{\log\left(2\right)}\frac{\mathbf{b}^T_{kl}\left(\mathbf{p}-\mathbf{q}\right)}{\left(\mathbf{z}^T_{kl}+\mathbf{b}^T_{kl}\right)\mathbf{q}+\sigma^2_{\text{n}}}\right) \\
& \geq R^*_{\text{min}}, \forall\left(k,l\right)\in\left(\mathcal{K},\mathcal{L}\right). && (5.32d)
\end{aligned}$$

The maximization Problem (5.32) becomes a concave optimization problem with both linear objective function and constraints, which can be iteratively solved by Algorithm 3 with the CVX package [117, 126].

The convergence of the proposed fractional SCA algorithm is proved below.

Proposition 3. *The fractional SCA algorithm in Algorithm 3 always converges to a Karush-Kuhn-Tucker (KKT) stationary solution of Problem (5.13).*

Algorithm 2 The SCA algorithm

Require:
$i = 0$ (iteration number)
$\mathbf{x}^{(0)}$ (initial value of $\mathbf{x}$ where $\mathbf{x} \in \mathcal{X}$)
ϵ_{SCA} (convergence tolerance)
Ensure:
$\mathbf{x}^*$ (optimal $\mathbf{x}$)
1: **while** $\|\mathbf{x}^{(i+1)} - \mathbf{x}^{(i)}\|_2 > \epsilon_{SCA}$ **do**
2: Generate the surrogate functions $y\left(\mathbf{x}, \mathbf{x}^{(i)}\right)$ and $c_j\left(\mathbf{x}, \mathbf{x}^{(i)}\right)$;
3: $\mathbf{x}^{(i+1)} = \underset{\substack{x\in\Omega \\ c_j\left(\mathbf{x},\mathbf{x}^{(i)}\right)\leq 0, j=1,2,\cdots,J}}{\arg\max} \quad y\left(\mathbf{x}, \mathbf{x}^{(i)}\right)$;
4: $i = i + 1$
5: **end while**

Proof. To any concave function, it is upper-bounded by its first-order Taylor expansion at any point. Meanwhile, it is noticeable that the numerator of objective function (5.13a) and the constraint (5.13d) are the difference of two concave functions. If $R_{kl}^{\mathrm{d}}(\mathbf{p})$ is represented as

$$R_{kl}^{\mathrm{d}}(\mathbf{p}) = r_{kl}^{+}(\mathbf{p}) - r_{kl}^{-}(\mathbf{p}), \tag{5.33}$$

for any $\mathbf{p}_j$, it thus have that

$$r_{kl}^{+}(\mathbf{p}) - r_{kl}^{-}(\mathbf{p}) \geq r_{kl}^{+}(\mathbf{p}) - \left[r_{kl}^{-}(\mathbf{p}_j) + \left(\triangledown R_{kl}^{\mathrm{d}}(\mathbf{p})\right)^{T}(\mathbf{p} - \mathbf{p}_j)\right]. \tag{5.34}$$

Consequently, (5.32a) and (5.32d) are lower bounds of (5.13a) and (5.13d). As the lower bounds in (5.33) is tight when evaluated in $\mathbf{p}_j$, when $\mathbf{p} = \mathbf{p}_j$, it comes to (5.32a) and (5.32d) are equal to (5.13a) and (5.13d). Similarly, the gradients of (5.32a) and (5.32d) are equal to (5.13a) and (5.13d) when $\mathbf{p} = \mathbf{p}_j$. Consequently, the proposition proof is completed. □

By utilizing the Algorithm 3, the EE will monotonically increase and the local-optimal solution, which meets the given constraints, will iteratively be founded within polynomial time and affordable complexity.

5.5 Numerical examples

In this section, the validity of the proposed optimization algorithms will be verified by numerical simulations.

Algorithm 3 The fractional SCA algorithm to solve Problem (5.13)

Initialization for SCA algorithm:
$\mathbf{q}^{(0)} \in \mathbb{R}^{KL\times 1}$ % an initial feasible downlink power vector
$\epsilon_1 \in \mathbb{R}$ % a small convergence threshold
$i = 0$;
repeat
  Given $\mathbf{q}^{(i)}$, generate the surrogate functions $R_{kl}^{\mathrm{d}}\left(\mathbf{p}, \mathbf{q}^{(i)}\right)$ based on Equation (5.31);
  Initialization for Dinkelbach method:
  $\lambda^{(0)} \geq 0$ % determined by a random power vector $\mathbf{p}^{(0)} \in \mathbb{R}^{KL\times 1}$
  $\epsilon_2 \in \mathbb{R}$ % a small convergence threshold
  $j = 0$;
  repeat
    Given $\lambda^{(j)}$, obtain the optimal solution $\mathbf{p}^{(j)}$ for Problem (5.32);
    $\lambda^{(j+1)} \leftarrow \frac{\sum_{l=1}^{L}\sum_{k=1}^{K} R_{kl}^{\mathrm{d}}\left(\mathbf{p}^{(j)},\mathbf{q}^{(i)}\right)}{P_{\mathrm{tot}}\left(\mathbf{p}^{(j)}\right)}$;
    $j \leftarrow j + 1$;
  until $|\lambda^{(j)} - \lambda^{(j-1)}| \leq \epsilon_1$;
  $i \leftarrow i + 1$;
  return $\mathbf{q}^{(i)} \leftarrow \mathbf{p}^{(j)}$;
until $||\mathbf{q}^{(i)} - \mathbf{q}^{(i-1)}||_2 \leq \epsilon_2$;
return a locally optimal solution $\mathbf{p}^* = \mathbf{q}^{(i)}$ for Problem (5.13).

Consider a massive MIMO system consisting of 19 hexagon shaped cells, where each cell has a central BS and randomly distributed UEs. The simulation parameters listed in Table 5.3, which includes both the configuration of BS antennas and UE distribution, plus the power consumption of circuit power for both BS and UE. Additionally, the circuit power of BS was chosen according to the prediction that by the year 2020 [2]. The pilot reuse scheme with $RF = 3$ was considered in the simulation with the same UE distribution that was proposed in Chapter 4. The codebook for the GLP-based uplink pilot utilized the algorithm that was proposed in [99].

Figure.5.3 shows the minimum UE rate versus the number of BS antennas. The GLP based pilot codebook design and pilot reuse scheme were both utilized with $RF = 3$ and $\tau = 16$. The maximization of the minimum UE rate were calculated with the CVX. It can be observed that the adoption of optimization has enhanced the QoS significantly. When $M = 64$, the minimum UE rate of the pilot reuse scheme almost doubled, and it almost tripled for the GLP-based pilot design after the maximization. When $M = 256$, the improvement of pilot reuse increased by more than three times and it is approximately four times for the GLP-based pilot design after maximization.

Number of cells, L	19
Number of antennas at BS, M	$64 \leq M \leq 256$
Cell radius	500 m
UE minimum distance from BS	25 m
Carrier frequency	1.9 GHz
System bandwidth	20 MHz
Maximum UL power, $P_{\text{max}}^{\text{UL}}$	200 mW
Maximum DL power, $P_{\text{max}}^{\text{DL}}$	40 W
Thermal noise, σ_{n}^2	-174 dBm/Hz [127]
Mobility speed	60 km/H
Path loss model	$35.3 + 37.6 \log_{10} d$ dB
Coherence bandwidth	100 kHz
Power consumption of circuit power at BS, P_{c}^{d}	0.2 W [128]
Loss factor from DC to DC power supply, σ_{DC}	7.5% [2]
Loss factor from mains supply, σ_{MS}	9% [2]
Loss factor from cooling, σ_{cool}	10% [2]
Power amplifier efficiency of BS, η_{BS}	50 % [128]
Power amplifier efficiency of UE, η_{UE}	20 % [129]
UE circuit power, P_{c}^{u}	0.1 W [130]
Convergence tolerance, ϵ	1×10^{-3}

Table 5.3: *Simulation parameters for the results in this section*

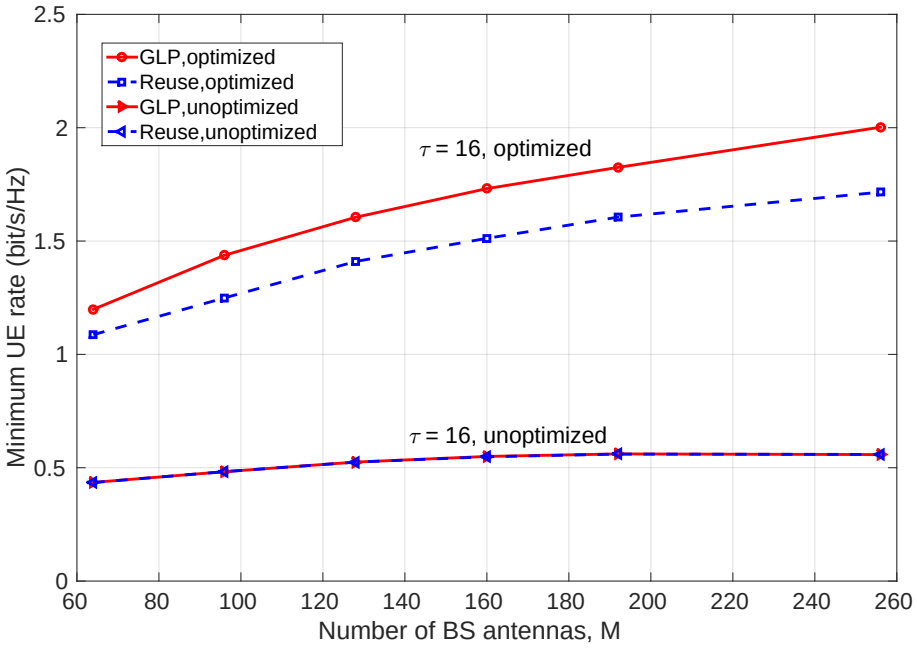

Figure 5.3: *Comparison of the minimum UE rate versus number of BS antennas M with and without maximization, with $RF = 3$, $\tau = 16$*

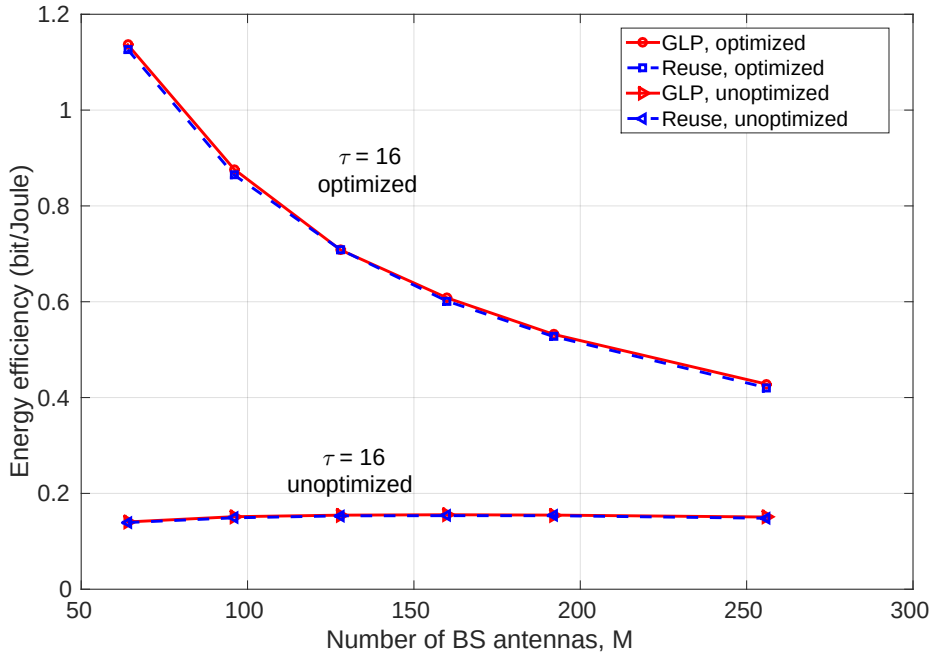

Figure 5.4: *Comparison of the energy efficiency versus the number of BS antennas with and without maximization, with* $RF = 3$, $\tau = 16$

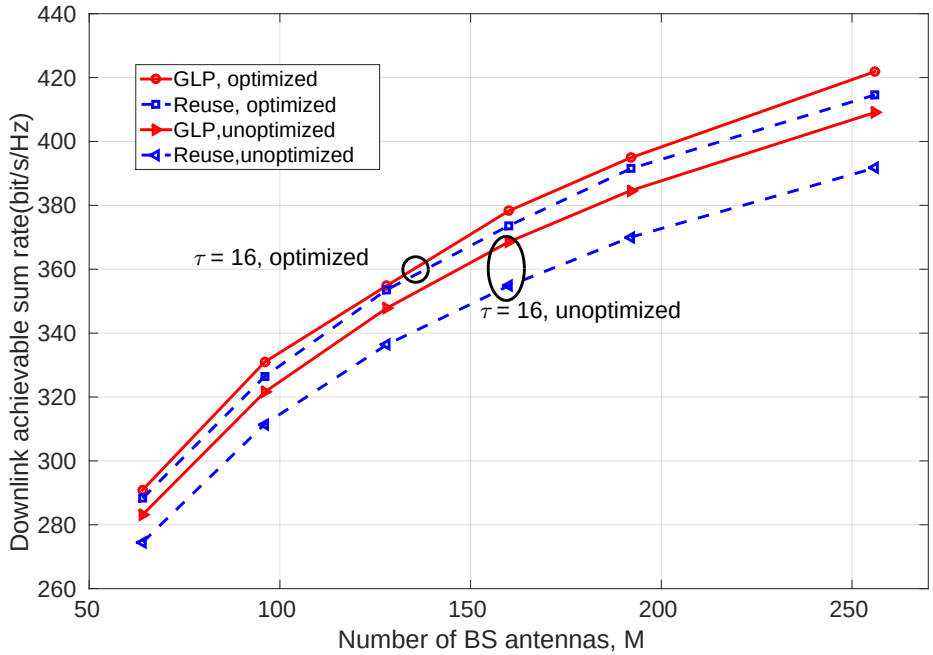

Figure 5.5: *Comparison of the downlink achievable sum rate versus the number of BS antennas* M *with and without optimization, with* $RF = 3$, $\tau = 16$.

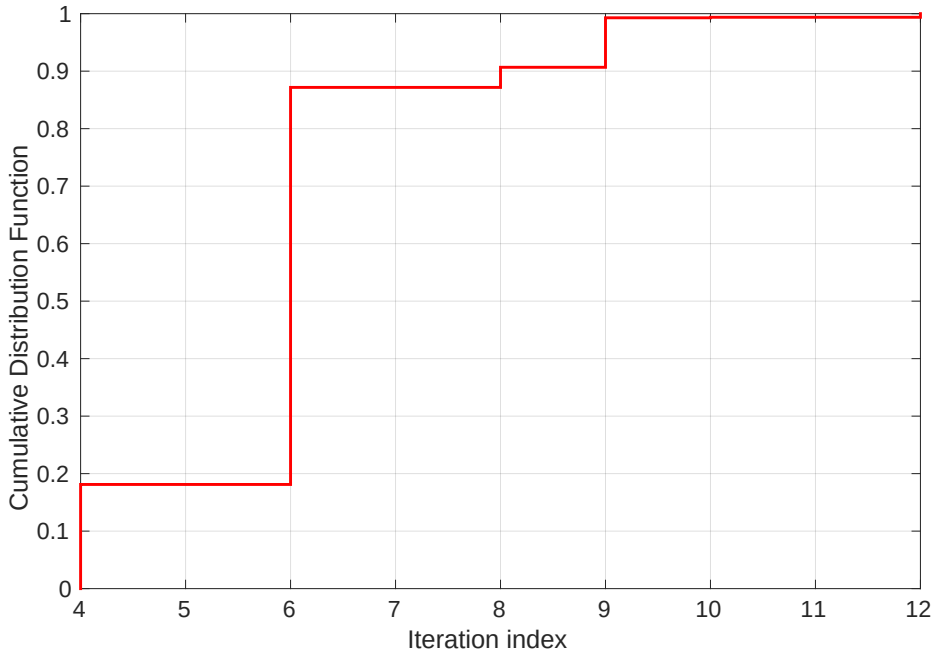

Figure 5.6: *Converge performance of Algorithm 3, with* $RF = 3$, $\tau = 16$, $\epsilon = 1 \times 10^{-3}$

Figure.5.4 shows the EE of multi-cell massive MIMO system versus the number of BS antennas. Again, the GLP based pilot codebook design and the pilot reuse scheme are both utilized, with $RF = 3$ and $\tau = 16$. The maximization of EE utilized Algorithm 3. For the unoptimized EE, the downlink transmit power was equally divided for each serving UE in the cell, i.e. $\frac{P_{\max}^{\mathrm{d}}}{K}$. It can be observed that the EE of both schemes decreased with the number of BS antennas, whereby, the EE without optimization slightly increased, but was almost consistent, mainly because, in the EE without optimization the downlink transmit power is dominant. The maximum power was utilized for downlink transmission and the increase of circuit power did not have a big influence on the EE. However, after the optimization, the downlink transmit power was greatly reduce, so the EE of both schemes decreased with the number of BS antenna adopted followed by the increase of BS circuit power.

Figure.5.5 shows the downlink achievable sum rate versus the number of BS antennas. A comparison has been made between the rates after downlink power allocation and the rate after the equal division of downlink transmission power has been utilized. Although the focus was on maximizing the EE, the optimal allocation of downlink power and the maximized minimum UE rate has improved the performance, with approximately 3% for GLP-based pilot codebook design and 5% for the pilot reuse scheme. The gap between two schemes has been reduced after

the power allocation. However, the GLP-based codebook design still performed better than the pilot reuse scheme. The main reason of the optimized rate has better performance than the unoptimized rate is that the optimal EE is computed with the maximum downlink achievable sum rate. According to the proposition in [108], the maximization of EE is equivalent with the downlink rate maximization.

Figure.5.6 shows the convergence performance of Algorithm 3. This is a Cumulative distribution function (CDF) plot of the iteration numbers to reach the $\epsilon = 10^{-}3$ in the maximization of EE with $RF = 3$ and $\tau = 16$. It can be observed that there are 90% of the results need 6 iterations to reaches the convergence point, and the optimization algorithm will 100% converge within 12 iterations.

5.6 Conclusion

In this chapter, motivated by the increasing demand for reducing energy consumption in cellular system designs, a general framework has been proposed for maximizing the energy efficiency of the system with a guaranteed minimum downlink rate constraint - a framework can be utilized in both multi-UE MIMO and massive MIMO systems. The optimal allocation of downlink transmit power was developed, which was based on the joint adoption of the fractional programming theory and sequential concave approximation. Because the difference of concave function problems exists in the objective functions and constraints, a first-order approximation has been considered for converting the non-concave problem into a series of concave problems. This was followed by converting the optimization problem from a fractional form into a linear form, in order for it to be solved iteratively.

Maximization of the minimum UE rate has also been considered in order to provide a feasible constraint. By applying the proposed optimization algorithm, the numerical results showed an improvement in the system's minimum UE rate, where the pilot reuse scheme has increased approximately 200% and the GLP-based codebook design almost increased 300% after utilizing the proposed optimization. In terms of the maximization of EE, compared with the equal division of downlink transmit power, it has been increased six times with $M = 64$ and two times with $M = 256$. The results have also shown that the energy efficiency of massive MIMO system decreases with the number of BS antennas after optimization, because of the increased circuit power consumption of BS. This suggests that an optimal number of BS antennas should

be considered for balancing the rate and energy performance of efficiency.

This chapter will be followed by the conclusion to this thesis in which the works and contributions in terms of both the conventional MIMO and massive MIMO systems will be summarized, after which a future extension of this research will be proposed.

Chapter 6
Conclusions and Future Work

This thesis has contributed to both conventional multiple-input multiple-output (MIMO) and massive MIMO systems. In this chapter, Section 6.1 will present a conclusion, which will summarize its main contributions and Section 6.2 will focus on the further research directions based on the findings from this thesis.

6.1 Conclusions

This thesis presented a study of both conventional MIMO and massive MIMO systems. The contributions focus on the following two important perspectives: (i) capacity enhancement, and (ii) energy efficiency improvement. The major research findings are summarized in the following section.

6.1.1 The K-best Detector and Adaptive Modulation Scheme

The joint utilization of K-best detector and adaptive modulation scheme has been presented in this thesis. The bit-error-rate (BER) performance estimation of the K-best algorithm in different channel conditions has been solved by the proposed estimation scheme, which is based on the union bound (UB) of maximum likelihood detector(MLD) with minimum Euclidean distance events that significantly reduced the computational complexity between 95% to 99%. The BER estimation has guaranteed accuracy with the pre-estimated look-up-table (LUT). With the reduced complexity and promising estimation accuracy, the K-best algorithm and adaptive modulation is very suitable for the practical application, especially for the parallel high performance hardware platform.

6.1.2 New Analytical Results

Three closed-form analytical expressions of down link achievable sum rate for massive MIMO systems with time-division-duplex (TDD) operation have been proposed in this thesis. The

adoption of analytical propositions helps to establish how the downlink achievable sum rate is affected by the pilot contamination phenomenon, which is considered to be one of the main limiting factors in terms of the performance of the massive MIMO systems. These propositions can be utilized for the performance analysis of single-cell, multi-cell and pilot reuse schemes respectively, since the numerical results have validated the analytical propositions.

This thesis has evaluated the performance of Grassmannian line packing (GLP) based pilot codebook design and a comparison has been made with the pilot reuse scheme. Furthermore, the numerical results have shown that the codebook design has significantly increased the downlink performance for both cell centre and edge user-equipments (UEs).

6.1.3 General framework of energy efficiency maximization

This thesis proposes a general framework of energy efficiency maximization that can be applied in both multi-UE and massive MIMO systems. The optimal allocation of downlink transmit power, which is based on the joint adoption of the fractional programming theory and sequential concave approximation, has been proposed. Since the difference of concave function problems exist in the objective function and constraints, the first-order approximation has been considered in order to convert the non-concave problem into a series of concave problems. It can be iteratively solved by converting the optimization problem from fractional into linear form. The numerical results proof the enhancement of minimum UE rate and the significant improvement of energy efficiency. It was found that the energy efficiency decreases with the number of base station (BS) antennas, because of the increase in circuit power consumption.

6.2 Future Work

Several directions may be taken that might possibly expand on the findings of this thesis.

- In Chapter 3, an assumption was made regarding the adaptive modulation scheme, whereby the perfect channel state information (CSI) was fully available at the receiver. Further improvements could be made for choosing the imperfect CSI for the performance prediction of the adaptive modulation scheme. This is because the imperfection comes from two different sources, (i) predicted errors from the channel estimation scheme, and (ii) the delay existed in the feedback from receiver to transmitter. The extension of imperfect

CSI is considered to be a more practical assumption and increases more difficulties for the performance prediction in adaptive modulation scheme.

- In Chapter 3, the transmission parameter considered in the adaptive scheme is the modulation. More parameters could be included in the adaptive scheme; for example, the coding schemes and transmit power could also be considered for the K-best detector as it is similar to the present adaptive modulation scheme, whereby the transmit power and coding method is adjusted to meet the varying channel conditions with the aim of maximizing the spectrum efficiency.

- In Chapter 4, the least square (LS) and maximum ratio transmission (MRT) methods were utilized for uplink channel estimation and downlink precoding. A possible expansion would be to consider other schemes. For example, zero-forcing (ZF) and minimum mean squared error (MMSE) are linear channel estimation methods, which have also been shown to perform well in massive MIMO systems. Similarly, the downlink precoding can also be considered for the ZF and MMSE scheme to further enhance the downlink rate.

- In Chapter 5, the power consumption model of downlink transmission adopted full radio frequency (RF) chains. An expansion could be made to optimize the number of RF chains for downlink transmission; this is known as the hybrid analogue and digital beamforming[131, 132]. The optimization problem could be extended in order to maximize the energy efficiency of the system with the number of RF chains being the variable, which subjects to the constraint of minimum UE rate requirement and maximum downlink power.

Appendix A

Proof of the Theorem 1

Proof.

$$
\begin{aligned}
&\left|\mathbf{h}_i^H\hat{\mathbf{h}}_m\right|^2 \\
&= \left(\sum_{n_1=1}^{K}\sqrt{\frac{\beta_{n_1}p_{n_1}^u}{p_m^u}}\rho_{m,n_1}\mathbf{h}_i^H\mathbf{h}_{n_1} + \frac{1}{\sqrt{p_m^u}}\mathbf{h}_i^H\mathbf{S}_m^H\mathbf{z}\right)^H \times \left(\sum_{n_2=1}^{K}\sqrt{\frac{\beta_{n_2}p_{n_2}^u}{p_m^u}}\rho_{m,n_2}\mathbf{h}_i^H\mathbf{h}_{n_2} + \frac{1}{\sqrt{p_m^u}}\mathbf{h}_i^H\mathbf{S}_m^H\mathbf{z}\right) \\
&= \sum_{n_1=1}^{K}\sum_{n_2=1}^{K}\sqrt{\frac{\beta_{n_1}p_{n_1}^u}{p_m^u}}\sqrt{\frac{\beta_{n_2}p_{n_2}^u}{p_m^u}}\rho_{m,n_1}\rho_{m,n_2}\mathbf{h}_{n_1}^H\mathbf{h}_i\mathbf{h}_i^H\mathbf{h}_{n_2} + \sum_{n_1=1}^{K}\sqrt{\frac{\beta_{n_1}p_{n_1}^u}{p_m^u}}\rho_{m,n_1}\mathbf{h}_{n_1}^H\mathbf{h}_i\mathbf{h}_i^H\mathbf{S}_m^H\mathbf{z} \\
&+ \sum_{n_2=1}^{K}\sqrt{\frac{\beta_{n_2}p_{n_2}^u}{p_m^u}}\rho_{m,n_2}\mathbf{z}^H\mathbf{S}_m^H\mathbf{h}_i\mathbf{h}_i^H\mathbf{h}_{n_2} + \frac{1}{p_m^u}\mathbf{z}^H\mathbf{S}_m\mathbf{h}_i\mathbf{h}_i^H\mathbf{S}_m^H\mathbf{z}. \qquad \text{(A.1)}
\end{aligned}
$$

Then, we have

$$
\begin{aligned}
&\mathrm{E}\left|\mathbf{h}_i^H\hat{\mathbf{h}}_m\right|^2 \\
&= \frac{1}{p_m^u}\left(\sum_{n_1=1}^{K}\sum_{n_2=1}^{K}\sqrt{\beta_{n_1}p_{n_1}^u}\sqrt{\beta_{n_2}p_{n_2}^u}\rho_{m,n_1}\rho_{m,n_2}\mathrm{E}\left[\mathbf{h}_{n_1}^H\mathbf{h}_i\mathbf{h}_i^H\mathbf{h}_{n_2}\right] + \mathrm{E}\left[\mathbf{z}^H\mathbf{S}_m\mathbf{h}_i\mathbf{h}_i^H\mathbf{S}_m^H\mathbf{z}\right]\right) \\
&= \frac{1}{p_m^u}\left(\beta_i p_i^u\rho_{m,i}^2\mathrm{E}\left[\mathbf{h}_i^H\mathbf{h}_i\mathbf{h}_i^H\mathbf{h}_i\right] + \sum_{n_1=n_2\neq i}^{K}\beta_{n_1}p_{n_1}^u\rho_{m,n_1}^2\mathrm{E}\left[\mathbf{h}_{n_1}^H\mathbf{h}_i\mathbf{h}_i^H\mathbf{h}_{n_1}\right]\right. \\
&\left.+ \sum_{n_1\neq n_2}^{K}\sqrt{\beta_{n_1}p_{n_1}^u}\sqrt{\beta_{n_2}p_{n_2}^u}\rho_{m,n_1}\rho_{m,n_2}\mathrm{E}\left[\mathbf{h}_{n_1}^H\mathbf{h}_i\mathbf{h}_i^H\mathbf{h}_{n_2}\right] + \mathrm{E}\left[\mathbf{z}^H\mathbf{S}_m\mathbf{h}_i\mathbf{h}_i^H\mathbf{S}_m^H\mathbf{z}\right]\right) \\
&= \frac{1}{p_m^u}\left(\beta_i p_i^u\rho_{m,i}^2(M^2+M) + M\sum_{n_1=n_2\neq i}^{K}\beta_{n_1}p_{n_1}^u\rho_{m,n_1}^2 + M\sum_{n_1=n_2}^{K}\beta_{n_1}p_{n_1}^u\rho_{m,n_1}^2 + M\sigma_z^2\right) \\
&= M\left(\frac{M}{p_m^u}\beta_i p_i^u\rho_{m,i}^2 + \frac{1}{p_m^u}\sum_{n=1}^{K}\beta_n p_n^u\rho_{m,n}^2 + \sigma_z^2\right) \\
&= M\left(\frac{M}{p_m^u}\beta_i p_i^u\rho_{m,i}^2 + \alpha_{m,n}\right) \qquad \text{(A.2)}
\end{aligned}
$$

where $\alpha_{m,n} = \left(\sum_{n=1}^{K} \beta_n p_n^u \rho_{m,n}^2 + \sigma_z^2 \right)$. As a result, we have the expression of γ_i^d as

$$\begin{aligned}
\gamma_i^d &= \frac{\frac{(\mathrm{E}\left[\mathbf{h}_i^{\mathrm{H}} \hat{\mathbf{h}}_i\right])^2 \beta_i p_i^d}{M\alpha_{i,n}}}{\frac{\mathrm{E}\left|\mathbf{h}_i^H \hat{\mathbf{h}}_i - \mathrm{E}\left[\mathbf{h}_i^H \hat{\mathbf{h}}_i\right]\right|^2 \beta_i p_i^d}{M\alpha_{i,n}} + \sum_{m \neq i}^{K} \frac{\mathrm{E}|\mathbf{h}_i^H \hat{\mathbf{h}}_m|^2 \beta_i p_m^d}{M\alpha_{m,n}} + \sigma^2} \\
&= \frac{\frac{M^2 \beta_i}{M\alpha_{i,n}} \beta_i p_i^d}{\beta_i p_i^d + \sum_{m \neq i}^{K} \frac{M\left(\frac{M}{p_m^u} \beta_i p_i^u \rho_{m,i}^2 + \alpha_{m,n}\right)}{M\alpha_{m,n}} \beta_i p_m^d + \sigma^2} \\
&= \frac{M\beta_i^2 p_i^d}{\alpha_{i,n} \left(\beta_i p_i^d + \sum_{m \neq i}^{K} \left(1 + \frac{M\beta_i p_i^u \rho_{m,i}^2}{p_m^u \alpha_{m,n}} \right) \beta_i p_m^d + \sigma^2 \right)}
\end{aligned} \tag{A.3}$$

□

Appendix B
Proof of the Theorem 2

Proof.

$$
\begin{aligned}
&\left|\mathbf{h}_{ij,j}^{H}\hat{\mathbf{h}}_{mj,j}\right|^{2} \\
&=\left(\sum_{l_1=1}^{L}\sum_{n_1=1}^{K}\sqrt{\frac{\beta_{n_1l_1,j}p_{n_1l_1}^{u}}{p_{mj}^{u}}}\rho_{mj,n_1l_1}\mathbf{h}_{ij,j}^{H}\mathbf{h}_{n_1l_1}+\frac{1}{\sqrt{p_{mj}^{u}}}\mathbf{h}_{ij,j}^{H}\mathbf{S}_{mj}^{H}\mathbf{z}\right)^{H} \\
&\times\left(\sum_{l_2=1}^{L}\sum_{n_2=1}^{K}\sqrt{\frac{\beta_{n_2l_2,j}p_{n_2l_2}^{u}}{p_{mj}^{u}}}\rho_{mj,n_2l_2}\mathbf{h}_{ij}^{H}\mathbf{h}_{n_2l_2}+\frac{1}{\sqrt{p_{mj}^{u}}}\mathbf{h}_{ij}^{H}\mathbf{S}_{mj}^{H}\mathbf{z}\right) \\
&=\sum_{l_1=1}^{L}\sum_{n_1=1}^{K}\sum_{l_2=1}^{L}\sum_{n_2=1}^{K}\sqrt{\frac{\beta_{n_1l_1,j}p_{n_1l_1}^{u}}{p_{mj}^{u}}}\sqrt{\frac{\beta_{n_2l_2,j}p_{n_2l_2}^{u}}{p_{mj}^{u}}}\rho_{mj,n_1l_1}\rho_{mj,n_2l_2}\mathbf{h}_{n_1l_1}^{H}\mathbf{h}_{ij}\mathbf{h}_{ij}^{H}\mathbf{h}_{n_2l_2} \\
&+\sum_{l_1=1}^{L}\sum_{n_1=1}^{K}\sqrt{\frac{\beta_{n_1l_1,j}p_{n_1l_1}^{u}}{p_{mj}^{u}}}\rho_{mj,n_1l_1}\mathbf{h}_{n_1l_1}^{H}\mathbf{h}_{ij}\mathbf{h}_{ij}^{H}\mathbf{S}_{mj}^{H}\mathbf{z} \\
&+\sum_{l_2=1}^{L}\sum_{n_2=1}^{K}\sqrt{\frac{\beta_{n_2l_2,j}p_{n_2l_2}^{u}}{p_{mj}^{u}}}\rho_{mj,n_2l_2}\mathbf{z}^{H}\mathbf{S}_{mj}^{H}\mathbf{h}_{ij}\mathbf{h}_{ij}^{H}\mathbf{h}_{n_2l_2}+\frac{1}{p_{mj}^{u}}\mathbf{z}^{H}\mathbf{S}_{mj}\mathbf{h}_{ij}\mathbf{h}_{ij}^{H}\mathbf{S}_{mj}^{H}\mathbf{z}. \qquad \text{(B.1)}
\end{aligned}
$$

Then, we have

$$
\begin{aligned}
&\mathrm{E}\left|\mathbf{h}_{ij}^{H}\hat{\mathbf{h}}_{mj}\right|^{2} \\
&=\frac{1}{p_{mj}^{u}}\Bigg(\sum_{l_1=1}^{L}\sum_{n_1=1}^{K}\sum_{l_2=1}^{L}\sum_{n_2=1}^{K}\sqrt{\beta_{n_1l_1,j}p_{n_1l_1}^{u}}\sqrt{\beta_{n_2l_2,j}p_{n_2l_2}^{u}}\rho_{mj,n_1l_1}\rho_{mj,n_2l_2}\mathrm{E}\left[\mathbf{h}_{n_1l_1}^{H}\mathbf{h}_{ij}\mathbf{h}_{ij}^{H}\mathbf{h}_{n_2l_2}\right] \\
&+\mathrm{E}\left[\mathbf{z}^{H}\mathbf{S}_{mj}\mathbf{h}_{ij}\mathbf{h}_{ij}^{H}\mathbf{S}_{mj}^{H}\mathbf{z}\right]\Bigg) \\
&=\frac{1}{p_{mj}^{u}}\Bigg(\beta_{ij,j}p_{ij}^{u}\rho_{mj,ij}^{2}\mathrm{E}\left[\mathbf{h}_{ij}^{H}\mathbf{h}_{ij}\mathbf{h}_{ij}^{H}\mathbf{h}_{ij}\right]+\sum_{n_1=n_2\neq i}^{K}\beta_{n_1j,j}p_{n_1j}^{u}\rho_{mj,n_1j}^{2}\mathrm{E}\left[\mathbf{h}_{n_1j}^{H}\mathbf{h}_{ij}\mathbf{h}_{ij}^{H}\mathbf{h}_{n_1j}\right] \\
&+\sum_{n_1\neq n_2}^{K}\sqrt{\beta_{n_1j,j}p_{n_1j}^{u}}\sqrt{\beta_{n_2j,j}p_{n_2j}^{u}}\rho_{mj,n_1j}\rho_{mj,n_2j}\mathrm{E}\left[\mathbf{h}_{n_1j}^{H}\mathbf{h}_{ij}\mathbf{h}_{ij}^{H}\mathbf{h}_{n_2j}\right]
\end{aligned}
$$

$$
\begin{aligned}
&+\sum_{l_1=l_2\neq j}^{L}\sum_{n_1\neq n_2}^{K}\sqrt{\beta_{n_1l_1,j}p^u_{n_1l_1}}\sqrt{\beta_{n_2l_1,j}p^u_{n_2l_1}}\rho_{mj,n_1l_1}\rho_{mj,n_2l_1}\mathrm{E}\left[\mathbf{h}^H_{n_1l_1}\mathbf{h}_{ij}\mathbf{h}^H_{ij}\mathbf{h}_{n_2l_1}\right]\\
&+\sum_{l_1\neq l_2}^{L}\sum_{n_1\neq n_2}^{K}\sqrt{\beta_{n_1l_1,j}p^u_{n_1l_1}}\sqrt{\beta_{n_2l_2,j}p^u_{n_2l_2}}\rho_{mj,n_1l_1}\rho_{mj,n_2l_2}\mathrm{E}\left[\mathbf{h}^H_{n_1l_1}\mathbf{h}_{ij}\mathbf{h}^H_{ij}\mathbf{h}_{n_2l_2}\right]\\
&+\mathrm{E}\left[\mathbf{z}^H\mathbf{S}_{mj}\mathbf{h}_{ij}\mathbf{h}^H_{ij}\mathbf{S}^H_{mj}\mathbf{z}\right]\Bigg)\\
&=\frac{1}{p^u_{mj}}\Bigg(\beta_{ij,j}p^u_{ij}\rho^2_{mj,ij}(M^2+M)+M\sum_{n_1=n_2\neq i}^{K}\beta_{n_1j,j}p^u_{n_1j}\rho^2_{mj,n_1j}\\
&+M\sum_{l_1=l_2\neq j}^{L}\sum_{n_1=n_2}^{K}\beta_{n_1l_1,j}p^u_{n_1l_1}\rho^2_{mj,n_1l_1}+M\sigma_z^2\Bigg)\\
&=M\left(\frac{M}{p^u_{mj}}\beta_{ij,j}p^u_{ij}\rho^2_{mj,ij}+\frac{1}{p^u_{mj}}\sum_{l=1}^{L}\sum_{n=1}^{K}\beta_{nl,j}p^u_{nl}\rho^2_{mj,nl}+\sigma_z^2\right)\\
&=M\left(\frac{M}{p^u_{mj}}\beta_{ij,j}p^u_{ij}\rho^2_{mj,ij}+\alpha_{mj,nl}\right)
\end{aligned}
\tag{B.2}
$$

where $\alpha_{mj,nl}=\left(\sum_{l=1}^{L}\sum_{n=1}^{K}\beta_{nl,j}p^u_{nl}\rho^2_{mj,nl}+\sigma_z^2\right)$. As a result, we have the expression of γ^d_{ij} as

$$
\begin{aligned}
\gamma^d_{ij}&=\frac{\frac{\left(\mathrm{E}\left[\mathbf{h}^{\mathrm{H}}_{ij,j}\hat{\mathbf{h}}_{ij,j}\right]\right)^2\beta_{ij,j}p^d_{ij}}{M\alpha_{ij,nl}}}{\frac{\mathrm{E}\left|\mathbf{h}^H_{ij,j}\hat{\mathbf{h}}_{ij,j}-\mathrm{E}\left[\mathbf{h}^H_{ij,j}\hat{\mathbf{h}}_{ij,j}\right]\right|^2\beta_{ij,j}p^d_{ij}}{M\alpha_{ij,nl}}+\sum_{m\neq i}^{K}\frac{\mathrm{E}|\mathbf{h}^H_{ij,j}\hat{\mathbf{h}}_{mj,j}|^2\beta_{ij,j}p^d_{mj}}{M\alpha_{mj,nl}}+\sum_{l\neq j}^{L}\sum_{k=1}^{K}\frac{\mathrm{E}|\mathbf{h}^H_{il,l}\hat{\mathbf{h}}_{kl,l}|^2\beta_{ij,l}p^d_{kl}}{M\alpha_{kl,nl}}+\sigma^2}\\
&=\frac{M\beta^2_{ij,j}p^d_{ij}}{\alpha_{ij,nl}\left(\beta_{ij,j}p^d_{ij}+\sum_{m\neq i}^{K}\left(1+\varphi_{mj,nl}\right)\beta_{ij,j}p^d_{mj}+\sum_{l\neq j}^{L}\sum_{k=1}^{K}\left(1+\varphi_{kl,nl}\right)\beta_{il,l}p^d_{kl}+\sigma^2\right)}
\end{aligned}
\tag{B.3}
$$

where

$$
\varphi_{mj,nl}=\frac{M\beta_{ij,j}p^u_{ij}\rho^2_{mj,ij}}{p^u_{mj}\alpha_{mj,nl}} \tag{B.4}
$$

$$
\varphi_{kl,nl}=\frac{M\beta_{il,l}p^u_{il}\rho^2_{kl,ij}}{p^u_{kl}\alpha_{kl,nl}} \tag{B.5}
$$

□

Appendix C
Original publications

C.1 Journal Papers

- W. Fu, P. Cao and J. Thompson, "Performance Analysis of Non orthogonal Pilots in Massive MIMO Systems and Energy Efficiency Optimization with Fractional SCA algorithm", to be submitted.

C.2 Conference Papers

- W. Fu, P. Cao and J. Thompson, "Achievable Rate Performance of TDD Multi-cell Massive MIMO with Non-Orthogonal Pilots," WSA 2016; 20th International ITG Workshop on Smart Antennas, Munich, Germany, 2016, pp. 1-5.
- W. Fu and J. S. Thompson, "Performance analysis of K-best detection with adaptive modulation," 2015 International Symposium on Wireless Communication Systems (ISWCS), Brussels, 2015, pp. 306-310 (invited paper).

Performance Analysis of K-Best Detection with Adaptive Modulation

Wenjun Fu and John S Thompson
Institute for Digital Communications, University of Edinburgh
Email:{w.fu, john.thompson}@ed.ac.uk

***Abstract*—In this paper, the K-best detection algorithm with an adaptive modulation scheme in multiple input multiple output (MIMO) systems is proposed. A simplified error probability approximation method based on the union bound (UB) of the Maximum-Likelihood detector (MLD) is proposed to predict the bit error rate (BER) of the K-best algorithm. In specific, the simplified approach only uses the minimum Euclidean distance (MED) events which is suitable for the adaptive modulation scheme with much reduced computational complexity. In order to improve the accuracy of prediction, the signal-to-noise ratio (SNR) gaps between the UB with MED events and the full UB are estimated. Finally, simulation results have clearly shown the adaptive K-best algorithm applying the simplified approximation method has much reduced computational complexities while maintaining a promising BER performance.**

***Index Terms*—Adaptive Modulation, K-best, Maximum Likelihood, Union Bound**

I. Introduction

Multiple input multiple output (MIMO) is an advanced wireless communication technology that has attracted great interests from both researchers and industrialists. The utilization of multiple antennas at both transmitter and receiver is a promising technique to increase spectrum efficiency with high diversity order [1]. The maximum likelihood detector (MLD) is an optimal receiver design of MIMO system which guarantees robust detection performance. However, the exhaustive search over the large lattice point space leads to high computational complexity which is unrealistic in practical application. To achieve quasi-MLD performance with acceptable complexity, many novel detection algorithms have been proposed including the fixed sphere decoder (FSD) [2] and the K-best detection algorithm [3]. The K-best algorithm is a non-linear detector that achieves the quasi-ML performance with fixed complexity. The detection can be executed simultaneously by applying the breadth-first tree search with fixed number of searching paths and it is very suitable for parallel hardware platforms implementations. In terms of spectrum efficiently transmission in MIMO systems, adaptive modulation scheme is an convincing technique to improve data throughput over time-varying channels [4], [5]. The adaptive modulation scheme estimates the MIMO channel at the receiver and feeds back the most suitable modulation schemes that matches the channel quality to users at the transmitter.

Recently the literature of the K-best algorithm mainly focused on the complexity reductions and detection performance improvements. In [6], the authors proposed an adaptive K-value method according to channel condition. An adaptive K values will be employed in the detection according to the varying channel conditions. In [7] the authors considered the complexity reduction on higher order modulation schemes. Furthermore, discussions have been made on real-value system versus complex-value system. In [8], the authors have made optimizations on tree pruning and small K values can achieve optimal detection performance.

978-1-4673-6540-6/15/$31.00 ©

Contribution: Different from the literature discussed above, the K-best algorithm with adaptive modulation technique is proposed in this paper. Because the channel condition number is used as the channel quality indicator, we proposed a simplified error probability approximation method based on the union bound (UB) of the MLD to estimate the bit error rate (BER) performance of the K-best algorithm. The proposed method utilises the minimum Euclidean distance (MED) events only in the approximation. Comparing with the conventional UB approach, the simplified approximation method has much reduced computational complexity so that it is more suitable to be used for performance predictions in real-time adaptive modulation setups. Furthermore, by setting up the target BER, a look-up table (LUT) approach is applied to approximate performance gaps between the proposed simplified approximation and the conventional UB or the K-best algorithm with different K values. Then the BER performance of the K-best algorithm can be predicted accurately in the adaptive modulation scheme. Based on the accurate prediction, the modulation schemes that achieve the target BER will be sent back to the users. As a result, a promising error rate performance under different channel conditions can be guaranteed with much reduced computational complexity.

Organization: the remainder of the paper will be organized as follows. Section II gives a general introduction of the system model and detection algorithms used in this paper. Also a brief description will be given on the UB of MLD. Section III specifies the procedures of how adaptation works and how the LUT is generated. Section IV demonstrates the simulation results. Section V provides the conclusions and future work.

II. System Model and Detection Algorithms

A. MIMO System Model

Consider an uncoded MIMO system with N_t transmit antennas and N_r receive antennas, denoted as $N_t \times N_r$. Note that $N_r \geq N_t$. The received vector $\mathbf{y}$ with size $N_r \times 1$ can be denoted as

$$\mathbf{y} = \mathbf{H}\mathbf{s} + \mathbf{n}, \tag{1}$$

where $\mathbf{s} = [s_1, s_2, \ldots, s_{N_t}]^T$ denotes the transmitted symbol vector of size $N_t \times 1$ and each symbol is modulated with a complex constellation based on M-ary quadrature amplitude modulation (MQAM). The received complex vector is denoted

as $\mathbf{y} = [y_1, y_2, \ldots, y_{N_r}]^T$ and $\mathbf{n} = [n_1, n_2, \ldots, n_{N_r}]^T$ denotes the additive white Gaussian noise vector with elements of independent and identical distributed (i.i.d) complex Gaussian noise. In addition, the complex noise elements have zero mean and variance of σ_n^2. The channel $\mathbf{H} \in \mathbb{C}^{N_r \times N_t}$ has i.i.d elements $h_{ji} \sim \mathcal{CN}(0,1)$ which indicates the uncorrelated Rayleigh fading propagation environment. The assumption is made that the channel matrix is perfectly estimated at the receiver side.

For non-linear detectors such as the K-best algorithm, they generally convert the received symbols $\mathbf{y}$ from a complex value into a real valued form, which can be represented as

$$\begin{aligned}\mathbf{y}_r &= \begin{bmatrix}\Re(\mathbf{y})\\ \Im(\mathbf{y})\end{bmatrix} = \begin{bmatrix}\Re(\mathbf{H}) & -\Im(\mathbf{H})\\ \Im(\mathbf{H}) & \Re(\mathbf{H})\end{bmatrix}\begin{bmatrix}\Re(\mathbf{s})\\ \Im(\mathbf{s})\end{bmatrix} + \begin{bmatrix}\Re(\mathbf{n})\\ \Im(\mathbf{n})\end{bmatrix}\\ &= \mathbf{H}_r\mathbf{s}_r + \mathbf{n}_r, \end{aligned} \tag{2}$$

where $\Re\{\cdot\}$ denotes the real part and $\Im\{\cdot\}$ denotes the imaginary part of the symbol vectors. The size of the real transmit and receive vector including the channel matrix is twice that of the complex valued form.

B. MLD and K-best algorithm

The MLD performs an exhaustive search over the lattice point space $\mathcal{S}^{N_t}$ where $\mathcal{S}$ denotes the constellation set of transmit symbols. The detection performed by the MLD considers all the lattice points with in the received signal space and the optimal result will be the lattice point that leads to the smallest Euclidean distance to the received symbols vector. It can be represented as

$$\hat{\mathbf{s}}_{\mathrm{MLD}} = \underset{\hat{\mathbf{s}}\in\mathcal{S}^{N_t}}{\arg\min} \|\mathbf{y} - \mathbf{H}\hat{\mathbf{s}}\|^2, \tag{3}$$

where $\hat{\mathbf{s}}$ is the transmit symbol vector with elements included in the constellation set $\mathcal{S}$ and the $\|(\cdot)\|$ denotes the norm of the vector. The computational complexity of the MLD increases exponentially with the large modulation size and the number of antennas in MIMO systems. For example, if the MLD is used on a 16×16 MIMO system with 256-QAM, the detection of one symbol vector searches over 256^{16} lattice points. This limits the practical use of the MLD.

The K-best algorithm is an attractive alternative to the MLD with fixed complexity and uses parallel searches of the closest lattice point. If the QR decomposition is applied on the real valued channel matrix, then it comes $\mathbf{H}_r = \mathbf{QR}$ where $\mathbf{Q}$ is a $2N_r \times 2N_t$ unitary real value matrix and $\mathbf{R}$ is a $2N_r \times 2N_t$ upper triangular real value matrix with elements r_{mn}. By multiplying the nulling term $\mathbf{Q^H}$ on the MLD equation, the reformulation is represented as

$$\begin{aligned}\hat{\mathbf{s}} &= \underset{\hat{\mathbf{s}}\in\mathcal{S}^{2N_t}}{\arg\min} \|\mathbf{y}_r - \mathbf{H}_r\mathbf{s}\|^2\\ &= \underset{\hat{\mathbf{s}}\in\mathcal{S}^{2N_t}}{\arg\min} \|\mathbf{QQ^H}(\mathbf{y}_r - \mathbf{H}_r\mathbf{s})\|^2\\ &= \underset{\hat{\mathbf{s}}\in\mathcal{S}^{2N_t}}{\arg\min} \|\mathbf{Q^H}\mathbf{y}_r - \mathbf{Q}^H\mathbf{QR}\mathbf{s}\|^2\\ &= \underset{\hat{\mathbf{s}}\in\mathcal{S}^{N_t}}{\arg\min} \sum_{m=1}^{2N_t}\left|\tilde{y}_m - \sum_{n=m}^{2N_t} r_{mn}\hat{s}_n\right|^2. \end{aligned} \tag{4}$$

As $\mathbf{R}$ is an upper triangular matrix with zero elements under the matrix diagonal, finding the closest lattice point in the K-best SD algorithm can be transformed into a tree structure

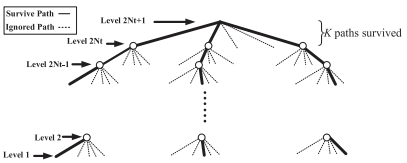

Fig. 1. The K-best detection tree diagram

search. Fig.1 shows an example of the expanded tree structure. The lattice point tree contains $2N_r + 1$ tree levels. Each node represents a real valued lattice point. Level *m* lies above the *m-1* level, so the nodes in level *m* are denoted as "parent nodes" and each node in level $m-1$ is a 10pt, "child node". Each parent node has $\sqrt{\mathcal{S}}$ real valued child nodes. The paths between parent nodes and child nodes denote the partial Euclidean distances (PED) between the lattice points. The PED of the level *m* can be represented as

$$PED_m = PED_{m+1} + \left|\tilde{y}_m - \sum_{n=m}^{2N_t} r_{mn}\hat{s}_n\right|^2, \tag{5}$$

where includes the PED of the previous level PED_{m+1} and the Euclidean distance (ED) of the current level. The K-best SD algorithm performs a breadth-first search over the tree which starts from the top to the bottom. At each level, only *K* nodes with the smallest PEDs are kept as surviving candidates. In the end the path with the smallest cumulative PED is chosen to be the detection result.

C. Union bound of the MLD

In this section, a brief introduction of the UB of MLD will be given. The UB P_{ub} of the MLD is a widely used upper bound that provides a theoretical approximation of the error probability [9]. The calculation of UB starts from the Pairwise Error Probability (PEP), denoted as $P_{\mathbf{s}_i\to\mathbf{s}'_j}$. PEP is the probability that the receiver detected vector $\mathbf{s}'_j$ but that vector $\mathbf{s}_i$ was actually sent and it can be expressed as

$$P_{\mathbf{s}_i\to\mathbf{s}'_j} = Q\left(\sqrt{\frac{d^2_{\mathbf{s}\to\mathbf{s}'}}{2\sigma_n^2}}\right), \tag{6}$$

where $Q(\cdot)$ denotes the Marcum Q-function and $d^2_{\mathbf{s}\to\mathbf{s}'}$ denotes the squared Euclidean distance between the vector $\mathbf{s}$ and the vector $\mathbf{s}'$. For given channel realizations $\mathbf{H}$, the $d^2_{\mathbf{s}\to\mathbf{s}'}$ can be expressed as

$$d^2_{\mathbf{s}\to\mathbf{s}'} = \mathrm{E}\|\mathbf{H}(\mathbf{s}_i - \mathbf{s}'_j)\|^2. \tag{7}$$

The mean PEP over i.i.d. Gaussian channels will be calculated for each pair of vectors. The UB of the MLD is sum of the mean PEP of all the symbol vectors and it is represented as

$$\begin{aligned}P_{\mathrm{ub}} = &\frac{1}{\sum_{n=1}^{N_t}\log_2(M_n)}\frac{1}{\prod_{n=1}^{N_t}M_n}\sum_{i=1}^{M_n^{N_t}}\sum_{j=1\&j\neq i}^{M_n^{N_t}} e_b(\mathbf{s}_i,\mathbf{s}_j^*)\\ &\times \mathrm{E}\left\{ Q\left(\sqrt{\frac{\|\mathbf{H}(\mathbf{s}_i - \mathbf{s}_j^*)\|^2}{2\sigma_n^2}}\right)\middle|\mathbf{H}\right\}, \end{aligned} \tag{8}$$

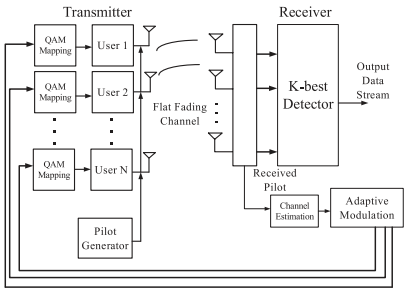

Fig. 2. System diagram of the K-best with adaptive modulation scheme

where $e_b(\mathbf{s}_i, \mathbf{s}_j^*)$ is the number of bit errors between the vectors $\mathbf{s}_i$ and $\mathbf{s}_j$ and M_n denotes the M-ary modulation size for transmit antennas.

III. The K-best algorithm with adaptive modulation scheme

In this section, firstly an overview of the proposed adaptive MIMO system with the K-best algorithm is given. Secondly we investigate how the detection performance is affected by the channel condition number. Finally a comprehensive introduction is presented on the simplified UB with MED events method.

A. proposed adaptive MIMO system with the K-best algorithm

Fig.2 shows the block diagram of this system. The transmitters are considered as users with single antenna devices. The receiver is the device with multiple antennas using the K-best algorithm as the detector. The detailed description of the system is given as follows.

1) Measure the MIMO channel and the transmit powers: each transmitter will first transmit pilot symbols to perform channel estimation. At the receiver, the channel estimation module predicts the channel state information (CSI) according to the received pilot symbols.
2) Estimate the error rate for different modulation scheme combinations: the adaptive modulation module computes the error probability using perfect CSI with different modulation scheme setups for users.
3) Select the modulation schemes combinations: after the calculation of error probabilities, the modulation combination reaches the target BER is chosen for the adaptive modulation.
4) Feed back the chosen modulation schemes to users at the transmitter side: finally, the combination of modulation schemes that maximises data throughput and still meets the target error rate is feed back to users. The users then transmit data symbols according to the feed back information.

B. Influence of channel condition number on detection performance

The propagation environment has a significant influence on the performance of the K-best SD detector. One of the channel quality metrics is the channel condition number, denoted as κ_H. The calculation of κ_H first applies singular value decomposition of the channel matrix. Then κ_H is defined as the ratio of the largest singular value over the smallest singular value, which is denoted as $\kappa_H = \frac{\lambda_{max}}{\lambda_{min}}$ where λ denotes the singular value of the channel matrix. The channel with $\kappa_H = 1$ is considered as well conditioned channel. The receiver can equalise the channel without loss of performance. When $\kappa_H > 1$, the channel quality gets worse with the increasing κ_H value. In [10], it has been shown how the κ_H influences the detection performance of the linear detectors (i.e., zero-forcing and MMSE). We are interested in the influence of κ_H on the non-linear detectors such as the K-best algorithm. Fig.3(a) illustrates how the BER

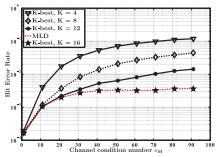

(a) Non-linear detector and the ML with increasing κ_H, in MIMO with $N_t = N_r = 4$, 16-QAM, i.i.d Rayleigh fading channel

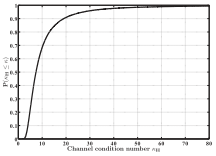

(b) Cumulative distribution function, in MIMO with $N_t = N_r = 4$, i.i.d Rayleigh fading channel

Fig. 3. The influences of channel condition number κ_H on non-linear detector

of K-best is degraded by the increasing value of κ_H. When $\kappa_H < 10$, only the MLD and $K = 16$ have acceptable BER performance which is below 10^{-3}. However, the performance drops dramatically when $\kappa > 10$. Furthermore, the degradation in BER is significant in both large K values (e.g.,$K = 16$) and small K values (e.g.,$K = 4$). Fig.3(b) plots the cumulative distribution function (CDF) simulation of κ_H for i.i.d Rayleigh fading channel. It is shown that there is approximately a 30% chance that $\kappa_H > 10$ and a 15% chance that $\kappa_H > 15$. The CDF result indicates that the high condition number channel events occur frequently, which significantly affects the overall detection performance. Thus, based on the characteristics of channel observed in Fig.3(b) and the degradation observed in Fig.3(a), we propose the adaptive K-best algorithm. The main goal of the adaptive K-best algorithm is to combat influences brought by the varying channel conditions. By selecting feasible modulation schemes that fit the channel condition, the detection performance can achieve the target BER.

C. The simplified UB with MED

In adaptive modulation, one important step is to get an accurate prediction of the error rate under varying channel conditions. It is mentioned in [3] that with a sufficiently large K value, the K-best algorithm has close performance to the MLD. Meanwhile, it is shown in [9] that the UB is a tight upper bound of the MLD. As a result, the approximation of the K-best error probability employs the UB of MLD for each channel realization. However, Equation (9) has shown high computational complexity that is not suitable for practical implementation of the adaptive modulation scheme. For example, if a 4×4 MIMO utilise 64-QAM scheme, the

UB needs to calculate 64^4 PEPs and each PEP is averaged over 64^4 pair of vectors which has very high computational complexity. The approximation needs to be accurate and with less computations. The simplified approximation method of the error probability is proposed to overcome the high computational requirement while maintaining good accuracy. To compare with the conventional UB of the MLD, the simplified approximation uses only the MED events for the calculation of the PEP. The MED events indicate error events of the constellation points that have the minimum Euclidean distance to the transmitted symbols.The minimum Euclidean distance is expressed as

$$d_{\min} = \min_{\mathbf{s}\in M^{N_t} \& \mathbf{s}\neq\mathbf{s}'} \|\mathbf{s}-\mathbf{s}'\|. \tag{9}$$

To compare with the non MED events, the MED events have the relation that

$$Q\left(\sqrt{\frac{d^2_{\mathbf{s}\to\mathbf{s}'}}{2\sigma_n^2}}\right) \leq Q\left(\sqrt{\frac{d^2_{\min}}{2\sigma_n^2}}\right). \tag{10}$$

In Equation (11), the reason of the MED events having higher probabilities than the other error events is the Q function is a decreasing function of Euclidean distance. Since the MED events have significant influence on the overall error probability approximation, the simplified UB utilizes MED events in the PEP calculation to obtain a rough approximation of the full UB. If the set Λ_{MED} denotes the subset of the constellation points with the minimum Euclidean distance to the transmit signal, then it is clear that Λ_{MED} is much less than the full constellation point set. And the lattice space of Λ_{MED} is also smaller than the full constellation point lattice space. The proposed simplified UB approximation of the K-best algorithm's performance is derived as

$$P_{e,MED} = \frac{1}{\sum_{n=1}^{N_t}\log_2(M_n)} \frac{1}{\prod_{n=1}^{N_t} M_n} \sum_{i=1}^{M_n^{N_t}} \sum_{MED=1}^{\Lambda_{\mathrm{MED}}} e_b(\mathbf{s}_i, \mathbf{s}^*_{MED})$$
$$\times \mathrm{E}\left\{ Q\left(\sqrt{\frac{\|\mathbf{H}(\mathbf{s}_i - \mathbf{s}'_{MED})\|^2}{2\sigma_n^2}} - \Delta SNR\right) \middle| \mathbf{H}\right\}, \tag{11}$$

where $P_{e,MED}$ denotes the error probability approximation using the UB with MED events only.

Although the UB approximations with the MED events are not tight enough to yield an accurate approximation, it has same PEP trend in high SNR region. The gaps between the UB with MED events and the full UB in SNR are estimated as error rate corrections for the use in the adaptive modulation algorithm. If the SNR gap is denoted as ΔSNR, it is represented as

$$\Delta SNR = \Delta SNR_{\mathrm{UB}} + \Delta SNR_{\mathrm{kbest}}. \tag{12}$$

The estimation of the ΔSNR value starts from setting the modulation combinations. The modulation combinations indicate the possible feeding of modulation schemes to different users. Then the channel condition numbers κ_H are divided into different groups with small value intervals based on the CDF of κ_H. The ΔSNR_{UB} between the simplified UB and the full UB within each group of κ_H are estimated. The other key point is to estimate the gap between the K-best algorithm with different K value configurations. Though a large K value

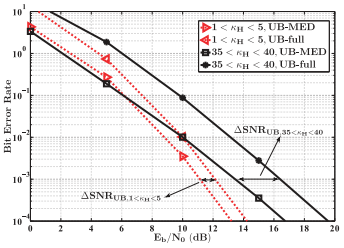

Fig. 4. The UB with MED events and the full UB, in MIMO with $N_t = N_r = 4$, 16-QAM

leads to a quasi-MLD performance, under well conditioned channels, small K values can also be used to get optimal result with less computations. Therefore, small K value cases are included in the adaptive scheme. The performance gaps $\Delta SNR_{\mathrm{kbest}}$ are estimated so that the simplified UB is able to predict the K-best algorithm with different K values. The accurate predications of error probability are based on the above two performance gaps. A LUT can be built with ΔSNR under different channel conditions and the LUT is crucial to the adaptive modulation scheme.

IV. Simulation Result

In this section, the simulation results are given on performance of the K-best algorithm with the adaptive modulation scheme. The first step of simulation is to build the LUT of ΔSNR_{t} and $\Delta SNR_{\mathrm{kbest}}$. For the ΔSNR estimations, simulations have been made on a 4×4 MIMO system. There are 4 users at the transmitter and the receiver has four antennas with the K-best SD algorithm as detector. The M-ary QAM modulation scheme is used in the simulation with $M = 4, 16$. Based on the CDF of κ_H, it has been divided into 8 groups with interval value of 5 from $\kappa_H = 1$ to $\kappa_H = 40$. For example, group 1 is from $\kappa_H = 1$ to $\kappa_H = 5$, and group 2 is from $\kappa_H = 6$ to $\kappa_H = 10$ etc.. Within each group of κ_H, there are minimum 10,000 randomly generated channel realizations with κ_H distributed within the range. Fig.4 shows an example of how the ΔSNR_{UB} between the UB with MED events and the full UB are constructed. The figure shows the BER performance as a function of SNR of the fully calculated UB versus the UB with MED events only. The BER curves of these two bounds are consistent with fixed SNR gaps between each other. With the target BER as 10^{-3}, the ΔSNR_{UB} values between the full UB and the UB with MED events are estimated. Fig.5 shows an example of how the $\Delta SNR_{\mathrm{kbest}}$ is estimated between the UB using only the MED events and the K-best algorithm with different K values within different κ_H value ranges. It is clear that with larger K values, the K-best algorithm will have better performance. The reduction of the performance of the K-best algorithm with different K values at the target BER are estimated. In the simulation, there are totally $M_n^{N_t} = 65536$ possible transmit vectors and for each vector, the subset Λ_{MED} approximately ranges from 2^4 to 8^4. Comparing with the full UB with the set 16^4, the reduction of computations is around 94% to 99.98%.

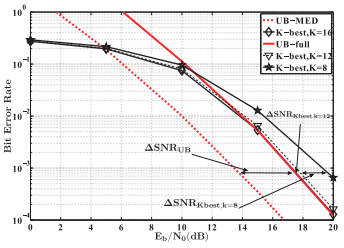

Fig. 5. The UB with MED events versus the full UB and K-best with different K values, in MIMO system with $N_t = N_r = 4$, 16-QAM, $35 \leq \kappa \leq 40$. The K values are $K = 8, 12, 16$

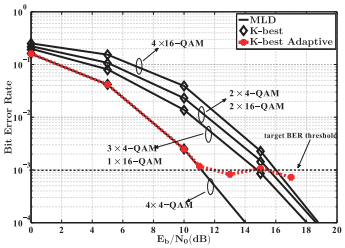

Fig. 6. BER of the K-best with adaptive modulation scheme versus the MLD and K-best with different modulation combinations, in MIMO system with $N_t = N_r = 4$ and modulation combinations listed in Table I.

Table 1 is built with the $\Delta SNR_{\text{kbest}}$ covering eight different ranges of κ_H values. The ΔSNR values of the K-best algorithm for both small and big K values are similar for small value of κ_H. It indicates that with the well-conditioned channels, the K-best algorithm can use small K values to reduce computational complexity. In the case of large κ_H, the difference of ΔSNR between different modulation configurations becomes significant. The performance degradations caused by high κ_H are obvious in higher order modulation scheme with small K values. Fig.6 shows the BER performance of the K-best adaptive modulation scheme versus the MLD and the fixed modulation K-best. For the users at the transmitter side, there are six different configurations to select according to the channel conditions following Table I. The target BER is set to $BER_T = 10^{-3}$. For each channel realization, the predicted performance of different modulation combinations will be calculated with the UB with MED events and the LUT. The modulation combination with the closest estimated performance to the target BER will be used for the transmission. In Fig.6, the K-best with the adaptive modulation scheme follows the BER of 4×4-QAM modulations until the SNR is approximately 11dB. Then it fluctuates around the target BER. The K-best with adaptive modulation scheme maintains a constant BER performance with a higher data rate than the other combinations.

TABLE I
LUT OF ΔSNR (dB)

κ_H	(1)	(2)	(3)	(4)	(5)	(6)
1∼5	0.33	1.66	1.66	1.43	1.43	1.43
6∼10	0.40	2.24	2.33	2.20	2.20	2.20
11∼15	0.46	2.40	2.65	2.60	2.60	2.60
16∼20	0.50	2.50	2.80	2.75	2.75	2.85
21∼25	0.55	2.62	2.90	2.82	2.84	3.10
26∼30	0.55	2.65	2.96	2.91	3.02	3.52
31∼35	0.60	2.65	3.00	2.94	3.15	4.61
36∼40	0.60	2.70	3.05	2.96	3.40	5.46

Notes: (1): $4 \times 4 -$ QAM, (2):$[16, 4, 4, 4]$ with $K = 16$ for 16-QAM and $K = 4$ for 4-QAM, (3):$[16, 16, 4, 4]$ with $K = 16$ for 16-QAM and $K = 4$ for 4-QAM, (4):$4 \times 16 -$ QAM with $K = 16$,(5):$4 \times 16 -$ QAM with $K = 12$, (6):$4 \times 16 -$ QAM with $K = 8$.

V. CONCLUSION

In this paper, the K-best algorithm with adaptive modulation scheme was proposed in this paper. A simplified approach was given to approximate the error probability with the minimum Euclidean distance events considered only. By estimating the performance gaps between the conventional union bound and the simplified union bound, accurate predictions can be made on the BER performance of the K-best algorithm with much less computations. From our simulations, the adaptive K-best has guaranteed the BER performance with an approximately 94% to 99% reduction of computations comparing with the conventional union bound in one search iteration. The future work will consider the performance in the cases of imperfect CSI and correlated channels.

REFERENCES

[1] G. J. Foschini, "Layered space-time architecture for wireless communication in a fading environment when using multi-element antennas," *Bell Labs Technical Journal*, vol. 1, no. 2, pp. 41–59, Oct. 1996.

[2] L. G. Barbero and J. S. Thompson, "Fixing the complexity of the sphere decoder for mimo detection," *IEEE Trans. Wireless Commun.*, vol. 7, no. 6, pp. 2131–2142, Jun. 2008.

[3] Z. Guo and P. Nilsson, "Algorithm and implementation of the k-best sphere decoding for mimo detection," *IEEE J. Sel. Areas Commun.*, vol. 24, no. 3, pp. 491–503, Mar. 2006.

[4] A. J. Goldsmith, *Wireless Communications*, Cambridge University Press, New York, 2005.

[5] Z. Zhou, B. Vucetic, M. Dohler, and Y. Li, "Mimo systems with adaptive modulation," *IEEE Trans. Veh. Technol.*, vol. 54, no. 5, pp. 1828–1842, Sept. 2005.

[6] M. Rahman, E. Rohani, and G. S. Choi, "An iterative soft decision based adaptive k-best decoder without snr estimation," *Proc. Asilomar Conference on Signals, Systems and Computers.*, pp. 1016–1020, Nov. 2014.

[7] R. Ma, P. Ren, S. Xue, and Q. Du, "Adaptive low-complexity constellation-reduction aided detection in mimo systems employing high-order modulation," *Proc. IEEE Wireless Communications and Networking Conference (WCNC).*, pp. 4083–4088, Apr. 2013.

[8] C. Shen and A.M. Eltawil, "An adaptive reduced complexity k-best decoding algorithm with early termination," *Proc. IEEE Consumer Communications and Networking Conference (CCNC).*, pp. 1–5, Jan. 2010.

[9] X. Zhu and R. D. Murch, "Performance analysis of maximum likelihood detection in a mimo antenna system," *IEEE Trans. Commun.*, vol. 50, no. 2, pp. 187–191, Feb. 2002.

[10] H. Artes, D. Seethaler, and F. Hlawatsch, "Efficient detection algorithms for mimo channels: a geometrical approach to approximate ml detection," *IEEE Trans. Signal Process.*, vol. 51, no. 11, pp. 2808–2820, Nov. 2003.

WSA 2016 • March 9-11, 2016, Munich, Germany

Achievable Rate Performance of TDD Multi-cell Massive MIMO with Non-Orthogonal Pilots

Wenjun Fu, Pan Cao and John Thompson
Institute for Digital Communications, University of Edinburgh
Email:{w.fu, p.cao, john.thompson}@ed.ac.uk

***Abstract*—Massive multiple-input multiple-output (MIMO) is a promising technology that provides high system capacity, and with excellent performance in energy efficiency and system robustness. However, pilot contamination restricts the system performance due to the limited length of orthogonal training sequences. In this paper, we propose optimization of non-orthogonal pilots for uplink training. The Grassmannian line packing method is applied in the design of pilots that leads to maximum chordal distances between training sequences which reduces pilot contamination. The analytical expression of the user equipments (UEs) signal-to-intereference-plus-noise ratio (SINR) in multi-cell massive MIMO system and the analytical SINR of UEs in Grassmannian manifold are presented. Simulation results show shown that non-orthogonal pilot sequences with the Grassmainn line packing method yield significant improvements of the system capacity.**

***Index Terms*—Massive MIMO, TDD, non-orthogonal pilots, Grassmannian line packing**

I. Introduction

Massive multiple-input-multiple-output (MIMO) system is an advanced wireless communication technology that has attracted great interest from both researchers and industrialists in recent years. The deployment of a large-scale array of antennas (tens or even hundreds of antennas) at the base station (BS) is desired to support increased numbers of user equipments (UEs) in the same time-frequency resource. It is shown that both spectrum and energy efficiency can be greatly improved through multiplexing gain and the pairwise orthogonal channel property [1]–[3]. Furthermore, the complexity of both detector and precoder designs can be much simplified.

However, the limited length of the coherence interval may cause *pilot contamination*, which seriously affects estimation of the channel state information (CSI) and consequently degrades the system performance. One solution is to reuse orthogonal pilots between UEs or cells and many novel reuse schemes have been proposed to reduce this effect. In [4] a precoding method was proposed for the multi-cell MIMO system to reduce the pilot contamination effect. An orthogonal pilot reuse scheme was proposed in [5] with reuse factor of seven. The pilot contamination was mitigated at the cost of increasing the sample duration of training sequences. In [6], the UEs are divided into cell-centre and cell-edge groups. Different pilot orthogonal pilots are assigned to these two groups which leads to a reduction of both the pilot contamination and the pilot sample duration.

Pan Cao and John Thompson acknowledge financial support for this research from the UK EPSRC grant number EP/L026147/1. Simulation data is available at http://www.homepages.ed.ac.uk/jst/.

In contrast with pilot reuse schemes, in this paper the focus is on the Grassmannian line packing (GLP) based pilot scheme. Although in [7], the GLP-based pilot sequence design is proposed to reduce contamination, the discussion relates to the estimation error performance and does not provide the theoretical analysis of pilot length on the throughput. The authors compare the throughput performance of different pilot schemes [8], but the study is limited to a single-cell scenario. In this paper we focus on evaluating the downlink achievable rate performance of a time-division-duplex (TDD) multi-cell massive MIMO system with the GLP based pilot scheme. The closed-form achievable sum rate expression for the multi-cell system is presented and comparisons are made with the conventional pilot reuse scheme. The numerical results show that the GLP-based pilot design significantly outperforms the pilot reuse scheme and it brings large gains in the system throughput.

The rest of the paper is organized as follows. In section II, an description of the multi-cell massive MIMO system model is given. In section III, we list the proposed analytical expressions and description of the Grassmannian line packing problem. The simulation results and discussions are given in section IV. Finally, the conclusion of the paper is given in section V.

Notation: The bold font notation is applied to represent matrix or vector. To a matrix $\mathbf{A}$, $\mathbf{A}^{\mathrm{T}}$ denotes its transpose, $\mathbf{A}^{\mathrm{H}}$ denotes its Hermitian transpose and $\mathbf{A}^{*}$ represents its conjugate transpose. $\mathcal{CN}(x, y)$ denotes the complex normal distribution with x as mean and y as variance, $\mathrm{diag}(\cdot)$ denotes the diagonal matrix, $\mathbb{E}[\cdot]$ and $\mathrm{Var}\{\cdot\}$ represents expection and variance, respectively. $\mathbf{I}_M$ is M-dimensional identity matrix. $\otimes$ is Kronecker product.

II. System model

We consider a multi-cell massive MIMO cellular network with L cells which is illustrated in Fig.1. Each cell includes a central BS equipped with M antennas serving K single-antenna UEs where $M \gg K$. We consider a block-fading channel and the channel vector from the k-th UE in the i-th cell to the BS in the j-th cell can be represented as

$$\mathbf{g}_{k,i,j} = \sqrt{\beta_{k,i,j}}\mathbf{h}_{k,i,j}, \quad (1)$$

ISBN 978-3-8007-4177-9

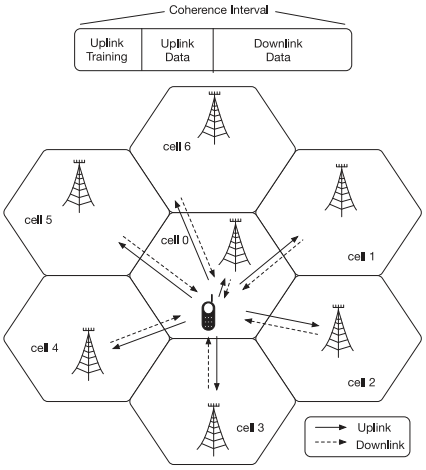

Fig. 1. A multi-cell massive MIMO system with signal antenna UE

where $\beta_{k,i,j}$ represents the large-scale fading coefficient that models the effect of path-loss and shadowing; $\mathbf{h}_{k,i,j}$ represents the small-scale fading and vector contains independent and identically distributed (i.i.d) random variables where $\mathbf{h}_{k,i,j} \in \mathcal{CN}(0, \mathbf{I}_M)$. The coherence interval is also illustrated in Fig.1, which can be divided into three parts: uplink training, uplink data transmission and downlink data transmission. With the coherence bandwidth B_c Hz and T_s seconds as the coherence time, the number of samples T_c equals to $T_c = T_s \times B_c$. It is assumed that the channel model $\sqrt{\beta_{k,i,j}}\mathbf{h}_{k,i,j}$ remains constant during one coherence interval.

A. Uplink Training

TDD operation is considered in this paper. The transmission starts with UEs sending their own training sequences to their BS simultaneously. To the UE i of the j-th cell, each UE will be assigned a pilot sequence vector which is denoted by $\mathbf{s}_{i,j}$. The $\mathbf{s}_{i,j} \in \mathbb{C}^{\tau \times 1}$ has a length of τ samples and $\mathbb{E}[|\mathbf{s}_{i,j}|^2] = 1$. The correlation coefficient of pilot sequences between the UE i and the UE k in the jth-cell is described as

$$\rho^2_{i,k,j} \triangleq |\mathbf{s}^{\mathrm{H}}_{i,j}\mathbf{s}_{k,j}|^2, \tag{2}$$

where $\rho^2_{i,k,j} \in [0, 1]$. To the BS in cell j, it is assumed to receive the uplink training sequences from the UEs in both cell j and the other $L-1$ cells, which can be represented as

$$\begin{aligned}\mathbf{y}_j &= \underbrace{\sum_{k=1}^{K}\sqrt{p_u\beta_{k,j,j}}\mathbf{S}_{k,j,j}\mathbf{h}_{k,j,j}}_{\text{cell } j} + \underbrace{\sum_{l\neq j}^{L}\sum_{k=1}^{K}\sqrt{p_u\beta_{k,l,j}}\mathbf{S}_{k,l,j}\mathbf{h}_{k,l,j}}_{\text{other } L-1 \text{ cells}} + \mathbf{n}_j \\ &= \sum_{l=1}^{L}\sum_{k=1}^{K}\sqrt{p_u\beta_{k,l,j}}\mathbf{S}_{k,l,j}\mathbf{h}_{k,l,j} + \mathbf{n}_j,\end{aligned} \tag{3}$$

where $\mathbf{y}_j \in \mathbb{C}^{\tau M \times 1}$ denotes the received pilot vector; p_u denotes the uplink transmission power; $\mathbf{n}_j \in \mathbb{C}^{\tau M \times 1}$ denotes matrix of additive white Gaussian noise (AWGN) at the BS with elements $n_{M,k,j} \in \mathcal{CN}(0, \sigma_n^2\mathbf{I}_M)$; $\mathbf{S}_{k,l,j}$ represents the matrix with pilot sequence and $\mathbf{S}_{k,l,j} = s_{k,l,j} \otimes \mathbf{I}_M$. Once the BS received the uplink training sequences, least squared (LS) algorithm is utilized for the channel estimation. The estimated CSI can be expressed as

$$\begin{aligned}\hat{\mathbf{h}}_{i,j,j} &= \mathbf{S}^{\mathrm{T}}_{i,j,j}\mathbf{y}_j \\ &= \sqrt{\beta_{i,j,j}}\mathbf{h}_{i,j,j} + \sum_{k\neq i}^{K}\rho_{i,k,j}\mathbf{h}_{k,j,j} + \sum_{l\neq j}^{L}\sum_{k=1}^{K}\rho_{i,k,l}\mathbf{h}_{k,l,i} + \mathbf{S}^{\mathrm{T}}_{i,j,j}\mathbf{n}_j.\end{aligned} \tag{4}$$

Equation (4) indicates that the correlation between pilots has a significant influence on the accuracy of the estimation. If both $\rho_{i,k,j}$ and $\rho_{i,k,l}$ are equal to 0, the estimated result will be the desired CSI corrupted only by noise. However, as mentioned above pilot contamination commonly exists in the massive MIMO systems. As a result, the interference between pilots might result in non-zero correlation coefficients which will reduce the estimation accuracy.

After uplink training, the UEs start the data transmission and the estimated CSI will be utilized in the BS for signal detection. The received uplink data at the j-th cell is given as

$$\mathbf{y}_{j,data} = \sum_{l=1}^{L}\sum_{k=1}^{K}\sqrt{p_u\beta_{k,l,j}}\mathbf{x}_{k,l,j}\mathbf{h}_{k,l,j} + \mathbf{n}_d, \tag{5}$$

where $\mathbf{y}_{j,data}$ denotes the received uplink data by the BS in the j-th cell; $\mathbf{x}_{k,l,j}$ represents the uplink transmit data; $\mathbf{n}_d$ denotes the additive noise. It is assumed that the power of data transmission is equal to that used for the uplink training.

B. Downlink Data Transmission

Recall that reciprocity in the TDD operation leads to the utilization of the estimated uplink CSI in the downlink data transmission. In addition, a linear precoding method is also adopted. We assume that the received noisy downlink signal by UE i in the j-th cell is denoted as $\mathbf{r}_{i,j}$, where it contains downlink data streams from both the BS in cell j and the other $L-1$ cells. It can be represented as

$$\mathbf{r}_{i,j} = \sum_{l=1}^{L}\sqrt{p^{DL}_{i,j,l}\beta_{i,j,l}}\mathbf{h}^{\mathrm{H}}_{i,j,l}\sum_{k=1}^{K}\mathbf{q}_{i,k,l}t_{i,k,l} + z_{i,j}, \tag{8}$$

where $p^{DL}_{i,j,l}$ represents the downlink transmission power; $\sqrt{\beta_{i,j,l}}\mathbf{h}^{\mathrm{H}}_{i,j,l}$ denotes the downlink CSI from the BS in the

ISBN 978-3-8007-4177-9

$$SINR_{i,j} = \frac{\beta_{i,j} p_{i,j}}{\beta_{i,j}\left(\sum\limits_{k\neq i}^{K} p_{k,j}\rho_{i,k,j}^2 + \sum\limits_{m=1}^{K} p_{m,j}\frac{\gamma_{m,j}}{M}\right) + \sum\limits_{l\neq j}^{L}\sum\limits_{\overline{k}=1}^{K} \beta_{i,l} P_{\overline{k},l}\frac{(M\rho_{i,\overline{k},l}^2+\gamma_{\overline{k},l})\gamma_{i,j}}{M\gamma_{\overline{k},l}} + \frac{\sigma_i^2\gamma_{i,j}}{M}} \tag{6}$$

$$\begin{aligned} SINR_{i,j} &= \frac{\beta_{i,j} p_{i,j}\frac{(\mathbb{E}[\mathbf{h}_{i,j}^H\hat{\mathbf{h}}_{i,j}])^2}{M\gamma_{k,j}}}{\beta_{i,j}\sum\limits_{k\neq i}^{K}\frac{p_{k,j}\mathbb{E}|\mathbf{h}_{i,j}^H\hat{\mathbf{h}}_{k,j}|^2}{M\gamma_{k,j}} + \beta_{i,j}p_{k,j}\frac{\mathbb{E}|(\mathbf{h}_{i,j}^H\hat{\mathbf{h}}_{i,j}-\mathbb{E}[\mathbf{h}_{i,j}^H\hat{\mathbf{h}}_{i,j}])|^2}{M\gamma_{i,j}} + \sum\limits_{l\neq j}^{L}\sum\limits_{\overline{k}=1}^{K}\frac{\beta_{\overline{k},j}p_{\overline{k},l}\mathbb{E}|\mathbf{h}_{i,l}^H\hat{\mathbf{h}}_{\overline{k},l}|^2}{M\gamma_{\overline{k},l}} + \sigma^2} \\ &= \frac{\beta_{i,j}p_{i,j}\frac{M^2}{M\gamma_{i,j}}}{\beta_{i,j}\sum\limits_{k\neq i}^{K} p_{k,j}\frac{M^2\rho_{i,k,j}^2+M\gamma_{k,j}}{M\gamma_{i,j}} + \beta_{i,j}p_{k,j}\frac{M\gamma_{i,j}}{M\gamma_{i,j}} + \sum\limits_{l\neq j}^{L}\sum\limits_{\overline{k}=1}^{K}\frac{\beta_{i,l}p_{\overline{k},l}(M^2\rho_{i,\overline{k},l}^2+M\gamma_{\overline{k},l})}{M\gamma_{\overline{k},l}} + \sigma^2} \\ &= \frac{\beta_{i,j}p_{i,j}}{\beta_{i,j}\sum\limits_{k\neq i}^{K} p_{k,j}\frac{(M\rho_{i,k,j}^2+\gamma_{k,j})}{M} + \beta_{i,j}p_{k,j}\frac{\gamma_{k,j}}{M} + \sum\limits_{l\neq j}^{L}\sum\limits_{\overline{k}=1}^{K}\beta_{i,l}p_{\overline{k},l}\frac{(M\rho_{i,\overline{k},l}^2+\gamma_{\overline{k},l})\gamma_{i,j}}{M\gamma_{\overline{k},l}} + \frac{\sigma^2\gamma_{i,j}}{M}} \\ &= \frac{\beta_{i,j}p_{i,j}}{\beta_{i,j}\left(\sum\limits_{k\neq i}^{K} p_{k,j}\rho_{i,k,j}^2 + \sum\limits_{m=1}^{K} p_{m,j}\frac{\gamma_{m,j}}{M}\right) + \sum\limits_{l\neq j}^{L}\sum\limits_{\overline{k}=1}^{K}\beta_{i,l}P_{\overline{k},l}\frac{(M\rho_{i,\overline{k},l}^2+\gamma_{\overline{k},l})\gamma_{i,j}}{M\gamma_{\overline{k},l}} + \frac{\sigma^2\gamma_{i,j}}{M}} \end{aligned} \tag{7}$$

l-th cell to the UE i in the j-th cell; $\mathbf{q}_{i,k,l}$ is linear precoding vector and $t_{i,k,l}$ denotes the data symbols streams transmitted by the BS in the l-th cell; $z_{i,j}$ is the AWGN and $z_{i,j} \in \mathcal{CN}(0, \sigma_z^2\mathbf{I}_M)$. As a result, the UE's received signal can be derived in the form of the desired signal plus the effective noise indicating the inter- and intra-cell interference. Let $G_{i,j,j} = \sqrt{p_{i,j,j}^{DL}\beta_{i,j,j}}\mathbf{h}_{i,j,j}^H$, then the received signal can be represented as

$$\mathbf{r}_{i,j} = \mathbb{E}[G_{i,j,j}]\mathbf{q}_{i,j,j}t_{i,j,j} + z_{i,j}^{'}, \tag{9}$$

where $z_{i,j}^{'}$ represents the effective noise and can be expressed as

$$\begin{aligned} z_{i,j}^{'} = &(G_{i,j,j} - \mathbb{E}[G_{i,j,j}])\mathbf{q}_{i,j,j}t_{i,j,j} + G_{i,j,j}\left(\sum_{k\neq i}^{K}\mathbf{q}_{i,k,j}t_{i,k,j}\right) \\ &+ \sum_{l\neq j}^{L}\sum_{k=1}^{K}\sqrt{\beta_{i,j,l}}\mathbf{h}_{i,j,l}^H\mathbf{q}_{i,k,l}t_{i,k,l} + z_{i,j}. \end{aligned} \tag{10}$$

According to the descriptions in [8], the precoding vector of the UE i in the j-th cell, $\mathbf{q}_{i,j,j}$, is given as

$$\mathbf{q}_{i,j,j} = \frac{\hat{\mathbf{h}}_{i,j,j}}{\sqrt{M\left(\sum\limits_{\overline{k}=1}^{K}\rho_{i,\overline{k},j}^2 + \sigma_w^2\right)}}. \tag{11}$$

In addition, it is assumed that if the number of antennas at the BS increase to infinity, we can get the following law of large number or the asymptotic orthogonality between channels in massive MIMO system

$$\lim_{M\to\infty}\frac{1}{M}\mathbf{h}_{i,j,j}^{\mathrm{H}}\mathbf{h}_{k,j,j} = \begin{cases} 0, & \text{if } i \neq k \\ 1, & \text{if } i = k. \end{cases} \tag{12}$$

In Lemma 1 of [8], they only considered the SINR of single-cell scenario. The following proposition gives the achievable sum rate with the SINR of multi-cell scenario.

Proposition 1. *For a L cells TDD massive MIMO system serving K UEs with a training sequence length of τ, the achievable sum rate of the system can be given as*

$$R = \sum_{l=1}^{L}\sum_{k=1}^{K}\left(1 - \frac{\tau}{T}\right)\log_2(1 + SINR_{k,l}) \tag{13}$$

where the $SINR_{k,l}$ is given by equation (12) at the top of the page.

Proof. As shown in Lemma 1 [8] , $\mathbb{E}[|\mathbf{h}_{i,j}^H\hat{\mathbf{h}}_{k,j}|] = M^2\rho_{i,k,j}^2 + M\gamma_{k,j}$ where $\gamma_{k,j} = \sum\limits_{z=1}^{k}\rho_{k,z,j}^2 + \sigma^2$, $\mathbb{E}[|\mathbf{h}_{i,j}^H\hat{h}_{i,j}|] = M^2$. By substituting into equation (6), we can get the proposed SINR and consequently the achievable sum rate. □

The proposed achievable sum rate in Proposition 1 has clearly shown how the varying length of pilots τ and the correlations between pilots $\rho_{i,k,j}$ influences the performance of the system. Assuming the training sequences are limited in length, different methods have been proposed to reduce the interference caused by pilot reuse in the denominator of the SINR [6], [7]. In the next section, the pilots design utilizing the GLP method will be introduced.

III. Grassmannian Line Packing based Pilot Design

The GLP design problem is to find the optimal packing of one-dimensional vectors in a vector space which has already been utilized for beamforming codebook design under the limited feedback in a multi-user MIMO system [9], [10]. In this section, we will introduce the GLP problem and investigate the application to pilot sequence design.

ISBN 978-3-8007-4177-9

Consider two 1-dimensional unit vectors $\mathbf{w}_1$ and $\mathbf{w}_2$ all belong to a matrix Φ_m with $\mathbf{w}_1 \equiv \mathbf{w}_2$. The equivalence of two vectors can be seen as two lines with same length in a complex vector space $\mathbb{C}^m$. The two lines can also be seen as two one-dimensional subspaces in $\mathbb{C}^m$. The set of all the one-dimensional subspaces in $\mathbb{C}^m$ is denoted as $\mathcal{G}(m,1)$, named the Grassmann Manifold. In the Grassmann manifold, the distance between the two subspaces $\mathbf{w}_1$ and $\mathbf{w}_2$ is defined as the sine of the angle $\theta_{\mathbf{w}_1,\mathbf{w}_2}$ between these two subspaces, which is formulated as

$$d_c(\mathbf{w}_1,\mathbf{w}_2) = \sin\theta_{\mathbf{w}_1,\mathbf{w}_2} = \sqrt{1-|\mathbf{w}_1^{\mathrm{H}}\mathbf{w}_2|^2}. \quad (14)$$

Assume that there are N one-dimensional subspaces in the Grassmann manifold $\mathcal{G}(m,1)$, the GLP problem is to optimally pack these N subspaces, i.e. the N subspaces are equally separated in space with the largest possible adjacent distances.

The GLP method can also be utilized in pilot sequence design. If each UE is assigned a training sequence with length τ and there are totally K UEs in the L cells, it forms a $K \times \tau$ matrix with the pilot sequence as the row vector. Due to the limited length of τ, it is not possible to assign each UE with orthogonal pilots in a TDD massive MIMO system. As a result, in the pilot reuse scheme [6], only some of the UEs are assigned with orthogonal pilots and the rest of UEs reuse these pilots. However, the pilot sequences can be treated as packing K one-dimensional subspaces in a $\mathcal{G}(\tau,1)$ Grassmann manifold. With maximum adjacent distances between pilots, the correlations between pilot sequences will be minimized. The correlation between pilot sequence $\mathbf{s}_1$ and $\mathbf{s}_2$ can be written as

$$\rho^2_{\mathbf{s}_1,\mathbf{s}_2} = |\mathbf{s}_1^{\mathrm{H}}\mathbf{s}_2|^2 = 1 - d_c^2(\mathbf{s}_1,\mathbf{s}_2). \quad (16)$$

In [11], [12] is proposed an upper bound of the distance in the Grassmannian manifold. To pack K subspaces (ie. K UEs) in the $\mathcal{G}(\tau,1)$ Grassmann manifold, the bound can be expressed as

$$d_c^2 \le \begin{cases} \frac{(\tau-1)}{\tau}\cdot\frac{K}{K-1}, & \text{if } K \le \tau(\tau+1)/2 \\ \frac{(\tau-1)}{\tau}, & \text{if } K > \tau(\tau+1)/2. \end{cases} \quad (17)$$

The above upper bound of distance can be utilized in bounding the correlations of the pilot sequences scheme with GLP. Consequently, we can estimate the achievable sum rate with the proposed pilot sequence design.

Corollary 1. *For a L cells TDD massive MIMO system serving K UEs with the length of training sequence equal to τ, the achievable sum rate of the system with the proposed pilot sequence design can be expressed as*

$$R_G = \sum_{l=1}^{L}\sum_{k=1}^{K}\left(1-\frac{\tau}{T}\right)\log_2\left(1+SINR_{k,l}^G\right) \quad (18)$$

where $SINR_{k,l}^G$ is given by equation (19) and ρ_G^2 is represented as

$$\rho_G^2 = \begin{cases} 1-\left(\frac{\tau-1}{\tau}\cdot\frac{K}{K-1}\right), & \text{if } K \le \tau(\tau+1)/2 \\ 1-\left(\frac{\tau-1}{\tau}\right), & \text{if } K > \tau(\tau+1)/2, \end{cases}$$

TABLE I
TABLE OF SYSTEM PARAMETERS

Number of cells L	7
Number of antennas at BS M	64-128
Cell radius	250 m
Minimum distance between UE and BS	35 m
Average transmit power at BS	40 W
System bandwidth	200 kHz
Carrier frequency	2 GHz
Velocity of mobile	10 km/h

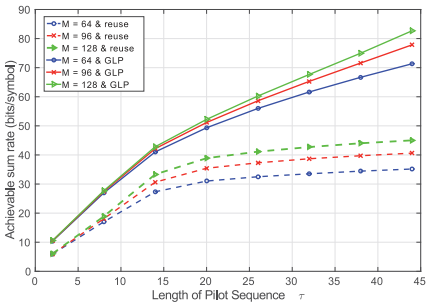

Fig. 2. Comparison of the achievable sum rate with pilot reuse scheme and non-orthogonal pilot scheme in the pilot contamination regions

Proof. Based on equations (16) and (17), we can get a lower bound on the correlation values. And by applying the GLP in pilot design, the correlation between pilots is same and by applying the bound of ρ in Proposition 1, it provides an upper bound on the achievable sum rate of the system. □

IV. Simulation Results and Discussions

A. Simulations results

The performance of the proposed GLP based pilot design is evaluated by Monte-Carlo simulations. Consider a massive MIMO system with 7 equal size hexagon shaped cells with a radius of 250 meters In [13], it pointed out that massive MIMO systems are likely to be installed in high-capacity hot-spot regions to serve a large number of UEs, such as in football stadia or shopping malls. As a result, the non-uniform distribution of UEs in a multi-cell massive MIMO system is considered in the simulation. The simulation includes seven cells with an equal number of antennas at each BS but the central cell is considered to serve more UEs than the neighbouring six cells. The UEs are randomly distributed in each cell with minimum 35 meters distance from BS. Furthermore, the velocity of each mobile is set to a small value (10 km/h). The calculation of path-loss follows the model $35.3 + 37.6\log_{10} d_{U,B}$ where $d_{U,B}$ denotes the distance (with unit meter) between UE and BS. The downlink transmit power is assumed to be equally distributed to the UEs in each cell.

Fig.2 shows the simulation results of achievable sum rate with increasing pilot length τ for different numbers of antennas at BS where $M = 64, 96$ or 128. The comparison

ISBN 978-3-8007-4177-9

$$SINR_{i,j} = \frac{\beta_{i,j} p_{i,j}}{\beta_{i,j}\left(\rho_G^2 \sum\limits_{k\neq i}^{K} p_{k,j} + \frac{K\rho_G^2+\sigma_w^2}{M} \sum\limits_{m=1}^{K} p_{m,j}\right) + \sum\limits_{l\neq j}^{L} \sum\limits_{k=1}^{K} \beta_{i,l} p_{k,l} \frac{(M+K)\rho_G^2+\sigma_w^2}{M} + \frac{K\rho_G^2+\sigma_w^2}{M}\sigma_i^2} \tag{15}$$

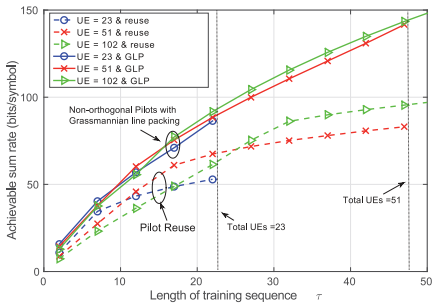

Fig. 3. Comparison of the achievable sum rate with pilot reuse scheme and non-orthogonal pilot scheme in the pilot contamination regions

TABLE II
TABLE OF UE GROUPS

	Central cell	Neighbouring 6 cells	Total UEs
Group 1	5 UEs	3 UEs	23 UEs
Group 2	15 UEs	6 UEs	51 UEs
Group 3	30 UEs	12 UEs	102 UEs

is made between pilot reuse scheme and the non-orthogonal pilot scheme with pilot contamination where $\tau < K$. The central cell contains 15 UEs while the neighbouring 6 cells contain 5 UEs. It can be observed that all the achievable sum rates linearly increase with the number of antennas at the BS. This is consistent with the proposition in [8] that the transmission rate is fundamentally limited by the length of the pilot sequences. When $\tau = 44$, the sum rate of the GLP based training sequence is doubled over the pilot reuse scheme. Furthermore, the GLP based pilot scheme has achieved significant improvements in transmission rate over the pilot reuse scheme for all the antenna configurations. This result is due to the small τ value leading to limited reuse of possibilities for the pilot signals so that the pilot contamination degrades the throughput performance significantly. Nevertheless, the GLP-based pilot design is able to mitigate the pilot contamination even with a small τ value. As a result, it has achieved much higher sum rate.

Fig.3 shows the achievable sum rate versus the varying number of UEs. Table II lists the three different groups of UE distributions that used in the simulation with $M = 256$. Again the GLP-based pilot design outperforms the pilot reuse schemes among the three UE distributions. The performance gaps between these two pilot schemes increase with the length of the training sequence. The GLP based pilot sequence brings approximately 70% increase of sum rate over the pilot reuse scheme. In addition, simulation results indicate the GLP-based pilot design is desired to be applied for a large number of UEs. For example, when τ is equal to 50, the gap of two schemes for $K = 51$ is about 60 bits/symbol and for $K = 102$ it is 80 bits/symbol.

V. Conclusions

The achievable sum rate performance of a massive MIMO system with a Grassmannian line packing based pilot scheme is investigated in this paper. A new closed-form achievable sum rate is proposed and simulations has been made with the TDD multi-cell massive MIMO systems with different configurations of the number of BS antennas, UE configurations and pilot sequence length. The results showed that the application of Grassmannian line packing in pilot design has significantly improved the throughput performance by at least 70%. In addition, it has shown that the Grassmannian line packing based pilot scheme is suitable to serve cells with large number of UEs. Future work will be focused on the joint optimization of capacity and energy efficiency.

References

[1] F. Rusek *et al.*, "Scaling up mimo: Opportunities and challenges with very large arrays," *IEEE Signal Process. Mag.*, vol. 30, no. 1, pp. 40–60, Jan 2013.

[2] F. Tufvesson E. Larsson, O. Edfors and T. Marzetta, "Massive mimo for next generation wireless systems," *IEEE Commun. Mag.*, vol. 52, no. 2, pp. 186–195, Feb 2014.

[3] H. Q. Ngo, E. G. Larsson, and T. L. Marzetta, "Energy and spectral efficiency of very large multiuser mimo systems," *IEEE Trans. on Commun.*, vol. 61, no. 4, pp. 1436–1449, April 2013.

[4] T. L. Marzetta J. Jose, A. Ashikhmin and S. Vishwanath, "Pilot contamination and precoding in multi-cell tdd systems," *IEEE Trans. Wireless Commun.*, vol. 10, no. 8, pp. 2640–2651, Aug. 2011.

[5] H. Yang and T. L. Marzetta, "Total energy efficiency of cellular large scale antenna system multiple access mobile networks," *IEEE Online Conference GreenCom*, pp. 27–32, Oct 2013.

[6] X. Zhu *et al.*, "Soft pilot reuse and multi-cell block diagonalization precoding for massive mimo systems," *IEEE Trans. Veh. Technol.*, vol. PP, no. 99, pp. 1–1, 2015.

[7] H. Wang *et al.*, "On design of non-orthogonal pilot signals for a multi-cell massive mimo system," *IEEE Wireless Commun. Letters*, vol. 4, no. 2, pp. 129–132, April 2015.

[8] J. C. Shen J. Zhang and K. B. Letaief, "Downlink user capacity of massive mimo under pilot contamination," *IEEE Trans. Wireless Commun.*, vol. 14, no. 6, pp. 3183–3193, June 2015.

[9] D. J. Love, R. W. Heath, and T. Strohmer, "Grassmannian beamforming for multiple-input multiple-output wireless systems," *IEEE Trans. Inf. Theory*, vol. 49, no. 10, pp. 2735–2747, Oct 2003.

[10] D. J. Love *et al.*, "An overview of limited feedback in wireless communication systems," *IEEE J. Sel. Areas Commun*, vol. 26, no. 8, pp. 1341–1365, October 2008.

[11] A. Barg and D. Yu. Nogin, "Bounds on packings of spheres in the grassmann manifold," *IEEE Trans. Inform. Theory*, vol. 48, no. 9, pp. 2450–2454, Sep 2002.

[12] J. H. Conway, R. H. Hardin, and N. J. A. Sloane, "Packing lines, planes etc.: Packings in grassmannian spaces," *Exper. Math.*, vol. 5, no. 2, pp. 139–159, 1996.

[13] R. E. Hattachi and J. Erfanian, "NGMN 5G white paper," http://tinyurl.com/ne6pxzo, Feb 2015.

ISBN 978-3-8007-4177-9

Non-Orthogonal Pilots Based Spectral and Energy Eff ciency Analysis for Multi-cell Massive MIMO Systems

Wenjun Fu, Pan Cao, Member, IEEE and John Thompson, Fellow, IEEE

Abstract

Channel estimation plays an important role in massive multiple-input multiple output (MIMO) systems in order to benef t from the high beamforming gain by forming very narrow beams. However, pilot contamination (PC) usually exists and inf uences the quality of estimated channel state information (CSI) due to the conf ict between the limited channel coherence interval and the large number of user equipments (UEs). Instead of utilizing the traditional pilot reuse scheme, we apply the principle of Grassmannian line packing (GLP) for the non-orthogonal pilot sequence design in order to mitigate the PC effect, where pairwise correlations between non-orthogonal pilot sequences has the same value between 0 and 1. In this work, for multi-cell massive MIMO systems with time-division-duplex (TDD) mode, we propose a new closed-form expression based on the use of non-orthogonal pilot sequences,which clearly shows how the PC, transmission power and number of base station (BS) antennas inf uence the system spectral eff ciency (SE). In addition, we also propose a general framework to optimize the energy eff ciency (EE) by effective downlink power control by two steps. We f rst solve a feasibility problem to determine maximum rate requirement for UEs, and then we apply the fractional sequential convex approximation algorithm to maximize the EE subject to feasible rate constraints to guarantee the QoS. Numerical results verify the propositions and show the improved performance of non-orthogonal pilot sequences to the traditional pilot reuse scheme in both SE and EE.

Index Terms

Massive multiple-input-and-multiple-output, spectral eff ciency, energy eff ciency, non-orthogonal pilot sequence, fractional programming

The work is partially supported by the UK EPSRC grant number EP/L026147/1. The authors are with the Institute for Digital Communications, The University of Edinburgh, Edinburgh EH3 9JL, United Kingdom (email: {w.fu, p.cao, john.thompson}@ed.ac.uk).

I. Introduction

Massive multiple-input-and-multiple-output (MIMO), also known as large-scale antenna systems, is a promising mobile communication technology to build the f fth generation (5G) cellular networks. A large array of antennas - hundreds or even thousands - deployed at a base station (BS) gives the potential of high data rates and reliability for tens or even hundreds of user equipments (UEs) within the same time-frequency resources [1]–[3].

However, these benef ts offered by massive MIMO heavily rely on the quality of the estimated channel state information (CSI) [4], [5]. In massive MIMO systems, the time-division-duplex (TDD) operation mode may be preferred to the frequency-division-duplex (FDD) mode because the feedback of high-dimensional channels can be avoided by utilizing channel reciprocity in the TDD mode. To obtain high quality CSI in TDD mode, long orthogonal pilot sequences are needed in order to avoid pilot contamination (PC). However, the transmission of such long pilot sequences usually conf icts with the f nite channel coherence interval. As a result, PC becomes a limiting factor for the spectral eff ciency (SE) when short pilot sequences are not properly designed [4], [5]. Therefore, much attention has been attracted on pilot sequences design in order to reduce inf uence of PC on the system performance.

Meanwhile, as the number of BS antennas increases greatly, massive MIMO may cause higher energy consumption. Due to the fact that the BSs accounts for more than 70% percent total energy consumption in the existing cellular network [6], [7], it has become a main concern for the 5G cellular operators how to realize the green network operation. Therefore, besides the SE performance, the energy eff ciency (EE) is also a crucial performance metric for massive MIMO system design and evaluation.

A. Related work

One widely used scheme for pilot sequence design for channel estimation in a massive MIMO system is pilot reuse. The basic idea of pilot reuse is for some UEs to reuse the same set of orthogonal pilot sequences as the others [5]. As the UEs who use the same pilots will interfere with each other in the uplink pilot transmission, PC highly depends on the how the orthogonal pilots are allocated to the UEs. Therefore, previous literature focused on how to smartly reuse pilots to reduce the PC effect. The authors in [4] utilize a common cell-based reuse, where the set of orthogonal pilot sequences are reused by the cells in a regular pattern. In [8], [9], the pilot sequence design has been improved by dividing sequences into several subsets while UEs are

divided into cell-centre and cell-edge groups according to path-loss and shadowing. Following this division, one subset is reused by the centre UEs and the remaining subsets are assigned to the edge UEs. This pilot allocation improved the QoS of edge UEs with a rate decrease of central UEs as compensation. In [10] the authors consider the covariance between the desired and the interfering UE channels because the channel estimation performance depends on the overlap of their dominant subspaces. The PC effect has been much reduced under the condition of limited angle of arrival at BS. In [11], the optimal schedule of UEs in each cell based on a given number of antennas and coherence interval is proposed.

Another pilot sequence design scheme is the recently proposed non-orthogonal pilots based scheme [12]. Unlike the pilot reuse scheme where the pairwise correlation value of pilot sequences is either 0 or 1, the non-orthogonal pilot sequence based scheme has a correlation value between 0 and 1. The authors in [12] investigate the error variance performance of channel estimation with non-orthogonal pilot sequences design, whereas the performance analysis of the SE and EE is excluded. In [13], the SE performance is analyzed for a single-cell massive MIMO system, which is extended to a multi-cell system in [14], [15]. However, the derivation for the SE expression is based on an unrealistic assumption in [14], which will be explained in Remark 1 in section III.

B. Contributions

This work aims to provide a complete and accurate analysis of both the SE and EE for a multi-cell massive MIMO system with TDD mode when the non-orthogonal pilots sequences are used. The main contributions are summarized as follows:

1) We derive a new closed-form sum rate expression based on the non-orthogonal pilot sequence scheme for a multi-cell massive MIMO system in Theorem 1 of Section III. This expression clearly shows how the PC, the number of BS antennas and uplink/downlink transmission power inf uence the SE performance. Furthermore, this expression can be formulated as the sum rate based on orthogonal pilots reuse scheme as shown in Corollary 1 of Section III;
2) We propose a general framework for the optimization of the EE. Based on the proposed rate expression, the framework f rst solve a feasibility problem to determine the maximum rate requirement for the UEs. Then, we utilize the fractional sequential convex approximation

(SCA) algorithm to optimize the EE subject to the feasible rate constraint by downlink power control.

3) We use the principle of Grassmannian line packing (GLP) to generate the non-orthogonal pilot sequences for channel estimation in numerical results. In addition, we also consider the existence of distortion in the non-orthogonal pilots due to the non-ideal hardware in practical systems.

The remainder of this paper is organized as follows: Section II introduces a multi-cell TDD massive MIMO system model; Section III proposes and analyzes a closed-form expression of downlink achievable rate; Section IV first formulate an EE maxmization problem and presents an algorithm to solve it; Finally, numerical results and discussions are provided in Section V.

The following notations are utilized through the paper. The bold font notation is applied to represent matrix or vector. For a matrix $\mathbf{A}$, $\mathbf{A}^T$, $\mathbf{A}^H$ and $\mathbf{A}^*$ represent its transpose, Hermitian transpose and conjugate transpose, respectively. $\mathcal{CN}(x, y)$ denotes the complex normal distribution with x as mean and y as variance, $\mathrm{diag}(\cdot)$ denotes the diagonal matrix, $\mathbb{E}[\cdot]$ and $\mathrm{Var}\{\cdot\}$ represents expectation and variance, respectively. $\mathbf{I}_M$ is M-dimensional identity matrix. $\otimes$ denotes the Kronecker product.

II. System model

Consider a multi-cell massive MIMO cellular network with TDD mode. In each cell, a BS is equipped with an M-antenna array serving K single-antenna UEs. Note that $M \gg K$. A block-fading channel model is considered and the channel vector from UE i in cell j to the BS l can be represented as $\sqrt{\beta_{ij,l}}\mathbf{h}_{ij,l}$, where $\beta_{ij,l}$ represents the large-scale fading coefficient that models path-loss and shadowing; $\mathbf{h}_{ij,l}$ represents the small-scale fading and each element in $\mathbf{h}_{ij,l}$ is independent and identically distributed (i.i.d) satisfying $\mathbf{h}_{ij,l} \in \mathcal{CN}(0, \mathbf{I}_M)$. It is assumed that the channel model $\sqrt{\beta_{ij,l}}\mathbf{h}_{ij,l}$ remains constant during one channel coherence interval.

1) Uplink Channel Estimation: The uplink transmission starts with UEs sending their own pilot sequences to their home cell BS simultaneously. Each UE i in cell j will be assigned a pilot sequence vector $\mathbf{s}_{ij}$, where $\mathbf{s}_{ij} \in \mathbb{C}^{\tau\times 1}$ has a length of τ samples and $\mathbb{E}[|\mathbf{s}_{ij}|^2] = 1$. The correlation coefficient of pilot sequences between the UE i and the UE $\tilde{i} \neq i$ in cell j is given as

$$\rho^2_{ij,\tilde{i}j} \triangleq |\mathbf{s}^H_{ij}\mathbf{s}_{\tilde{i}j}|^2, \tag{1}$$

where in the perfect orthogonality condition it follows:

$$\rho^2_{ij,\bar{i}j} = \begin{cases} 0, & if \quad i \neq \bar{i} \\ 1, & if \quad i = \bar{i}. \end{cases} \tag{2}$$

It is assumed that all active UEs send their uplink pilot sequences simultaneously and the BS receives the uplink pilot sequences from both the home cell and the other $L-1$ cells, where the received signal at BS j is expressed as

$$\begin{aligned} \mathbf{y}_j &= \underbrace{\sum_{k=1}^{K} \sqrt{p^u_{kj}\beta_{kj,j}}\mathbf{S}_{kj}\mathbf{h}_{kj,j}}_{\text{cell } j} + \underbrace{\sum_{l\neq j}^{L}\sum_{k=1}^{K} \sqrt{p^u_{kl}\beta_{kl,j}}\mathbf{S}_{kl}\mathbf{h}_{kl,j}}_{\text{other } L-1 \text{ cells}} + \mathbf{n}_j \\ &= \sum_{l=1}^{L}\sum_{k=1}^{K} \sqrt{p^u_{kl}\beta_{kl,j}}\mathbf{S}_{kl}\mathbf{h}_{kl,j} + \mathbf{n}_j, \end{aligned} \tag{3}$$

where $\mathbf{y}_j \in \mathbb{C}^{\tau M \times 1}$ is the received signal; p^u_{kj} denotes the uplink transmit power; $\mathbf{n}_j \in \mathbb{C}^{\tau M \times 1}$ represents additive white Gaussian noise (AWGN) at the BS, where each element satisfies the distribution $\mathcal{CN}(0, \sigma_n^2)$; $\mathbf{S}_{kj} \in \mathbb{C}^{\tau M \times M}$ denotes the matrix includes the pilot sequence from UE k to BS j and $\mathbf{S}_k = s_k \otimes \mathbf{I}_M$. Once the BS receives the uplink pilot sequences, the least square (LS) method is applied for estimating CSI, where the estimated CSI for UE i is represented as

$$\widehat{\mathbf{h}}_{ij,j} = \sqrt{\beta_{ij,j}}\mathbf{h}_{ij,j} + \frac{1}{\sqrt{p^u_{ij}}}\left(\sum_{k\neq i}^{K}\sqrt{p^u_{kj}\beta_{kj,j}}\rho_{ij,kj}\mathbf{h}_{kj,j} + \sum_{l\neq j}^{L}\sum_{k=1}^{K}\sqrt{p^u_{kl}\beta_{kl,j}}\rho_{ij,kl}\mathbf{h}_{kl,j} + \mathbf{S}^{\mathrm{T}}_{ij}\mathbf{n}_j\right). \tag{4}$$

Equation (4) shows how the correlation between uplink pilot sequences influence the accuracy of estimation result. If there is no PC, the desired CSI is only affected by thermal noise. However, PC exists when the length of pilot sequence is shorter than the total number of UEs ($K \times L$ in total). Therefore, an uplink pilot design and PC mitigation are important to Massive MIMO systems.

2) Multi-cell Downlink Transmission: It is assumed that the estimated uplink CSI can be utilized for downlink transmission because of the channel reciprocity. To reduce the complexity and latency for online strategy design, MRT beamforming is applied for downlink precoding. Then, the received noisy signal by UE i in cell j can be expressed as

$$\begin{aligned} r_{ij} &= \underbrace{\sqrt{p^d_{ij}\beta_{ij,j}}\mathbf{h}^H_{ij,j}(\sum_{k=1}^{K}\mathbf{h}^H_{ij,j}\mathbf{t}_{ij,j}x_{ij,j})}_{cell\ j} + \underbrace{\sum_{l\neq j}^{L}\sum_{k=1}^{K}\sqrt{p^d_{il}\beta_{ij,l}}\mathbf{h}^H_{ij,l}\mathbf{t}_{kl,l}x_{kl,l}}_{other\ L-1\ cells} + z_{ij} \\ &= \sum_{l=1}^{L}\sum_{k=1}^{K}\sqrt{p^d_{ij,l}\beta_{ij,l}}\mathbf{h}^H_{ij,l}\mathbf{t}_{kl,l}x_{kl,l} + z_{ij}, \end{aligned} \tag{5}$$

where p_{ij}^{d} is the downlink transmit power; $\sqrt{\beta_{ij,j}}\mathbf{h}_{ij,j}^{H}$ denotes the downlink CSI, which utilized the uplink CSI; z_{ij} represents the AWGN satisfying $z_{ij} \in \mathcal{CN}(0, \sigma_n^2 \mathbf{I}_M)$; $x_{kl,l}$ represents the data symbols streams to UE k in cell l from BS l and $\mathbf{t}_{kl,l}$ denotes MRT beamforming direction based on the estimated CSI, i.e., $\mathbf{t}_{kl,l} = \widehat{\mathbf{h}}_{kl,l}/\|\widehat{\mathbf{h}}_{kl,l}\|$.

III. The Proposed Downlink Achievable Sum Rate

A. Multi-cell Massive MIMO Downlink Achievable Sum Rate

The channel property of the asymptotically favourable propagation environment [1] can also be applied in massive MIMO due to the very large number of antennas, which implies that two different channels can be considered to be approximately orthogonal, i.e.,

$$\lim_{M\to\infty} \frac{1}{M}\mathbf{h}_{ij,j}^{H}\mathbf{h}_{kj,j} = \begin{cases} 0, & \text{if } i \neq k \\ 1, & \text{if } i = k. \end{cases} \tag{6}$$

Based on (6), the term $\mathbb{E}\,\|\widehat{\mathbf{h}}_{ij,j}^{H}\widehat{\mathbf{h}}_{ij,j}\|$ can be simplified as

$$\mathbb{E}\,\|\widehat{\mathbf{h}}_{ij,j}^{H}\widehat{\mathbf{h}}_{ij,j}\| = M\left(\frac{1}{p_{ij,j}}\sum_{l=1}^{L}\sum_{n=1}^{K}\left(p_{nl}^{u}\beta_{nl}\rho_{ij,nl}^{2} + \sigma_n^2\right)\right) = M\alpha_{ij,nl} \tag{7}$$

As a result, the beamforming direction $\mathbf{t}_{ij,j}$ used by BS j for UE i in cell j can also be expressed as

$$\mathbf{t}_{ij,j} = \frac{1}{\sqrt{M\alpha_{ij,nl}}}\widehat{\mathbf{h}}_{ij,j}. \tag{8}$$

Based on Equation (5), the received signal at a UE can be interpreted as the desired signal and effective noise when the intra-cell and inter-cell interference are treated as additive noise. Let $g_{ij} = \sqrt{p_{ij}^{d}\beta_{ij,j}}\mathbf{h}_{ij,j}^{\mathrm{H}}\mathbf{t}_{ij}$, then the received signal at UE i in cell j is represented as

$$r_{ij} = \mathbb{E}[g_{ij}]x_{ij} + z_{ij}^{'}, \tag{9}$$

where $z_{ij}^{'}$ represents the effective noise and is expressed as

$$z_{ij}^{'} = (g_{ij} - \mathbb{E}[g_{ij}])x_{ij} + \sum_{k\neq i}^{K} g_{kj}x_{kj} + \sum_{l\neq j}^{L}\sum_{k=1}^{K} g_{kl}x_{kl} + z_{ij}. \tag{10}$$

The multi-cell average downlink achievable rate for UE i in cell j is given as [16]

$$R_{ij}^{d} = \left(1 - \frac{\tau}{T}\right)\log_2\left(1 + \gamma_{ij}^{d}\right), \tag{11}$$

where the downlink SINR γ_{ij}^d is

$$\gamma_{ij}^d = \frac{\left(\mathbb{E}\left[\mathbf{h}_{ij,j}^{\mathrm{H}}\mathbf{t}_{ij,j}\right]\right)^2 \beta_{ij,j}p_{ij}^d}{\mathrm{Var}\left[\mathbf{h}_{ij,j}^{\mathrm{H}}\mathbf{t}_{ij,j}\right]\beta_{ij,j}p_{ij,j}^d + \sum\limits_{m\neq i}^{K}\mathbb{E}\left|\mathbf{h}_{ij,j}^{\mathrm{H}}\mathbf{t}_{mj,j}\right|^2\beta_{ij,j}p_{mj}^d + \sum\limits_{l\neq j}^{L}\sum\limits_{k=1}^{K}\mathbb{E}\left|\mathbf{h}_{ij,l}^{\mathrm{H}}\mathbf{t}_{kl,l}\right|^2\beta_{ij,l}p_{kl}^d + \sigma_n^2}. \quad (12)$$

Based on Equation (11), we derive a closed-form expression for average downlink rate as follows.

Theorem 1. *Consider a multi-cell massive MIMO system with TDD mode. When we utilize the LS method for uplink channel estimation and MRT beamforming as downlink precoding, the average downlink rate for UE i in cell j can be expressed as*

$$R_{ij}^d = \left(1 - \frac{\tau}{T}\right)\log_2\left(1 + \gamma_{ij}^d\right) \quad (13)$$

where γ_{ij}^d denotes the SINR of UE i in Cell j, i.e.,

$$\gamma_{ij}^d = \frac{M\beta_{ij,j}^2 p_{ij}^d}{\alpha_{ij,nm}\left(\beta_{ij,j}p_{ij}^d + \sum\limits_{m\neq i}^{K}\left(1 + \frac{M\beta_{ij,j}p_{ij}^u\rho_{mj,ij}^2}{p_{mj}^u\alpha_{mj,nm}}\right)\beta_{ij,j}p_{mj}^d + \sum\limits_{l\neq j}^{L}\sum\limits_{k=1}^{K}\left(1 + \frac{M\beta_{il,l}p_{il}^u\rho_{kl,ij}^2}{p_{kl}^u\alpha_{kl,nm}}\right)\beta_{il,l}p_{kl}^d + \sigma_n^2\right)}, \quad (14)$$

with $\alpha_{ij,nm} = \sum\limits_{m=1}^{L}\sum\limits_{n=1}^{K}\frac{1}{p_{ij}^u}\left(\beta_{nm,j}\rho_{ij,nm}^2 + \sigma_n^2\right)$.

Proof. See Appendix. □

Remark 1. *The proposed expression of* (14) *in Theorem 1 is more accurate than [14], since the uplink power control assumption of $p_{ij}\beta_{ij,l} = 1$ for all l used in [14] does not hold in general. For example, if $\beta_{ij,1} = 2$, $\beta_{ij,2} = 3$, we cannot make both $p_{ij}\beta_{ij,1} = 1$ and $p_{ij}\beta_{ij,2} = 1$ hold at the same time by controlling a single variable p_{ij}.*

The achievable rate expression given in (8) clearly shows how the system spectral efficiency is affected by the correlations between the pilot sequences.

B. Pilot Reuse Scheme

When the length of pilot sequences is less than the number of UEs, pilot reuse is usually needed as in previous work. A trade-off exists between reuse factor and training overhead. If a larger reuse factor value is utilized, there will be less UEs that suffer inter-cell interference and the downlink SINR might be improved. However, it also causes higher training overhead at the same time, which will reduce the time period for downlink transmission. Therefore, based

on the results in Theorem 1, we characterize the downlink achievable rate for the pilot reuse scheme as follows.

Corollary 1. *For a positive integer pilot reuse factor U, the achievable downlink rate for each UE with pilot reuse scheme is given as*

$$R_{ij}^{d,pr} = \left(1 - \frac{\tau}{T}\right) \log_2 \left(1 - \gamma_{ij}^{d,pr}\right), \tag{15}$$

where $\gamma_{ij}^{d,pr}$ denotes the SINR for UE i in cell j, i.e.,

$$\gamma_{ij}^{d,pr} = \frac{M\beta_{ij,j}^2 p_{ij}^d}{\alpha_{ij,nm}\left(\sum\limits_{k=1}^{K} \beta_{ij,j} p_{kj}^d + \xi_{l_1} + \xi_{l_2} + \xi_{l_3} + \sigma_n^2\right)} \tag{16}$$

with the definitions of

$$\xi_{l_1} \triangleq \sum_{l_1 \neq j}^{L-\frac{L}{U}} \sum_{k_1=1}^{K} \beta_{ij,l_1} p_{k_1 l_1}^d, \tag{17a}$$

$$\xi_{l_2} \triangleq \sum_{l_2 \neq j}^{L/U} \sum_{k_2=1}^{K-1} \beta_{ij,l_2} p_{k_2 l_2}^d, \tag{17b}$$

$$\xi_{l_3} \triangleq \sum_{l_2 \neq j}^{L/U} \sum_{k_3}^{1} \left(1 + \frac{M\beta_{il_2,l_2} p_{il_2}^u}{p_{k_3 l_2}^u \alpha_{k_3 l_2,nl}}\right) \beta_{il_2,l_2} p_{k_3 l_2}^d. \tag{17c}$$

Proof. Under the assumption that pilot reuse factor U is a positive integer, the number of UEs which can be assigned to the set of orthogonal pilots is $\left(L - \frac{L}{U}\right) \times K + \frac{L}{U} \times (K-1)$. The other $\frac{L}{U}$ UEs who reuse this set of pilots have correlation value $\rho = 1$. As a result, Equation (16) can be specialized from Equation (14) for the reuse case. □

Equation (15) shows the impact to the reuse factor N on the downlink achievable rate.

IV. Optimization of Energy Efficiency

The BSs in massive MIMO systems are equipped with large scale antenna arrays and also require complicated hardware and high signal processing capacity, which will cause very high energy consumption. Therefore, energy efficiency, measured in bit/Joule, is also an important metric for system design and managementi.e.,

$$\text{Energy Efficiency} = \frac{\text{Downlink achievable sum rate}}{\text{Total power consumption}}. \tag{18}$$

The objective of this work is to develop an efficient power allocation algorithm to jointly allocate the power to all the UEs in the multi-cell massive MIMO systems, and meanwhile

satisfy the transmit power limitation and minimum UE rate constraints, in order to maximize the EE as defined in (18).

A. Power Consumption Model

To formulate the EE maximization problem, the total power consumption P_{tot} of the system will be first modelled, which is expressed as

$$P_{tot} = P_u + P_d, \tag{19}$$

where P_u and P_d denotes the total power for the uplink and downlink transmission respectively. In terms of the total power consumption model for the uplink transmission P_u, it includes: (i) the transmit power for transmitting uplink pilot of single antenna UEs, and (ii) the circuit and signal processing power associated with transmission of uplink pilot. Without loss of generality, it follows the assumption below

Assumption 1. *For all the single-antenna UEs in the multi-cell massive MIMO systems with TDD mode, it is assumed that all the UEs have the same power amplifier (PA) efficiency, circuit and signal processing power consumption for each coherence interval. For all the BSs, it follows the assumptions below*

1) *All the BSs have the same PA ratio, circuit and signal processing power consumption for each coherence interval.*
2) *Each transceiver serves one antenna at the BS.*

Consequently, following Assumption 1, the total power consumption for the uplink transmission P_u is defined as

$$P_u = \underbrace{\sum_{l=1}^{L}\sum_{k=1}^{K}\frac{\tau}{T}\frac{p_{kl}^u}{\eta_{UE}}}_{uplink\ transmit\ power} + \underbrace{L\cdot K\cdot p_{\mathrm{c}}^u}_{\substack{uplink\ circuits\ and\\ signal\ processing\ power}}, \tag{20}$$

where p_{kl}^u denotes the uplink transmit power of UE k in cell l and $k \in \mathcal{K}$, $l \in \mathcal{L}$, η_{UE} is the PA efficiency of UE, the product $\frac{\tau}{T}p_{kl}^u$ denotes the transmit power for uplink pilot transmission and p_c^u represents the circuits and signal processing power of UEs.

Parameter	Description
P_u	Total uplink power consumption
p_{kl}^u	Uplink transmit power from the UE k in cell l
η_{UE}	Power amplifier efficiency ratio of UE
p_c^u	Total Circuit and signal processing power consumption of UE

TABLE I: Power model parameters for the uplink transmission

The total power consumption model for BS in downlink transmission P_d includes (i) the downlink transmit power, and (ii) the circuit and signal processing power for the BS in receiving and transmitting signals. The value of P_d is expressed as [17], [18]

$$P_d = \frac{1}{\sigma_{BS}} \left(\sum_{l=1}^{L} \sum_{k=1}^{K} \left(1 - \frac{\tau}{T}\right) \frac{p_{kl}^d}{\eta_{BS}} + L \cdot M \cdot p_c^d \right), \tag{21}$$

where p_{kl}^d denotes the downlink transmit power for UE k by the BS in cell l and $k \in \mathcal{K}$, $l \in \mathcal{L}$, η_{BS} denotes the PA efficiency and σ_{BS} represents the loss factors of BS, which is expressed as

$$\sigma_{BS} = (1 - \sigma_{DC})(1 - \sigma_{MS})(1 - \sigma_{cool}), \tag{22}$$

where η_{PA} is the PA efficiency of BS, σ_{DC}, σ_{MS} and σ_{cool} represents the loss factor due to (i) direct-current (DC) to DC power supply, (ii) mains supply indicating Alternating Current (AC) to DC unit and (iii) cooling system respectively [17] [18]. The p_c^d is the circuit and signal processing power consumption of BS, which is modelled as

$$p_c^d = p_{c,dac}^d + p_{c,mix}^d + p_{c,filt}^d + p_{c,syn}^d + p_{bf}^d, \tag{23}$$

where $p_{c,dac}^d$, $p_{c,mix}^d$ and $p_{c,filt}^d$ represents the circuit power consumption of each BS antenna for the operation of (i) digital-analogue-conversion, (ii) mixing, and (iii) filtering [19]. The values $p_{c,syn}^d$ and p_{bf}^d represents the consumption of frequency synthesizer and beamforming respectively. For the sake of understanding, the power model parameters for the uplink and downlink transmission utilized in this paper have been listed in Table I and Table II respectively. Following the formulation of the total power consumption of the system, the problem of maximizing the EE can be mathematically formulated in the next section.

Parameter	Description
P_d	Total downlink power consumption
p_{kl}^d	Downlink transmit power to the UE k from BS l
η_{BS}	Power amplifier efficiency of BS
σ_{BS}	Loss factors of BS
σ_{DC}	Loss factor from direct-current to direct-current power supply
σ_{MS}	Loss factor from main supply
σ_{cool}	Loss factor from cooling
p_c^d	Total circuit and signal processing power consumption of BS
$p_{c,dac}^d$	BS power consumption of digital-analogue-converting
$p_{c,mix}^d$	BS power consumption of mixing
$p_{c,filt}^d$	BS power consumption of filtering
$p_{c,syn}^d$	BS power consumption of synchronization
$p_{c,syn}^d$	BS power consumption of beamforming

TABLE II: Power model parameters for the downlink transmission

B. Problem Formulation

The EE of the multi-cell massive MIMO systems with TDD mode is defined as follows.

$$EE\left(p_{kl}^u, p_{kl}^d\right) = \frac{\sum_{l=1}^{L}\sum_{k=1}^{K}\left(1-\frac{\tau}{T}\right)\log_2\left(1+\gamma_{kl}\left(p_{kl}^u, p_{kl}^d\right)\right)}{\sum_{l=1}^{L}\sum_{k=1}^{K}\frac{\tau}{T}\frac{p_{kl}^u}{\eta_{UE}} + L\left(MP_c^u\right) + \frac{1}{\sigma_{BS}}\sum_{l=1}^{L}\sum_{k=1}^{K}\left(1-\frac{\tau}{T}\right)\frac{p_{kl}^d}{\eta_{BS}} + L\left(MP_c^d\right)} \tag{24}$$

where γ_{kl} denotes the signal-to-interference-plus-noise-ratio (SINR) of UE k in cell l. Following the EE definition in equation (24), power allocation will be applied on both uplink and downlink for maximizing the EE of the overall system. The optimization problem can be formulated as

$$\underset{p_{kl}^u, p_{kl}^d}{\text{maximize}} \quad EE\left(p_{kl}^u, p_{kl}^d\right) \tag{25a}$$

$$\text{subject to} \quad 0 < p_{kl}^u \le p_{max}^u, \ \forall (k,l) \in (\mathcal{K}, \mathcal{L}) \tag{25b}$$

$$p_{kl}^d \ge 0, \ \forall (k,l) \in (\mathcal{K}, \mathcal{L}) \tag{25c}$$

$$\sum_{k=1}^{K} p_{kl}^d \le p_{max}^d, \ \forall (l) \in (\mathcal{L}) \tag{25d}$$

$$R_{kl}^D\left(p_{kl}^u, p_{kl}^d\right) \ge R_{min}, \ \forall (k,l) \in (\mathcal{K}, \mathcal{L}), \tag{25e}$$

where p_{max}^u and p_{max}^d are the maximum uplink and downlink transmit power constraints at the UE and BS side due to the hardware limitations, R_{min} represents the minimum downlink

rate that guarantees the QoS. In (25), Constraint (25b) ensures that the uplink power is less or equal to the maximum limitation but larger than 0. Constraints (25c) and (25d) ensure that the downlink power to each UE is larger or equal to 0, and the sum power to all the UEs in one cell meets the maximum limit. Constraint (25e) ensures that the downlink achievable rate of each UE needs to larger or equal to the pre-defined minimum UE rate.

It is noticeable from Problem (25a) that the maximization of EE is challenging to solve directly. Although Problem (24) has a ratio form with a fractional structure, it cannot be directly solved with existing algorithms for the fractional programming theory [20], [21]. It is because the numerator in Problem (25a) and the Constraint (25e) includes the downlink achievable sum rate of a multi-cell massive MIMO system, which is a difference of two concave functions. Optimization problems with DC functions are generally non-concave and it is challenging to find the globally optimal solution.

C. EE optimization

In this paper, a general framework is proposed to solve the EE maximization problem efficiently. The proposed framework starts with the reformulation of (25), which aims to convert the variables in equation (24) into vector form. The purpose of conversion for the algorithm is to enable the joint allocation of the transmit power for all the UEs in the multi-cell scenario. Following this reformulation, the optimization focuses on one single power vector, rather than multiple scalar power values.

1) Problem Reformulation: In terms of the downlink achievable sum rate, the problem utilizes the proposition in Theorem 1. For solving the problem efficiently, it is assumed that all the UEs utilize full power for the transmission of uplink pilot sequences. By observing the downlink SINR expression in equation (14), it can be found that the downlink achievable sum rates increase monotonically with the uplink power. Consequently, the optimization only considers the downlink transmit power as the variable, which is expressed as

$$\mathbf{p} \triangleq \left[p_{k-2l}^{d}, p_{k-1l}^{d}, \cdots, p_{kl}^{d}\right]^{T} \in \mathbb{R}_{+}^{(LK\times 1)}, \tag{26}$$

where $\mathbf{p}$ is the vector which contains elements of the downlink power for each UE. Consequently, the downlink SINR expression in equation (14) is reformulated as

$$\gamma_{ij}\left(\mathbf{p}\right) = \frac{\mathbf{z}_{ij}^{T}\mathbf{p}}{\mathbf{b}_{ij}^{T}\mathbf{p} + \sigma_{n}^{2}}, \tag{27}$$

with $\mathbf{z}_{ij} \triangleq \left[0, 0, \cdots, \frac{M}{\alpha_{ij,nj}}\beta_{ij,j}^2, 0, 0, \cdots\right]^T \in \mathbb{R}^{(LK\times 1)}$ and $\mathbf{b}_{ij} \triangleq \left[0, 0, \cdots, \beta_{ij,j}, \sum_{k\neq i}^{K} \frac{(M\beta_{ij,j}\rho_{kj,ij}^2+\alpha_{kj,nm})}{\alpha_{kj,nm}}\beta_{ij,j}, \sum_{l\neq j}^{L}\sum_{k=1}^{K} \frac{(M\beta_{ij,l}\rho_{kl,ij}^2+\alpha_{kl,nm})}{\alpha_{kl,nm}}\beta_{ij,l}, \cdots\right]^T$. The vector $\mathbf{z}_{ij}$ is a $LK \times 1$ all zero vector except for one corresponding position and $\mathbf{b}_{ij} \in \mathbb{R}^{LK\times 1}$ is similarly defined, but for multiple non-zero entries. For example, in terms of the the calculation of γ_{ij}, it has p_{ij}^d in the numerator. Consequently, the non-zero entry in $\mathbf{z}_{ij}$ will be $\frac{M}{\alpha_{ij,nj}}\beta_{ij,j}^2$ and all the other entries will be zero. Then, the numerator of γ_{ij} equals to $\frac{M}{\alpha_{ij,nj}}\beta_{ij,j}^2 p_{ij}^d$. In terms of $\mathbf{b}_{ij}$ in the denominator, it is similarly defined.

The total power consumption of the system can also be reformulated as

$$P_{sum}\left(\mathbf{p}\right) = P_u + \left(\frac{1}{\sigma_{BS}}\left(\sum_{l=1}^{L}\sum_{k=1}^{K}\mathbf{c}_\eta^T\mathbf{p} + L\cdot M\cdot p_c^d\right)\right), \tag{28}$$

where $\mathbf{c}_\eta$ is a $LK \times 1$ vector with all the entries are $\left(1-\frac{\tau}{T}\right)\frac{1}{\eta_{BS}}$. Following the reformulation of the SINR and the sum power consumption given above, Problem (25a) can be rewritten as

$$\underset{\mathbf{p}}{\text{maximize}} \quad EE\left(\mathbf{p}\right) = \frac{\sum_{l=1}^{L}\sum_{k=1}^{K}\left(1-\frac{\tau}{T}\right)\log_2\left(1+\gamma_{kl}\left(\mathbf{p}\right)\right)}{P_u + \left(\frac{1}{\sigma_{BS}}\left(\sum_{l=1}^{L}\sum_{k=1}^{K}\mathbf{c}_\eta^T\mathbf{p} + L\cdot M\cdot p_c^d\right)\right)} \tag{29a}$$

$$\text{subject to} \quad \mathbf{t}_{kl}^T\mathbf{p} \geq 0, \ \forall\left(k,l\right) \in \left(\mathcal{K},\mathcal{L}\right) \tag{29b}$$

$$\sum_{k=1}^{K}\mathbf{t}_{kl}^T\mathbf{p} \leq p_{max}^d \ , \ \forall\left(l\right) \in \left(\mathcal{L}\right) \tag{29c}$$

$$R_{kl}^d\left(\mathbf{p}\right) \geq R_{min} \ , \ \forall\left(k,l\right) \in \left(\mathcal{K},\mathcal{L}\right), \tag{29d}$$

where $\mathbf{t}_{kl} \triangleq \left[0, 0, \cdots, 1, 0, 0, \cdots\right]^T$ is a vector with $KL\times 1$ length and all zero elements but unit elements at corresponding position. The aim of the optimization framework is to jointly optimize the downlink transmit power for all the UEs of the cell, and it can be easily achieved after the reformulation. Also, the reformulated problem is suitable for utilizing CVX [22] to solve it. The second step will be the maximization of QoS UE rate R_{min}. The QoS UE rate is the minimum downlink achievable rate, which guarantees the service provided by BS. It is aimed not only to maximize the QoS rate for all the UEs, but also to provide a feasible constraint for the EE optimization in the varying quality propagation environment.

2) Maximization of QoS UE rate: For the constraint that shown in (29d), a fixed value of R_{min} is obviously not suitable. It is because the UE positions and propagation environment are always changing, where the QoS UE rate also varies. For example, the cell edge UEs may

suffer strong interference which might influence the channel estimation quality and therefore the downlink transmission rate might be reduced. In order to tackle Problem (29a), a proper constraint value of QoS UE rate is required at the beginning of EE maximization.On the other hand, fairness should also be considered in the system design, which is achieved by enhancing the QoS UE rate.

The maximization problem of the QoS UE rate is formulated as follows

$$\underset{\mathbf{P}}{\text{maximize}} \quad \min_{k,l} \quad R_{kl}^{d}(\mathbf{p}) \tag{30a}$$

$$\text{Subject to} \quad \mathbf{t}_{kl}^{T}\mathbf{p} \geq 0,\ \forall\,(k,l) \in (\mathcal{K},\mathcal{L}) \tag{30b}$$

$$\sum_{k=1}^{K} \mathbf{t}_{kl}^{T}\mathbf{p} \leq p_{max}^{d}\ ,\ \forall\,(l) \in (\mathcal{L})\,. \tag{30c}$$

To solve Problem (30a), it can be transferred into a epigraph form, which is commonly used for solving the concave optimization problem [21]. The epigraph form is a reformulation of the concave problem by replacing the original objective function with a new variable and an equal constraints. Consequently, Problem (30a) can be reformulated as

$$\underset{\chi,\mathbf{p}}{\text{maximize}} \quad \chi \tag{31a}$$

$$\text{subject to} \quad R_{kl}(\mathbf{p}) \geq \chi, \forall\,(k,l) \in (\mathcal{K},\mathcal{L}) \tag{31b}$$

$$\mathbf{t}_{kl}^{T}\mathbf{p} \geq 0,\ \forall\,(k,l) \in (\mathcal{K},\mathcal{L}) \tag{31c}$$

$$\sum_{k=1}^{K} \mathbf{t}_{kl}^{T}\mathbf{p} \leq p_{max}^{d}\ ,\ \forall\,(l) \in (\mathcal{L})\,, \tag{31d}$$

where χ is the introduced variable. It can be found that Problem (31) is a linear programming problem and it is concave. It can be solved by the common optimization method, e.g. CVX, where the proof of concavity is presented below.

Lemma 1. *Problem (31) can be solved optimally.*

Proof. First, the constraint (31b) can be reformulated as

$$\begin{aligned} &\left(1-\frac{\tau}{T}\right)\log_2\left(1+\frac{\mathbf{z}_{ij}^{T}\mathbf{p}}{\mathbf{b}_{ij}^{T}\mathbf{p}+\sigma_n^2}\right) \geq \chi \\ \Leftrightarrow \quad &\left(\mathbf{z}_{ij}^{T}-\left(2^{\frac{\chi}{\left(1-\frac{\tau}{T}\right)}}-1\right)\mathbf{b}_{ij}^{T}\right)\mathbf{p} \geq \left(2^{\frac{\chi}{\left(1-\frac{\tau}{T}\right)}}-1\right)\sigma_n^2 \end{aligned} \tag{32}$$

With a given χ, Problem (31) becomes a linear programming problem with respect to $\mathbf{p}$. Thus, we can find the optimal $\mathbf{p}$ and χ by jointly using bisection search method of χ and solving the linear programmes with respect to $\mathbf{p}$. □

After maximizing the QoS UE rate, it provides a feasible constraint for the EE maximization. As Problem $(29a)$ is in fractional form, the Dinkelbach method [23], which is a useful algorithm that belongs to fractional programming [20], can be utilized for solving the problem. The utilization of fractional programming theory converts the EE maximization problem into a series of concave problems, and the globally optimal solution can be iteratively found by utilizing the Dinklebach method [23]. However, the directly adoption of fractional programming theory requires conditions on both the objective function and constraints, where $y(\mathbf{x})$ needs to be a concave function, $z(\mathbf{x})$ is a concave function and the constraints are all concave as well. In terms of the multi-cell massive MIMO system with TDD mode, the expression of downlink rate, which is the numerator in Problem (29a) and the constraint (29d), is a non-concave function [24], [25]. Consequently, the fractional SCA algorithm is proposed for solving the maximization of EE in multi-cell massive MIMO systems.

3) The introduction of SCA Algorithm: The SCA algorithm is an advanced scheme that is utilized to solve non-concave optimization problems, where locally optimal solutions can be found efficiently with acceptable complexity [26], [27]. Consider a non-concave optimization problem

$$\underset{\mathbf{x}\in\mathbb{R}^M}{\text{maximize}} \quad y(\mathbf{x}) \tag{33a}$$

$$\text{s.t.} \quad c_j(\mathbf{x}) \leq 0\ ,\ j = 1, 2, \cdots, J, \mathbf{x} \in \Omega \tag{33b}$$

where y, c_j are both continuous and differentiable functions over $\mathbb{R}^M$. It is assumed that both y and c_j can be expanded as the difference of two non-negative concave functions, which are expressed as

$$y(\mathbf{x}) \triangleq y^+(\mathbf{x}) - y^-(\mathbf{x}) \tag{34}$$

$$c_j(\mathbf{x}) \triangleq c_j^+(\mathbf{x}) - c_j^-(\mathbf{x}) \tag{35}$$

where $y^+, y^-, c_j^+, c_j^- : \mathbb{R}^M \to \mathbb{R}$. It can be observed that both the objective function (33a) and the constraint (33b) are typical DC programming of variable $\mathbf{x}$ [28] with a DC constraint, which is generally considered as a non-concave problem. Consequently, common concave optimization algorithms cannot be directly applied for solving these problems.

The approximation of concave functions is common scheme of solving a non-concave problem with local convergence. The SCA algorithm adopts this scheme in solving the non-concave problem iteratively. A surrogate function is generated for the approximation iteratively by utilizing the first order Taylor series expansion, which is given as

$$y(\mathbf{x},\mathbf{z}) = y(\mathbf{x})^{+} - \left(y^{-}(\mathbf{z}) + (\nabla y(\mathbf{z}))^{T}(\mathbf{x}-\mathbf{z})\right). \tag{36}$$

Equation (36) is an approximation of function $y(\mathbf{x})$, which is tight when $\mathbf{x} = \mathbf{z}$. Otherwise it comes to $y(\mathbf{x},\mathbf{z}) < y(\mathbf{x})$. Similarly, the surrogate functions can also be generated for the constraints which are difference of two concave functions. By replacing the non-concave functions in both the objective function and constraints with their surrogate functions, problem (33a) can be linearly approximated by a series of concave functions, which can be iteratively solved with acceptable complexity.

After the introduction of fractional programming and the SCA algorithm, the proposed fractional SCA algorithm in solving the EE problem will be presented in the following section.

4) The Fractional SCA Algorithm: To solve the maximization of EE in multi-cell massive MIMO system with TDD mode, the combination of fractional programming and the SCA algorithm is utilized to jointly find the optimal downlink power allocation [29]. The optimization firstly calculates the maximized QoS UE rate R^{*}_{min}, which provides a feasible constraint. Secondly, the surrogate function is generated for the downlink achievable rate, which is the numerator of the objective function (29a) and constraints (29d), where with feasible vector $\mathbf{q}$, the surrogate functions for the SCA algorithm are expressed as

$$R^{d}_{kl}(\mathbf{p},\mathbf{q}) \triangleq \left(1-\frac{\tau}{T}\right)\left(\log_2\left(\frac{\left(\mathbf{z}^{T}_{kl}+\mathbf{b}^{T}_{kl}\right)\mathbf{p}+\sigma^{2}_{n}}{\left(\mathbf{z}^{T}_{kl}+\mathbf{b}^{T}_{kl}\right)\mathbf{q}+\sigma^{2}_{n}}\right) - \frac{1}{\log(2)}\frac{\mathbf{b}^{T}_{kl}(\mathbf{p}-\mathbf{q})}{\left(\mathbf{z}^{T}_{kl}+\mathbf{b}^{T}_{kl}\right)\mathbf{q}+\sigma^{2}_{n}}\right). \tag{37}$$

Thirdly, by utilizing the fractional programming in the (29a) with equation (37), the maximization problem is reformulated as

$$\underset{\mathbf{p}}{\text{maximize}} \quad \sum_{l=1}^{L}\sum_{k=1}^{K}\left(1-\frac{\tau}{T}\right)\left(\log_2\left(\frac{\left(\mathbf{z}_{kl}^T+\mathbf{b}_{kl}^T\right)\mathbf{p}+\sigma_n^2}{\left(\mathbf{z}_{kl}^T+\mathbf{b}_{kl}^T\right)\mathbf{q}+\sigma_n^2}\right)-\frac{1}{\log(2)}\frac{\mathbf{b}_{kl}^T(\mathbf{p}-\mathbf{q})}{\left(\mathbf{z}_{kl}^T+\mathbf{b}_{kl}^T\right)\mathbf{q}+\sigma_n^2}\right)$$
$$-\lambda P_{tot}(\mathbf{p}) \tag{38a}$$

$$\text{subject to} \quad \mathbf{t}_{kl}^T\mathbf{p}\geq 0, \quad \forall(k,l)\in(\mathcal{K},\mathcal{L}) \tag{38b}$$

$$\sum_{k=1}^{K}\mathbf{t}_{kl}^T\mathbf{p}\leq p_{max}^d, \quad \forall(l)\in(\mathcal{L}) \tag{38c}$$

$$\left(\mathbf{z}_{kl}^T-\left(2^{\frac{R_{min}^*}{\left(1-\frac{\tau}{T}\right)}}-1\right)\mathbf{b}_{kl}^T\right)\mathbf{p}\geq\left(2^{\frac{R_{min}^*}{\left(1-\frac{\tau}{T}\right)}}-1\right)\sigma_n^2, \quad \forall(k,l)\in(\mathcal{K},\mathcal{L}). \tag{38d}$$

Around the point $\mathbf{q}$, Problem (38) becomes a convex optimization problem with respect to $\mathbf{p}$, which can be optimally solved by CVX. The convergence of the proposed fractional SCA algorithm is proved below.

Proposition 1. *The fractional SCA algorithm in Algorithm 1 always converges to a Karush-Kuhn-Tucker (KKT) stationary solution of Problem (29).*

Proof. For any concave function, it is upper-bounded by its first order Taylor approximation at any point. Meanwhile, it can be seen that the numerator of objective function (29a) is the difference of two concave functions. If $R_{kl}^d(\mathbf{p})$ is represented as

$$R_{kl}^d(\mathbf{p})=r_{kl}^+(\mathbf{p})-r_{kl}^-(\mathbf{p}), \tag{39}$$

for any $\mathbf{p}_j$, it thus holds that

$$r_{kl}^+(\mathbf{p})-r_{kl}^-(\mathbf{p})\geq r_{kl}^+(\mathbf{p})-\left[r_{kl}^-(\mathbf{p}_j)+\left(\nabla R_{kl}^d(\mathbf{p})\right)^T(\mathbf{p}-\mathbf{p}_j)\right]. \tag{40}$$

Consequently, (38a) is lower bounds of (29a). As the lower bounds in (39) is tight when evaluated in $\mathbf{p}_j$, when $\mathbf{p}=\mathbf{p}_j$, it comes to (38a) are equal to (29a). Similarly, the gradients of (38a) is equal to (29a) when $\mathbf{p}=\mathbf{p}_j$. Consequently, the proof is completed. □

By utilizing Algorithm 1, the EE will monotonically increase and the local-optimal solution, which meets the given constraints, will iteratively be founded within polynomial time and affordable complexity.

Algorithm 1 The fractional SCA algorithm to solve Problem (29)

Initialization for SCA algorithm:

$\mathbf{q}^{(0)} \in \mathbb{R}^{KL\times 1}$ % an initial feasible downlink power vector

$\epsilon_1 \in \mathbb{R}$ % a small convergence threshold

$i = 0$;

repeat

Given $\mathbf{q}^{(i)}$, generate the surrogate functions $R_{kl}^{d}\left(\mathbf{p}, \mathbf{q}^{(i)}\right)$ based on Equation (37);

Initialization for Dinkelbach method:

$\lambda^{(0)} \geq 0$ % determined by a random power vector $\mathbf{p}^{(0)} \in \mathbb{R}^{KL\times 1}$

$\epsilon_2 \in \mathbb{R}$ % a small convergence threshold

$j = 0$;

repeat

Given $\lambda^{(j)}$, obtain the optimal solution $\mathbf{p}^{(j)}$ for Problem (38);

$\lambda^{(j+1)} \leftarrow \frac{\sum_{l=1}^{L}\sum_{k=1}^{K} R_{kl}^{d}\left(\mathbf{p}^{(j)},\mathbf{q}^{(i)}\right)}{P_{tot}\left(\mathbf{p}^{(j)}\right)}$;

$j \leftarrow j + 1$;

until $|\lambda^{(j)} - \lambda^{(j-1)}| \leq \epsilon_1$;

$i \leftarrow i + 1$;

return $\mathbf{q}^{(i)}$;

until $||\mathbf{q}^{(i)} - \mathbf{q}^{(i-1)}||_2 \leq \epsilon_2$;

return a locally optimal solution $\mathbf{p}^{*} = \mathbf{q}^{(i)}$ for Problem (29).

V. Numerical examples

In this section, the validity of the proposed closed-form downlink achievable sum rate and the optimization algorithm will be verified by numerical simulations. Consider a massive MIMO system consisting of 19 hexagon shaped cells as illustrated in Figure 1, where each cell has a central BS and randomly distributed UEs. The pilot reuse scheme with $U = 3$ was considered in the simulation with the UE distribution listed in Table III. The simulation parameters listed in Table IV, which includes both the configuration of BS antennas and UE distribution, plus the power consumption of circuit power for both BS and UE. Additionally, the circuit power of BS was chosen according to the prediction that by the year 2020 [18]. The codebook for the GLP-based uplink pilots were generated from the algorithm that was proposed in [30].

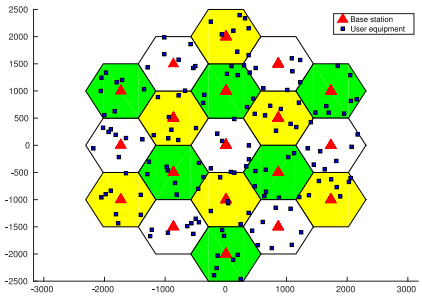

Fig. 1: Illustration of multi-cell massive MIMO systems with $L = 19$, $U = 3$. Each fill color represents the assignment of one set orthogonal pilot sequences. In this example, $K = 8$.

pilot length,τ	K in white cell	K in green cell	K in yellow cell	Total number of UE
$\tau = 8$	$K = 2$	$K = 3$	$K = 3$	50
$\tau = 16$	$K = 5$	$K = 5$	$K = 6$	101
$\tau = 32$	$K = 10$	$K = 11$	$K = 11$	202
$\tau = 64$	$K = 20$	$K = 22$	$K = 22$	404

TABLE III: UE distribution when $U = 3$

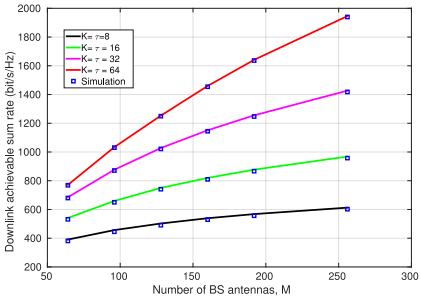

Fig. 2: Average downlink achievable sum rate versus the number of BS antennas M, with $L = 19$, $\tau = K = 8, 16, 32, 64$ and $U = 1$

Number of cells, L	19
Number of antennas at BS, M	$64 \leq M \leq 256$
Cell radius	500 m
UE minimum distance from BS	25 m
Carrier frequency	1.9 GHz
System bandwidth	20 MHz
Maximum UL power,P_{max}^{UL}	200 mW
Maximum DL power,P_{max}^{DL}	40 W
Thermal noise, σ_n^2	-174 dBm/Hz [31]
Mobility speed	60 km/H
Path loss model	$35.3 + 37.6 \log_{10} d$ dB
Coherence bandwidth	100 kHz
Power consumption of circuit power at BS, P_c^d	0.2 W [32]
Loss factor from DC to DC power supply, σ_{DC}	7.5% [18]
Loss factor from mains supply, σ_{MS}	9% [18]
Loss factor from cooling, σ_{cool}	10% [18]
Power amplifier efficiency of BS, η_{BS}	50 % [32]
Power amplifier efficiency of UE, η_{UE}	20 % [33]
UE circuit power, P_c^u	0.1 W [34]
Convergence tolerance, ϵ	1×10^{-3}

TABLE IV: Simulation parameters for the results in this section

A. The Performance of Downlink Achievable Sum Rate

Firstly, the proposed Theorem 1 will be verified. Figure.2 shows the downlink achievable sum rate with $U = 1$ versus number of BS antennas. Four different configurations of K are considered with $K = 8, 16, 32, 64$ for each cell. The analytical results are calculated by adopting equation (13) in Theorem 1 and simulation results from equation (11) with 10,000 channel realizations. It can be observed that the downlink achievable sum rate increases linearly with M. Additionally, the proposed analytical results match well with the simulation results, which has shown the validity of Theorem 1.

Figure.3 shows the downlink achievable sum rate with $U = 3$ versus the number of BS antennas. The analytical results are calculated by adopting equation (15) in Corollary 1 and the simulation results are calculated by adopting equation (11). It can be observed that the analytical results match well with the simulation results, which again shows the usefulness of the proposed analytical expression.

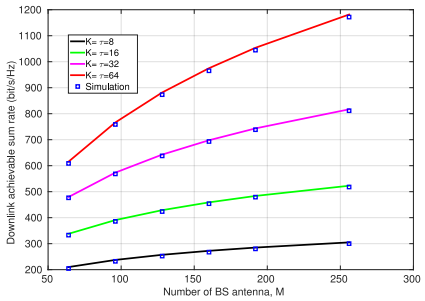

Fig. 3: Average downlink achievable sum rate versus the number of BS antennas M, with $L = 19$, $\tau = K = 8, 16, 32, 64$ and $U = 3$

The performance comparison considers not only the average downlink achievable sum rate, but also the rate of both cell central and edge UEs. The classification method in each cell is consistent, which is compared with the following threshold β_j^t [8]

$$\beta_j^t = \frac{\varphi}{K} \sum_{i=1}^{K} \beta_{ij}^2, \tag{41}$$

where φ denotes the coefficient that is defined based on the system configurations. The value φ is chosen as 0.2 in this paper. As a result, the classification of central and edge UE in cell j is expressed as

$$\begin{cases} \beta_{ij}^2 \geq \beta_j^t, & \text{central UE} \\ \beta_{ij}^2 < \beta_j^t, & \text{edge UE} \end{cases}. \tag{42}$$

The system parameters are consistent with the previous simulation of $U = 3$. Figure.4 shows the average downlink achievable sum rate versus the number of BS antennas. The GLP-based design utilizes the codebook generated from the algorithm proposed in [30], which has constant modulus and a finite alphabet (i.e. phase-shift keying (PSK)). It can be observed that the GLP-based pilot codebook outperforms the pilot reuse scheme. Additionally, with the increase of τ, the rate gain becomes more significant. In the case of $\tau = 8$, the average improvement is about 0.5%. When τ increases to 16 and 32, the average improvement is about 3.4 %. In the case of $\tau = 64$, the rate improvement becomes 4.7%. The reason is due to the increase of choral distance between lines in Grassmannian manifold along with the vector space dimension.

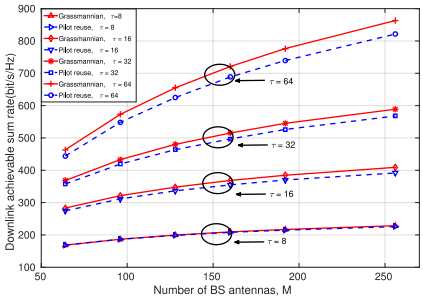

Fig. 4: Comparison of average downlink achievable sum rate versus the number of BS antennas M between GLP-based pilot codebook and pilot reuse scheme, with $L = 19$, $\tau = K = 8, 16, 32, 64$ and $U = 3$

This means that the correlation between codewords decreases as indicated by the upper bound. Figure.5 shows the downlink spectrum efficiency of both central and edge UEs. The simulation

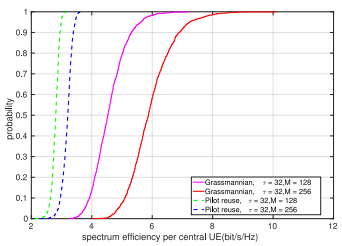

(a) Cumulative distribution function of spectrum efficiency per central UE, with $\tau = 32$ and $M = 128, 256$

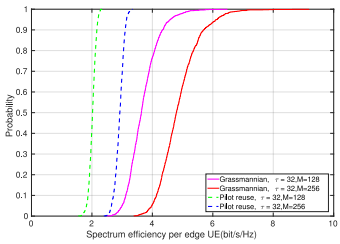

(b) Cumulative distribution function of spectrum efficiency per edge UE, with $\tau = 32$ and $M = 128, 256$

Fig. 5: The downlink spectrum efficiency comparison of central and edge UEs

considers $\tau = 32$ with $M = 128, 256$. By observing the 10th percentile, i.e., the rate met by 90% UEs, the improvement of the central UE is about 70% and nearly two fold for edge UEs.

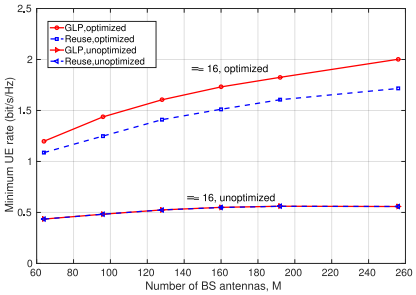

Fig. 6: Comparison of the minimum UE rate versus number of BS antennas M with and without maximization, with $U = 3, \tau = 16$

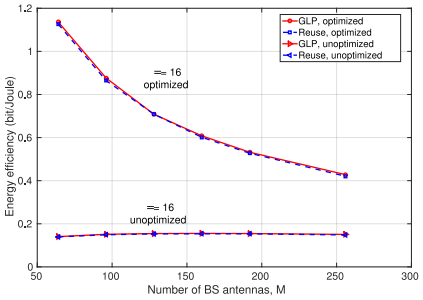

Fig. 7: Comparison of the energy eff ciency versus the number of BS antennas with and without maximization, with $U = 3, \tau = 16$

B. The Performance of Fractional SCA Algorithm

Fig.6 shows the QoS UE rate versus the number of BS antennas. The GLP based pilot codebook design and pilot reuse scheme were both utilized with $U = 3$ and $\tau = 16$. The maximization of the QoS UE rate were calculated with the CVX. It can be observed that the adoption of this optimization has enhanced the QoS signif cantly. When $M = 64$, the QoS UE rate of the pilot reuse scheme almost doubled, and it almost tripled for the GLP-based pilot design after the maximization. When $M = 256$, the improvement of pilot reuse increased by more than three

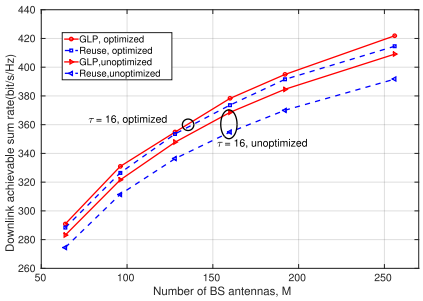

Fig. 8: Comparison of the downlink achievable sum rate versus the number of BS antennas M with and without optimization, with $U = 3$, $\tau = 16$.

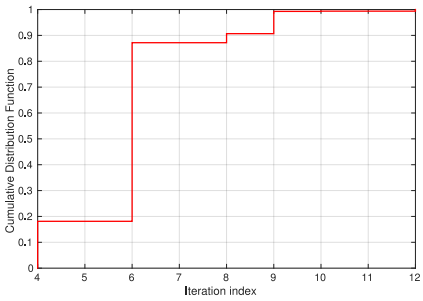

Fig. 9: Converge performance of Algorithm 1, with $U = 3$, $\tau = 16$, $\epsilon = 1 \times 10^{-3}$

times and it is approximately four times for the GLP-based pilot design after maximization.

Fig.7 shows the EE of multi-cell massive MIMO system versus the number of BS antennas. Again, the GLP based pilot codebook design and the pilot reuse scheme are both utilized, with $U = 3$ and $\tau = 16$. The maximization of EE utilized Algorithm 1. For the unoptimized EE, the downlink transmit power was equally divided for each serving UE in the cell, i.e. $\frac{P_{max}^{d}}{K}$. It can be observed that the EE of both schemes decreased as the number of BS antennas increases, whereby, the results for EE without optimization are almost consistent, because, in that scenario the downlink transmit power is dominant. The maximum power was utilized for

downlink transmission and the increase of circuit power did not have a big inf uence on the EE. However, after the optimization, the downlink transmit power was greatly reduced, so the EE of both schemes decreased with the number of BS antenna adopted followed by the increase of BS circuit power.

Fig.8 shows the downlink achievable sum rate versus the number of BS antennas. A comparison has been made between the rates after downlink power allocation and the rate after the equal division of downlink transmission power has been utilized. Although the focus was on maximizing the EE, the optimal allocation of downlink power and the maximized minimum UE rate has improved the rate performance, with about the improvement of 3% for GLP-based pilot codebook design and 5% for the pilot reuse scheme. The gap between two schemes has been reduced after the power allocation. However, the GLP-based codebook design still performed better than the pilot reuse scheme.

Fig.9 shows the convergence performance of Algorithm 3. This is a Cumulative distribution function (CDF) plot of the iteration numbers to reach the value $= 10^{-3}$ in the maximization of EE with $U = 3$ and $\tau = 16$. It can be observed that there are 90% of the results need 6 iterations to reaches the convergence point, and the optimization algorithm will always converge within 12 iterations.

VI. Conclusion

In this paper, we investigate the spectral eff ciency (SE) and energy eff ciency (EE) performance of non-orthogonal pilot sequence design in multi-cell massive MIMO systems with the time-division-duplex mode. We derive a new closed-form analytical expression of downlink achievable sum rate for SE analysis, which clearly demonstrates the impact from the pilot contamination and the number of base station antennas. The Grassmannian line packing (GLP) based pilot sequence design is considered for channel estimation, with the aim of increasing system SE. Furthermore, we propose a general framework of optimization for maximizing the QoS constrained EE, which includes two steps. Firstly, the feasibility problem is solved to optimize the QoS rate of user-equipments (UEs). Then, we utilize the fractional sequential convex approximation algorithm to maximize the EE, subject to the optimized QoS rate and power constraints by eff cient downlink power allocation. Numerical results have demonstrated the validity of the proposed analytical expressions and the non-orthogonal pilot sequence design achieves a 4% average improvement in SE over the traditional pilot reuse scheme. In addition,

there is a significant improvement of QoS rate and EE by utilizing the proposed optimization framework.

APPENDIX

Prove of Lemma 1

Proof.

$$\begin{aligned}
&\left|\mathbf{h}_{ij,j}^H\widehat{\mathbf{h}}_{mj,j}\right|^2\\
&=\left(\sum_{l_1=1}^{L}\sum_{n_1=1}^{K}\sqrt{\frac{\beta_{n_1l_1,j}p_{n_1l_1}^u}{p_{mj}^u}}\rho_{mj,n_1l_1}\mathbf{h}_{ij,j}^H\mathbf{h}_{n_1l_1}+\frac{1}{\sqrt{p_{mj}^u}}\mathbf{h}_{ij,j}^H\mathbf{S}_{mj}^H\mathbf{z}\right)^H\\
&\times\left(\sum_{l_2=1}^{L}\sum_{n_2=1}^{K}\sqrt{\frac{\beta_{n_2l_2,j}p_{n_2l_2}^u}{p_{mj}^u}}\rho_{mj,n_2l_2}\mathbf{h}_{ij}^H\mathbf{h}_{n_2l_2}+\frac{1}{\sqrt{p_{mj}^u}}\mathbf{h}_{ij}^H\mathbf{S}_{mj}^H\mathbf{z}\right)\\
&=\sum_{l_1=1}^{L}\sum_{n_1=1}^{K}\sum_{l_2=1}^{L}\sum_{n_2=1}^{K}\sqrt{\frac{\beta_{n_1l_1,j}p_{n_1l_1}^u}{p_{mj}^u}}\sqrt{\frac{\beta_{n_2l_2,j}p_{n_2l_2}^u}{p_{mj}^u}}\rho_{mj,n_1l_1}\rho_{mj,n_2l_2}\mathbf{h}_{n_1l_1}^H\mathbf{h}_{ij}\mathbf{h}_{ij}^H\mathbf{h}_{n_2l_2}\\
&+\sum_{l_1=1}^{L}\sum_{n_1=1}^{K}\sqrt{\frac{\beta_{n_1l_1,j}p_{n_1l_1}^u}{p_{mj}^u}}\rho_{mj,n_1l_1}\mathbf{h}_{n_1l_1}^H\mathbf{h}_{ij}\mathbf{h}_{ij}^H\mathbf{S}_{mj}^H\mathbf{z}\\
&+\sum_{l_2=1}^{L}\sum_{n_2=1}^{K}\sqrt{\frac{\beta_{n_2l_2,j}p_{n_2l_2}^u}{p_{mj}^u}}\rho_{mj,n_2l_2}\mathbf{z}^H\mathbf{S}_{mj}^H\mathbf{h}_{ij}\mathbf{h}_{ij}^H\mathbf{h}_{n_2l_2}+\frac{1}{p_{mj}^u}\mathbf{z}^H\mathbf{S}_{mj}\mathbf{h}_{ij}\mathbf{h}_{ij}^H\mathbf{S}_{mj}^H\mathbf{z}.
\end{aligned}\tag{43}$$

Then, we have

$$\begin{aligned}
&\mathbb{E}\left|\mathbf{h}_{ij}^H\widehat{\mathbf{h}}_{mj}\right|^2\\
&=\frac{1}{p_{mj}^u}\left(\sum_{l_1=1}^{L}\sum_{n_1=1}^{K}\sum_{l_2=1}^{L}\sum_{n_2=1}^{K}\sqrt{\beta_{n_1l_1,j}p_{n_1l_1}^u}\sqrt{\beta_{n_2l_2,j}p_{n_2l_2}^u}\rho_{mj,n_1l_1}\rho_{mj,n_2l_2}\,\mathbb{E}\left[\mathbf{h}_{n_1l_1}^H\mathbf{h}_{ij}\mathbf{h}_{ij}^H\mathbf{h}_{n_2l_2}\right]\right.\\
&\left.+\,\mathbb{E}\left[\mathbf{z}^H\mathbf{S}_{mj}\mathbf{h}_{ij}\mathbf{h}_{ij}^H\mathbf{S}_{mj}^H\mathbf{z}\right]\right)\\
&=\frac{1}{p_{mj}^u}\left(\beta_{ij,j}p_{ij}^u\rho_{mj,ij}^2\,\mathbb{E}\left[\mathbf{h}_{ij}^H\mathbf{h}_{ij}\mathbf{h}_{ij}^H\mathbf{h}_{ij}\right]+\sum_{n_1=n_2\neq i}^{K}\beta_{n_1j,j}p_{n_1j}^u\rho_{mj,n_1j}^2\,\mathbb{E}\left[\mathbf{h}_{n_1j}^H\mathbf{h}_{ij}\mathbf{h}_{ij}^H\mathbf{h}_{n_1j}\right]\right.\\
&\left.+\sum_{n_1\neq n_2}^{K}\sqrt{\beta_{n_1j,j}p_{n_1j}^u}\sqrt{\beta_{n_2j,j}p_{n_2j}^u}\rho_{mj,n_1j}\rho_{mj,n_2j}\,\mathbb{E}\left[\mathbf{h}_{n_1j}^H\mathbf{h}_{ij}\mathbf{h}_{ij}^H\mathbf{h}_{n_2j}\right]\right.
\end{aligned}$$

$$
\begin{aligned}
&+\sum_{l_1=l_2\neq j}^{L}\sum_{n_1\neq n_2}^{K}\sqrt{\beta_{n_1l_1,j}p^u_{n_1l_1}}\sqrt{\beta_{n_2l_1,j}p^u_{n_2l_1}}\rho_{mj,n_1l_1}\rho_{mj,n_2l_1}\,\mathbb{E}\left[\mathbf{h}^H_{n_1l_1}\mathbf{h}_{ij}\mathbf{h}^H_{ij}\mathbf{h}_{n_2l_1}\right]\\
&+\sum_{l_1\neq l_2}^{L}\sum_{n_1\neq n_2}^{K}\sqrt{\beta_{n_1l_1,j}p^u_{n_1l_1}}\sqrt{\beta_{n_2l_2,j}p^u_{n_2l_2}}\rho_{mj,n_1l_1}\rho_{mj,n_2l_2}\,\mathbb{E}\left[\mathbf{h}^H_{n_1l_1}\mathbf{h}_{ij}\mathbf{h}^H_{ij}\mathbf{h}_{n_2l_2}\right]\\
&+\mathbb{E}\left[\mathbf{z}^H\mathbf{S}_{mj}\mathbf{h}_{ij}\mathbf{h}^H_{ij}\mathbf{S}^H_{mj}\mathbf{z}\right]\Bigg)\\
&=\frac{1}{p^u_{mj}}\Bigg(\beta_{ij,j}p^u_{ij}\rho^2_{mj,ij}(M^2+M)+M\sum_{n_1=n_2\neq i}^{K}\beta_{n_1j,j}p^u_{n_1j}\rho^2_{mj,n_1j}\\
&+M\sum_{l_1=l_2\neq j}^{L}\sum_{n_1=n_2}^{K}\beta_{n_1l_1,j}p^u_{n_1l_1}\rho^2_{mj,n_1l_1}+M\sigma_z^2\Bigg)\\
&=M\left(\frac{M}{p^u_{mj}}\beta_{ij,j}p^u_{ij}\rho^2_{mj,ij}+\frac{1}{p^u_{mj}}\sum_{l=1}^{L}\sum_{n=1}^{K}\beta_{nl,j}p^u_{nl}\rho^2_{mj,nl}+\sigma_z^2\right)\\
&=M\left(\frac{M}{p^u_{mj}}\beta_{ij,j}p^u_{ij}\rho^2_{mj,ij}+\alpha_{mj,nl}\right)
\end{aligned}
\tag{44}
$$

where $\alpha_{mj,nl}=\left(\sum_{l=1}^{L}\sum_{n=1}^{K}\beta_{nl,j}p^u_{nl}\rho^2_{mj,nl}+\sigma_z^2\right)$. As a result, we have the expression of γ^d_{ij} as

$$
\begin{aligned}
\gamma^d_{ij}&=\frac{\frac{\left(\mathbb{E}\left[\mathbf{h}^{\mathrm{H}}_{ij,j}\widehat{\mathbf{h}}_{ij,j}\right]\right)^2\beta_{ij,j}p^d_{ij}}{M\alpha_{ij,nl}}}{\frac{\mathbb{E}\left|\mathbf{h}^H_{ij,j}\widehat{\mathbf{h}}_{ij,j}-\mathbb{E}\left[\mathbf{h}^H_{ij,j}\widehat{\mathbf{h}}_{ij,j}\right]\right|^2\beta_{ij,j}p^d_{ij}}{M\alpha_{ij,nl}}+\sum_{m\neq i}^{K}\frac{\mathbb{E}\left|\mathbf{h}^H_{ij,j}\widehat{\mathbf{h}}_{mj,j}\right|^2\beta_{ij,j}p^d_{mj}}{M\alpha_{mj,nl}}+\sum_{l\neq j}^{L}\sum_{k=1}^{K}\frac{\mathbb{E}\left|\mathbf{h}^H_{il,l}\widehat{\mathbf{h}}_{kl,l}\right|^2\beta_{ij,l}p^d_{kl}}{M\alpha_{kl,nl}}+\sigma^2}\\
&=\frac{M\beta^2_{ij,j}p^d_{ij}}{\alpha_{ij,nl}\left(\beta_{ij,j}p^d_{ij}+\sum_{m\neq i}^{K}\left(1+\varphi_{mj,nl}\right)\beta_{ij,j}p^d_{mj}+\sum_{l\neq j}^{L}\sum_{k=1}^{K}\left(1+\varphi_{kl,nl}\right)\beta_{il,l}p^d_{kl}+\sigma^2\right)}
\end{aligned}
\tag{45}
$$

where

$$\varphi_{mj,nl}=\frac{M\beta_{ij,j}p^u_{ij}\rho^2_{mj,ij}}{p^u_{mj}\alpha_{mj,nl}} \tag{46}$$

$$\varphi_{kl,nl}=\frac{M\beta_{il,l}p^u_{il}\rho^2_{kl,ij}}{p^u_{kl}\alpha_{kl,nl}} \tag{47}$$

□

REFERENCES

[1] T. L. Marzetta, "Noncooperative cellular wireless with unlimited numbers of base station antennas," *IEEE Trans. Wireless Commun.*, vol. 9, no. 11, pp. 3590–3600, November 2010.

[2] E. G. Larsson, O. Edfors, F. Tufvesson, and T. L. Marzetta, "Massive MIMO for next generation wireless systems," *IEEE Commun. Mag.*, vol. 52, no. 2, pp. 186–195, February 2014.

[3] F. Rusek, D. Persson, B. K. Lau, E. G. Larsson, T. L. Marzetta, O. Edfors, and F. Tufvesson, "Scaling up MIMO: Opportunities and challenges with very large arrays," *IEEE Signal Process. Mag.*, vol. 30, no. 1, pp. 40–60, Jan 2013.

[4] J. Jose, A. Ashikhmin, T. L. Marzetta, and S. Vishwanath, "Pilot contamination and precoding in multi-cell tdd systems," *IEEE Trans. Wireless Commun.*, vol. 10, no. 8, pp. 2640–2651, August 2011.

[5] O. Elijah, C. Y. Leow, T. A. Rahman, S. Nunoo, and S. Z. Iliya, "A comprehensive survey of pilot contamination in massive MIMO-5G system," *IEEE Communications Surveys Tutorials*, vol. 18, no. 2, pp. 905–923, Secondquarter 2016.

[6] C. Han, T. Harrold, S. Armour, I. Krikidis, S. Videv, P. M. Grant, H. Haas, J. S. Thompson, I. Ku, C. X. Wang, T. A. Le, M. R. Nakhai, J. Zhang, and L. Hanzo, "Green radio: radio techniques to enable energy-efficient wireless networks," *IEEE Commun. Mag.*, vol. 49, no. 6, pp. 46–54, June 2011.

[7] C. X. Wang, F. Haider, X. Gao, X. H. You, Y. Yang, D. Yuan, H. M. Aggoune, H. Haas, S. Fletcher, and E. Hepsaydir, "Cellular architecture and key technologies for 5G wireless communication networks," *IEEE Commun. Mag.*, vol. 52, no. 2, pp. 122–130, February 2014.

[8] X. Zhu, Z. Wang, C. Qian, L. Dai, J. Chen, S. Chen, and L. Hanzo, "Soft pilot reuse and multicell block diagonalization precoding for massive MIMO systems," *IEEE Trans. Veh. Technol.*, vol. 65, no. 5, pp. 3285–3298, May 2016.

[9] I. Atzeni, J. Arnau, and M. Debbah, "Fractional pilot reuse in massive MIMO systems," in *2015 IEEE International Conference on Communication Workshop (ICCW)*, June 2015, pp. 1030–1035.

[10] H. Yin, D. Gesbert, M. Filippou, and Y. Liu, "A coordinated approach to channel estimation in large-scale multiple-antenna systems," *IEEE J. Sel. Areas Commun.*, vol. 31, no. 2, pp. 264–273, February 2013.

[11] E. Bjrnson, E. G. Larsson, and M. Debbah, "Massive MIMO for maximal spectral efficiency: How many users and pilots should be allocated?," *IEEE Trans. Wireless Commun.*, vol. 15, no. 2, pp. 1293–1308, Feb 2016.

[12] H. Wang, W. Zhang, Y. Liu, Q. Xu, and P. Pan, "On design of non-orthogonal pilot signals for a multi-cell massive MIMO system," *IEEE Wireless Commun. Lett.*, vol. 4, no. 2, pp. 129–132, April 2015.

[13] J. C. Shen, J. Zhang, and K. B. Letaief, "Downlink user capacity of massive MIMO under pilot contamination," *IEEE Trans. Wireless Commun.*, vol. 14, no. 6, pp. 3183–3193, June 2015.

[14] N. Akbar, N. Yang, P. Sadeghi, and R. A. Kennedy, "Multi-cell multiuser massive MIMO networks: User capacity analysis and pilot design," *IEEE Transactions on Communications*, vol. 64, no. 12, pp. 5064–5077, Dec 2016.

[15] W. Fu, P. Cao, and J. Thompson, "Achievable rate performance of tdd multi-cell massive MIMO with non-orthogonal pilots," in *WSA 2016; 20th International ITG Workshop on Smart Antennas*, March 2016, pp. 1–5.

[16] J. Hoydis, S. ten Brink, and M. Debbah, "Massive MIMO in the ul/dl of cellular networks: How many antennas do we need?," *IEEE J. Sel. Areas Commun.*, vol. 31, no. 2, pp. 160–171, February 2013.

[17] W. Liu, S. Han, and C. Yang, "Is massive MIMO energy efficient?," *CoRR*, vol. abs/1505.07187, 2015.

[18] G. Auer, V. Giannini, C. Desset, I. Godor, P. Skillermark, M. Olsson, M. A. Imran, D. Sabella, M. J. Gonzalez, O. Blume, and A. Fehske, "How much energy is needed to run a wireless network?," *IEEE Wireless Commun.*, vol. 18, no. 5, pp. 40–49, October 2011.

[19] H. Kim, C. B. Chae, G. de Veciana, and R. W. Heath, "A cross-layer approach to energy efficiency for adaptive MIMO systems exploiting spare capacity," *IEEE Trans. Wireless Commun.*, vol. 8, no. 8, pp. 4264–4275, August 2009.

[20] A. Zappone and E. Jorswieck, "Energy efficiency in wireless networks via fractional programming theory," *Foundations and Trends in Communications and Information Theory*, vol. 11, no. 3-4, pp. 185–396, 2015.

[21] S. Boyd and L. Vandenberghe, *Convex Optimization*, Cambridge University Press, New York, NY, USA, 2004.

[22] M. Grant and S. Boyd, "CVX: Matlab software for disciplined convex programming, version 2.1," http://cvxr.com/cvx, Mar. 2014.

[23] W. Dinkelbach, "On nonlinear fractional programming," *Management Science*, vol. 13, no. 7, pp. 492–498, 1967.

[24] A. Zappone, E. Bjrnson, L. Sanguinetti, and E. Jorswieck, "Achieving global optimality for energy efficiency maximization in wireless networks," 2016.

[25] C. Avin, Y. Emek, E. Kantor, Z. Lotker, D. Peleg, and L. Roditty, "SINR diagrams: Convexity and its applications in wireless networks," *J. ACM*, vol. 59, no. 4, pp. 18:1–18:34, Aug. 2012.

[26] P. Cao, W. Liu, J. S. Thompson, C. Yang, and E. A. Jorswieck, "Semidynamic green resource management in downlink heterogeneous networks by group sparse power control," *IEEE J. Sel. Areas Commun.*, vol. 34, no. 5, pp. 1250–1266, May 2016.

[27] A. Beck, A.and Ben-Tal and L. Tetruashvili, "A sequential parametric convex approximation method with applications to nonconvex truss topology design problems," *Journal of Global Optimization*, vol. 47, no. 1, pp. 29–51, 2010.

[28] P. D. Tao and L. T. H. An, "Convex analysis approach to dc programming: Theory, algorithms and applications," *Acta Mathematica Vietnamica*, vol. 22, no. 1, pp. 289–355, 1997.

[29] A. Zappone and E.A. Jorswieck, "Energy-efficient resource allocation in future wireless networks by sequential fractional programming," *Digital Signal Processing*, vol. 60, pp. 324 – 337, 2017.

[30] A. Medra and T. N. Davidson, "Flexible codebook design for limited feedback systems via sequential smooth optimization on the grassmannian manifold," *IEEE Trans. Signal Process.*, vol. 62, no. 5, pp. 1305–1318, March 2014.

[31] 3GPP TR 36.814, "Further advancements for e-utra physical layer aspects (release 9)," Tech. Rep., 2010.

[32] C. Desset, B. Debaillie, and F. Louagie, "Modeling the hardware power consumption of large scale antenna systems," in *IEEE Online Conference on Green Communications (OnlineGreenComm)*, Nov 2014, pp. 1–6.

[33] D. Nguyen, L. N. Tran, P. Pirinen, and M. Latva-aho, "Precoding for full duplex multiuser MIMO systems: Spectral and energy efficiency maximization," *IEEE Trans. Signal Process.*, vol. 61, no. 16, pp. 4038–4050, Aug 2013.

[34] E. Bjrnson, L. Sanguinetti, J. Hoydis, and M. Debbah, "Designing multi-user MIMO for energy efficiency: When is massive MIMO the answer?," in *2014 IEEE Wireless Communications and Networking Conference (WCNC)*, April 2014, pp. 242–247.

Bibliography

[1] Y. S. Cho, J. Kim, W. Y. Yang, and C. G. Kang, *MIMO-OFDM Wireless Communications with MATLAB*. Wiley Publishing, 2010.

[2] G. Auer, V. Giannini, C. Desset, I. Godor, P. Skillermark, M. Olsson, M. A. Imran, D. Sabella, M. J. Gonzalez, O. Blume, and A. Fehske, "How much energy is needed to run a wireless network?," *IEEE Wireless Commun.*, vol. 18, pp. 40–49, October 2011.

[3] Cisco, "Cisco Visual Networking Index: Global Mobile Data Traffic Forecast Update, 2015-2020," tech. rep., February 2016.

[4] Ericsson, "Ericsson Mobility Report-on the pulse of the networked society," tech. rep., November 2016.

[5] D. Brake, "5G and next generation wireless: Implications for policy and competition," tech. rep., June 2016.

[6] I. Qualcomm Technologies, "Leading the world to 5G," tech. rep., February 2016.

[7] Ericsson, "5G systems enabling the transformation of industry and society," tech. rep., January 2017.

[8] A. J. PAULRAJ, D. A. GORE, R. U. NABAR, and H. BOLCSKEI, "An overview of MIMO communications - a key to gigabit wireless," *Proceedings of the IEEE*, vol. 92, pp. 198–218, Feb 2004.

[9] S. Yang and L. Hanzo, "Fifty years of MIMO detection: The road to large-scale MIMOs," *IEEE Communications Surveys Tutorials*, vol. 17, pp. 1941–1988, Fourthquarter 2015.

[10] E. G. Larsson, "MIMO detection methods: How they work [lecture notes]," *IEEE Signal Process. Mag.*, vol. 26, no. 3, 2009.

[11] Z. Guo and P. Nilsson, "Algorithm and implementation of the k-best sphere decoding for MIMO detection," *IEEE J. Sel. Areas Commun.*, vol. 24, pp. 491–503, March 2006.

[12] S. Chen, T. Zhang, and Y. Xin, "Relaxed K -best MIMO signal detector design and vlsi implementation," *IEEE Transactions on Very Large Scale Integration (VLSI) Systems*, vol. 15, pp. 328–337, March 2007.

[13] A. Svensson, "An introduction to adaptive qam modulation schemes for known and predicted channels," *Proceedings of the IEEE*, vol. 95, pp. 2322–2336, Dec 2007.

[14] V. Jungnickel, K. Manolakis, W. Zirwas, B. Panzner, V. Braun, M. Lossow, M. Sternad, R. Apelfrojd, and T. Svensson, "The role of small cells, coordinated multipoint, and massive MIMO in 5G," *IEEE Commun. Mag.*, vol. 52, pp. 44–51, May 2014.

[15] A. Osseiran, F. Boccardi, V. Braun, K. Kusume, P. Marsch, M. Maternia, O. Queseth, M. Schellmann, H. Schotten, H. Taoka, H. Tullberg, M. A. Uusitalo, B. Timus, and M. Fallgren, "Scenarios for 5G mobile and wireless communications: the vision of the metis project," *IEEE Commun. Mag.*, vol. 52, pp. 26–35, May 2014.

[16] T. L. Marzetta, "Massive MIMO: An introduction," *Bell Labs Technical Journal*, vol. 20, pp. 11–22, 2015.

[17] H. Q. Ngo, T. L. Marzetta, and E. G. Larsson, "Analysis of the pilot contamination effect in very large multicell multiuser MIMO systems for physical channel models," in *2011 IEEE International Conference on Acoustics, Speech and Signal Processing (ICASSP)*, pp. 3464–3467, May 2011.

[18] C. Han and S. Armour, "Energy efficient radio resource management strategies for green radio," *IET Communications*, vol. 5, pp. 2629–2639, Dec 2011.

[19] Y. S. Soh, T. Q. S. Quek, M. Kountouris, and H. Shin, "Energy efficient heterogeneous cellular networks," *IEEE J. Sel. Areas Commun.*, vol. 31, pp. 840–850, May 2013.

[20] Z. Niu, Y. Wu, J. Gong, and Z. Yang, "Cell zooming for cost-efficient green cellular networks," *IEEE Commun. Mag.*, vol. 48, pp. 74–79, November 2010.

[21] A. J. Fehske, F. Richter, and G. P. Fettweis, "Energy efficiency improvements through micro sites in cellular mobile radio networks," in *2009 IEEE Globecom Workshops*, pp. 1–5, Nov 2009.

[22] E. Oh, B. Krishnamachari, X. Liu, and Z. Niu, "Toward dynamic energy-efficient operation of cellular network infrastructure," *IEEE Commun. Mag.*, vol. 49, pp. 56–61, June 2011.

[23] R. Bolla, R. Bruschi, F. Davoli, and F. Cucchietti, "Energy efficiency in the future internet: A survey of existing approaches and trends in energy-aware fixed network infrastructures," *IEEE Communications Surveys Tutorials*, vol. 13, pp. 223–244, Second 2011.

[24] J. Wu, Y. Zhang, M. Zukerman, and E. K. N. Yung, "Energy-efficient base-stations sleep-mode techniques in green cellular networks: A survey," *IEEE Communications Surveys Tutorials*, vol. 17, pp. 803–826, Secondquarter 2015.

[25] B. Sklar, *Digital Communications: Fundamentals and Applications (2nd Edition)*. Prentice Hall, 2 ed., Jan. 2001.

[26] D. Tse and P. Viswanath, *Fundamentals of Wireless Communication*. New York, NY, USA: Cambridge University Press, 2005.

[27] T. L. Marzetta, E. G. Larsson, H. Yang, and H. Q. Ngo, *Fundamentals of Massive MIMO*. Cambridge Press, 1st ed., 2016.

[28] H. Sampath, S. Talwar, J. Tellado, V. Erceg, and A. Paulraj, "A fourth-generation MIMO-ofdm broadband wireless system: design, performance, and field trial results," *IEEE Commun. Mag.*, vol. 40, pp. 143–149, Sep 2002.

[29] J. G. Andrews, S. Buzzi, W. Choi, S. V. Hanly, A. Lozano, A. C. K. Soong, and J. C. Zhang, "What will 5G be?," *IEEE J. Sel. Areas Commun.*, vol. 32, pp. 1065–1082, June 2014.

[30] L. Zheng and D. N. C. Tse, "Diversity and multiplexing: a fundamental tradeoff in multiple-antenna channels," *IEEE Trans. Inf. Theory*, vol. 49, pp. 1073–1096, May 2003.

[31] S. M. Alamouti, "A simple transmit diversity technique for wireless communications," *IEEE J. Sel. Areas Commun.*, vol. 16, pp. 1451–1458, Oct 1998.

[32] P. W. Wolniansky, G. J. Foschini, G. D. Golden, and R. A. Valenzuela, "V-blast: an architecture for realizing very high data rates over the rich-scattering wireless channel," in *Signals, Systems, and Electronics, 1998. ISSSE 98. 1998 URSI International Symposium on*, pp. 295–300, Sep 1998.

[33] M. Jankiraman, *Space-time Codes and MIMO Systems*. Artech House universal personal communications series, Artech House, 2004.

[34] E. Telatar, "Capacity of multi-antenna gaussian channels," *European Transactions on Telecommunications*, vol. 10, no. 6, pp. 585–595, 1999.

[35] M. O. Damen, H. E. Gamal, and G. Caire, "On maximum-likelihood detection and the search for the closest lattice point," *IEEE Trans. Inf. Theory*, vol. 49, pp. 2389–2402, Oct 2003.

[36] L. Bai, J. Choi, and Q. Yu, *Low Complexity MIMO Receivers*. Springer Publishing Company, Incorporated, 2014.

[37] G. J. Foschini, "Layered space-time architecture for wireless communication in a fading environment when using multi-element antennas," *Bell Labs Technical Journal*, vol. 1, pp. 41–59, Autumn 1996.

[38] W.-K. Ma, P.-C. Ching, and Z. Ding, "Semidefinite relaxation based multiuser detection for M-ary PSK multiuser systems," *IEEE Transactions on Signal Processing*, vol. 52, pp. 2862–2872, Oct 2004.

[39] P. H. Tan, L. K. Rasmussen, and T. M. Aulin, "The application of semidefinite programming for detection in cdma," in *Proceedings. 2001 IEEE International Symposium on Information Theory (IEEE Cat. No.01CH37252)*, pp. 9–, 2001.

[40] M. Kisialiou, X. Luo, and Z. Q. Luo, "Efficient implementation of quasi- maximum-likelihood detection based on semidefinite relaxation," *IEEE Transactions on Signal Processing*, vol. 57, pp. 4811–4822, Dec 2009.

[41] A. Wiesel, Y. C. Eldar, and S. Shamai, "Semidefinite relaxation for detection of 16-qam signaling in mimo channels," *IEEE Signal Processing Letters*, vol. 12, pp. 653–656, Sept 2005.

[42] A. Jamalipour, T. Wada, and T. Yamazato, "A tutorial on multiple access technologies for beyond 3g mobile networks," *IEEE Commun. Mag.*, vol. 43, pp. 110–117, Feb 2005.

[43] P. W. C. Chan, E. S. Lo, R. R. Wang, E. K. S. Au, V. K. N. Lau, R. S. Cheng, W. H. Mow, R. D. Murch, and K. B. Letaief, "The evolution path of 4g networks: FDD or tdd?," *IEEE Commun. Mag.*, vol. 44, pp. 42–50, Dec 2006.

[44] M. Vu and A. Paulraj, "MIMO wireless linear precoding," *IEEE Signal Process. Mag.*, vol. 24, pp. 86–105, Sept 2007.

[45] D. Gesbert, M. Shafi, D. shan Shiu, P. J. Smith, and A. Naguib, "From theory to practice: an overview of MIMO space-time coded wireless systems," *IEEE J. Sel. Areas Commun.*, vol. 21, pp. 281–302, Apr 2003.

[46] L. G. Barbero and J. S. Thompson, "Fixing the complexity of the sphere decoder for MIMO detection," *IEEE Trans. Wireless Commun.*, vol. 7, pp. 2131–2142, June 2008.

[47] M. Wenk, M. Zellweger, A. Burg, N. Felber, and W. Fichtner, "K-best MIMO detection vlsi architectures achieving up to 424 mbps," in *2006 IEEE International Symposium on Circuits and Systems*, pp. 4 pp.–1154, May 2006.

[48] S. Mondal, A. Eltawil, C. A. Shen, and K. N. Salama, "Design and implementation of a sort-free K-Best sphere decoder," *IEEE Transactions on Very Large Scale Integration (VLSI) Systems*, vol. 18, pp. 1497–1501, Oct 2010.

[49] A. Goldsmith, *Wireless Communications*. New York, NY, USA: Cambridge University Press, 2005.

[50] S. Catreux, V. Erceg, D. Gesbert, and R. W. Heath, "Adaptive modulation and MIMO coding for broadband wireless data networks," *IEEE Commun. Mag.*, vol. 40, pp. 108–115, Jun 2002.

[51] Z. Zhou, B. Vucetic, M. Dohler, and Y. Li, "MIMO systems with adaptive modulation," *IEEE Trans. Veh. Technol.*, vol. 54, pp. 1828–1842, Sept 2005.

[52] J. Huang, *Adaptive MIMO Systems with Channel State Information at Transmitter*. PhD thesis, KTH Royal Institute of Technology in Stockholm, 2009.

[53] Z. Xie, C. K. Rushforth, R. T. Short, and T. K. Moon, "A tree-search algorithm for signal detection and parameter estimation in multi-user communications," in *Military Communications Conference, 1990. MILCOM '90, Conference Record, A New Era. 1990 IEEE*, pp. 796–800 vol.2, Sep 1990.

[54] M. Rahman, E. Rohani, and G. S. Choi, "An iterative soft decision based adaptive k-best decoder without snr estimation," in *2014 48th Asilomar Conference on Signals, Systems and Computers*, pp. 1016–1020, Nov 2014.

[55] R. Ma, P. Ren, S. Xue, and Q. Du, "Adaptive low-complexity constellation-reduction aided detection in MIMO systems employing high-order modulation," in *2013 IEEE*

Wireless Communications and Networking Conference (WCNC), pp. 4083–4088, April 2013.

[56] Q. Zhou and X. Ma, "An improved lr-aided k-best algorithm for MIMO detection," in *Wireless Communications Signal Processing (WCSP), 2012 International Conference on*, pp. 1–5, Oct 2012.

[57] C. Y. Hung, R. Y. Chang, and W. H. Chung, "A hybrid mmse and K-Best detection scheme for MIMO systems," in *Vehicular Technology Conference (VTC Fall), 2012 IEEE*, pp. 1–5, Sept 2012.

[58] S. Han, T. Cui, and C. Tellambura, "Improved K-Best sphere detection for uncoded and coded MIMO systems," *IEEE Wireless Commun. Lett.*, vol. 1, pp. 472–475, October 2012.

[59] E. Dahlman, S. Parkvall, and J. Skold, *4G: LTE/LTE-Advanced for Mobile Broadband*. Academic Press, 1st ed., 2011.

[60] Y. Zhou, C. Zhong, S. Jin, Y. Huang, and Z. Zhang, "A low-complexity multiuser adaptive modulation scheme for massive MIMO systems," *IEEE Signal Process. Lett.*, vol. 23, pp. 1464–1468, Oct 2016.

[61] J. Jiang, J. S. Thompson, and H. Sun, "A singular-value-based adaptive modulation and cooperation scheme for virtual-MIMO systems," *IEEE Trans. Veh. Technol.*, vol. 60, pp. 2495–2504, July 2011.

[62] Z. Zhou, B. Vucetic, Z. Chen, and Y. Li, "Design of adaptive modulation in MIMO systems using outdated csi," in *2005 IEEE 16th International Symposium on Personal, Indoor and Mobile Radio Communications*, vol. 2, pp. 1101–1105 Vol. 2, Sept 2005.

[63] S. Zhou and G. B. Giannakis, "Adaptive modulation for multiantenna transmissions with channel mean feedback," *IEEE Trans. Wireless Commun.*, vol. 3, pp. 1626–1636, Sept 2004.

[64] B. Hassibi and H. Vikalo, "On the sphere-decoding algorithm i. expected complexity," *IEEE Transactions on Signal Processing*, vol. 53, pp. 2806–2818, Aug 2005.

[65] X. Zhu and R. D. Murch, "Performance analysis of maximum likelihood detection in a MIMO antenna system," *IEEE Trans. Commun.*, vol. 50, pp. 187–191, Feb 2002.

[66] G. Lindell, "Some exact union bound results for maximum likelihood detection in MIMO systems," in *Proceedings. International Symposium on Information Theory, 2005. ISIT 2005.*, pp. 2223–2227, Sept 2005.

[67] H. Artes, D. Seethaler, and F. Hlawatsch, "Efficient detection algorithms for MIMO channels: a geometrical approach to approximate ml detection," *IEEE Trans. Signal Process.*, vol. 51, pp. 2808–2820, Nov 2003.

[68] J. Proakis, *Digital Communications*. Electrical engineering series, McGraw-Hill, 2001.

[69] O. Elijah, C. Y. Leow, T. A. Rahman, S. Nunoo, and S. Z. Iliya, "A comprehensive survey of pilot contamination in massive MIMO-5G system," *IEEE Communications Surveys Tutorials*, vol. 18, pp. 905–923, Secondquarter 2016.

[70] E. G. Larsson, O. Edfors, F. Tufvesson, and T. L. Marzetta, "Massive MIMO for next generation wireless systems," *IEEE Commun. Mag.*, vol. 52, pp. 186–195, February 2014.

[71] T. L. Marzetta, "Noncooperative cellular wireless with unlimited numbers of base station antennas," *IEEE Trans. Wireless Commun.*, vol. 9, pp. 3590–3600, November 2010.

[72] F. Rusek, D. Persson, B. K. Lau, E. G. Larsson, T. L. Marzetta, O. Edfors, and F. Tufvesson, "Scaling up MIMO: Opportunities and challenges with very large arrays," *IEEE Signal Process. Mag.*, vol. 30, pp. 40–60, Jan 2013.

[73] C. X. Wang, F. Haider, X. Gao, X. H. You, Y. Yang, D. Yuan, H. M. Aggoune, H. Haas, S. Fletcher, and E. Hepsaydir, "Cellular architecture and key technologies for 5G wireless communication networks," *IEEE Commun. Mag.*, vol. 52, pp. 122–130, February 2014.

[74] F. Boccardi, R. W. Heath, A. Lozano, T. L. Marzetta, and P. Popovski, "Five disruptive technology directions for 5G," *IEEE Commun. Mag.*, vol. 52, pp. 74–80, February 2014.

[75] N. Alliance, "Next generation mobile networks (ngmn) 5G white paper." `http://tinyurl.com/ne6pxzo`, Feb 2015.

[76] J. Shen, J. Zhang, K. Chen, and K. B. Letaief, "High-dimensional CSI acquisition in massive MIMO: sparsity-inspired approaches," *CoRR*, vol. abs/1505.00426, 2015.

[77] X. Rao and V. K. N. Lau, "Distributed compressive csit estimation and feedback for FDD multi-user massive MIMO systems," *IEEE Trans. Signal Process.*, vol. 62, pp. 3261–3271, June 2014.

[78] J. C. Shen, J. Zhang, E. Alsusa, and K. B. Letaief, "Compressed csi acquisition in FDD massive MIMO with partial support information," in *2015 IEEE International Conference on Communications (ICC)*, pp. 1459–1464, June 2015.

[79] J. Jose, A. Ashikhmin, T. L. Marzetta, and S. Vishwanath, "Pilot contamination and precoding in multi-cell tdd systems," *IEEE Trans. Wireless Commun.*, vol. 10, pp. 2640–2651, August 2011.

[80] J. Hoydis, S. ten Brink, and M. Debbah, "Massive MIMO in the ul/dl of cellular networks: How many antennas do we need?," *IEEE J. Sel. Areas Commun.*, vol. 31, pp. 160–171, February 2013.

[81] H. Q. Ngo, E. G. Larsson, and T. L. Marzetta, "Energy and spectral efficiency of very large multiuser MIMO systems," *IEEE Trans. Commun.*, vol. 61, pp. 1436–1449, April 2013.

[82] H. Huh, G. Caire, H. C. Papadopoulos, and S. A. Ramprashad, "Achieving "massive MIMO" spectral efficiency with a not-so-large number of antennas," *IEEE Trans. Wireless Commun.*, vol. 11, pp. 3226–3239, September 2012.

[83] X. Zhu, Z. Wang, C. Qian, L. Dai, J. Chen, S. Chen, and L. Hanzo, "Soft pilot reuse and multicell block diagonalization precoding for massive MIMO systems," *IEEE Trans. Veh. Technol.*, vol. 65, pp. 3285–3298, May 2016.

[84] I. Atzeni, J. Arnau, and M. Debbah, "Fractional pilot reuse in massive MIMO systems," in *2015 IEEE International Conference on Communication Workshop (ICCW)*, pp. 1030–1035, June 2015.

[85] H. Yin, D. Gesbert, M. Filippou, and Y. Liu, "A coordinated approach to channel estimation in large-scale multiple-antenna systems," *IEEE J. Sel. Areas Commun.*, vol. 31, pp. 264–273, February 2013.

[86] E. Bjrnson, E. G. Larsson, and M. Debbah, "Massive MIMO for maximal spectral efficiency: How many users and pilots should be allocated?," *IEEE Trans. Wireless Commun.*, vol. 15, pp. 1293–1308, Feb 2016.

[87] H. Wang, W. Zhang, Y. Liu, Q. Xu, and P. Pan, "On design of non-orthogonal pilot signals for a multi-cell massive MIMO system," *IEEE Wireless Commun. Lett.*, vol. 4, pp. 129–132, April 2015.

[88] J. C. Shen, J. Zhang, and K. B. Letaief, "Downlink user capacity of massive MIMO under pilot contamination," *IEEE Trans. Wireless Commun.*, vol. 14, pp. 3183–3193, June 2015.

[89] N. Akbar, N. Yang, P. Sadeghi, and R. A. Kennedy, "User capacity analysis and pilot design for multi-cell multiuser massive MIMO networks," *CoRR*, vol. abs/1511.07568, 2015.

[90] P. Lioliou and M. Viberg, "Least-squares based channel estimation for MIMO relays," in *2008 International ITG Workshop on Smart Antennas*, pp. 90–95, Feb 2008.

[91] J. Zhou and J. Thompson, "Linear precoding for the downlink of multiple input single output coexisting wireless systems," *IET Communications*, vol. 2, pp. 742–752, July 2008.

[92] T. L. Marzetta, "How much training is required for multiuser mimo?," in *2006 Fortieth Asilomar Conference on Signals, Systems and Computers*, pp. 359–363, Oct 2006.

[93] B. Hassibi and B. M. Hochwald, "How much training is needed in multiple-antenna wireless links?," *IEEE Transactions on Information Theory*, vol. 49, pp. 951–963, April 2003.

[94] J. H. Conway, R. H. Hardin, and N. J. A. Sloane, "Packing lines, planes, etc.: packings in grassmannian spaces," *Experiment. Math.*, vol. 5, no. 2, pp. 139–159, 1996.

[95] D. J. Love, R. W. Heath, and T. Strohmer, "Grassmannian beamforming for multiple-input multiple-output wireless systems," *IEEE Trans. Inf. Theory*, vol. 49, pp. 2735–2747, Oct 2003.

[96] D. J. Love, R. W. Heath, V. K. N. Lau, D. Gesbert, B. D. Rao, and M. Andrews, "An overview of limited feedback in wireless communication systems," *IEEE J. Sel. Areas Commun.*, vol. 26, pp. 1341–1365, October 2008.

[97] W. Dai, Y. Liu, and B. Rider, "Quantization bounds on grassmann manifolds and applications to MIMO communications," *IEEE Trans. Inf. Theory*, vol. 54, pp. 1108–1123, March 2008.

[98] H. Zorlein and M. Bossert, "Coherence optimization and best complex antipodal spherical codes," *IEEE Trans. Signal Process.*, vol. 63, pp. 6606–6615, Dec 2015.

[99] A. Medra and T. N. Davidson, "Flexible codebook design for limited feedback systems via sequential smooth optimization on the grassmannian manifold," *IEEE Trans. Signal Process.*, vol. 62, pp. 1305–1318, March 2014.

[100] A. Fehske, G. Fettweis, J. Malmodin, and G. Biczok, "The global footprint of mobile communications: The ecological and economic perspective," *IEEE Commun. Mag.*, vol. 49, pp. 55–62, August 2011.

[101] Z. Hasan, H. Boostanimehr, and V. K. Bhargava, "Green cellular networks: A survey, some research issues and challenges," *IEEE Communications Surveys Tutorials*, vol. 13, pp. 524–540, Fourth 2011.

[102] O. Blume, H. Eckhardt, S. Klein, E. Kuehn, and W. M. Wajda, "Energy savings in mobile networks based on adaptation to traffic statistics," *Bell Labs Technical Journal*, vol. 15, pp. 77–94, Sept 2010.

[103] H. Kim, C. B. Chae, G. de Veciana, and R. W. Heath, "A cross-layer approach to energy efficiency for adaptive MIMO systems exploiting spare capacity," *IEEE Trans. Wireless Commun.*, vol. 8, pp. 4264–4275, August 2009.

[104] F. Han, Z. Safar, W. S. Lin, Y. Chen, and K. J. R. Liu, "Energy-efficient cellular network operation via base station cooperation," in *2012 IEEE International Conference on Communications (ICC)*, pp. 4374–4378, June 2012.

[105] G. Wang, C. Guo, S. Wang, and C. Feng, "A traffic prediction based sleeping mechanism with low complexity in femtocell networks," in *2013 IEEE International Conference on Communications Workshops (ICC)*, pp. 560–565, June 2013.

[106] Z. Chong and E. A. Jorswieck, "Energy efficiency in random opportunistic beamforming," in *2011 IEEE 73rd Vehicular Technology Conference (VTC Spring)*, pp. 1–5, May 2011.

[107] C. Hellings and W. Utschick, "Energy efficiency optimization in the multiantenna downlink with linear transceivers," in *2013 IEEE 24th Annual International Symposium on Personal, Indoor, and Mobile Radio Communications (PIMRC)*, pp. 414–418, Sept 2013.

[108] P. Cao, Z. Chong, Z. K. M. Ho, and E. Jorswieck, "Energy-efficient power allocation for amplify-and-forward MIMO relay channel," in *2012 IEEE 17th International Workshop on Computer Aided Modeling and Design of Communication Links and Networks (CAMAD)*, pp. 333–337, Sept 2012.

[109] K. T. K. Cheung, S. Yang, and L. Hanzo, "Achieving maximum energy-efficiency in multi-relay ofdma cellular networks: A fractional programming approach," *IEEE Trans. Commun.*, vol. 61, pp. 2746–2757, July 2013.

[110] A. Zappone and E. Jorswieck, "Energy efficiency in wireless networks via fractional programming theory," *Foundations and Trends in Communications and Information Theory*, vol. 11, no. 3-4, pp. 185–396, 2015.

[111] E. Bjrnson, L. Sanguinetti, J. Hoydis, and M. Debbah, "Optimal design of energy-efficient multi-user MIMO systems: Is massive MIMO the answer?," *IEEE Trans. Wireless Commun.*, vol. 14, pp. 3059–3075, June 2015.

[112] H. Yang and T. L. Marzetta, "Total energy efficiency of cellular large scale antenna system multiple access mobile networks," in *Online Conference on Green Communications (GreenCom), 2013 IEEE*, pp. 27–32, Oct 2013.

[113] L. Zhao, H. Zhao, F. Hu, K. Zheng, and J. Zhang, "Energy efficient power allocation algorithm for downlink massive MIMO with mrt precoding," in *Vehicular Technology Conference (VTC Fall), 2013 IEEE 78th*, pp. 1–5, Sept 2013.

[114] W. Liu, S. Han, and C. Yang, "Is massive MIMO energy efficient?," *CoRR*, vol. abs/1505.07187, 2015.

[115] G. J. Foschini, G. D. Golden, R. A. Valenzuela, and P. W. Wolniansky, "Simplified processing for high spectral efficiency wireless communication employing multi-element arrays," *IEEE J. Sel. Areas Commun.*, vol. 17, pp. 1841–1852, Nov 1999.

[116] S. Boyd and L. Vandenberghe, *Convex Optimization*. New York, NY, USA: Cambridge University Press, 2004.

[117] M. Grant and S. Boyd, "CVX: Matlab software for disciplined convex programming, version 2.1." `http://cvxr.com/cvx`, Mar. 2014.

[118] W. Dinkelbach, "On nonlinear fractional programming," *Management Science*, vol. 13, no. 7, pp. 492–498, 1967.

[119] A. Zappone, E. Bjrnson, L. Sanguinetti, and E. Jorswieck, "Achieving global optimality for energy efficiency maximization in wireless networks," 2016.

[120] C. Avin, Y. Emek, E. Kantor, Z. Lotker, D. Peleg, and L. Roditty, "SINR diagrams: Convexity and its applications in wireless networks," *J. ACM*, vol. 59, pp. 18:1–18:34, Aug. 2012.

[121] P. Cao, W. Liu, J. S. Thompson, C. Yang, and E. A. Jorswieck, "Semidynamic green resource management in downlink heterogeneous networks by group sparse power control," *IEEE J. Sel. Areas Commun.*, vol. 34, pp. 1250–1266, May 2016.

[122] A. Beck, A.and Ben-Tal and L. Tetruashvili, "A sequential parametric convex approximation method with applications to nonconvex truss topology design problems," *Journal of Global Optimization*, vol. 47, no. 1, pp. 29–51, 2010.

[123] P. D. Tao and L. T. H. An, "Convex analysis approach to dc programming: Theory, algorithms and applications," *Acta Mathematica Vietnamica*, vol. 22, no. 1, pp. 289–355, 1997.

[124] L. Thi, T. Duc, and P. Dinh, "A dc programming approach for a class of bilevel programming problems and its application in portfolio selection," *Numerical Algebra, Control and Optimization*, vol. 2, no. 1, pp. 167–185, 2012.

[125] J.-B. Hiriart-Urruty, *Generalized Differentiability / Duality and Optimization for Problems Dealing with Differences of Convex Functions*, pp. 37–70. Berlin, Heidelberg: Springer Berlin Heidelberg, 1985.

[126] M. Grant and S. Boyd, "Graph implementations for nonsmooth convex programs," in *Recent Advances in Learning and Control* (V. Blondel, S. Boyd, and H. Kimura, eds.), Lecture Notes in Control and Information Sciences, pp. 95–110, Springer-Verlag Limited, 2008. `http://stanford.edu/~boyd/graph_dcp.html`.

[127] G. T. 36.814, "Further advancements for e-utra physical layer aspects (release 9)," tech. rep., 2010.

[128] C. Desset, B. Debaillie, and F. Louagie, "Modeling the hardware power consumption of large scale antenna systems," in *IEEE Online Conference on Green Communications (OnlineGreenComm)*, pp. 1–6, Nov 2014.

[129] D. Nguyen, L. N. Tran, P. Pirinen, and M. Latva-aho, "Precoding for full duplex multiuser MIMO systems: Spectral and energy efficiency maximization," *IEEE Trans. Signal Process.*, vol. 61, pp. 4038–4050, Aug 2013.

[130] E. Bjrnson, L. Sanguinetti, J. Hoydis, and M. Debbah, "Designing multi-user MIMO for energy efficiency: When is massive MIMO the answer?," in *2014 IEEE Wireless Communications and Networking Conference (WCNC)*, pp. 242–247, April 2014.

[131] A. F. Molisch, V. V. Ratnam, S. Han, Z. Li, S. L. H. Nguyen, L. Li, and K. Haneda, "Hybrid beamforming for massive MIMO - A survey," *CoRR*, vol. abs/1609.05078, 2016.

[132] S. Han, C. l. I, Z. Xu, and C. Rowell, "Large-scale antenna systems with hybrid analog and digital beamforming for millimeter wave 5G," *IEEE Commun. Mag.*, vol. 53, pp. 186–194, January 2015.